NOVEL INSIGHTS INTO THE GENETICS OF GROWTH DISORDERS

EDITED BY: Mara Giordano and Liborio Stuppia
PUBLISHED IN: Frontiers in Genetics, Frontiers in Endocrinology and Frontiers in Pediatrics

frontiers Research Topics

ISSN 1664-8714
ISBN 978-2-88976-341-2
DOI 10.3389/978-2-88976-341-2

About Frontiers

Frontiers is more than just an open-access publisher of scholarly articles: it is a pioneering approach to the world of academia, radically improving the way scholarly research is managed. The grand vision of Frontiers is a world where all people have an equal opportunity to seek, share and generate knowledge. Frontiers provides immediate and permanent online open access to all its publications, but this alone is not enough to realize our grand goals.

Frontiers Journal Series

The Frontiers Journal Series is a multi-tier and interdisciplinary set of open-access, online journals, promising a paradigm shift from the current review, selection and dissemination processes in academic publishing. All Frontiers journals are driven by researchers for researchers; therefore, they constitute a service to the scholarly community. At the same time, the Frontiers Journal Series operates on a revolutionary invention, the tiered publishing system, initially addressing specific communities of scholars, and gradually climbing up to broader public understanding, thus serving the interests of the lay society, too.

Dedication to Quality

Each Frontiers article is a landmark of the highest quality, thanks to genuinely collaborative interactions between authors and review editors, who include some of the world's best academicians. Research must be certified by peers before entering a stream of knowledge that may eventually reach the public - and shape society; therefore, Frontiers only applies the most rigorous and unbiased reviews.
Frontiers revolutionizes research publishing by freely delivering the most outstanding research, evaluated with no bias from both the academic and social point of view. By applying the most advanced information technologies, Frontiers is catapulting scholarly publishing into a new generation.

What are Frontiers Research Topics?

Frontiers Research Topics are very popular trademarks of the Frontiers Journals Series: they are collections of at least ten articles, all centered on a particular subject. With their unique mix of varied contributions from Original Research to Review Articles, Frontiers Research Topics unify the most influential researchers, the latest key findings and historical advances in a hot research area! Find out more on how to host your own Frontiers Research Topic or contribute to one as an author by contacting the Frontiers Editorial Office: frontiersin.org/about/contact

NOVEL INSIGHTS INTO THE GENETICS OF GROWTH DISORDERS

Topic Editors:
Mara Giordano, University of Eastern Piedmont, Italy
Liborio Stuppia, University of Studies G. d'Annunzio Chieti and Pescara, Italy

Citation: Giordano, M., Stuppia, L., eds. (2022). Novel Insights into the Genetics of Growth Disorders. Lausanne: Frontiers Media SA. doi: 10.3389/978-2-88976-341-2

Table of Contents

frontiers | Frontiers in Genetics

EDITORIAL
published: 08 June 2022
doi: 10.3389/fgene.2022.920469

Editorial: Novel Insights Into the Genetics of Growth Disorders

Mara Giordano[1]* *and Liborio Stuppia*[2]

[1]*Laboratory of Genetics, SCDU Clinical Biochemistry, University Hospital "Maggiore della Carità", Novara and Department of Health Sciences, University of Eastern Piedmont, Novara, Italy,* [2]*Department of Psychological, Health and Territorial Sciences and Center for Advanced Sciences and Technology (CAST), G. d'Annunzio University, Chieti-Pescara, Italy*

Keywords: growth disorder, SHOX, COL1A, Acan, Lamc3, Smad4

Editorial on the Research Topic

Novel Insights Iinto the Genetics of Growth Disorders

Although in the popular culture the definition of "genetic disease" is mainly associated to the presence of clinical signs such as intellectual disability, heart malformations or facial dysmorphisms, the history of Medical Genetics demonstrates that actually one of the first conditions associated to a genetic disease has been represented by short stature. This disorder, representing a common medical concern that paediatricians have to face in their daily practice, can be associated to different genetic conditions, with the first evidence coming from the identification of the 45, X karyotype as the cause of the Turner Syndrome (TS), characterized by short stature as one of the main clinical signs (Zinn et al., 1993). The comparison between the phenotype of TS and Klinefelter syndrome, due to a 47, XXY karyotype and characterized by tall stature, suggested the presence of one or more genes affecting human stature mapping on both X and Y sex chromosomes. Since these two chromosomes share genes only on their pseudoautosomal regions (PAR1 and PAR2), it was quite obvious to conclude that the gene(s) involved in short stature was located within these regions. Finally, in 1997, the SHOX gene, mapping within the PAR1 region, was cloned and identified as responsible both for a number of cases of idiopathic short stature and for the majority of cases of Leri-Weill dyschondrosteosis (Rao et al., 1997). In a short time, search for alterations in *SHOX* has become crucial in the molecular diagnosis of short stature (Stuppia et al., 2003; Stuppia et al., 2010; Genoni et al., 2018), in particular due to the evidence of a good response to GH treatment showed by patients with SHOX deficit (Benabbad et al., 2017). Moreover, the presence of variants affecting height also outside the *SHOX* coding region extended the spectrum of genotype–phenotype correlation in short stature (Benito- Sanz et al., 2005; Babu et al., 2021; Fanelli et al., 2022). The identification of the *SHOX* gene and its analysis in the diagnostic workflow of children with short stature prompted other researchers to investigate the role played by other genes in the pathogenesis of different forms of short stature.

Currently there are more than 200 mendelian syndromes or skeletal dysplasia associated with short stature for which the genetic cause have been identified. In some patients with short stature, variants of moderate effect explain less extreme phenotypes than those seen in disorders with classical syndromic phenotype. For example, biallelic variants in the natriuretic peptide receptor 2 (*NPR2)* (Wu et al., 2022) lead to acromesomelic displasia weather monoallelic mutations have been detected in short stature patients without any other distinctive feature (Hisado-Oliva et al., 2018) Pathogenic variants in *FGFR3*, have been found in a wide range of phenotypes, namely achondroplasia, hypochondroplasia and more recently in patients with milder forms short stature (Kant et al., 2015).

OPEN ACCESS

Edited and reviewed by:
Jordi Pérez-Tur,
Institute of Biomedicine of Valencia (CSIC), Spain

***Correspondence:**
Mara Giordano
mara.giordano@med.uniupo.it

Specialty section:
This article was submitted to Genetics of Common and Rare Diseases, a section of the journal Frontiers in Genetics

Received: *14 April 2022*
Accepted: *27 April 2022*
Published: *08 June 2022*

Citation:
Giordano M and Stuppia L (2022) Editorial: Novel Insights Into the Genetics of Growth Disorders. Front. Genet. 13:920469. doi: 10.3389/fgene.2022.920469

At present, a clear example of the strong interest devoted to short stature and in general to growth disorders by the international scientific community is provided by this Research Topic on *Novel Insights into the Genetics of Growth Disorders*, reporting a series of very interesting papers exploring the most relevant topics in this field.

SHOX and SHOX-regulated genes still represents a very promising field of study, as reported in the paper by Hoffmann et al., who analysed differentially expressed genes in SHOX-overexpressing human fibroblasts, confirming *NPPB* and *FGFR* among the most strongly regulated genes, together with 143 novel candidates. Among these, multiple Sox family members were significantly dysregulated in Shox-deficient pectoral fins highlighting an important role for these genes in Shox-related growth disorders.

Another very promising field of studies is represented by the application of the novel technologies, mainly the Next Generation Sequencing (NGS) in the identification of gene variants involved in the short stature. In this view, several papers in this Research Topic report very interesting data about the usefulness of this approach. Tang et al. investigated the genetics of 16 Chinese foetuses with skeletal dysplasia by whole exome sequencing (WES) and identified 12 cases carrying clinically relevant variants, including one deletion in *DMD* and 14 variants in other six genes. Furthermore WES allowed to detect two cases of somatic mosaicism for two distinct variants in COL1A1, one in a foetus and the other in the healthy mother of an affected carrier foetus, thus elucidating the usefulness of NGS in improving the diagnosis yield of skeletal dysplasia.

The NGS approach revealed that mutations in the aggrecan encoding gene, *ACAN*, represent one of the main causes of idiopathic and syndromic forms of short stature. Several studies retrospectively analyzed cohorts of patients that tested negative for *SHOX* alteration as the paper of Mancioppi et al., where NGS targeted analysis detected a novel *ACAN* heterozygous pathogenic variant in a family with idiopathic short stature, early-onset osteoarthritis and osteoarthritis dissecans.

The identification of novel gene variants associated with different form of growth disorders is also the topic of the two manuscripts by Li et al., Li et al. as well as of the submissions of. In the first study Li et al., authors collected clinical data and biological samples from a 12-year-old boy with Cornelia de Lange syndrome (CdLS) referred for short stature. A *de novo* pathogenic variant in *SMC3* in the proband, c.1942A>G, was evidenced by whole-exome sequencing. A review of the literature carried out by authors reported other 27 CdLS cases with variants in *SMC3*, all showing symptoms of verbal development delay and intellectual disability to different degrees. In the second paper of Li et al., the *GHR* gene was analysed in four patients with Laron Syndrome (LS). Four *GHR* variants were identified, two of which were novel mutations. Wild type and mutant GHR expression plasmids were constructed, and transiently transfected into HepG2 cells and HEK293T cells to observe the subcellular distribution of the GHR protein by immunofluorescence. It is worth underlying that as well as for other genes for which biallelic mutations cause severe syndromic forms, *GHR* is also involved in milder phenotypes such as idiopathic short stature in patients carrying monoallelic variants (Dias et al., 2017; Andrews et al., 2021).

Finally, the paper of Quian et al. investigated Occipital cortical malformation (OCCM), a disease caused by malformations of cortical development characterized by polymicrogyria and pachygyria of the occipital lobes and childhood-onset seizures, and identified novel complex heterozygous variants of *LAMC3* in a Chinese female with childhood-onset seizures. This issue also includes a study on Congenital hypertiroidism (CH), one of the most frequent endocrine disease in childhood which causes intellectual disability and short stature if untreated. Whereas most previous studies conducted on the genetic causes of CH focused on single genes, the research of Huang et al. utilized NGS to analyse a panel of 28 candidate genes related to CH. Clinically relevant variants were identified in eight genes in 14 of the 15 investigated patients (93.33%), underlying the efficiency of this approach with an important implications in clinical diagnosis and therapeutic choices.

The therapeutic perspectives in the field of short stature have also been considered in this Research Topic. The paper of Wu et al. takes into account a case of Myhre syndrome, a rare disorder caused by heterozygous mutations in *SMAD4* and characterized by dysmorphic facial features, intrauterine growth retardation, short stature, obesity, muscle hypertrophy and varying degrees of psychomotor developmental disorder. The patient, who also showed the novel symptom of giant testicles, was treated with growth hormone combined with letrozole, that successfully improved his short stature.

In conclusion, the present Research Topic provides novel information about the genetics of growth disorders, and demonstrates the usefulness of the modern technologies in disclosing novel gene variants associated to this condition.

The identification of novel genetic variants associated to growth disorders, as well as the identification of the pathogenic mechanism leading to the clinical phenotype, will improve both the diagnosis and the treatment of these disorders, leading to a "precision medicine "strategy able to identify specific solutions based on the genetic defect and avoiding a "one size fits all" approach, which can be useless, when not dangerous, for patients.

AUTHOR CONTRIBUTIONS

MG and LS contributed to the writing of the editorial with direct and intellectual contribution.

REFERENCES

Andrews, A., Maharaj, A., Cottrell, E., Chatterjee, S., Shah, P., Denvir, L., et al. (2021). Genetic Characterization of Short Stature Patients with Overlapping Features of Growth Hormone Insensitivity Syndromes. *J. Clin. Endocrinol. Metab.* 106, e4716–e4733. doi:10.1210/clinem/dgab437

Babu, D., Vannelli, S., Fanelli, A., Mellone, S., Baffico, A. M., Corrado, L., et al. (2021). Variants in the 5′UTR Reduce SHOX Expression and Contribute to SHOX Haploinsufficiency. *Eur. J. Hum. Genet.* 29, 110–121. doi:10.1038/s41431-020-0676-y

Benabbad, I., Rosilio, M., Child, C. J., Carel, J.-C., Ross, J. L., Deal, C. L., et al. (2017). Safety Outcomes and Near-Adult Height Gain of Growth Hormone-Treated Children with SHOX Deficiency: Data from an Observational Study and a Clinical Trial. *Horm. Res. Paediatr.* 87, 42–50. doi:10.1159/000452973

Benito-Sanz, S., Thomas, N. S., Huber, C., del Blanco, D. G., Aza-Carmona, M., Crolla, J. A., et al. (2005). A Novel Class of Pseudoautosomal Region 1 Deletions Downstream of SHOX Is Associated with Léri-Weill Dyschondrosteosis. *Am. J. Hum. Genet.* 77, 533–544. doi:10.1086/449313

Dias, C., Giordano, M., Frechette, R., Bellone, S., Polychronakos, C., Legault, L., et al. (2017). Genetic Variations at the Humangrowth Hormone Receptor (GHR)gene Locus Are Associated with Idiopathic Short Stature. *J. Cell. Mol. Med.* 21, 2985–2999. doi:10.1111/jcmm.13210

Fanelli, A., Vannelli, S., Babu, D., Mellone, S., Cucci, A., Monzani, A., et al. (2022). Copy Number Variations Residing outside the SHOX Enhancer Region Are Involved in Short Stature and Léri-Weill Dyschondrosteosis. *Molec Gen Gen Med* 10, e1793. doi:10.1002/mgg3.1793

Genoni, G., Monzani, A., Castagno, M., Ricotti, R., Rapa, A., Petri, A., et al. (2018). Improving Clinical Diagnosis in SHOX Deficiency: the Importance of Growth Velocity. *Pediatr. Res.* 83, 438–444. doi:10.1038/pr.2017.247

Hisado-Oliva, A., Ruzafa-Martin, A., Sentchordi, L., Funari, M. F. A., Bezanilla-López, C., Alonso-Bernáldez, M., et al. (2018). Mutations in C-Natriuretic Peptide (NPPC): a Novel Cause of Autosomal Dominant Short Stature. *Genet. Med.* 20, 91–97. doi:10.1038/gim.2017.66

Kant, S. G., Cervenkova, I., Balek, L., Trantirek, L., Santen, G. W. E., de Vries, M. C., et al. (2015). A Novel Variant of FGFR3 Causes Proportionate Short Stature. *Eur. J. Endocrinol.* 172, 763–770. doi:10.1530/EJE-14-0945

Rao, E., Weiss, B., Fukami, M., Rump, A., Niesler, B., Mertz, A., et al. (1997). Pseudoautosomal Deletions Encompassing a Novel Homeobox Gene Cause Growth Failure in Idiopathic Short Stature and Turner Syndrome. *Nat. Genet.* 16, 54–63. doi:10.1038/ng0597-54

Stuppia, L., Gatta, V., Antonucci, I., Giuliani, R., and Palka, G. (2010). Different Approaches in the Molecular Analysis of the SHOX Gene Dysfunctions. *J. Endocrinol. Invest.* 33 (6 Suppl. l), 30–33. doi:10.1002/ajmg.a.20198

Stuppia, L., Calabrese, G., Gatta, V., Pintor, S., Morizio, E., Fantasia, D., et al. (2003). SHOX Mutations Detected by FISH and Direct Sequencing in Patients with Short Stature. *J. Med. Genet.* 40, 11e–11. doi:10.1136/jmg.40.2.e11

Wu, J., Wang, M., Jiao, Z., Dou, B., Li, B., Zhang, J., et al. (2022). Novel Loss-Of-Function Mutations in NPR2 Cause Acromesomelic Dysplasia, Maroteaux Type. *Front. Genet.* 13, 823861. doi:10.3389/fgene.2022.823861

Zinn, A. R., Page, D. C., and Fisher, E. M. C. (1993). Turner Syndrome: The Case of the Missing Sex Chromosome. *Trends Genet.* 9, 90–93. doi:10.1016/0168-9525(93)90230-f

Conflict of Interest: The authors declare that the research was conducted in the absence of any commercial or financial relationships that could be construed as a potential conflict of interest.

Publisher's Note: All claims expressed in this article are solely those of the authors and do not necessarily represent those of their affiliated organizations, or those of the publisher, the editors and the reviewers. Any product that may be evaluated in this article, or claim that may be made by its manufacturer, is not guaranteed or endorsed by the publisher.

frontiers in Genetics

ORIGINAL RESEARCH
published: 10 March 2021
doi: 10.3389/fgene.2021.599863

Whole Exome Sequencing Aids the Diagnosis of Fetal Skeletal Dysplasia

Hui Tang[1,2†], *Qin Zhang*[1,2†], *Jingjing Xiang*[1,2†], *Linliang Yin*[1,2], *Jing Wang*[3*] and *Ting Wang*[1,2*]

[1] Center for Reproduction and Genetics, The Affiliated Suzhou Hospital of Nanjing Medical University, Suzhou, China, [2] Center for Reproduction and Genetics, Suzhou Municipal Hospital, Suzhou, China, [3] Suzhou Guangji Hospital, Suzhou, China

Skeletal dysplasia is a complex group of bone and cartilage disorders with strong clinical and genetic heterogeneity. Several types have prenatal phenotypes, and it is difficult to make a molecular diagnosis rapidly. In this study, the genetic cause of 16 Chinese fetuses with skeletal dysplasia were analyzed, and 12 cases yielded positive results including one deletion in *DMD* gene detected by SNP-array and 14 variants in other 6 genes detected by whole exome sequencing (WES). In addition, somatic mosaicism was observed. Our study expanded the pathogenic variant spectrum and elucidated the utilization of WES in improving the diagnosis yield of skeletal dysplasia.

Keywords: skeletal dysplasia, prenatal diagnosis, whole-exome sequencing, SNP-array, novel variants

OPEN ACCESS

Edited by:
Liborio Stuppia,
University of Studies G. d'Annunzio Chieti and Pescara, Italy

Reviewed by:
Marco Savarese,
University of Helsinki, Finland
Damian Smedley,
The Wellcome Sanger Institute, United Kingdom

***Correspondence:**
Ting Wang
biowt@njmu.edu.cn
Jing Wang
804745036@qq.com

†These authors have contributed equally to this work

Specialty section:
This article was submitted to Genetics of Common and Rare Diseases, a section of the journal Frontiers in Genetics

Received: *28 August 2020*
Accepted: *27 January 2021*
Published: *10 March 2021*

Citation:
Tang H, Zhang Q, Xiang J, Yin L, Wang J and Wang T (2021) Whole Exome Sequencing Aids the Diagnosis of Fetal Skeletal Dysplasia. Front. Genet. 12:599863. doi: 10.3389/fgene.2021.599863

INTRODUCTION

Unexpected skeletal dysplasia affects approximately 1 per 5,000 and is a complex group of bone and cartilage disorders with strong clinical and genetic heterogeneity (Geister and Camper, 2015). In the 2015 revision of the Nosology and Classification of Genetic Skeletal Disorders, 436 disorders are classified into 42 groups according to syndromes, publication, genetic information, and nosologic autonomy, and 364 different genes are associated with genetic skeletal disorders (Bonafe et al., 2015). Many of these disorders can give rise to prenatal phenotypes. In the past, ultrasound evaluation was a widely used method for detection of congenital anomalies (Krakow et al., 2009). However, the lack of family history and non-specific and limited clinical symptoms *in utero* may introduce difficulties in prenatal diagnosis. Recently, with the advances in molecular technology, especially next-generation sequencing, high-throughput sequencing has been considered as an effective method for different genetic diagnosis (Retterer et al., 2016; LaDuca et al., 2017). Based on the statements released by the International Society for Prenatal Diagnosis (ISPD), the Society for Maternal Fetal Medicine (SMFM), and the Perinatal Quality Foundation (PQF), and the American College of Medical Genetics and Genomics (ACMG), next-generation sequencing can be used with ultrasound anomalies when standard diagnostic genetic testing, such as chromosomal microarray analysis, failed to yield a definitive diagnosis. Especially, if a specific diagnosis is suspected, molecular testing for the suggested disorder should be the initial test. Thus, many studies have adopted this for prenatal evaluation (International Society for Prenatal et al., 2018; Monaghan et al., 2020). Thirty-one studies conducted prenatal analysis by whole exome sequencing (WES) with the diagnostic rates between 6.2 and 80% (Best et al., 2018). Notably, the application of targeted exome sequencing in prenatal diagnosis of skeletal dysplasia is outstanding as several researches have reported high detection rates from 75 to 83.3% (Chandler et al., 2018; Zhou et al., 2018; Liu et al., 2019; Han et al., 2020). Definitive molecular diagnosis can provide accurate results instead of a suspected clinical impression and information about subsequent development of the disease and treatment regimens; thus, parents could get genetic counseling, and birth-defect intervention could be implemented for future pregnancies.

In this study, we analyzed 16 cases of fetuses with suspected skeletal dysplasia by WES and aimed to elucidate WES as a useful and efficient aid to precise diagnosis.

MATERIALS AND METHODS

Patients

This study was approved by the institutional ethics committee of the Affiliated Suzhou Hospital of Nanjing Medical University. Sixteen affected patients and available family members were recruited with informed consent. All fetuses were diagnosed with suspected skeletal abnormalities by prenatal ultrasound and some ultrasound pictures were listed in **Figure 2**. Their clinical symptoms are summarized in **Table 1**. We obtained fetal muscle tissue or cord blood and parents' peripheral blood with the exception of cases 9 and 10 that we only got the samples from the patients. Genomic DNA was extracted using the QIAamp DNA Blood Mini Kit (Qiagen, Hilden, Germany) according to standard extraction methods.

SNP-array

Single nucleotide polymorphism array analysis was performed on the Affymetrix CytoScan platform (Affymetrix, Santa Clara, CA, USA) following the protocol. After amplified, DNA was hybridized to the Affymetrix 750K array containing 550,000 copy number variation (CNV) markers and 200,000 SNP markers. Data were analyzed by Chromosome Analysis Suite 3.2 (Affymetrix, Santa Clara, CA, USA). CNVs were analyzed and classified according to the guidelines released by American College of Medical Genetics and Genomics (Kearney et al., 2011).

Whole-Exome Sequencing and Mutation Analysis

WES was performed by the Fulgent Genetics Company (Fuzhou, China). DNA of the fetus and their parents were used to create the DNA libraries, enriched by IDT xGen Exome V2 reagent (Integrated DNA Technologies, Inc., Iowa, United States), sequenced on the Illumina Nova6000 (Illumina, San Diego, CA, United States), and mapped to the human genome (NCBI37/hg19) by the Sentieon software package. Over 99% coverage of targeted bases was achieved, with an average sequencing depth of over 100. Then Picard was used to compare the results to remove redundancy, and the variants were detected by vVarscan. An in-house algorithm CNVexon developed by Fulgent Genetics was used for exon-based CNV detection based on reads counts, and a misalignment detection algorithm was used for pseudogenes' optimization. All variants were searched in multiple databases including gnomAD, Exome Aggregation Consortium (ExAC), dbSNP, 1000 Genome Project, Human Gene Mutation Database (HGMD), ClinVar and Leiden Open Variation Database (LOVD). Four prediction tools were used for variant interpretation: DANN, MutationTaster, REVEL, and SIFT. For splicing variants, Human Splicing Finder was used. Variants were classified according to the recommended guidelines released by the American College of Medical Genetics and Genomics and the Association for Molecular Pathology (Richards et al., 2015).

Verification of Gene Mutations

If microdeletions or microduplications were detected, these would be verified by multiplex ligation-dependent probe amplification (MLPA) in patients and parents. And if mutations were detected for a single gene, Sanger sequencing would be conducted to validate the mutations.

RESULTS

A total of 16 cases with suspected skeletal dysplasia were investigated, and all of them underwent detailed ultrasound examination during pregnancy. Several parameters were examined by ultrasound: biparietal diameter, head circumference, abdominal circumference, chest circumference, length of the long bones, shape of long bones, mandibular size and shape, abnormal posturing of the extremities, and other congenital anomalies. In 16 cases, we detected one deletion in *DMD* and causative variants in six genes, including *FGFR3*, *COL1A1*, *COL1A2*, *ALPL*, *HSPG2,* and *DYNC2H1* with a detection rate of 75% (**Table 1**).

Abnormalities Detected by SNP-array

Twelve cases were tested for CNVs first by SNP-array. We found a 184 kb deletion in chromosome Xp21.1, which spanned from exon 49 to exon 53 of the *DMD* gene in case 1. At 24 weeks of gestation, the ultrasound scan showed that the fetal feet were ballet-shaped, and the angle of tibiofibula and dorsum of foot was near 180°. However, the fetus didn't receive a prenatal genetic test. When he was born, an SNP-array was conducted using his cord blood. Further analysis by MLPA verified the deletion in the patient, and his mother was heterozygous for this deletion (**Figure 1A**).

Abnormalities Detected by WES

WES was performed for 11 cases with negative results of SNP-array analysis and other four new cases. A total of 14 variants in 6 genes associated with skeletal dysplasia were detected in 11 cases (**Table 1**) and confirmed by Sanger sequencing (**Figure 1B**).

In case 2, two compound heterozygous causative mutations c.5984C>T (p.A1995V) and c.10606C>T (p.R3536X) (Qiao et al., 2018) in *DYNC2H1* gene were detected. Mutations in *DYNC2H1* were associated with short-rib thoracic dysplasia 3 (Merrill et al., 2009). Short rib-polydactyly syndrome 3 (SRPS 3) was an autosomal recessive disease overlapping with Jeune asphyxiating thoracic dystrophy belonging to the ciliopathy, but it was more severe and characterized by early prenatal expression, lethality and variable malformations (Dagoneau et al., 2009), which was correlated with patient 2′s presentations.

Hypophosphatasia resulting from mutations in *ALPL* gene was found in case 3 (c.984_986del, c.1463C>G) and case 4 (c.2T>C, c.984_986del), respectively. Both of the mutations in these two cases presented compound heterozygous condition. c.984_986del leaded to the deletion of phenylalanine at position 328 at the β-sheet. c.2T>C caused the loss of the start codon, and the alanine residue at position 488 (c.1463C>G, p.A488G) was conserved in several species.

TABLE 1 | Summary of clinical findings and molecular diagnoses.

Case	Family history	Gestation (w)	Ultrasound findings		Molecular result		Variant Type (ACMG)	MAF (gnomAD)	References or *in silico* prediction
			Skeletal anomalies	Other anomalies	Variant	Inheritance			
1	One previous pregnancies with the same anomalies	24	Feet were ballet-shaped, and the angle of tibiofibula and dorsum of foot was near 180°	Polyhydramnios	arr[hg19] Xp21.1(31,690,978-31,875,673)x0	Maternal	Pathogenic (PVS1, PS4, PM2)	-	Murugan et al., 2010
2	Previous pregnancy with short long bones and narrow thorax	25	Narrow thorax TH = 118 mm, short long bones FL = 23 mm HL = 19 mm, polydactylia	Renalsinusseparation	*DYNC2H1* NM_001080463 c.5984C>T and c.10606C>T	AR; Biparental inheritance	Pathogenic (PS4, PM2, PM3, PP4)and Pathogenic (PS4, PM2, PM3, PP4)	0.000004030 (1/248124); 0.00003 (1/31386)	(c.5984C>T and c.10606C>T: Qiao et al., 2018)
3		26	Short and curved long bones, FL = 34 mm HL = 36 mm, curved cubitus		*ALPL* NM_000478.5 c.984_986del and c.1463C>G	AR; Biparental inheritance	Pathogenic (PS4, PS3, PM4) and Likely Pathogenic (PM1, PM2, PM3)	0.00001062 (3/282562); -	(c.984_986del : Chang et al., 2012; Taillandier et al., 2015; c.1463C>G: 0.9885, P, B, B)
4		22	Short and curved long bones	Cloverleaf skull, enteric canal echo enhancement	*ALPL* NM_000478.5 c.984_986del and c.2T>C	AR; Biparental inheritance	Pathogenic (PS4, PS3, PM4) and Pathogenic (PVS1, PM2, PM3)	0.000008 (2/251166); 0.000004 (1/251344)	(c.984_986del : Chang et al., 2012; Taillandier et al., 2015; c.2T>C: 0.9808, P, P, P)
5		25	Narrow thorax, short long bones, FL = 24 mm HL = 17.6 mm, short rib		*FGFR3* NM_000142.4 c.742C>T	*De novo*	Pathogenic (PS2, PS4)	-	Pokharel et al., 1996; Sawai et al., 1999; Chen et al., 2001; Tonni et al., 2010
6		24^{+6}	Short long bones, FL = 29.4 mm HL = 17 mm		*COL1A2* NM_000089 c.2189G>T	*De novo*	Pathogenic (PS2, PS1, PM1, PM2)	-	0.9871, P, P, P
7		14^{+3}	X-type lower limbs, upper limbs adductus,nasalbonelength 2.2 mm	NT = 4 mm anasarca					
8	Two previous pregnancies with the same anomalies	19	Short long bones with fracture, short rib, wide orbilal septum		*COL1A2* NM_000089 c.1764+3_1764+6del	Maternal	VOUS (PM2, PP1, PP3)	-	-, P, -, -
9		25	Short long bones, lumbosacral portion bent						
10		24	Short limbs, micrognathia, spine misaligned		*HSPG2* NM_005529.6 c.8553del and c.12532+1G>T	U	Likely Pathogenic (PVS1, PM2) and Pathogenic (PVS1, PM2, PM3)	-; 0.00000401 (2/249388)	c.8553del: -, P, -, -; c.12532+1G>T: 0.9958, P, -, -
11		31	Abnormal morphology of ulna						
12	Two previous pregnancies with the same anomalies	23	Short limbs, narrow thorax, bell-shaped chest	Anasarca CTR>0.5 pleural effusion	*COL1A1* NM_000088.3 c.3389G>A	Maternal	Likely Pathogenic (PM1, PM2, PP3, PP5)	-	ClinVar
13		20	Short long bones with abnormal thorax	NT = 4.4 mm	*COL1A1* NM_000088.3 c.1921G>A	*De novo*	Pathogenic (PS2, PM1, PM2, PM5)	-	0.9981, P, P, P
14		25	Short and curved long bones		*COL1A2* NM_000089 c.1010G>A	*De novo*	Pathogenic (PS2, PM1, PM2, PM5)	-	0.9974, P, P, P
15		22	Short left humerus and curved ulnaandradius						
16		U	Short long bones		*FGFR3* NM_000142.4c.1138G>A	*De novo*	Pathogenic (PS2, PS4)	-	Xue et al., 2014

TH, Thoracic Circumference; FL, Femur length; HL, humerus length; NT, nuchal translucency; CTR,cardiothoracic ration; AD, autosomal dominant; AR, autosomal recessive; U, unknown; Four prediction tools: DANN, MutationTaster, REVEL and SIFT:-, unpredictable; P, Pathogenic; B, Benign. The value range of DANN is 0 to 1, with 1 given to the variants predicted to be the most damaging.

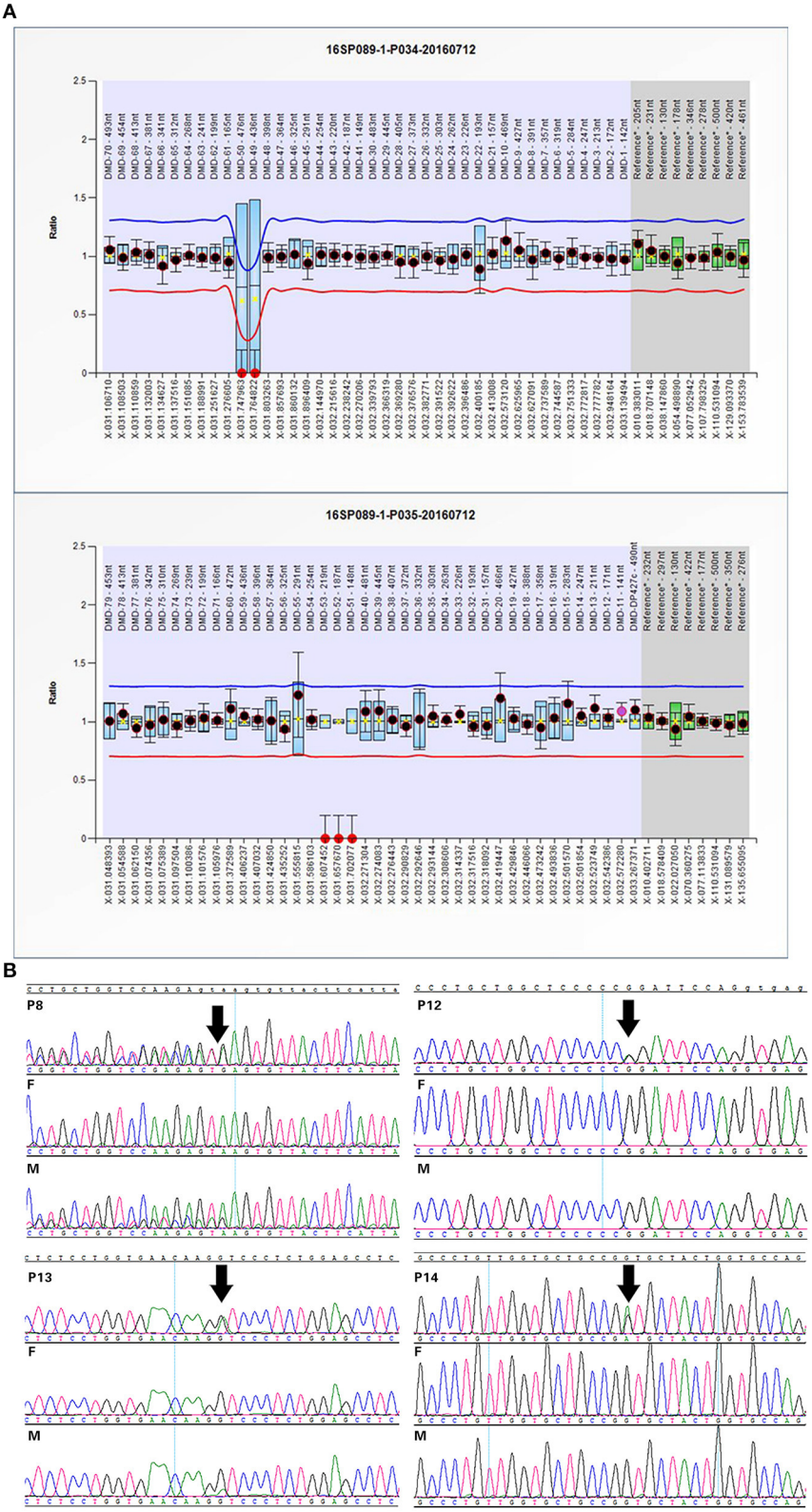

FIGURE 1 | Confirmation of SNP-array or WES results: **(A)** The MLPA results of case 1 indicated the deletion spanning from exon 49 to exon 53 in *DMD* gene. **(B)** Sanger sequencing confirmed mutations in some cases with OI. Variants are indicated by black arrows.

Mutations c.742C>T was detected in case 5, and c.1138G>A was detected in case 16, which were mutation hotspots of *FGFR3* gene. Mutations in collagen genes were identified in five cases, of which c.2189G>T (p.G730V) in *COL1A2* of case 6, c.1921G>A (p.G641R) in *COL1A1* of case 13, and c.1010G>A (p.G337D) in *COL1A2* of case 14 were *de novo*, while c.1764+3_1764+6delAAGT in *COL1A2* of case 8 and c.3389G>A in *COL1A1* of case 12 were maternally inherited. Four missense mutations resulted in glycine substitutions in Gly-X-Y, which could create severe damage to collagen. The splicing mutation c.1764+3_1764+6delAAGT was predicted to disrupt normal splicing by Human Splicing Finder.

In case 10, clinically significant mutations in *HSPG2* were found (c.8553del and c.12532+1G>T). c.8553del produced a truncated protein that terminated at 2878 amino acid residues lacking part of domain IV and the whole domainV, and c.12532+1G>T at the C-terminal region may lead to abnormal splicing as predicted by Human Splicing Finder. However, no pathogenic variants were identified in cases 7, 9, 11, and 15.

DISCUSSION

Many aspects could affect the detection rate of WES, such as the number of cases, selected criteria of study, proband-only WES, or trio WES, and so on (Best et al., 2018). It was reported that trio WES had a higher diagnostic rate; fetuses with multiple anomalies also had a higher diagnostic rate and when testing single structural anomalies, a particular organ system may have a higher diagnostic yield (Best et al., 2018; International Society for Prenatal et al., 2018). Among the 16 cases in the present study, 12 cases received a definitive molecular diagnosis, including a microdeletion and 8 novel variants, and the detection rate is 75%, which is consistent with the high detection rates of skeletal dysplasia from 75 to 83.3% revealed by previous studies (Chandler et al., 2018; Zhou et al., 2018; Liu et al., 2019; Han et al., 2020).

In case 1, a deletion spanning from exon 49 to exon 53 of the *DMD* gene was detected in a male patient and inherited from his mother. He exhibited abnormal posturing of the lower extremities, which were not reported previously during the intrauterine period in patients with DMD/BMD. And the family has experienced one pregnancy with the same anomalies before without other information and further genetic analysis. To our knowledge, only one fetus with a deletion of exons 17–29 of the *DMD* gene was reported to present prenatal phenotypes including fetal growth restriction and oligohydramnios (Lin et al., 2017). And the deletion of exons 49–53 of the *DMD* gene were detected in three patients with DMD/BMD as reported previously (Covone et al., 1991; Murugan et al., 2010; Yang et al., 2019). However, our patient was dead, and we could not get more information. Therefore, it is difficult to define these new symptoms in intrauterine period as phenotype expansion of DMD/BMD or genotype-phenotype discordance.

Moreover, we found mutations in *ALPL* in cases 3 and 4. Pathogenic variants in *ALPL* cause hypophosphatasia characterized by defective mineralization of bone and/or teeth in the presence of low activity of serum and bone alkaline phosphatase (ALP) (Millan and Whyte, 2016). c.984_986del in cases 3 and 4 was reported previously (Chang et al., 2012; Taillandier et al., 2015), which result in the deletion of phenylalanine at the β-sheet and decreased activity of its coding protein the tissue-nonspecific isoenzymes of alkaline phosphatase (TNSALP) (Michigami et al., 2005). Thus, c.984_986del may reduce the enzymatic activity too. c.1460C>T (p.A487V) and c.1466G>C (p.C489S) were reported early, of which the latter one exhibited a diminished ALP activity, less located on the cell surface and failed to become the mature form (Satou et al., 2012; Porntaveetus et al., 2017). This suggested that p.487-489 of ALPL protein may play an important role in enzymatic activity. c.2T>C caused the loss of the start codon and generated a transcript starting at Met56 as c.3G>A did, which did not exhibit enzymatic activity, had no significant effect on the wild type ALPL protein, and could not be attached to the cell membrane (Mentrup et al., 2011).

Patient 5 harbored c.742C>T in *FGFR3* gene, which has been detected in different populations (Pokharel et al., 1996; Sawai et al., 1999; Chen et al., 2001; Tonni et al., 2010). And patient 16 had a hotspot mutation c.1138G>A in *FGFR3* (Xue et al., 2014). These fetuses' ultrasound scans all revealed a narrow chest with shortening of the long bones. Besides, c.8553del and c.12532+1G>T in *HSPG2* were identified in case 10. *HSPG2* is an essential gene, and its mutations could lead to Schwartz-Jampel syndrome, type 1(SJS) and severe neonatal lethal Dyssegmental dysplasia, Silverman-Handmaker type (DDSH) (Arikawa-Hirasawa et al., 2002; Martinez et al., 2018). However, the compound heterozygous condition couldn't be confirmed because the parents' samples were not available. Trio sequencing of patient 7 and the parents detected a heterozygous missense variation c.4813C>T in *FLNB*, which was inherited from the normal father with 62 of 120 (51.7%) reads. Though several cases with family history presenting an autosomal dominant trait has been reported (Doren et al., 1998; Xu et al., 2018), the father in case 7 didn't have malformations associated with FLNB-related disorders such as short stature, club feet, and facial dysmorphisms (Bicknell et al., 2007).

Furthermore, variants of type I collagen genes related to osteogenesis imperfect (OI) were identified in five cases. Type I collagen is a heterotrimer containing two α1(I) and one α2(I) chains assembled by procollagen chains with N-terminal and C-terminal globular propeptides flanking the helical domain (Forlino and Marini, 2016). The helical domains contain Gly-X-Y triplets where glycine substitutions are the most frequent cause of OI (Marini et al., 2007). In our study, we detected four missense mutations and one splicing variant: c.1921G>A and c.3389G>A in *COL1A1* and c.1010G>A, c.2189G>T, and c.1764+3_1764+6del in *COL1A2*, respectively (**Figure 2B**). Four missense mutations were glycine substitutions in Gly-X-Y, which would delay helical folding and prolong access time for modifying enzymes. Previous researches have described two infants with c.2188G>T (p.G730C) and c.2188G>C (p.G730R) in *COL1A2* changing the same amino acid residue as c.2189G>T (p.G730V) and exhibited the same phenotypes such as blue sclera, wormian bones, and shortening and bowing of the

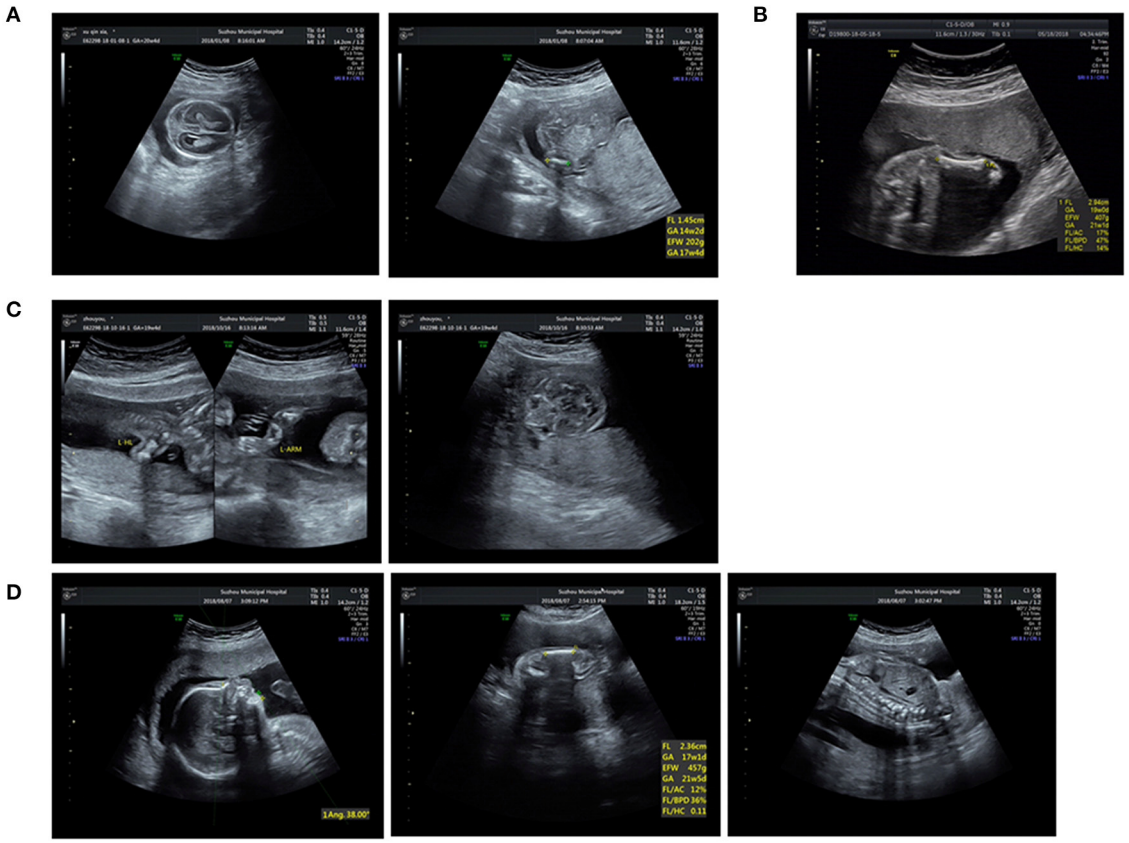

FIGURE 2 | Ultrasound pictures of cases 4, 6, 8, and 10: **(A)** Short femur and cloverleaf skull of P4. **(B)** Short femur of P6. **(C)** Short long bones and wide orbital septum of P8. **(D)** Short limbs, micrognathia, and spine misaligned of P10.

upper and lower limbs (Gomez-Lira et al., 1994; Hachiya et al., 2012). The similar situation was observed in c.1010G>A and c.1921G>A. And c.3389G>A in *COL1A1* has been classified as likely pathogenic in ClinVar (https://www.ncbi.nlm.nih.gov/clinvar/). The splicing mutation c.1764+3_1764+6del in *COL1A2* in case 8 may yield abnormal splicing transcript as predicted by Human Splicing Finder. Notably, the variants in cases 8 and 12 were maternally inherited. Both of the mothers experienced induced abortion twice in the second trimester due to the same skeletal dysplasia malformation, suggesting the somatic mosaicism. The mutated allele c.3389G>A was present in 17 of 66 (25.8%) reads in WES, and the peak of mutated allele was lower than that of the wild-type allele in sanger sequencing, suggesting that it is a mosaic mutation in the mother of case 12. After that, we tried to recall the asymptomatic mother; however, she didn't receive radiographical examination, and we only knew that her sclera and height were normal and didn't suffer bone fracture before. Similarly, the mutated allele c.1764+3_1764+6del was present in 22 of 68 (32.3%) reads in the mother of case 8 who presented extremely mild symptoms such as short stature compared with the fetus. Nevertheless, the ratio of the fetus was 37.8% (17/45) similar to the mother. We supposed that other factors such as underlying genetic modifiers may affect the phenotypes.

Four cases did not have a definitive molecular diagnosis, and the negative WES results could be attributed to limited phenotypes or the limitations of WES. For fetuses, several aspects could affect the detection rate, especially incomplete prenatal phenotypes (Aarabi et al., 2018). Meanwhile, many challenges should be considered, such as ethical concerns, analysis of variants of unknown significance, and secondary findings (Best et al., 2018; Monaghan et al., 2020). In the future, with the development of fetal specific phenotype genotype database, the uncertainty in cases will become less frequent (Aarabi et al., 2018). Furthermore, the causative variants of these four cases may reside in the noncoding-regulatory or deep-intronic regions could not be detected by WES, which could be analyzed by whole genome sequencing in the future.

CONCLUSION

In summary, one CNV and 14 single nucleotide variants of 6 genes were identified in 16 families with suspected skeletal abnormalities by prenatal ultrasound scan. The results of this study elucidated that the utilization of WES improved the diagnosis yield of skeletal dysplasia and provided useful genetic counseling guidance for parents. In addition, two cases with

type I collagen variants from asymptomatic parent were also found, indicating the advantage of next generation sequencing in the detection of somatic mosaicism. Further studies will be needed to evaluate the application of prenatal WES for skeletal dysplasia.

DATA AVAILABILITY STATEMENT

The datasets for this article are not publicly available due to concerns regarding participant/patient anonymity. Requests to access the datasets should be directed to the corresponding author.

ETHICS STATEMENT

The studies involving human participants were reviewed and approved by The Affiliated Suzhou Hospital of Nanjing Medical University. Written informed consent to participate in this study was provided by the participants' legal guardian/next of kin. Written informed consent was obtained from the minor(s)' legal guardian/next of kin for the publication of any potentially identifiable images or data included in this article.

AUTHOR CONTRIBUTIONS

TW and JW were responsible for testing strategy design. HT and JX analyzed the data and drafted the manuscript. QZ and LY provided clinical information. HT and JX carried out the molecular analyses. All authors read and approved the final manuscript.

FUNDING

This study was supported by Suzhou Science and Technology Support Program (SS2019066) Research on population and family planning development in Jiangsu Province, Jiangsu Provincial Medical Innovation Team (CXTDB2017013), Suzhou Clinical Medical Expert Team (SZYJTD201708), and Jiangsu Maternal and Children health care key discipline (FXK201748).

ACKNOWLEDGMENTS

The manuscript was submitted as a preprint at Research Square (Tang et al., 2020). We thank all the healthy individuals and the family members for their participation and support in this study.

REFERENCES

Aarabi, M., Sniezek, O., Jiang, H., Saller, D. N., Bellissimo, D., Yatsenko, S. A., et al. (2018). Importance of complete phenotyping in prenatal whole exome sequencing. *Hum. Genet.* 137, 175–181. doi: 10.1007/s00439-017-1860-1

Arikawa-Hirasawa, E., Le, A. H., Nishino, I., Nonaka, I., Ho, N. C., Francomano, C. A., et al. (2002). Structural and functional mutations of the perlecan gene cause Schwartz-Jampel syndrome, with myotonic myopathy and chondrodysplasia. *Am. J. Hum. Genet.* 70, 1368–1375. doi: 10.1086/340390

Best, S., Wou, K., Vora, N., Van der Veyver, I. B., Wapner, R., and Chitty, L. S. (2018). Promises, pitfalls and practicalities of prenatal whole exome sequencing. *Prenat. Diagn.* 38, 10–19. doi: 10.1002/pd.5102

Bicknell, L. S., Farrington-Rock, C., Shafeghati, Y., Rump, P., Alanay, Y., Alembik, Y., et al. (2007). A molecular and clinical study of Larsen syndrome caused by mutations in FLNB. *J. Med. Genet.* 44, 89–98. doi: 10.1136/jmg.2006.043687

Bonafe, L., Cormier-Daire, V., Hall, C., Lachman, R., Mortier, G., Mundlos, S., et al. (2015). Nosology and classification of genetic skeletal disorders: 2015 revision. *Am. J. Med. Genet. Part A* 167, 2869–2892. doi: 10.1002/ajmg.a.37365

Chandler, N., Best, S., Hayward, J., Faravelli, F., Mansour, S., Kivuva, E., et al. (2018). Rapid prenatal diagnosis using targeted exome sequencing: a cohort study to assess feasibility and potential impact on prenatal counseling and pregnancy management. *Genet. Med.* 20, 1430–1437. doi: 10.1038/gim.2018.30

Chang, K. C., Lin, P. H., Su, Y. N., Peng, S. S., Lee, N. C., Chou, H. C., et al. (2012). Novel heterozygous tissue-nonspecific alkaline phosphatase (TNAP) gene mutations causing lethal perinatal hypophosphatasia. *J. Bone Miner. Metab.* 30, 109–113. doi: 10.1007/s00774-011-0282-8

Chen, C. P., Chern, S. R., Wang, W., and Wang, T. Y. (2001). Second-trimester molecular diagnosis of a heterozygous 742 –> T (R248C) mutation in the FGFR3 gene in a thanatophoric dysplasia variant following suspicious ultrasound findings. *Ultrasound Obstet. Gynecol.* 17, 272–273. doi: 10.1046/j.1469-0705.2001.00377.x

Covone, A. E., Lerone, M., and Romeo, G. (1991). Genotype-phenotype correlation and germline mosaicism in DMD/BMD patients with deletions of the dystrophin gene. *Hum. Genet.* 87, 353–360. doi: 10.1007/BF00200919

Dagoneau, N., Goulet, M., Genevieve, D., Sznajer, Y., Martinovic, J., Smithson, S., et al. (2009). DYNC2H1 mutations cause asphyxiating thoracic dystrophy and short rib-polydactyly syndrome, type III. *Am. J. Hum. Genet.* 84, 706–711. doi: 10.1016/j.ajhg.2009.04.016

Doren, M., Rehder, H., and Holzgreve, W. (1998). Prenatal diagnosis and obstetric management of Larsen's syndrome in a patient with an unrecognized family history of the disease. *Gynecol. Obstet. Invest.* 46, 274–278. doi: 10.1159/000010050

Forlino, A., and Marini, J. C. (2016). Osteogenesis imperfecta. *Lancet* 387, 1657–1671. doi: 10.1016/S0140-6736(15)00728-X

Geister, K. A., and Camper, S. A. (2015). Advances in skeletal dysplasia genetics. *Annu. Rev. Genomics Hum. Genet.* 16, 199–227. doi: 10.1146/annurev-genom-090314-045904

Gomez-Lira, M., Sangalli, A., Pignatti, P. F., Digilio, M. C., Giannotti, A., Carnevale, E., et al. (1994). Determination of a new collagen type I alpha 2 gene point mutation which causes a Gly640 Cys substitution in osteogenesis imperfecta and prenatal diagnosis by DNA hybridisation. *J. Med. Genet.* 31, 965–968. doi: 10.1136/jmg.31.12.965

Hachiya, Y., Hayashi, M., Negishi, T., Atsumi, S., Kubota, M., and Nishihara, T. (2012). A case of osteogenesis imperfecta type II caused by a novel COL1A2 gene mutation: endoscopic third ventriculostomy to prevent hydrocephalus. *Neuropediatrics* 43, 225–228. doi: 10.1055/s-0032-1324405

Han, J., Yang, Y. D., He, Y., Liu, W. J., Zhen, L., Pan, M., et al. (2020). Rapid prenatal diagnosis of skeletal dysplasia using medical trio exome sequencing: benefit for prenatal counseling and pregnancy management. *Prenat. Diagn.* 40, 577–584. doi: 10.1002/pd.5653

International Society for Prenatal Diagnosis (ISPD), the Society for Maternal Fetal Medicine (SMFM), and the Perinatal Quality Foundation (PQF) (2018). Joint Position Statement from the International Society for Prenatal Diagnosis (ISPD), the Society for Maternal Fetal Medicine (SMFM), and the Perinatal Quality Foundation (PQF) on the use of genome-wide sequencing for fetal diagnosis. *Prenat. Diagn.* 38, 6–9. doi: 10.1002/pd.5195

Kearney, H. M., Thorland, E. C., Brown, K. K., Quintero-Rivera, F., South, S. T., and Working Group of the American College of Medical Genetics Laboratory Quality Assurance Committee (2011). American College of Medical Genetics standards and guidelines for interpretation and reporting of postnatal constitutional copy number variants. *Genet. Med.* 13, 680–685. doi: 10.1097/GIM.0b013e3182217a3a

Krakow, D., Lachman, R. S., and Rimoin, D. L. (2009). Guidelines for the prenatal diagnosis of fetal skeletal dysplasias. *Genet. Med.* 11, 127–133. doi: 10.1097/GIM.0b013e3181971ccb

LaDuca, H., Farwell, K. D., Vuong, H., Lu, H. M., Mu, W., Shahmirzadi, L., et al. (2017). Exome sequencing covers >98% of mutations identified on targeted next generation sequencing panels. *PLoS ONE* 12:e0170843. doi: 10.1371/journal.pone.0170843

Lin, S., Zhou, Y., Zhou, B., and Gu, H. (2017). Unexpected discovery of a fetus with DMD gene deletion using single nucleotide polymorphism array. *Chin. J. Med. Genet.* 34, 563–566. doi: 10.3760/cma.j.issn.1003-9406.2017.04.021

Liu, Y., Wang, L., Yang, Y. K., Liang, Y., Zhang, T. J., Liang, N., et al. (2019). Prenatal diagnosis of fetal skeletal dysplasia using targeted next-generation sequencing: an analysis of 30 cases. *Diagn. Pathol.* 14:76. doi: 10.1186/s13000-019-0853-x

Marini, J. C., Forlino, A., Cabral, W. A., Barnes, A. M., San Antonio, J. D., Milgrom, S., et al. (2007). Consortium for osteogenesis imperfecta mutations in the helical domain of type I collagen: regions rich in lethal mutations align with collagen binding sites for integrins and proteoglycans. *Hum. Mutat.* 28, 209–221. doi: 10.1002/humu.20429

Martinez, J. R., Dhawan, A., and Farach-Carson, M. C. (2018). Modular proteoglycan perlecan/HSPG2: mutations, phenotypes, and functions. *Genes (Basel)* 9:9110556. doi: 10.3390/genes9110556

Mentrup, B., Marschall, C., Barvencik, F., Amling, M., Plendl, H., Jakob, F., et al. (2011). Functional characterization of a novel mutation localized in the start codon of the tissue-nonspecific alkaline phosphatase gene. *Bone* 48, 1401–1408. doi: 10.1016/j.bone.2011.03.676

Merrill, A. E., Merriman, B., Farrington-Rock, C., Camacho, N., Sebald, E. T., Funari, V. A., et al. (2009). Ciliary abnormalities due to defects in the retrograde transport protein DYNC2H1 in short-rib polydactyly syndrome. *Am. J. Hum. Genet.* 84, 542–549. doi: 10.1016/j.ajhg.2009.03.015

Michigami, T., Uchihashi, T., Suzuki, A., Tachikawa, K., Nakajima, S., and Ozono, K. (2005). Common mutations F310L and T1559del in the tissue-nonspecific alkaline phosphatase gene are related to distinct phenotypes in Japanese patients with hypophosphatasia. *Eur. J. Pediatr.* 164, 277–282. doi: 10.1007/s00431-004-1612-9

Millan, J. L., and Whyte, M. P. (2016). Alkaline phosphatase and hypophosphatasia. *Calcif. Tissue Int.* 98, 398–416. doi: 10.1007/s00223-015-0079-1

Monaghan, K. G., Leach, N. T., Pekarek, D., Prasad, P., Rose, N. C., Practice, A. P., et al. (2020). The use of fetal exome sequencing in prenatal diagnosis: a points to consider document of the American College of Medical Genetics and Genomics (ACMG). *Genet. Med.* 22, 675–680. doi: 10.1038/s41436-019-0731-7

Murugan, S., Chandramohan, A., and Lakshmi, B. R. (2010). Use of multiplex ligation-dependent probe amplification (MLPA) for Duchenne muscular dystrophy (DMD) gene mutation analysis. *Indian J. Med. Res.* 132, 303–311.

Pokharel, R. K., Alimsardjono, H., Takeshima, Y., Nakamura, H., Naritomi, K., Hirose, S., et al. (1996). Japanese cases of type 1 thanatophoric dysplasia exclusively carry a C to T transition at nucleotide 742 of the fibroblast growth factor receptor 3 gene. *Biochem. Biophys. Res. Commun.* 227, 236–239. doi: 10.1006/bbrc.1996.1495

Porntaveetus, T., Srichomthong, C., Suphapeetiporn, K., and Shotelersuk, V. (2017). Monoallelic FGFR3 and Biallelic ALPL mutations in a Thai girl with hypochondroplasia and hypophosphatasia. *Am. J. Med. Genet. A* 173, 2747–2752. doi: 10.1002/ajmg.a.38370

Qiao, L., Li, H., Wang, T., Gao, A., Zhao, N., and Zhang, Q. (2018). A novel variant in a family with short rib-polydactyly syndrome type 3. *Chin. J. Clin. Lab. Sci.* 36, 834–836.

Retterer, K., Juusola, J., Cho, M. T., Vitazka, P., Millan, F., Gibellini, F., et al. (2016). Clinical application of whole-exome sequencing across clinical indications. *Genet. Med.* 18, 696–704. doi: 10.1038/gim.2015.148

Richards, S., Aziz, N., Bale, S., Bick, D., Das, S., Gastier-Foster, J., et al. (2015). Standards and guidelines for the interpretation of sequence variants: a joint consensus recommendation of the American College of Medical Genetics and Genomics and the Association for Molecular Pathology. *Genet. Med.* 17, 405–424. doi: 10.1038/gim.2015.30

Satou, Y., Al-Shawafi, H. A., Sultana, S., Makita, S., Sohda, M., and Oda, K. (2012). Disulfide bonds are critical for tissue-nonspecific alkaline phosphatase function revealed by analysis of mutant proteins bearing a C(201)-Y or C(489)-S substitution associated with severe hypophosphatasia. *Biochim. Biophys. Acta* 1822, 581–588. doi: 10.1016/j.bbadis.2012.01.007

Sawai, H., Komori, S., Ida, A., Henmi, T., Bessho, T., and Koyama, K. (1999). Prenatal diagnosis of thanatophoric dysplasia by mutational analysis of the fibroblast growth factor receptor 3 gene and a proposed correction of previously published PCR results. *Prenat. Diagn.* 19, 21–24. doi: 10.1002/(SICI)1097-0223(199901)19:1<21::AID-PD457>3.0.CO;2-5

Taillandier, A., Domingues, C., De Cazanove, C., Porquet-Bordes, V., Monnot, S., Kiffer-Moreira, T., et al. (2015). Molecular diagnosis of hypophosphatasia and differential diagnosis by targeted next generation sequencing. *Mol. Genet. Metab.* 116, 215–220. doi: 10.1016/j.ymgme.2015.09.010

Tang, H., Zhang, Q., Yin, L. L., et al. (2020). Whole exome sequencing aids the diagnosis of fetal skeletal dysplasia. *Res. Sqaure*[Preprint]. Available online at: https://www.researchsquare.com/article/rs-46976/v1 (accessed July 28, 2020).

Tonni, G., Azzoni, D., Ventura, A., Ferrari, B., Felice, C. D., and Baldi, M. (2010). Thanatophoric dysplasia type I associated with increased nuchal translucency in the first trimester: early prenatal diagnosis using combined ultrasonography and molecular biology. *Fetal. Pediatr. Pathol.* 29, 314–322. doi: 10.3109/15513811003796938

Xu, Q., Wu, N., Cui, L., Lin, M., Thirumal Kumar, D., George Priya Doss, C., et al. (2018). Comparative analysis of the two extremes of FLNB-mutated autosomal dominant disease spectrum: from clinical phenotypes to cellular and molecular findings. *Am. J. Transl. Res.* 10, 1400–1412.

Xue, Y., Sun, A., Mekikian, P. B., Martin, J., Rimoin, D. L., Lachman, R. S., et al. (2014). FGFR3 mutation frequency in 324 cases from the International Skeletal Dysplasia Registry. *Mol. Genet. Genomic. Med.* 2, 497–503. doi: 10.1002/mgg3.96

Yang, Y. M., Yan, K., Liu, B., Chen, M., Wang, L. Y., Huang, Y. Z., et al. (2019). Comprehensive genetic diagnosis of patients with Duchenne/Becker muscular dystrophy (DMD/BMD) and pathogenicity analysis of splice site variants in the DMD gene. *J. Zhejiang Univ. Sci. B* 20, 753–765. doi: 10.1631/jzus.B1800541

Zhou, X., Chandler, N., Deng, L., Zhou, J., Yuan, M., and Sun, L. (2018). Prenatal diagnosis of skeletal dysplasias using a targeted skeletal gene panel. *Prenat. Diagn.* 38, 692–699. doi: 10.1002/pd.5298

Conflict of Interest: The authors declare that the research was conducted in the absence of any commercial or financial relationships that could be construed as a potential conflict of interest.

frontiers in Endocrinology

ORIGINAL RESEARCH
published: 12 April 2021
doi: 10.3389/fendo.2021.605736

Identification and *In Vitro* Functional Verification of Two Novel Mutations of *GHR* Gene in the Chinese Children with Laron Syndrome

*Ran Li, Fengying Gong, Hui Pan, Hanting Liang, Hui Miao, Yuxing Zhao, Lian Duan, Hongbo Yang, Linjie Wang, Shi Chen and Huijuan Zhu**

Key Laboratory of Endocrinology of National Health Commission, Department of Endocrinology, Peking Union Medical College Hospital, Chinese Academy of Medical Science and Peking Union Medical College, Beijing, China

OPEN ACCESS

Edited by:
Liborio Stuppia, University of Studies G. d'Annunzio Chieti and Pescara, Italy

Reviewed by:
Anita Morandi, Integrated University Hospital Verona, Italy
Andrew Whatmore, The University of Manchester, United Kingdom

***Correspondence:**
Huijuan Zhu
shengxin2004@163.com

Specialty section:
This article was submitted to Pediatric Endocrinology, a section of the journal Frontiers in Endocrinology

Received: *13 September 2020*
Accepted: *15 March 2021*
Published: *12 April 2021*

Citation:
Li R, Gong F, Pan H, Liang H, Miao H, Zhao Y, Duan L, Yang H, Wang L, Chen S and Zhu H (2021) Identification and In Vitro Functional Verification of Two Novel Mutations of GHR Gene in the Chinese Children with Laron Syndrome. Front. Endocrinol. 12:605736. doi: 10.3389/fendo.2021.605736

Purpose: Laron syndrome (LS) is a severe growth disorder caused by *GHR* gene mutation or post-receptor pathways defect. The clinical features of these patients collected in our present study were summarized, *GHR* gene variants were investigated and further *in vitro* functional verification was carried out.

Methods: Four patients with LS were collected, their clinical characteristics were summarized, genomic DNA was extracted, and *GHR* gene was amplified and sequenced. GHR wild type (GHR-WT) and mutant GHR expression plasmids were constructed, and transiently transfected into HepG2 cells and HEK293T cells to observe the subcellular distribution of the GHR protein by immunofluorescence and to determine the expression of GHR and its post-receptor signaling pathway changes by Western blotting.

Results: All of the four patients were male, and the median height was -4.72 SDS. Four *GHR* gene variants including c.587A>C (p.Y196S), c.766C>T (p.Q256*), c.808A>G (p.I270V) and c.1707-1710del (p.E570Afs*30) were identified, and the latter two were novel mutations. The results of mutant GHR plasmids transfection experiments and immunofluorescence assay showed that the subcellular distribution of GHR-Q256* and GHR-E570Afs*30 mutant proteins in HepG2 and HEK293T cells presented with a unique ring-like pattern, gathering around the nucleus, while GHR-Y196S mutant protein was evenly distributed on HepG2 cell membrane similar to GHR-WT. The GHR protein levels of HepG2 cells transiently transfected with GHR-Y196S, GHR-Q256* and GHR-E570Afs*30 were all significantly lower when compared with cells transfected with GHR-WT ($P<0.05$). Further mutant GHR post-receptor signal transduction investigation demonstrated that GH induced phosphorylated STAT5 levels of HepG2 cells transfected with three mutant plasmids were all significantly decreased in comparison with that of GHR-WT ($P<0.05$).

Conclusions: Two novel *GHR* gene mutations (I270V and E570Afs*30) were found in our patients with LS. GHR mutations influenced the subcellular distribution and GHR protein

levels, then led to the impaired post-receptor signal transduction, suggesting that the *GHR* mutations contributed to the pathological condition of LS patients.

Keywords: Laron syndrome, *GHR* gene mutation, subcellular distribution, STAT5, HepG2 cells

INTRODUCTION

Laron syndrome (LS) is a rare inherited disorder characterized by severe postnatal growth failure, normal or increased circulating growth hormone (GH) secretion and insulin-like growth factor 1 (IGF-1) deficiency (1). Classical LS was first described by Laron et al. in 1966 who reported three siblings with severe growth retardation from a consanguineous Jewish family, and the disorder was termed "Laron-type dwarfism" or "growth hormone insensitivity" subsequently (2, 3). LS is a kind of autosomal recessive disease which often occurred in families with parental consanguinity and sporadic cases have also been reported (3). Since 1966 when LS was firstly reported, more than 250 patients have been reported so far (4, 5).

LS is mainly caused by growth hormone receptor (GHR) gene mutations and monogenic defects of post-receptor components in the GH signal transduction pathway, such as signal transducer and activator of transcription 5B (*STAT5B*), *IGFALS*, *IGF1*, *IGF-1R* and pregnancy-associated plasma protease A2 (*PAPPA2*) (5–13). Among the various genetic aberrations, *GHR* gene mutations are most commonly reported (4).

GH, also known as somatotropin, plays a critical role in the promotion of growth, cell division and regeneration (3, 4). The effects of GH are directly mediated through its cell surface receptor, GHR. *GHR* gene is located on chromosome 5p13.1-p12 and is composed of 10 exons, with exon 1 being an untranslated region (3, 14). Exons 2 to 10 encode a peptide of 638 amino acid residues. After GHR proteins are synthesized in the endoplasmic reticulum, they are transported to the cell membrane through a protein-conducting channel and inserted in the cell membrane (15, 16). The mature GHR protein is comprised of three domains: an extracellular domain of 246 residues (encoded by exons 2-7 of GHR), a transmembrane domain of 24 residues (encoded by exon 8), and an intracellular domain of 350 residues (encoded by exons 9 and 10) (17). GH binds with GHRs to form a trimolecular complex and changes the conformation of the GHRs, triggers signaling molecules, such as Janus kinase 2 (JAK2), STAT5, and Src family kinases (2, 18–20). Activated, tyrosine-phosphorylated STAT5 proteins translocate into the nucleus and promote the transcription of the downstream IGF-1 gene (6, 21).

To date, more than 100 *GHR* gene defects have been identified, and the majority of the mutations occur in the extracellular domain of *GHR* gene, while mutations in the transmembrane domain and intracellular domain are relatively rare (4, 17, 22, 23). Several studies investigated the effects of *GHR* gene variations on the GH post-receptor signal transduction *in vitro* experiments. Fang et al. reported a compound heterozygous *GHR* mutations, C94S and H150Q, in an Austrian family, and functional studies showed that both the compound heterozygous mutation and C94S heterozygous mutation resulted in deficiency in activating GH-induced gene expression and diminished GH-induced STAT5b activation (24). Rughani et al. reported a novel W267* heterozygous nonsense mutation in the transmembrane domain in a Caucasian child, and the W267* mutation was shown to inhibit GH-induced STAT5 activation (25). Besides missense and nonsense mutation, the c.784G>C splicing mutation was investigated in a Turkish child, and *in vitro* studies revealed that the c.784G>C splicing mutation destroyed the intron 7 donor site and led to an absence of functional GHR (26). While, intragenic GHR deletion of 1454 nucleotides led to exon 8 skipping from the GHR mRNA transcript and translated a truncated GHR protein (27).

In the present study, four Chinese children diagnosed with LS in our Department of Endocrinology were collected and their clinical and biochemical characteristics were summarized. *GHR* gene variants were investigated and further *in vitro* functional verification was performed by cellular experiments to further elucidate the effects of *GHR* gene variations on *GHR* gene expression, subcellular distribution and GH-induced signal transduction.

MATERIALS AND METHODS

Clinical and Biochemical Characteristics

Four Chinese patients with severe growth retardation were admitted to Peking Union Medical College Hospital from 2012 to 2017. Height and weight were recorded as standard deviation scores (SDSs) based on the age- and sex-appropriate reference ranges of Chinese children. Blood samples were collected in the morning after an overnight fast, and the concentrations of GH and IGF-1 were measured by a solid-phase, two-site, chemiluminescent immunometric assay (IMMULITE 2000, Siemens, UK). Blood biochemical parameters and whole blood cell count were measured. The L-dopa GH provocative test was conducted as follows: L-dopa was given at a dosage of 125mg to patients weighing less than 10 kilograms (kg), 250 mg for patients weighing 10-30 kg, and for patients weighing more than 30 kg, 500 mg L-dopa was given (28). The basal GH level was quantified before medication, and peripheral serum was sampled every 30 minutes for up to 2 hours to measure GH concentration. The insulin-induced hypoglycemia GH provocative test was carried out by subcutaneously injecting insulin at a dosage of 0.1 U/kg, and the time-point of blood collection was 0, 30, 60, 90 and 120 minutes after medication (29). A peak GH concentration after stimulation of <5 ng/ml was

Abbreviations: LS, Laron syndrome; GHR, Growth hormone receptor; GHR-WT, GHR wild type; rhGH, Recombinant human growth hormone; rhIGF-1, Recombinant human IGF-1.

used to diagnose growth hormone deficiency (28). Pituitary magnetic resonance imaging (MRI) was conducted in each patient. LS was suspected when patients presented with extreme postnatal growth failure and midfacial hypoplasia. Biochemically, LS was featured by normal or elevated GH secretion and subnormal serum IGF-1 concentration, demonstrating the inability to generate normal quantities of IGF-1. *GHR* gene sequencing was then performed for patients suspected of LS, and the detailed process was described in the following part. The parents of the patients have given their written informed consent. The study was approved by the Ethics Committee of Peking Union Medical College Hospital and the reference number was JS-1663.

DNA Extraction and *GHR* Gene Sequencing

Genomic DNA was extracted from peripheral blood leukocytes using the Qiagen DNeasy Blood Kit (Qiagen, 69504, Germany) according to the standard protocol. Coding exons (exon 2 to exon 10) and the boundaries between introns and exons of the *GHR* gene were amplified by polymerase chain reaction (PCR) method. The primers used for PCR amplification were shown in **Table 1**. All PCR products were sequenced (Tianyi Huiyuan Biotech Corporation, Beijing, China) and aligned with the standard *GHR* sequence (RefSeq NM_000163.5) in UCSC BLAT (http://genome.ucsc.edu/cgi-bin/hgBlat). Our sequencing data is uploading to GenBank, and the accession numbers are MW701347, MW701348 and MW701349.

Construction of the *GHR* Wild-Type and Mutant Expression Plasmids

The full-length human *GHR* gene cDNA (NM_000163.5) was obtained by RT-PCR method from human total RNA isolated from white blood cells using EZNA Total RNA Kit (Omega Bio-Tek, Doraville, USA). GHR wild-type (GHR-WT) expression plasmid was yielded by inserting the *GHR* gene whole cDNA (+193~+2109) into pcDNA3.1(+) vector, both *GHR* gene cDNA and the pcDNA3.1(+) vector were digested by Kpnl and EcoRI enzymes and were ligated by T4 DNA ligase (Thermo Fisher Scientific, USA). The HA tag sequence (TACCCCTACGAC GTGCCCGACTACGCC) was inserted after the signal peptide sequence, then the plasmid was sequenced. Site-directed mutagenesis experiments were performed by Vigene Biosciences Company (Beijing, China) to construct GHR-Y196S, GHR-Q256* and GHR-E570Afs*30 mutant expression plasmids and Sanger sequencing was performed to verify the *GHR* gene mutations. Expression plasmids were extracted with a Qiagen Plasmid Maxi Kit (Qiagen 12162, Germany).

Cell Culture

Human embryonic kidney (HEK293T) cells and HepG2 cells were purchased from Cell Resource Center of Institute of Basic Medicine, Chinese Academy of Medical Sciences. HEK293T cells were cultured in DMEM medium (Hyclone, USA) supplemented with 10% fetal bovine serum (Cell Resource Center of Institute of Basic Medicine, Beijing, China) and antibiotics (100U/ml penicillin and 100U/ml streptomycin from Gibco, USA) under 5% CO_2 and 95% O_2 at 37°C. HepG2 cells were maintained in MEM medium (Hyclone, USA) containing 10% fetal bovine serum (Cell Resource Center of Institute of Basic Medicine, Beijing, China), nonessential amino acids (Gibco, USA) and antibiotics.

Transient Transfection

HEK293T cells and HepG2 cells were seeded on 12-well plates at a density of 6×10^5 cells/well. The cells were grown to 50~60% confluence prior to removal of antibiotic-containing medium and then incubated with 1ml antibiotic-free medium per well. The cells were transfected with 1.0 μg expression plasmids (GHR-WT, GHR-Y196S, GHR-Q256* and GHR-E570Afs*30 expression plasmids) and 1.5 μl of Lipofectamine 3000 (Thermo Fisher Scientific, USA) in 100 μl of OPTI-MEM serum-free medium (Hyclone, USA) for 5 hours, then the culture medium was replaced with fresh medium containing 10% fetal calf serum for 48h. The vector group was transfected with 1.0 μg pcDNA3.1(+) empty vector instead of expression plasmids.

Immunofluorescence Assays

Immunofluorescence was performed on fixed cells to determine the subcellular distribution of GHR. HEK293T cells and HepG2 cells were plated on 12-well plates treated with polylysine and transfected with either GHR-WT or mutant GHR expression plasmids. 48 hours after transfection, the cells were fixed with 4% paraformaldehyde for 20 minutes and permeabilized with saponin (Beyotime Biotechnology, P0095, China) for 20 minutes. QuickBlockTM blocking solution (Beyotime Biotechnology, P0220, China) was added to block non-specific

TABLE 1 | Primers used in the PCR amplification for *GHR* gene.

Exon	Forward primer sequence	Reverse primer sequence	Length of PCR products
Exon 2	AGCTCATTCATGTCTTACCC	AAAACTTGGATGTAGCGAAT	252bp
Exon 3	AGCCACAAAATGACCTGTTTAGC	GCCACACACTTTTAAACAACCAGA	781bp
Exon 4	CTAGACACGGAATACACTGG	AACAAATCACTTCCATTCCCACA	347bp
Exon 5	GAAGTACCAAACGGCCTC	TCTTCTTCACAACATTTACTGC	611bp
Exon 6	AAAATATTGGAAGAAATAAGAGCA	GGCCTCCATATATACATAAGCATC	516bp
Exon 7	AAAATGGGAGAATACCTG	ATATTTTGATTTGGACAACAC	349bp
Exon 8	GCTGAAACCTTTATGATACTCCC	CTGGAATGAATGGGTCAACT	758bp
Exon 9	ACACTCCAATTATATAAAGTACCA	TCCAGGAGAAGAGACACAAG	331bp
Exon 10	ACTGTTGTTCTTATTGTAACCAT	AAGGCATTTTAGAATCCATACCC	1213bp

antibody binding sites for 10 minutes. The cells were then stained with anti-HA monoclonal antibody (Abcam, USA, ab18181, 1:200 dilution) at 4°C overnight. Anti-mouse secondary antibody conjugated with Alexa Fluor 488 (CST, Danvers, MA, USA, 4408s, 1:1000 dilution) were added and incubated at room temperature in dark for 1 hour. DAPI was added to stain nucleus at room temperature in dark for 10 minutes. Fluorescence was detected using a Leica TCS SP5 II confocal fluorescence microscope (Leica, Germany).

Western Blotting for Detection of *GHR* and Phosphorylated-STAT5

To assess the influence of *GHR* mutations on the expression of GHR protein, the GHR protein levels were determined by Western blotting method in HepG2 cells. HepG2 cells were transfected with GHR-WT or mutant GHR expression plasmids as described above. Total proteins were extracted using RIPA cell lysis buffer. 30 μg of proteins were separated by electrophoresis on 8% SDS-PAGE gels. The proteins were then transferred to nitrocellulose membranes (Applygen, Beijing, China) through a wet transfer method (Bio-Rad, California, USA) followed by the immunodetection. The primary rabbit anti-GHR antibody (Abcam, USA, ab65304, 1:1000 dilution) was incubated at 4°C overnight, followed by incubation with the HRP-coupled secondary antibody for 1 hour at room temperature (anti-rabbit antibody from CST, 7074, 1:3000 dilution). Signals were detected by using high sensitivity SuperSignal West Pico PLUS reagent (ThermoFisher Scientific, USA, 34577) and visualized using the Tanon 5200 Chemiluminescence imager (China). The bands were analyzed using Image J. A similar process was also conducted to assay β-actin as an internal reference.

To further investigate whether the mutant GHRs affect GH-induced signal transduction, the levels of the total and phosphorylated-STAT5 (p-STAT5) protein was further determined by Western blotting method in HepG2 cells. As described previously, HepG2 cells were transfected with GHR-WT or mutant GHR expression plasmids for 5 hours, and the cell culture medium was changed to low serum medium (1% fetal bovine serum) 16 hours. Then, 100 ng/ml rhGH was supplemented for 30 minutes. Total proteins were extracted with a phosphatase inhibitor cocktail (MedChemExpress, USA, HY-K0022) which protected the proteins from being dephosphorylated during protein extraction procedure. The following western blotting process were conducted as described above. The primary rabbit anti-phospho-STAT5-Y694 (Abcam, ab32364), rabbit anti-STAT5 (Abcam, ab16276) and rabbit anti-β-actin (CST, 4970s) were incubated at 1:1000 dilution at 4°C overnight, while the secondary anti-rabbit antibody (CST, 7074) was incubated at 1:2000 dilution for 1 hour at room temperature. All immunoblot data shown were representative of at least three independent experiments.

Statistical Analysis

Each experiment was carried out three times. Samples in each group of experiments were repeated in triplicate. Normally distributed data are expressed as the mean ± standard deviation (SD), and skewness distribution data are expressed as the median. Statistical analysis was performed by t-test for two groups or one-way ANOVA for more than two groups. The Kruskal-Wallis test was used for skewed data. $P<0.05$ was considered significant. All statistical computations were performed with SPSS 23.0, and GraphPad Prism 6 was used for all statistical graphs.

RESULTS

The Demographic Characteristics and Biochemical Measurements of LS Patients

The demographic characteristics and biochemical measurements of the four patients are shown in **Table 2**. All of the four patients with LS were male, the median age was 6.2 years old. Three patients had a severe short stature with height SDS of -5.49, -6.71 and -3.95, while the height SDS of patient 2 was -2.80. The median height was -4.72 SDS, and the median weight was -2.77 SDS.

As shown in **Table 2**, three patients (P1, P2, P3) had higher basal GH levels than the normal reference range (<2.0 ng/ml), ranging from 2.10 to 15.44 ng/ml, whereas the basal GH levels of P4 patient was 1.59 ng/ml (<2.0 ng/ml). The peak GH levels during the GH stimulation test were extremely high in P1, P3 and P4 patients with unknown peak GH levels of P2. However, IGF-1 levels of P2, P3 and P4 patients was less than the lower limit of normal range (<25 ng/ml), and IGF-1 concentration of P1 was only 32 ng/ml. As expected, all four patients had bone age retardation with the median retardation time of 18 months. Finally, none of the patients showed abnormalities in the pituitary MRI.

Patient 1 received recombinant human GH (rhGH) treatment at a dosage of 0.053 mg/kg/d for 2 months, and his height increased by 3.3 cm and IGF-1 increased from 32 ng/ml to 91 ng/ml. Patient 4 was given rhGH treatment at a dosage of 0.057 mg/kg/d for 32 months. During the last follow-up, the height increased by 17.8 cm (from -3.95 SDS to -2.96 SDS) with an annual growth rate of 6.8 cm/year, and IGF-1 increased from less than 25 ng/ml to 64 ng/ml.

GHR Gene Variations of Four Patients With LS

Exon 2 to exon 10 of *GHR* gene of four patients with LS were amplified and sequenced. The results were shown in **Table 3** and **Figure 1**. Two single nucleotide polymorphism (SNP) sites, c.1483C>A (p.P495T, rs6183) and c.1630A>C (p.I544L, rs6180), were detected in Patient 1. Patient 2 carried a novel homozygous mutation, c.808A>G (p.I270V) as shown in **Figure 1A**, and neither of his parents had the c.808A>G mutation. A novel heterozygous nonsense mutation, c.766C>T (p.Q256*) was identified in patient 3 as shown in **Figure 1B**, and the C>T base substitution led to a premature stop codon, which produced a truncated GHR protein. Patient 4 carried *GHR* gene compound heterozygous mutations including a novel heterozygous mutation, c.1707_1710del (p.E570Afs*30) in exon 10 (**Figure 1D**), which was inherited from his father and a previously reported

TABLE 2 | Clinical and biochemical features of patients with Laron Syndrome.

	Age	Gender	Birth weight (kg)	Birth length (cm)	Weight SDS	Height SDS	Basal GH (ng/ml)	Peak GH (ng/ml)	IGF-1 (ng/ml)	IGF-1 SDS	IGFBP3 (mg/L)	Bone age retardation (months)	GH treatment and duration	ΔHeight after rhGH (cm)
P1	7.6	Male	2.65	Unknown	-2.96	-5.49	15.44	23.36	32	-3.0	1.2 (1.3~5.6)	12	Yes, 0.053mg/kg/d for 2 months	3.3
P2	3.5	Male	3.15	46	-2.93	-2.80	2.10	Unknown	<25	-3.0	Unknown	6	No	
P3	14.3	Male	Unknown	Unknown	-2.61	-6.71	9.60	31.7	<25	-3.0	0.6 (0.7~3.9)	28	No	
P4	4.8	Male	3.20	51	-1.82	-3.95	1.59	>33.80	<25	-3.0	1.14 (1.0~4.7)	24	Yes, 0.057mg/kg/d for 32 months	17.8

SDS, standard deviation score; rhGH, recombinant human growth hormone.

heterozygous mutation, c.587A>C (p.Y196S, rs747888560) in exon 6 (**Figure 1C**), which was inherited from his mother as presented in **Figure 1E**. However, neither of his parents manifested a short phenotype. The height SDS of his father and mother was 0.14 SDS (177 cm) and -0.03 SDS (157 cm), respectively.

Abnormal Subcellular Localization of Mutant *GHR*s Observed by Immunofluorescence Assays

To visualize the mutant GHR subcellular distribution, GHR-WT and mutant GHR expression plasmids were transfected into HepG2 cells and immunofluorescence assay was performed with a monoclonal anti-HA tag (HA tag was inserted after the signal peptide in the extracellular domain) antibody. As presented in **Figure 2**, GHR-WT proteins in green color were evenly distributed on the cell membrane of HepG2 cells. However, when Q256* mutant GHR expression plasmids were transfected into HepG2 cells, mutant GHR proteins gathered around the nucleus and presented in a unique ring-like pattern, which was apparently different from the GHR-WT. Similar to the GHR-Q256* truncated protein, the same ring-like pattern was observed in cells transfected with GHR-E570Afs*30 expression plasmids, the mutant GHR proteins were concentrated in the cytoplasm. However, unlike the subcellular distribution of mutant GHR-Q256* and GHR-E570Afs*30, the mutant GHR-Y196S proteins had a similar subcellular localization of GHR-WT with an even GHR distribution on the cell membrane.

Next, the subcellular distribution of mutant GHRs were again conducted in HEK293T cells by the same transient transfection method and immunofluorescence assays as shown in **Figure 3**, and the localization of the GHR-WT and mutant GHRs were similar to that of HepG2 cells. GHR-WT proteins in HEK293T cells presented with a uniform distribution on cell surface as observed in HepG2 cells transfected with GHR-WT. Q256* truncated proteins and E570Afs*30 proteins in HEK293T cells were localized in a region adjacent to the nucleus, similar to the subcellular distribution pattern seen in HepG2 cells. In HEK293T cells transfected with Y196S, GHRs had a similar subcellular localization as GHR-WT, evenly distributed on the cell membrane.

The Significantly Decreased Protein Levels of Mutant *GHR*s Transfected Into HepG2 Cells

Since the cellular localization of the mutant GHR has changed, has its protein levels also changed? In order to answer this issue, pcDNA3.1(+) empty vector, GHR-WT and mutant GHR expression plasmids were transfected into HepG2 cells, total proteins were extracted and Western blotting was performed. As shown in **Figures 4A, B**, GHRs could be detected in HepG2 cells transfected with pcDNA3.1(+) empty vector, and the molecular weight of GHRs were about 130 kDa. GHR-WT proteins were overexpressed compared to cells transfected with empty vector and the difference was statistically significant (**Figure 4C**, $P<0.05$). The GHR protein levels in HepG2 cells transfected with GHR-Y196S were significantly lower than that of GHR-WT

TABLE 3 | Genetic variants of the *GHR* gene in patients with Laron Syndrome.

Patient	Exon	Nucleotide	Protein	rs number	Homozygote/ Heterozygote	Novel	Clinical Significance
P1	Exon 10	c.1483C>A	p.P495T	6183	Heterozygote	No	Likely benign
	Exon 10	c.1630A>C	p.I544L	6180	Heterozygote	No	benign
P2	Exon 8	c.808 A>G	p.I270V		Homozygote	Yes	Uncertain significance
P3	Exon 7	c.766C>T	p.Q256*		Heterozygote	No	pathogenic
P4	Exon 6	c.587A>C	p.Y196S	747888560	Heterozygote	No	Likely pathogenic
	Exon 10	c.1707_1710del	p.E570Afs*30		Heterozygote	Yes	pathogenic

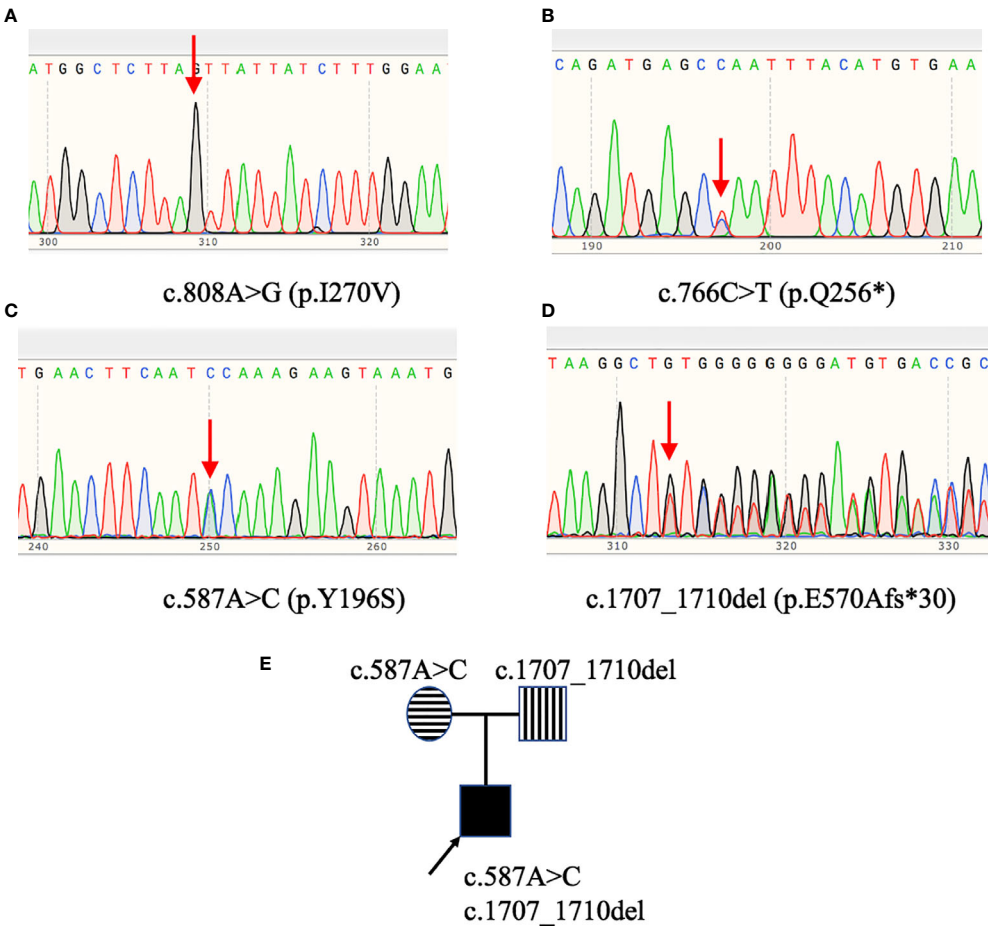

FIGURE 1 | *GHR* gene variants in patients with Laron syndrome. Patient 2 **(A)** carried the c.808A>G (p.I270V) homozygous mutation. Patient 3 **(B)** harbored the c.766C>T (p.Q256*) heterozygous mutation. Patient 4 **(C, D)** had *GHR* gene compound heterozygous mutations: c.587A>C (p.Y196S) and c.1707_1710del (p.E570Afs*30). Pedigree analysis of patient 4 **(E)** revealed that the c.587A>C variant was inherited from his mother, while the c.1707_1710del variant was inherited from his father.

and decreased by 19.65% as shown in **Figure 4C** ($P<0.05$). Specifically, unlike GHR-Y196S, HepG2 cells transfected with GHR-Q256* mutant expression plasmid produced a truncated protein, with a molecular weight of approximately 43 kDa as presented in **Figure 4B**. Protein bands corresponding to the molecular weight of 130kDa could be detected in HepG2 cells transfected with Q256*, and the GHR protein level was significantly decreased by 81.34% when compared to GHR-WT ($P<0.05$). Similar to GHR-Q256*, HepG2 cells transfected with GHR-E570Afs*30 mutant plasmid also had significantly diminished GHR protein expression at a molecular weight of 130kDa, which was decreased by 60.22% when compared to

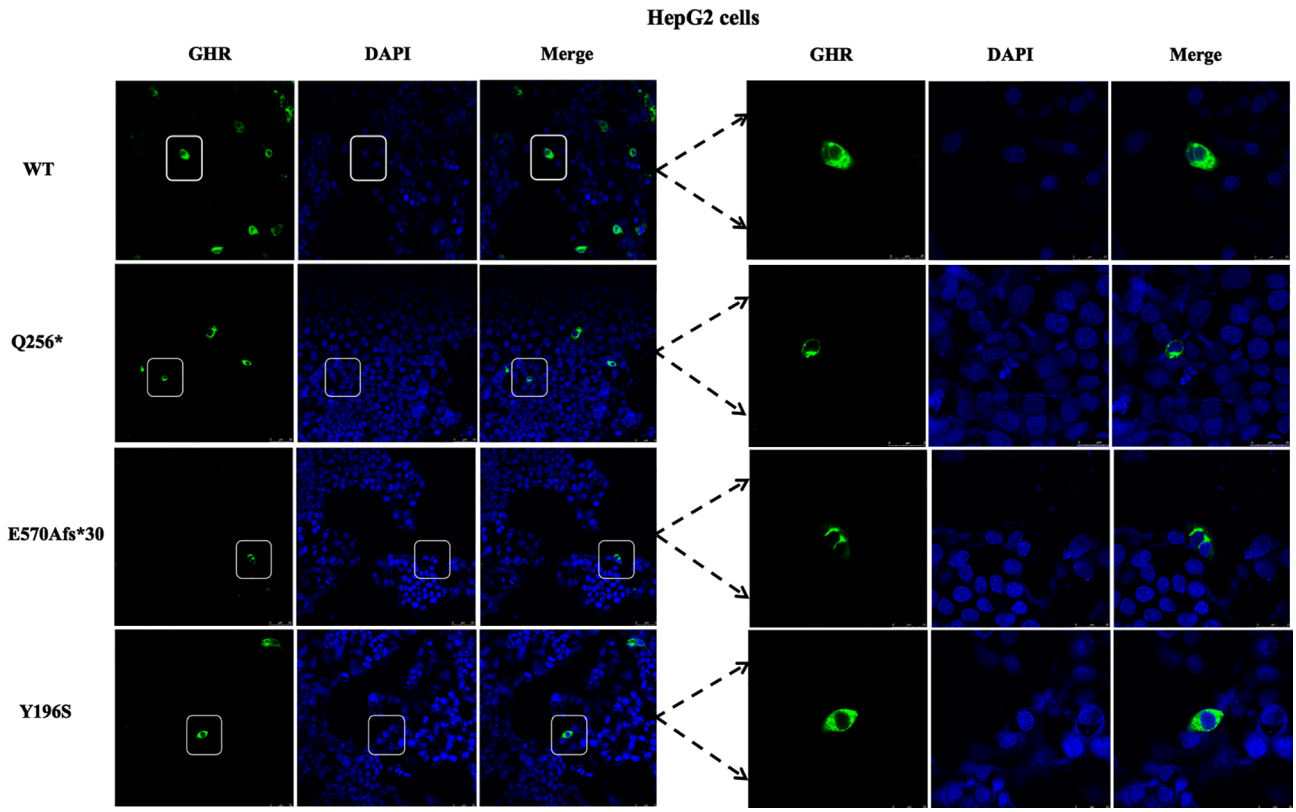

FIGURE 2 | Immunofluorescence images of HepG2 cells transfected with *GHR* wild type (WT) and mutant expression plasmids (Q256*, E570Afs*30 and Y196S). The *GHR* protein was labeled by anti-HA primary antibody in green, the nucleus was labeled by DAPI in blue, and the merged images were displayed in the right column.

GHR-WT as presented in **Figure 4C** ($P<0.05$). However, no visible truncated GHR protein band was identified in western blot gel.

The Significantly Decreased GH-Induced Phosphorylated STAT5 Levels of HepG2 Cells Transfected With Mutant *GHR*s

Since *GHR* gene mutations lead to abnormal subcellular location and the decreased expression of GHR proteins, it was not clear whether the transduction of post-receptor signal pathway was also affected. To further elucidate this problem, HepG2 cells were transfected with GHR-WT and mutant GHR expression plasmids, and cells were treated with 100ng/ml rhGH for 30 minutes before the total proteins were extracted. The levels of the total and p-STAT5 protein was measured by Western blotting. As shown in **Figures 5A, B**, both total STAT5 (t-STAT5) and p-STAT5 were detected at a molecular weight of 95 kDa in HepG2 cells. The relative levels of p-STAT5 among different groups was marked as the ratio of p-STAT5 to t-STAT5. As shown in **Figure 5C**, the levels of p-STAT5 proteins were significantly decreased in HepG2 cells transfected with GHR-Y196S mutant plasmid in comparison with cells transfected with GHR-WT, and decreased by 32.67% ($P<0.05$). In consistent with the results of GHR-Y196S, the levels of p-STAT5 proteins were also significantly reduced in HepG2 cells transfected with GHR-Q256* and GHR-E570Afs*30 mutant plasmids and reduced by 40.57% and 29.63%, respectively, as shown in **Figure 5C**, which indicated an impaired post-receptor signal transduction.

DISCUSSION

This study described the demographic characteristic and biochemical features of four Chinese patients with LS. Molecular genetic analysis revealed two novel *GHR* gene mutations, c.808A>G (p.I270V) and c.1707_1710del (p.E570Afs*30). Further *in vitro* functional experiments demonstrated that the novel *GHR* gene mutations disrupted the subcellular translocation of GHR proteins, affected the expression of GHR proteins and impaired the post-receptor signal transduction.

Patient 4 carried a compound heterozygous mutation, c.1707_1710del (p.E570Afs*30) and c.587A>C (p.Y196S). c.1707_1710del mutation was located in the intracellular region of GHR. Deletion of four bases resulted in a frameshift mutation, introducing a premature termination codon (TAG) at codon 600. The novel E570Afs*30 mutation influenced the subcellular distribution of GHR protein. Immunofluorescence

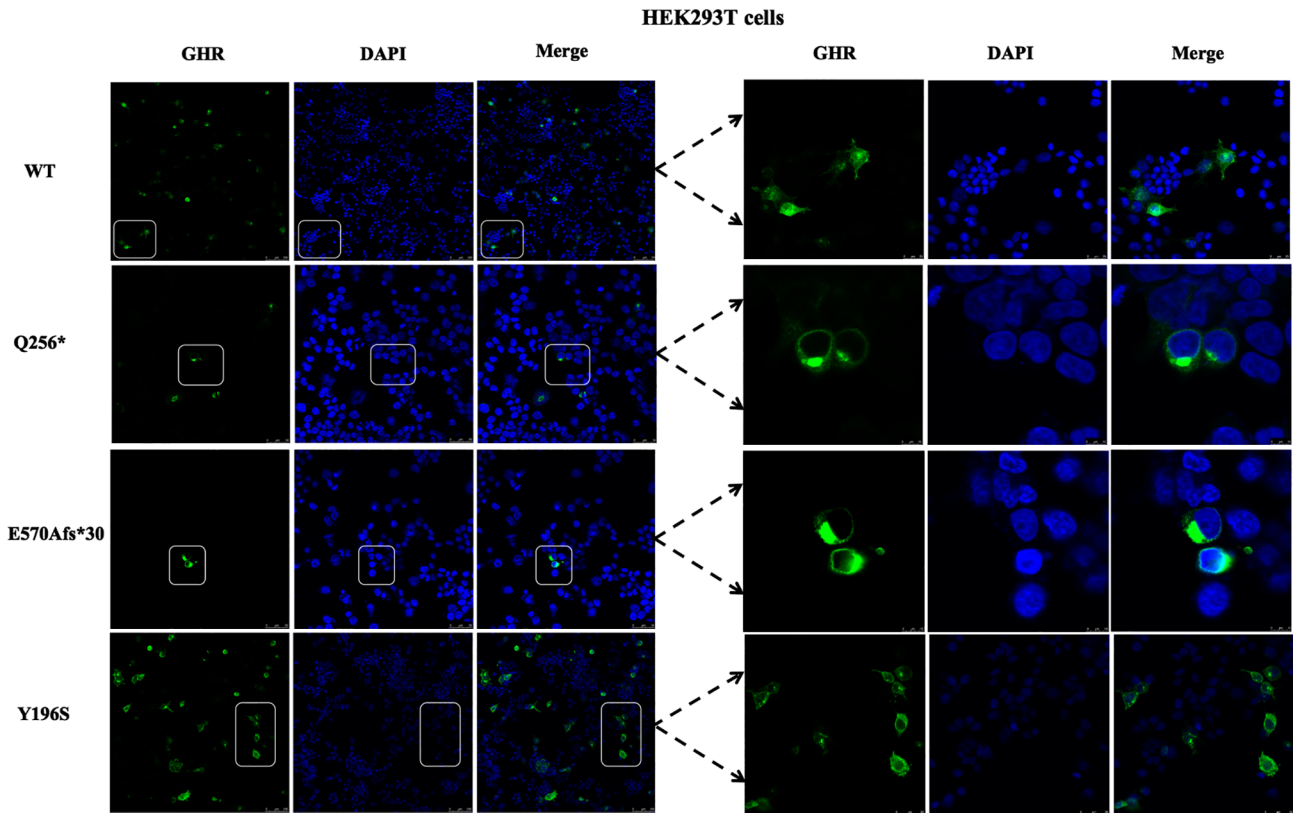

FIGURE 3 | Immunofluorescence images of HEK293T cells transfected with *GHR* wild type (WT) and mutant expression plasmids (Q256*, E570Afs*30 and Y196S). The *GHR* protein was labeled by anti-HA primary antibody in green, the nucleus was labeled by DAPI in blue, and the merged images were displayed in the right column.

demonstrated that the mutated GHR had a ring-like distribution pattern gathering around the nucleus, while GHR-WT were evenly distributed on the cell membrane. The GHR trafficking process from the endoplasmic reticulum to the cell membrane might be interrupted. E570Afs*30 mutation not only effected the translocation of GHR protein, but also influenced the expression of GHR and the GH-induced signal transduction. The expression of E570Afs*30 mutant protein was significantly decreased compared to the GHR-WT. The predicted consequence of this frameshift mutation would produce a truncated protein. However, no truncated protein was detected in Western blotting. The possible explanation of the result may be that the E570Afs*30 mutant *GHR* gene activated nonsense-mediated mRNA decay (30), which led to the GHR mRNA degradation. Milward et al. reported a homozygous 22-bp deletion in exon 10 of the GHR, resulting in a truncated GHR protein at amino acid 449 (GHR1-449) (31). Although both the GHR1-449 mutation and the E570Afs*30 mutation located in the intracellular domain, the mutant GHR1-449 protein had a similar cell surface distribution pattern as the GHR-WT, suggesting that GHR1-449 did not affect protein trafficking to the cell membrane, which was different from E570Afs*30 mutation in our study.

The other heterozygous mutation in patient 4, c.587A>C (p.Y196S), was first reported by Oh PS et al. in two Korean patients with LS. However, the *in vitro* cellular function studies were not performed in this study (32). The heterozygous c.587A>C substitution did not change the length of the GHR protein, and the mature Y196S mutant protein had the same molecular weight as the GHR-WT protein as demonstrated by Western blotting in our present study. However, the expression of GHR-Y196S was significantly lower than that of the GHR-WT, and the GHR post-receptor signal transduction was significantly impaired although the subcellular distribution of GHR-Y196S was similar to GHR-WT. Pedigree analysis revealed that the c.1707_1710del variant was inherited from his father, and the c.587A>C variant was inherited from his mother, nevertheless, neither of his parents had a short stature, suggesting that c.1707_1710del and the c.587A>C mutation had an additive effect on the phenotype of the patients.

In patient 3, a c.766C>T (p.Q256*) heterozygous nonsense mutation located in the extracellular domain was discovered. The substitution of C to T in exon 7 introduced a premature termination codon in place of a glutamic acid at amino acid 256 and produced a truncated GHR, leading to a deletion of the entire transmembrane domain and intracellular domain. The unique ring-like distribution

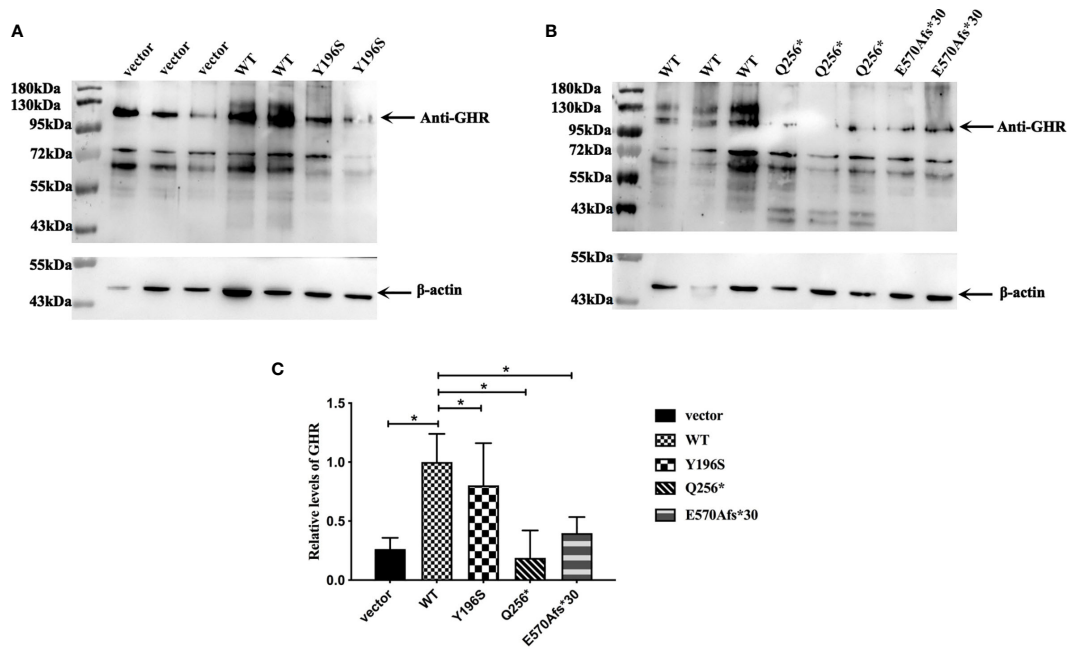

FIGURE 4 | **(A, B)** Expression of *GHR* protein in HepG2 cells transfected with pcDNA3.1(+) empty vector, *GHR* wild type (WT) and mutant expression plasmids (Y196S, Q256* and E570Afs*30). The *GHR* protein has a molecular weight of around 130 kDa. Protein bands corresponding to 130 kDa could be detected in HepG2 cells transfected with Q256* and E570Afs*30, and the relative expression of both of them were significantly decreased compared to GHR-WT (**C**, P<0.05). HepG2 cells transfected with Q256* mutant plasmid produced a truncated protein, with a molecular with of around 43kD. However, no truncated protein was detected in HepG2 cells transfected with E570Afs*30 mutant plasmid.

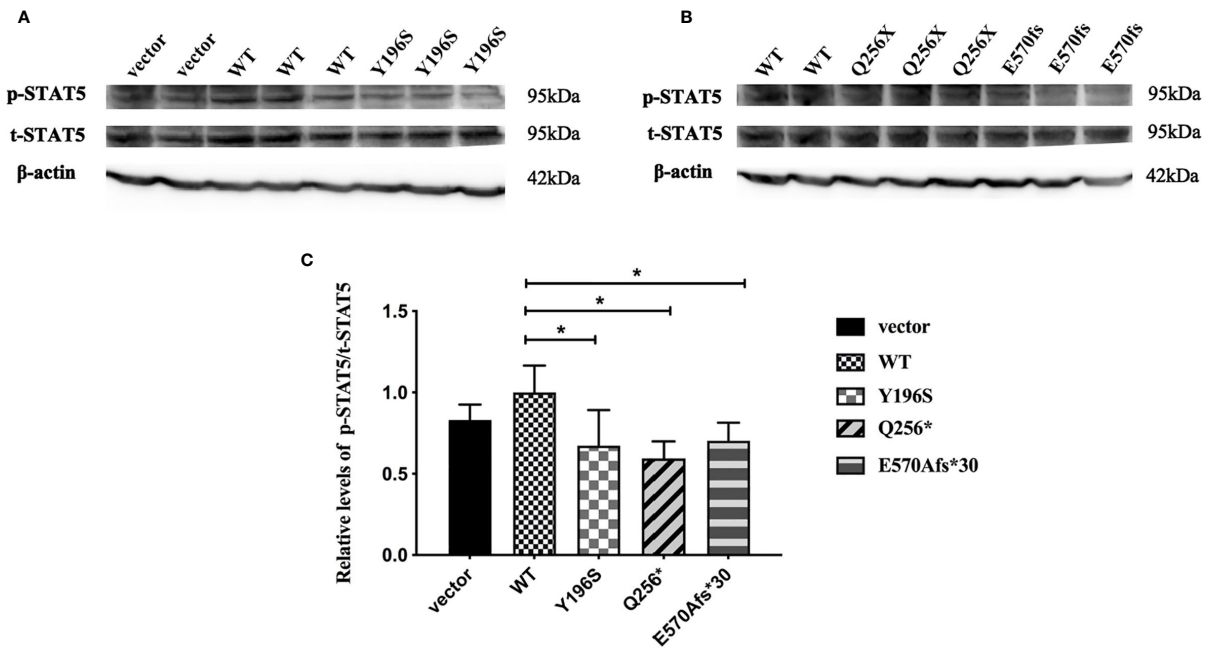

FIGURE 5 | Phosphorylated STAT5 (p-STAT5) expression in HepG2 cells transfected with wild type *GHR* (WT), mutant *GHR* Y196S, Q256* and E570Afs*30 after 100ng/ml rhGH was added in the cell culture medium for 30 minutes. Both p-STAT5 and total STAT5 (t-STAT5) had a molecular weight of around 95 kDa **(A, B)**. The ratio of p-STAT5 to t-STAT5 was converted to gray-scale value by Image J. The expression of p-STAT5 was significantly decreased in *GHR*-Y196S, *GHR*-Q256* and *GHR*-E570Afs*30 when compared to *GHR*-WT as shown in **(C)** (P<0.05).

pattern of GHR protein shown by immunofluorescence assay may be attributed to the mutant GHR-Q256* interfered with the translocation of mature GHR protein from the endoplasmic reticulum to the cell membrane. Western blot analysis demonstrated that the truncated protein had a molecular weight of 43 kDa, and the expression of both GHR and p-STAT5 were remarkably reduced compared to GHR-WT. The c.766C>T *GHR* gene mutation may explain the pathogenesis of the severe growth retardation in patient 3. A novel compound heterozygous mutation of the *GHR* gene, the c.724G>T (p.E224*) in exon 7 and c.981delC in exon 10, was reported by Kaji et al. in a Japanese girl whose height was -7.6 SDS (33). RT-PCR of the lymphocytes and sequencing of its cDNA revealed that no GHR mRNA was measured in the patient, suggesting that neither of the mutant alleles could generate a functional GHR mRNA.

In patient 2, a novel c.808A>G (p.I270V) homozygous missense mutation in the transmembrane domain was identified. *GHR* mutations occurring in the transmembrane domain were extremely rare. To our knowledge, in addition to c.839_875 +1417del (D262Gfs*5) reported by Klammt et al. (27), c.875G>C (p.R274T) reported by Woods et al. (34) and c.800G>A (p.W267*) reported by Rughani et al. (25), the c.808A>G (p.I270V) in the present study was the only mutation located in the transmembrane domain of GHR. The I270V recombinant expression plasmid was not successfully constructed in our study. Therefore, the *in vitro* functional verification of this mutation was not performed in our present study.

Various mutations in the *GHR* gene have been documented, including missense, deletion, nonsense, frameshift, and splice site mutations, which affect the expression of GHR, ligand binding, GHR dimerization, or signal transduction and result in the dysfunction of GHR (4, 17). We performed a literature review to summarize the published *GHR* gene mutation locus as shown in **Figure 6** (detailed information could be found in **Supplementary Table 1**). Among the 120 known *GHR* mutations, 77 mutations occurred extracellularly, 17 occurred in the GHR introns, 17 occurred intracellularly, and 5 occurred in the transmembrane domain (detailed information was shown in **Supplementary Material**). The remaining four mutations were large fragments deletion. Mutations in transmembrane domain were extremely scarce. Storr et al. found that the expression of milder gene defects might show significant variability within each kindred, explaining why some patients were clinically easy to diagnose, whereas others may be under-diagnosed (5). The short stature phenotype did not always parallel the *GHR* gene defect. Among our four patients with LS, patient 3 had the most severe genetic defect, and the loss of function of one *GHR* allele (Q256*) led to a severe height deficit. However, as for patient 1, who manifested a severe

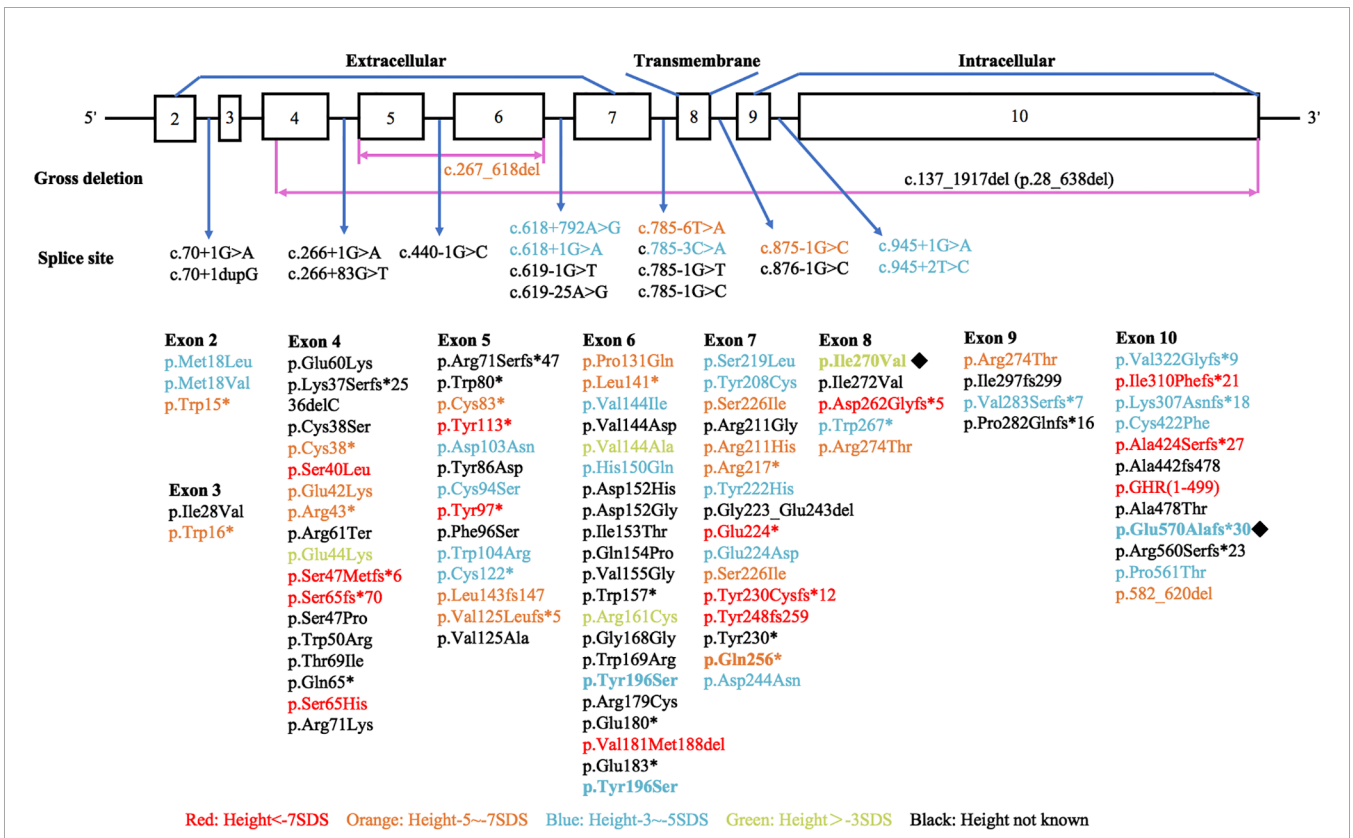

FIGURE 6 | Diagrammatic representation of the human *GHR* gene mutations published in patients with Laron syndrome. Different colors stand for variant severity of height defect. Red stands for patients with height less than -7 SDS, orange stands for patients with height between -5 SDS to -7 SDS, blue stands for patients with height between -3 SDS to -5 SDS, and green stands for patients with height above -3 SDS. Novel mutations found in our present study were labeled with ◆.

short phenotype with a height of -5.49 SDS, no *GHR* gene mutation was detected. Further genetic study about this patient needs to be done in the future.

Recombinant human IGF-1 (rhIGF-1) replacement is the recommended treatment for severe LS (35). However, the efficacy in mild or moderate LS patients remains unclear. Moreover, due to the unavailability of rhIGF-1 in China, the management of patients with LS is difficult. A study of combined rhGH plus rhIGF-1 therapy in children with short stature, low IGF-1 (below -1.0 SD) and normal GH levels assessed growth responses according to the dose of rhIGF-1. In the group receiving the highest dose of rhIGF-1 (150 μg/kg/d) combined with rhGH at 45 μg/kg/d, the year 1 height velocity was 11.2 ± 2.1 compared with 9.3 ± 1.7 cm/y in the group receiving rhGH at 45 μg/kg/d alone (36). rhGH was administered in patient 4 at 57 μg/kg/d for 32 months in our center, and the growth velocity was 6.8 cm/y with the height increased by 17.8 cm in total. The IGF-1 level increased from 25 ng/ml to 64 ng/ml. This finding may be attributed to the direct effect of GH to promote epiphyseal growth. Our clinical experience provides evidence and possibility in growth-promotion with rhGH under circumstance of unavailability of rhIGF-1.

Several limitations existed in our study. Since the phenotype of the patients was typical of LS, we conducted Sanger sequencing of the *GHR* gene, it was unclear whether defects of post-receptor components exist in the GH signal transduction pathway, such as *STAT5B, IGFALS, IGF-1* and *PAPPA2* genes. Besides, overlapping phenotypes and attenuated presentations can complicate the clinical picture, in which whole-exon sequencing or even whole-genome sequencing should be performed to discover underlying genetic abnormalities.

DATA AVAILABILITY STATEMENT

The datasets presented in this study can be found in online repositories. The names of the repository/repositories and accession number(s) can be found below: GenBank [accession: MW701347-MW701349].

ETHICS STATEMENT

The studies involving human participants were reviewed and approved by Ethics Committee of Peking Union Medical College Hospital. Written informed consent to participate in this study was provided by the participants' legal guardian/next of kin. Written informed consent was obtained from the individual(s), and minor(s)' legal guardian/next of kin, for the publication of any potentially identifiable images or data included in this article.

AUTHOR CONTRIBUTIONS

RL conducted the *in vitro* experiments and finished the rough draft. FG and HZ designed the experiments and revised the draft, and FG polished the language. HP supervised the experiments. HL and HM helped with the genetic data analysis. YZ and SC contribute to statistical analysis. LD, HY and LW revised the initial draft and provided useful suggestions. All authors agree to be accountable for the content of the work. All authors contributed to the article and approved the submitted version.

FUNDING

The study was supported by grants of The National Key Research and Development Program of China (No.2016YFC0901501) and the CAMS Innovation Fund for Medical Sciences (CAMS-2016-I2M-1-002).

SUPPLEMENTARY MATERIAL

The Supplementary Material for this article can be found online at: https://www.frontiersin.org/articles/10.3389/fendo.2021.605736/full#supplementary-material

REFERENCES

1. Rosenfeld RG, Rosenbloom AL, Guevara-Aguirre J. Growth hormone (GH) insensitivity due to primary GH receptor deficiency. *Endocr Rev* (1994) 15:369–90. doi: 10.1210/edrv-15-3-369
2. Laron Z, Pertzelan A, Mannheimer S. Genetic pituitary dwarfism with high serum concentation of growth hormone–a new inborn error of metabolism? *Isr J Med Sci* (1966) 2:152–5. doi: 10.1016/j.jtbi.2005.02.019
3. Laron Z. Laron syndrome (primary growth hormone resistance or insensitivity): the personal experience 1958-2003. *J Clin Endocrinol Metab* (2004) 89:1031–44. doi: 10.1210/jc.2003-031033
4. David A, Hwa V, Metherell LA, Netchine I, Camacho-Hubner C, Clark AJ, et al. Evidence for a continuum of genetic, phenotypic, and biochemical abnormalities in children with growth hormone insensitivity. *Endocr Rev* (2011) 32:472–97. doi: 10.1210/er.2010-0023
5. Storr HL, Chatterjee S, Metherell LA, Foley C, Rosenfeld RG, Backeljauw PF, et al. Nonclassical GH Insensitivity: Characterization of Mild Abnormalities of GH Action. *Endocrine Rev* (2019) 40:476–505. doi: 10.1210/er.2018-00146
6. Kofoed EM, Hwa V, Little B, Woods KA, Buckway CK, Tsubaki J, et al. Growth hormone insensitivity associated with a STAT5b mutation. *New Engl J Med* (2003) 349:1139–47. doi: 10.1056/NEJMoa022926
7. Dauber A, Munoz-Calvo MT, Barrios V, Domene HM, Kloverpris S, Serra-Juhe C, et al. Mutations in pregnancy-associated plasma protein A2 cause short stature due to low IGF-I availability. *EMBO Mol Med* (2016) 8:363–74. doi: 10.15252/emmm.201506106
8. Scalco RC, Hwa V, Domene HM, Jasper HG, Belgorosky A, Marino R, et al. STAT5B mutations in heterozygous state have negative impact on height: another clue in human stature heritability. *Eur J Endocrinol* (2015) 173:291–6. doi: 10.1530/EJE-15-0398
9. Domene HM, Bengolea SV, Martinez AS, Ropelato MG, Pennisi P, Scaglia P, et al. Deficiency of the circulating insulin-like growth factor system associated with inactivation of the acid-labile subunit gene. *New Engl J Med* (2004) 350:570–7. doi: 10.1056/NEJMoa013100
10. Hess O, Khayat M, Hwa V, Heath KE, Teitler A, Hritan Y, et al. A novel mutation in IGFALS, c.380T>C (p.L127P), associated with short stature, delayed puberty, osteopenia and hyperinsulinaemia in two siblings: insights

into the roles of insulin growth factor-1 (IGF1). *Clin Endocrinol* (2013) 79:838–44. doi: 10.1111/cen.12200
11. Walenkamp MJ, Losekoot M, Wit JM. Molecular IGF-1 and IGF-1 receptor defects: from genetics to clinical management. *Endocrine Dev* (2013) 24:128–37. doi: 10.1159/000342841
12. Woods KA, Camacho-Hübner C, Savage MO, Clark AJ. Intrauterine growth retardation and postnatal growth failure associated with deletion of the insulin-like growth factor I gene. *New Engl J Med* (1996) 335:1363–7. doi: 10.1056/NEJM199610313351805
13. Abuzzahab MJ, Schneider A, Goddard A, Grigorescu F, Lautier C, Keller E, et al. IGF-I receptor mutations resulting in intrauterine and postnatal growth retardation. *New Engl J Med* (2003) 349:2211–22. doi: 10.1056/NEJMoa010107
14. Barton DE, Foellmer BE, Wood WI, Francke U. Chromosome mapping of the growth hormone receptor gene in man and mouse. *Cytogenet Cell Genet* (1989) 50:137–41. doi: 10.1159/000132743
15. Rapoport TA. Protein translocation across the eukaryotic endoplasmic reticulum and bacterial plasma membranes. *Nature* (2007) 450:663–9. doi: 10.1038/nature06384
16. Rapoport TA, Li L, Park E. Structural and Mechanistic Insights into Protein Translocation. *Annu Rev Cell Dev Biol* (2017) 33:369–90. doi: 10.1146/annurev-cellbio-100616-060439
17. Lin S, Li C, Li C, Zhang X. Growth Hormone Receptor Mutations Related to Individual Dwarfism. *Int J Mol Sci* (2018) 19(5):1–20. doi: 10.3390/ijms19051433
18. Bieniek JM, Kashanian JA, Deibert CM, Grober ED, Lo KC, Brannigan RE, et al. Influence of increasing body mass index on semen and reproductive hormonal parameters in a multi-institutional cohort of subfertile men. *Fertil Steril* (2016) 106:1070–5. doi: 10.1016/j.fertnstert.2016.06.041
19. Yakar S, Liu JL, Stannard B, Butler A, Accili D, Sauer B, et al. Normal growth and development in the absence of hepatic insulin-like growth factor I. *Proc Natl Acad Sci USA* (1999) 96:7324–9. doi: 10.1073/pnas.96.13.7324
20. Wu Y, Sun H, Yakar S, LeRoith D. Elevated levels of insulin-like growth factor (IGF)-I in serum rescue the severe growth retardation of IGF-I null mice. *Endocrinology* (2009) 150:4395–403. doi: 10.1210/en.2009-0272
21. Hwa V, Little B, Adiyaman P, Kofoed EM, Pratt KL, Ocal G, et al. Severe growth hormone insensitivity resulting from total absence of signal transducer and activator of transcription 5b. *J Clin Endocrinol Metab* (2005) 90:4260–6. doi: 10.1210/jc.2005-0515
22. Birzniece V, Sata A, Ho KK. Growth hormone receptor modulators. *Rev Endocr Metab Disord* (2009) 10:145–56. doi: 10.1007/s11154-008-9089-x
23. Rosenfeld RG, Belgorosky A, Camacho-Hubner C, Savage MO, Wit JM, Hwa V. Defects in growth hormone receptor signaling. *Trends Endocrinol Metabol: TEM* (2007) 18:134–41. doi: 10.1016/j.tem.2007.03.004
24. Fang P, Riedl S, Amselem S, Pratt KL, Little BM, Haeusler G, et al. Primary growth hormone (GH) insensitivity and insulin-like growth factor deficiency caused by novel compound heterozygous mutations of the GH receptor gene: genetic and functional studies of simple and compound heterozygous states. *J Clin Endocrinol Metab* (2007) 92:2223–31. doi: 10.1210/jc.2006-2624
25. Rughani A, Zhang D, Vairamani K, Dauber A, Hwa V, Krishnan S. Severe growth failure associated with a novel heterozygous nonsense mutation in the GHR transmembrane domain leading to elevated growth hormone binding protein. *Clin Endocrinol* (2020) 92:331–7. doi: 10.1111/cen.14148
26. Akıncı A, Rosenfeld RG, Hwa V. A novel exonic GHR splicing mutation (c.784G > C) in a patient with classical growth hormone insensitivity syndrome. *Hormone Res Paediatrics* (2013) 79:32–8. doi: 10.1159/000341527
27. Klammt J, Shen S, Kiess W, Kratzsch J, Stobbe H, Vogel M, et al. Clinical and biochemical consequences of an intragenic growth hormone receptor (GHR) deletion in a large Chinese pedigree. *Clin Endocrinol* (2015) 82:453–61. doi: 10.1111/cen.12606
28. Frasier SD. A preview of growth hormone stimulation tests in children. *Pediatrics* (1974) 53:929–37.
29. Roth J, Glick SM, Yalow RS, Bersonsa. Hypoglycemia: a potent stimulus to secretion of growth hormone. *Sci (N Y NY)* (1963) 140:987–8. doi: 10.1126/science.140.3570.987
30. Kurosaki T, Popp MW, Maquat LE. Quality and quantity control of gene expression by nonsense-mediated mRNA decay. *Nat Rev Mol Cell Biol* (2019) 20:406–20. doi: 10.1038/s41580-019-0126-2
31. Milward A, Metherell L, Maamra M, Barahona MJ, Wilkinson IR, Camacho-Hübner C, et al. Growth hormone (GH) insensitivity syndrome due to a GH receptor truncated after Box1, resulting in isolated failure of STAT 5 signal transduction. *J Clin Endocrinol Metab* (2004) 89:1259–66. doi: 10.1210/jc.2003-031418
32. Oh PS KI, Moon YH. *A molecular genetic study on the two Korean patients with Laron syndrome, Program of the 81st Annual Meeting of The Endocrine Society*. San Diego, CA (1999). p. 140.
33. Kaji H, Nose O, Tajiri H, Takahashi Y, Iida K, Takahashi T, et al. Novel compound heterozygous mutations of growth hormone (GH) receptor gene in a patient with GH insensitivity syndrome. *J Clin Endocrinol Metab* (1997) 82:3705–9. doi: 10.1210/jc.82.11.3705
34. Woods KA, Fraser NC, Postel-Vinay MC, Savage MO, Clark AJ. A homozygous splice site mutation affecting the intracellular domain of the growth hormone (GH) receptor resulting in Laron syndrome with elevated GH-binding protein. *J Clin Endocrinol Metab* (1996) 81:1686–90. doi: 10.1210/jcem.81.5.8626815
35. Chernausek SD, Backeljauw PF, Frane J, Kuntze J, Underwood LE. Long-term treatment with recombinant insulin-like growth factor (IGF)-I in children with severe IGF-I deficiency due to growth hormone insensitivity. *J Clin Endocrinol Metab* (2007) 92:902–10. doi: 10.1210/jc.2006-1610
36. Backeljauw PF, Miller BS, Dutailly P, Houchard A, Lawson E, Hale DE, et al. Recombinant human growth hormone plus recombinant human insulin-like growth factor-1 coadministration therapy in short children with low insulin-like growth factor-1 and growth hormone sufficiency: results from a randomized, multicenter, open-label, parallel-group, active treatment-controlled trial. *Hormone Res Paediatrics* (2015) 83:268–79. doi: 10.1159/000371799

Conflict of Interest: The authors declare that the research was conducted in the absence of any commercial or financial relationships that could be construed as a potential conflict of interest.

frontiers in Genetics

ORIGINAL RESEARCH
published: 27 May 2021
doi: 10.3389/fgene.2021.688808

Identification and Tissue-Specific Characterization of Novel SHOX-Regulated Genes in Zebrafish Highlights SOX Family Members Among Other Genes

*Sandra Hoffmann[1,2], Ralph Roeth[1,3], Sabrina Diebold[4], Jasmin Gogel[1], David Hassel[5], Steffen Just[4] and Gudrun A. Rappold[1,2]**

[1]Department of Human Molecular Genetics, Institute of Human Genetics, University Hospital Heidelberg, Heidelberg, Germany, [2]DZHK (German Centre for Cardiovascular Research), Partner Site Heidelberg/Mannheim, Heidelberg, Germany, [3]nCounter Core Facility, Institute of Human Genetics, University of Heidelberg, Heidelberg, Germany, [4]Clinic for Internal Medicine II - Molecular Cardiology, University Hospital Ulm, Ulm, Germany, [5]Department of Internal Medicine III - Cardiology, University Hospital Heidelberg, Heidelberg, Germany

OPEN ACCESS

Edited by:
Liborio Stuppia,
University of Studies G. d'Annunzio Chieti and Pescara, Italy

Reviewed by:
Tsutomu Ogata,
Hamamatsu University School of Medicine, Japan
Emanuele Micaglio,
IRCCS Policlinico San Donato, Italy

***Correspondence:**
Gudrun A. Rappold
gudrun.rappold@med.uni-heidelberg.de

Specialty section:
This article was submitted to Genetics of Common and Rare Diseases, a section of the journal Frontiers in Genetics

Received: 31 March 2021
Accepted: 27 April 2021
Published: 27 May 2021

Citation:
Hoffmann S, Roeth R, Diebold S, Gogel J, Hassel D, Just S and Rappold GA (2021) Identification and Tissue-Specific Characterization of Novel SHOX-Regulated Genes in Zebrafish Highlights SOX Family Members Among Other Genes. Front. Genet. 12:688808. doi: 10.3389/fgene.2021.688808

SHOX deficiency causes a spectrum of clinical phenotypes related to skeletal dysplasia and short stature, including Léri-Weill dyschondrosteosis, Langer mesomelic dysplasia, Turner syndrome, and idiopathic short stature. SHOX controls chondrocyte proliferation and differentiation, bone maturation, and cellular growth arrest and apoptosis *via* transcriptional regulation of its direct target genes *NPPB*, *FGFR3*, and *CTGF*. However, our understanding of SHOX-related pathways is still incomplete. To elucidate the underlying molecular mechanisms and to better understand the broad phenotypic spectrum of *SHOX* deficiency, we aimed to identify novel SHOX targets. We analyzed differentially expressed genes in *SHOX*-overexpressing human fibroblasts (NHDF), and confirmed the known SHOX target genes *NPPB* and *FGFR* among the most strongly regulated genes, together with 143 novel candidates. Altogether, 23 genes were selected for further validation, first by whole-body characterization in developing *shox*-deficient zebrafish embryos, followed by tissue-specific expression analysis in three *shox*-expressing zebrafish tissues: head (including brain, pharyngeal arches, eye, and olfactory epithelium), heart, and pectoral fins. Most genes were physiologically relevant in the pectoral fins, while only few genes were also significantly regulated in head and heart tissue. Interestingly, multiple *sox* family members (*sox5*, *sox6*, *sox8*, and *sox18*) were significantly dysregulated in *shox*-deficient pectoral fins together with other genes (*nppa*, *nppc*, *cdkn1a*, *cdkn1ca*, *cyp26b1*, and *cy26c1*), highlighting an important role for these genes in *shox*-related growth disorders. Network-based analysis integrating data from the Ingenuity pathways revealed that most of these genes act in a common network. Our results provide novel insights into the genetic pathways and molecular events leading to the clinical manifestation of *SHOX* deficiency.

Keywords: short stature, skeletal dysplasia, pectoral fins, zebrafish, *SHOX* deficiency, skeletal disease associations

INTRODUCTION

Linear growth and skeletal development are highly dynamic processes that depend on transcription factors, signaling molecules, and extracellular matrix proteins. Long bones grow by endochondral ossification, a sequential replacement of cartilaginous tissue by bone. The growth plate, located near the ends of the long bones, provides a continuous supply of chondrocytes for endochondral ossification, which is initiated during early fetal development and continues until adolescence (Kronenberg, 2003; Lui et al., 2018). Any failure in this process causes a wide range of skeletal disorders. SHOX is one of several critical factors regulating chondrogenesis in the growth plate (Marchini et al., 2016).

Alterations in *SHOX* expression impairs human growth and causes a spectrum of clinical phenotypes related to skeletal dysplasia and short stature including Léri-Weill dyschondrosteosis, Langer mesomelic dysplasia, Turner syndrome, and idiopathic short and tall stature (Rao et al., 1997; Belin et al., 1998; Shears et al., 1998; Oliveira and Alves, 2011; Fukami et al., 2016; Marchini et al., 2016; Monzani et al., 2019). However, no genotype-phenotype correlation exists in individuals with *SHOX* mutation/deletion within the coding region (Binder et al., 2004), and also downstream enhancer deletions do not seem to greatly differ from those with coding mutations/deletions with respect to phenotypic characteristics and severity (Benito-Sanz et al., 2005; Rosilio et al., 2012). Although the penetrance of *SHOX* deficiency is high, its clinical expression is variable, even among family members (Schiller et al., 2000; Binder, 2011). *CYP26C1* has been identified as a modifier of severity in patients with *SHOX* deficiency, but certainly others will follow that contribute to the variable expressivity (Montalbano et al., 2016).

SHOX is a transcriptional regulator in chondrocyte proliferation and differentiation, bone maturation, cartilage synthesis, and cellular growth arrest and apoptosis *via* its direct target genes *NPPB*, *FGFR3*, and *CTGF* (Marchini et al., 2004, 2007; Decker et al., 2011; Beiser et al., 2014; Hristov et al., 2014). It also promotes linear growth at the growth plate *via* interaction with the SOX trio (SOX5, SOX6, and SOX9; Aza-Carmona et al., 2011). Further characterization of SHOX-dependent networks is critical, not only for elucidating SHOX functions and their link to disease, but also for discovering novel therapeutic targets in SHOX-related disorders.

To better understand the disease mechanisms underlying *SHOX* deficiency, we first performed genome-wide expression profiling in *SHOX*-overexpressing human fibroblasts to uncover novel SHOX target genes. Considering the complexity of the growth plate and the spatiotemporal expression of SHOX during bone development, we aimed to validate the physiological relevance of the identified genes in an animal model.

A *SHOX* ortholog is not present in rodents, so zebrafish has been a valuable model for studying the role of SHOX during development. Zebrafish embryos are excellent models for studying bone physiology and pathology (Carnovali et al., 2019) because they are small, have rapid external development, have a transparent larval body, and can easily be manipulated genetically. Another important consideration is that a *shox* ortholog and conserved non-coding elements (CNEs) are present in the zebrafish genome (Kenyon et al., 2011; Verdin et al., 2015). Several studies have already confirmed that *shox* deficiency impairs early embryonic growth and bone formation in zebrafish and that *shox* morphants have a shorter body length and reduced pectoral fin size (Sawada et al., 2015; Montalbano et al., 2016; Yokokura et al., 2017). Therefore, we used zebrafish as a read-out animal model to validate our putative target genes and confirm their physiological relevance. Our study highlights the importance of various gene families in *shox*-related growth disorders including the cyclin-dependent kinase inhibitors (*CKI*), cytochrome P450 26 subfamily (*CYP26*), natriuretic peptides (*NP*), and SRY-related HMG-box (*SOX*) genes.

MATERIALS AND METHODS

Cell Culture

Normal human dermal fibroblasts (NHDF cells; PromoCell: C12300) were cultured in Dulbecco's Modified Eagle Medium (DMEM; Gibco, Thermo Fisher Scientific), supplemented with 10% fetal bovine serum, penicillin (100 U/ml), and streptomycin (100 µg/ml) in a 5% CO_2-humidified incubator at 37°C. 1×10^6 NHDF cells were transfected with 3.5 µg pcDNA4/TO-*SHOX*-WT using the Amaxa® Human Dermal Fibroblasts Nucleofector® Kit (Lonza) according to the manufacturer's instructions. In control experiments, NHDF were transfected with 3.5 µg pcDNA4/TO-*SHOX*-HM, which encodes a homeodomain-mutant of SHOX leading to the amino acid exchange Y141D.

Microarray Analysis

Gene expression profiling was performed using the Sentrix® HumanRef-8 Expression BeadChips from Illumina according to the manufacturer's protocol. Total RNA from NHDF cells was isolated using Illustra RNAspin Isolation Kit (Cytiva) according to the manufacturer's instructions. For array hybridization, we prepared biotin-labeled cRNA from 250 µg total RNA according to Illumina's recommended sample labeling procedure using the MessageAmp™ II aRNA Amplification Kit (Thermo Fisher Scientific). Hybridization was performed at 58°C in GEX-HCB buffer (Illumina) at a concentration of 100 ng cRNA/µl for 20 h. Microarrays were washed twice in E1BC buffer (Illumina) at room temperature for 5 min. After blocking for 5 min in 1% Blocker Casein in PBS, array signals were developed by a 10 min incubation in 1 µg/ml Cy3-streptavidin (Cytiva) solution and 1% blocking solution. After final wash in E1BC, the arrays were dried and scanned using a Beadstation array scanner. Data extraction was done for all beads individually, and outliers were removed if >2.5 median absolute deviation (MAD). All remaining data points were used for the calculation of the mean average signal and SD for each probe. For each analyzed time point, we compared signals of normalized gene expression of *SHOX*-WT transfected samples to

SHOX-HM transfected controls. Differentially expressed genes were defined by a change in expression of more than 3-fold (*SHOX*-WT/*SHOX*-HM).

Zebrafish Embryos and Microinjections

Zebrafish (*Danio rerio*) were maintained as previously described (Westerfield, 2000). For all morpholino injection procedures, the Tg (myl7:GFP) strain was used (Rottbauer et al., 2006). Morpholino-modified antisense oligonucleotides (MO; Gene Tools) were directed against the exon 2 intron 2 junction in *shox*, causing reduction of pectoral fins as described previously (Montalbano et al., 2016). *Shox* antisense oligonucleotides or a standard control oligonucleotide (MO control), diluted in 0.2 M KCl, were microinjected into one-cell-stage zebrafish embryos (Just et al., 2011).

nCounter Expression Analysis

Zebrafish tissues were isolated at 55 hours post-fertilization (hpf) and total RNA was extracted with the Direct-zol RNA Microprep Kit (Zymo Research) according to the manufacturer's instructions. For each experiment, whole zebrafish embryos (10–15), hearts (30–70), heads (~20), or pectoral fins (30–40) were pooled per condition to obtain 50 ng of input material. Three to five independent experiments (*n*) were performed. mRNA expression levels were measured at the nCounter Core Facility Heidelberg using the nCounter SPRINT Profiler. This RNA quantification technology utilizes a direct digital detection of mRNA molecules and allows multiplexed target measurement in a single reaction with high sensitivity and specificity even with low amounts of input material (50 ng). A detailed probe design is given in **Supplementary Table 1**. The workflow is described at http://www.nanostring.com/elements/workflow. Background correction and data normalization were performed using the nSolver Analysis Software 4.0 (NanoString Technologies). The most stably expressed genes were chosen for normalization based on the geNorm method.

Statistical Analyses

Statistical analysis was carried out using GraphPad Prism 9 (GraphPad Software, La Jolla, CA, United States). For multiple *t*-tests, the two-stage step-up method of Benjamini, Krieger, and Yekutieli with a desired false discovery rate (FDR) of 5% was used to correct the values of *p*. All conditions statistically different from the control were indicated by $*p < 0.05$, $**p < 0.01$, and $***p < 0.001$.

Ingenuity Pathway Analysis

Ingenuity pathway analysis (IPA) is a web-based software application for the evaluation, integration, and interpretation of omics data (Kramer et al., 2014; QIAGEN Inc.).[1] IPA analysis indicates relationships and interactions between genes based on published data. A list of 24 selected genes (including *SHOX*) was uploaded to perform a pathway and core analysis. The core analysis comprises enrichment pathway analysis to identify significant biological processes and molecular functions in which these genes are involved. These include, for example, differentiation and development of chondrocytes, cartilage and connective tissue, as well as growth failure, short stature, and limb defects.

Databases

DisGeNET database (Pinero et al., 2015).[2] This database enables browsing, searching, and analyzing of genetic information linked to human diseases based on expert curated repositories, GWAS catalogues, animal models, and the scientific literature. DisGeNET is a discovery platform containing one of the largest publicly available collections of genes and variants associated to human diseases. The current version of DisGeNET (v7.0) contains 1,134,942 gene-disease associations, between 21,671 genes and 30,170 diseases, disorders, traits, and clinical or abnormal human phenotypes, and 369,554 variant-disease associations, between 194,515 variants and 14,155 diseases, traits, and phenotypes.

RESULTS

SHOX expression is low in tissues and cell lines (Durand et al., 2011) and only detectable at a very low level in mammalian organs during development (**Supplementary Figure 1**). The highest endogenous expression of *SHOX* so far was found in primary human fibroblasts (NHDF; Durand et al., 2011) and zebrafish embryos (Sawada et al., 2015; Montalbano et al., 2016). But even in fibroblasts, expression levels are too low to perform reliable knockdown experiments.

To investigate SHOX regulatory pathways and identify novel SHOX targets, we analyzed transcriptional changes following overexpression of *SHOX* wild type (WT) compared with a functional homeodomain mutant (HM) in NHDF fibroblast cells. *SHOX*-HM was previously detected in a patient with short stature carrying a c.421T>G missense mutation that led to an amino acid exchange (p.Y141D) in the homeodomain, which impairs SHOX function by reducing DNA-binding and transactivation capacity (Schneider et al., 2005). Therefore, this variant is an ideal negative control for differential expression analysis.

Gene expression profiling was carried out in NHDF cells at three different stages: 6, 12, and 24 h after transfection (**Figure 1A**). Whole-genome Illumina HumanRef8 expression beadchips (Human Sentrix-8 V2) were used to measure gene expression at each time point. Normalized expression of *SHOX*-WT was compared with normalized expression of *SHOX*-HM in the cells and displayed as ratios (**Supplementary Tables 2–4**). Microarray data of all three time points were then merged to analyze all differentially expressed genes (**Supplementary Table 5**). Out of 24,500 annotated transcripts targeted by the Illumina expression beadchips, 145 genes were differentially expressed with a more than 3-fold

[1]https://www.qiagenbioinformatics.com/products/ingenuity-pathway-analysis

[2]https://www.disgenet.org/home/

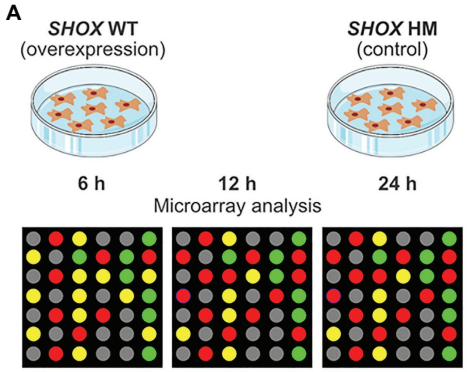

B

6h		12h		24h	
SOX8	6.4	HES5	20.2	SOX8	44.6
HES5	2.5	SOX8	16.2	HES5	36.1
NUAK2	2.3	RRAD	11.5	VGF	22.0
RGS16	2.2	ARC	11.3	ARC	19.8
BCOR	2.1	CYP26B1	8.3	RRAD	17.7
SNF1LK	2.1	VGF	7.4	CYP26B1	17.3
HSPA6	2.1	FGFR3	7.1	RASD1	15.2
LOH3CR2A	1.9	SOX18	6.4	NPPB	12.2
ARC	1.9	KRT17	5.1	FGFR3	10.5
TRIB1	1.9	RASD1	4.4	KRT17	9.9

FIGURE 1 | Microarray analysis of *SHOX* overexpressing wild type (WT) and mutant (HM) normal human dermal fibroblast (NHDF) cells. **(A)** Overview of experimental design. **(B)** Top 10 regulated genes in *SHOX* overexpressing NHDF cells after 6, 12, and 24 h. Identical colors indicate the same genes at different time points. Relative expression ratios are indicated next to the gene's name.

change. Forty-eight genes were downregulated and 97 genes were upregulated upon *SHOX* overexpression. The top 10 upregulated genes at all three time points are shown in **Figure 1B**. At the earliest time point (6 h), only one gene (*SOX8*) was significantly upregulated after *SHOX* overexpression based on a threshold 3-fold change in expression. At 12 and 24 h after transfection, the top 10 differentially expressed genes were all upregulated more than 3-fold (**Figure 1B**).

We identified two known SHOX target genes in the top 10 list – *NPPB* (Marchini et al., 2007) and *FGFR3* (Decker et al., 2011). In addition, we found novel target genes from families already associated with SHOX (**Supplementary Table 6**). These included *SOX8* and *SOX18* of the *SOX* gene family and *CYP26B1* of the *CYP26* gene family. *SOX18*, which was in the top 10 list upon 12 h of *SHOX* expression, fell to position 11 after 24 h despite a 9-fold upregulation. *NPPB* only appeared in the top 10 list after 24 h of *SHOX* expression. To further investigate family-based regulations, we selected further gene members (n = 4) of these families for validation, as well as eight genes that were previously associated with SHOX in the literature. The 11 genes from our list of top-regulated genes (**Figure 1B**) and the additional 12 genes from the literature are summarized in **Table 1**.

We used zebrafish embryos as an *in vivo* model to verify our selected putative SHOX-regulated genes. The expression of the zebrafish orthologs (n = 22; *ARC* does not have an ortholog) was analyzed at 55 hpf after morpholino-mediated knockdown of *shox*. Differential expression was found for 5/22 analyzed genes (*shox2*, *her15.1*, *cdkn1a*, *rasd1*, and *cyp26c1*) after *shox* knockdown using RNA isolated from whole zebrafish embryos (**Figure 2A**). Knockdown efficiency was only nominally significant for *shox* (p = 0.0284; q = 0.0635). To provide a possible explanation for this, we addressed its tissue-specific regulations. Thus, we performed analyses in *shox*-expressing zebrafish tissues from three different regions: pectoral fins, head (brain, pharyngeal arches, eye, and olfactory epithelium), and heart of *shox*-deficient and control embryos at 55 hpf (**Figures 2B–D**).

After *shox* knockdown, *shox* was significantly downregulated in the pectoral fin (p = 0.0149; q = 0.0118) but not in the head (p = 0.0648; q = 0.2381), and nominally significant downregulation was detected in the heart (p = 0.0142; q = 0.0566) as measured by nCounter analysis (**Figures 2B–D**). Almost all analyzed genes (16/22) were significantly dysregulated in the pectoral fins at the developmental time point 55 hpf (**Figure 3**). Of the top 10 regulated genes in NHDF cells, seven were dysregulated in zebrafish fins (*cyp26b1*, *her15.1*, *krt17*, *rasd1*, *sox8a*, *sox18*, and *vgf*), although the regulatory direction was not always the same as in NHDF cells. Interestingly, members of the *sox* and *cki* family were

TABLE 1 | Genes selected for validation.

Gene	6 h	12 h	24 h
ARC	1.9	11.3	19.8
BMP4	1	1	1
CDKN1A	1.2	2.9	5.4
CDKN1B	1.4	0.7	1
CDKN1C	1.1	1.8	5.1
CYP26A1	1.1	1.1	1
CYP26B1	1	8.3	17.3
CYP26C1	1	1.1	1
FGFR3	1.7	7.1	10.5
HES5	2.5	20.2	36.1
KRT17	1.4	5.1	9.9
NPPA	1	1.1	1.4
NPPB	1	1.7	12.2
NPPC	1	0.9	1
RASD1	1.5	4.4	15.2
RRAD	1	11.5	17.7
SHOX2	1	1	1
SOX5	1	1	1
SOX6	1.2	1	1
SOX8	6.4	16.2	44.6
SOX9	1	0.8	0.8
SOX18	1.1	6.4	9.0
VGF	1.1	7.4	22.0

The selection is based on the top regulated genes in SHOX overexpressing NHDF cells after 12 and 24 h (blue; n = 11). Already known SHOX-associated genes are highlighted in green (n = 8) and additionally analyzed members of gene families in light gray (n = 4).

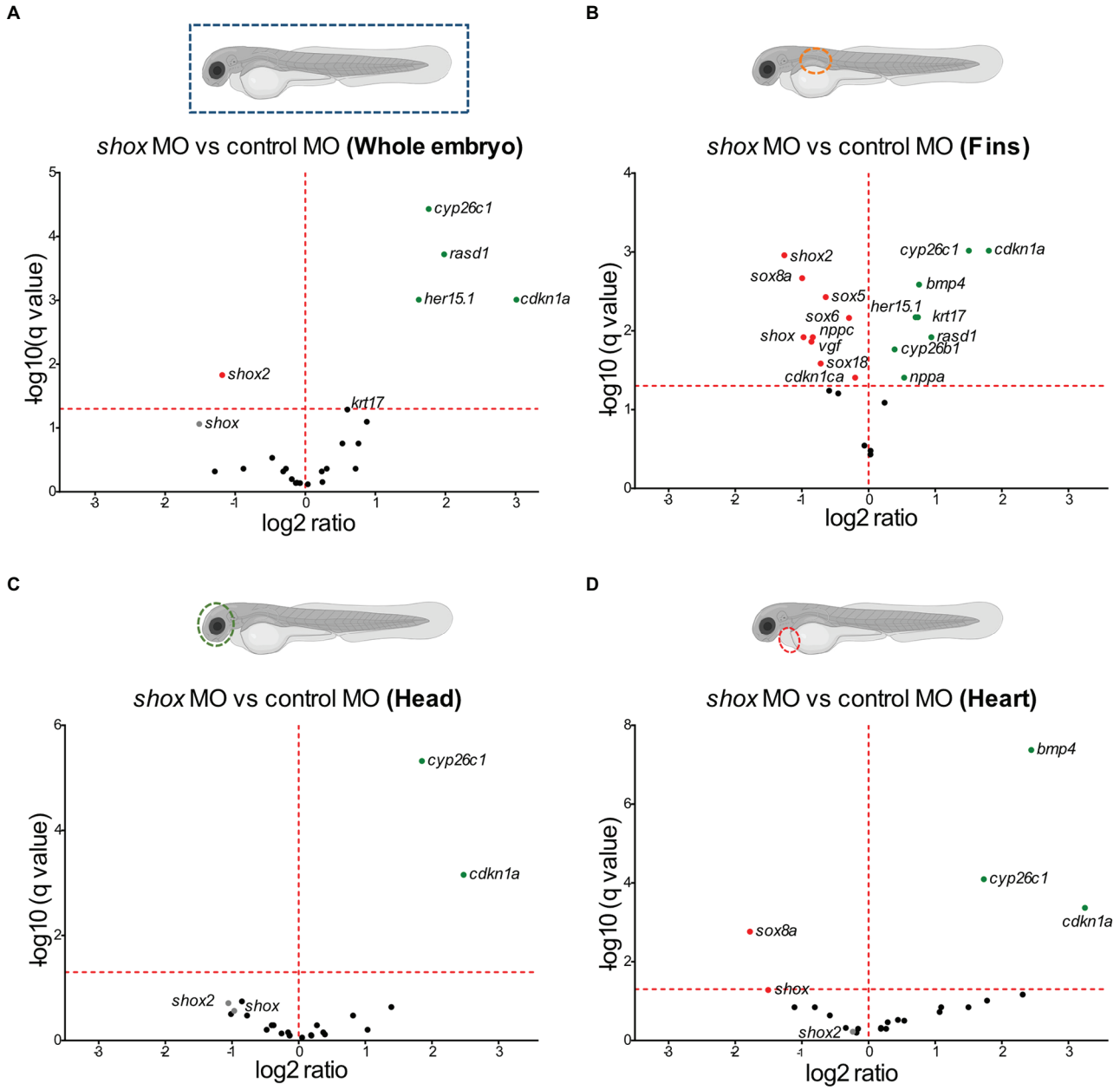

FIGURE 2 | Tissue-specific validation of putative Shox target genes in zebrafish embryos after *shox* knockdown. Volcano plot presentations of expression ratio of selected shox target genes in **(A)** whole zebrafish tissue (n = 6 *shox* MO, n = 6 control MO), **(B)** fins (n = 3 *shox* MO, n = 3 control MO), **(C)** head (n = 4 *shox* MO, n = 4 control MO), and **(D)** heart (n = 4 *shox* MO, n = 5 control MO) at 55 hours post-fertilization (hpf) after morpholino-mediated knockdown of shox compared to controls. Genes above the red horizontal dashed line are significantly regulated. Genes shown to the left of the dashed vertical line are downregulated, those on the right are upregulated. Statistical significance was determined by multiple unpaired t-tests adjusted by the two-stage step-up method of Benjamini, Krieger, and Yekutieli (adjusted values of $p = q$-values). MO, morpholino.

significantly dysregulated in the pectoral fin (**Figure 4**), highlighting the important role of these gene families in Shox-related growth defects.

To identify transcriptional pathways in which the novel SHOX-dependent genes play a role, we performed a functional network analysis, integrating the 23 selected genes with SHOX using the IPA software tool. Our analysis demonstrates that the majority of the newly identified/selected genes are connected within the same network of the known SHOX-regulated genes (except *CYP26A1*, *RASD1*, and *SOX18*). We also identified significant biological processes and molecular functions that involve these genes (**Supplementary Table 7**). These included differentiation and development of chondrocytes, cartilage, and connective tissue. The most

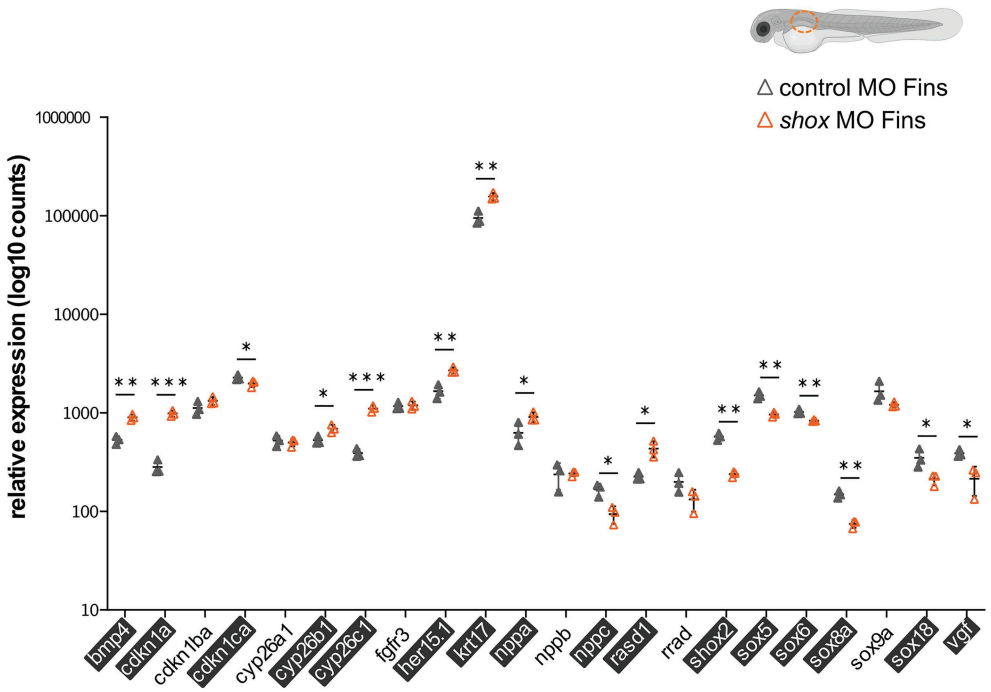

FIGURE 3 | Validation of putative Shox target genes in zebrafish fins. Tissue-specific analysis of all selected shox targets upon morpholino-mediated *shox* knockdown in zebrafish fins 55 hpf (orange) compared to controls (gray); $n = 3$ experiments per condition. Significantly regulated genes are highlighted. For *ARC*, no Zebrafish otholog exists. *HES5* corresponds to *her15.1* in zebrafish. Statistical significance was determined by multiple unpaired *t*-tests adjusted by the two-stage step-up method of Benjamini, Krieger, and Yekutieli (adjusted values of *p* are indicated by $^{*}p < 0.05$; $^{**}p < 0.01$; and $^{***}p < 0.001$). MO, morpholino; hpf, hours post-fertilization.

important annotated pathways relevant to SHOX-associated diseases included genes involved in growth failure, short stature, and limb defects (**Figure 5A**).

To predict the pathological relevance of the SHOX-regulated genes, we used the DisGeNET database (see footnote 2; Pinero et al., 2015) to summarize the known disease associations for each of the selected 23 genes (**Figure 5B**). Thirteen genes were associated with skeletal phenotypes such as short stature, skeletal abnormalities, and height; 10 genes had no such associations to date and, therefore, might represent novel candidates for skeletal disease.

DISCUSSION

Identifying SHOX-regulated genes is essential to understanding how SHOX signaling exerts its diverse effects in individuals with *SHOX* deficiency. To identify novel target genes, we compared the transcriptional activity of wild type SHOX with a non-functional mutant form of SHOX in NHDF cells by microarray analysis. Although derived from human fibroblasts, NHDF cells do not fully reflect the situation in the growth plate. Despite this limitation, all identified 145 differentially up- and downregulated target genes downstream of SHOX can now be further investigated as candidates for various disorders. The proteins encoded by this list of SHOX-regulated genes are implicated in a wide variety of functions, consistent with the diverse effects of SHOX on development (Marchini et al., 2016). These functions include chondrocyte proliferation and differentiation, bone maturation, cartilage synthesis, cellular growth arrest, and apoptosis. Some genes represent known direct targets or have been previously associated with SHOX, but most are unknown SHOX-regulated genes. The known SHOX target genes *NPPB* and *FGFR3* (Marchini et al., 2007; Decker et al., 2011) were among the top regulated genes after 12 and 24 h of overexpression. These findings show that NHDF cells are a valid and valuable model for analyzing the gene networks regulated by SHOX *in vitro*.

Considering the complexity of bone development and the spatiotemporal expression of *SHOX*, 11 of the upregulated and 12 additional genes were chosen for *in vivo* validation in zebrafish. Previous evidence has highlighted the role of SHOX as a transcriptional activator (Rao et al., 2001); therefore, we focused in this study only on those transcripts that were upregulated in NHDF cells and selected these for validation. *Shox* knockdown in whole zebrafish embryos altered embryonic growth and bone formation as previously described (Sawada et al., 2015; Montalbano et al., 2016; Yokokura et al., 2017). Gene expression analysis in *shox*-deficient whole zebrafish embryos also demonstrated a significant downregulation of *shox2*, the only *shox* paralog, and upregulation of four selected target candidates (*cyp26c1*, *rasd1*, *her15.1*, and *cdkn1a*). A *shox2*-associated cardiac phenotype is not present in whole embryos (Blaschke et al., 2007; Hoffmann et al., 2013), despite

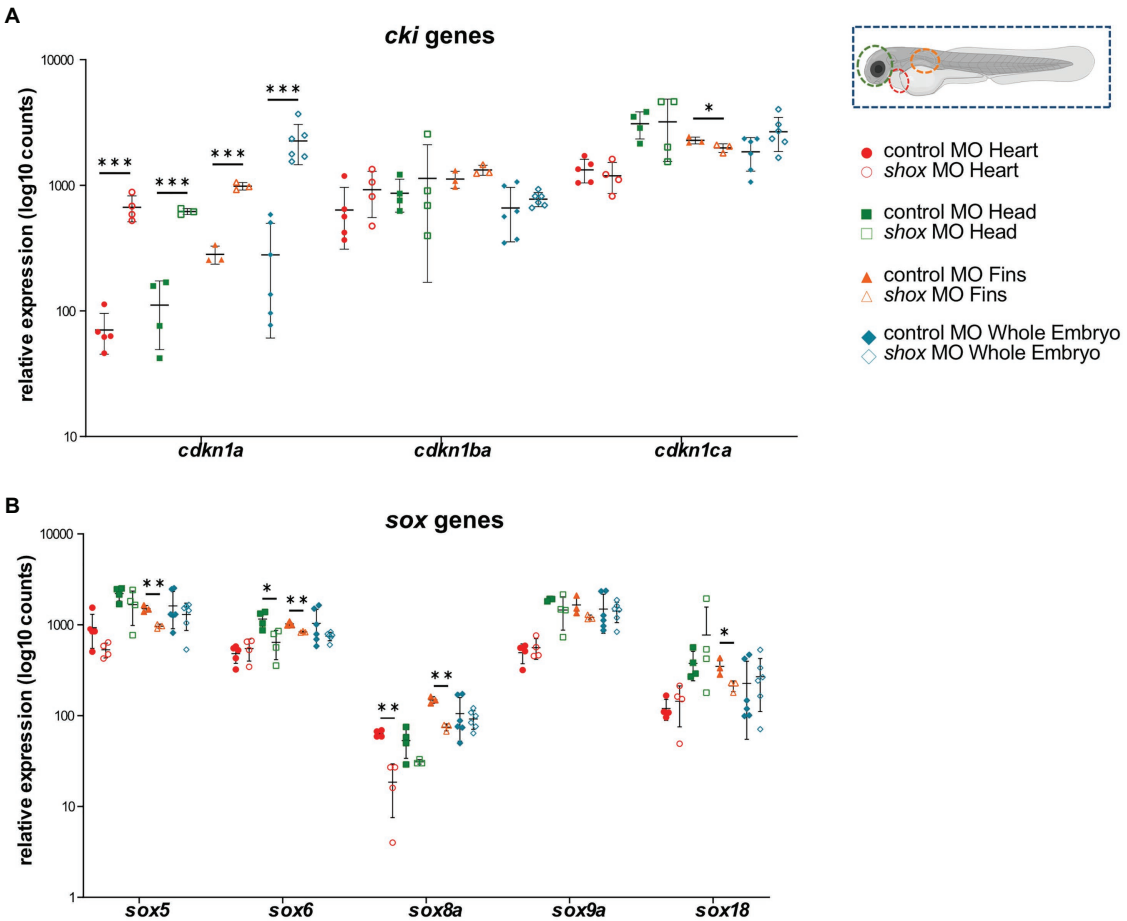

FIGURE 4 | Tissue-specific analysis of gene families upon morpholino-mediated *shox* knockdown in zebrafish embryos 55 hpf compared to controls. Relative expression levels for **(A)** the cyclin-dependent kinase inhibitor (*cki*) family members *cdkn1a*, *cdkn1ba*, and *cdkn1ca*; **(B)** members of the SRY-related HMG-box (*sox*) genes *sox5*, *sox6*, *sox8a*, *sox9a*, and *sox18* in heart (red; $n = 4$–5), head (green; $n = 4$), fin (orange; $n = 3$) or whole embryo (blue; $n = 6$). Statistical significance was determined by multiple unpaired *t*-tests adjusted by the two-stage step-up method of Benjamini, Krieger, and Yekutieli (adjusted values of *p* are indicated as $^{*}p < 0.05$, $^{**}p < 0.01$, and $^{***}p < 0.001$). MO, morpholino.

its strong downregulation ($p = 0.0029$; $q = 0.0010$) and known role in the orchestration of heart function.

To uncover any tissue-specific differences in SHOX-mediated gene expression, we performed separate analyses in fin, heart, and head tissue. Some genes (e.g., *shox2*) were downregulated in fin and head tissue after *shox* knockdown but not in heart tissue. This explains why we did not observe a cardiac phenotype in these embryos (**Figure 2**). *Bmp4* and *sox8a* were significantly dysregulated in fin and heart but not in whole zebrafish embryos, indicating the importance of tissue-specific analyses to identify cell-specific effects that may not be detected in whole embryos.

A more specific investigation, particularly in the fins, provided further insight: indeed, 16 of the 22 analyzed target candidates revealed significantly differential expression in zebrafish fins. The most downregulated gene was *shox2*, while *cdkn1a* was the most upregulated one. SHOX and SHOX2 proteins are known to interact (Aza-Carmona et al., 2014), but this is the first published evidence that *shox2* is a downstream target of Shox in the zebrafish fin. *Cdkn1a*, on the other hand, is a known cellular mediator of SHOX and is upregulated in *SHOX*-expressing cells (Marchini et al., 2004); however, we observed an upregulation of *cdkn1a* after *shox* knockdown in zebrafish fins. The known SHOX targets *NPPB* and *FGFR3* were dysregulated in NHDF cells but not in zebrafish. Different directions of regulation in different model systems have been observed for SHOX targets. SHOX was shown to positively regulate *FGFR3* expression in NHDF cells, confirming our results, but *Shox* overexpression in limb bud-derived chicken micromass cultures resulted in downregulation of *Fgfr3* and may explain the almost mutually exclusive expression patterns of *Fgfr3* and *Shox* in embryonic chicken limbs (Decker et al., 2011). Tissue-specific and cofactor-dependent opposing regulation of genes by specific transcription factors has been reported before (Lambert et al., 2018). Cofactors (coactivator or corepressor) vary in their availability and interaction with transcription factors in different tissues and this variation mediates distinct cell-specific effects. For example, *Bmp4* is a direct transcriptional target of Shox2 and is positively regulated

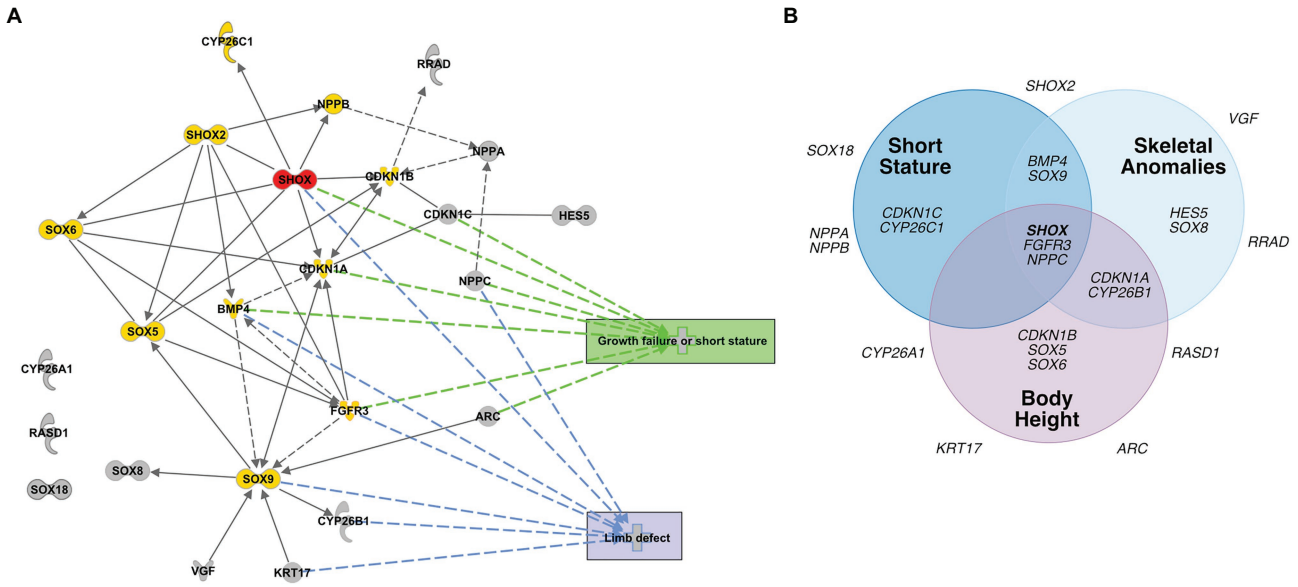

FIGURE 5 | Database analyses of SHOX-regulated genes. **(A)** Network-based pathway analysis of SHOX-regulated genes using the Ingenuity pathway analysis (IPA) software. SHOX is highlighted in red. Known SHOX-associated genes are shown in yellow. Novel SHOX-regulated genes are shown in gray. Direct regulations are indicated by arrows and interactions as lines; indirect regulations or interactions are presented as dotted arrows/lines, respectively. The most important annotated pathways relevant to SHOX-associated diseases or function are highlighted in green (genes involved in growth failure and short stature) and blue (genes involved in limb defects). **(B)** Gene-disease association according to DisGeNET. Venn diagram showing associations between SHOX and 23 SHOX-regulated genes with respect to skeletal phenotypes based on the DisGeNET database (https://www.disgenet.org/home/; Pinero et al., 2015).

during cardiogenesis, whereas an opposite regulation has been described in limb development (Yu et al., 2007; Puskaric et al., 2010; Bobick and Cobb, 2012). This may explain why some genes that are upregulated after *SHOX* overexpression in NHDF cells are not downregulated after *shox* knockdown in zebrafish fins. Yet, differential expression was identified for many genes in both zebrafish and human cells, indicating conserved regulatory mechanisms between these two species.

Multiple members of the sex determining region Y-box (*sox*) family (*sox5*, *sox6*, *sox8a*, and *sox18*) were shown to be significantly dysregulated in *shox*-deficient pectoral fins among other genes (*nppa*, *nppc*, *cdkn1a*, *cdkn1ca*, *cyp26b1*, and *cyp26c1*), highlighting the important role of various gene family members in Shox-related growth disorders. SHOX is known to interact with the SOX trio (SOX5/SOX6 and SOX9; Aza-Carmona et al., 2011), but we show for the first time that Shox transcriptionally regulates *sox5* and *sox6* but not *sox9*. Knockdown of *Sox6* downregulates *Shox* expression in chicken (Lin et al., 2018), suggesting a reciprocal regulation between *shox* and *sox6*. Two other SOX family members, *SOX8* and *SOX18*, were among the most upregulated genes in NHDF cells and confirmed to be significantly downregulated in *shox*-deficient pectoral fins. Among the SOX proteins, SOX9 exhibits the closest similarity to SOX8 (Schepers et al., 2000), but the role of SOX8 during chondrogenesis is not completely understood. *SOX8* is highly upregulated during chondrogenesis *in vitro*, most likely under the control of SOX9 and both together with SOX5 and SOX6 are required for transcription of *COL2A1* and many other chondrogenic molecules (Herlofsen et al., 2014). Thus, *SOX8/sox8a* might promote chondrogenesis *via* a *SHOX/shox* network. *SOX18* silencing significantly induces cell cycle arrest and apoptosis, and inhibits cell migration, invasion, and cell growth *in vitro* and *in vivo*. In contrast, *SOX18* is overexpressed in osteosarcoma, and promotes cell proliferation, migration, and invasion, inhibiting cell cycle arrest and apoptosis (Zhu et al., 2018). Given the role of SHOX as a modulator of cell proliferation and apoptosis (Marchini et al., 2004; Hristov et al., 2014), shox-dependent regulation of *sox18* might play a role in these processes.

Other interesting gene family members regulated by Shox are the cyclin-dependent kinase inhibitor 1 (*cki*) genes. Two members, *CDKN1A* and *CDKN1B*, have previously been reported as cellular mediators of SHOX. In human osteosarcoma cells, the induction of *SHOX* expression elevates *CDKN1A* and *CDKN1B* levels (Marchini et al., 2004). Together with *CDKN1C*, this gene family contributes to the regulation of cell cycle progression by regulating the activity of cell cycle kinases during chondrogenic differentiation (Yan et al., 1997; Negishi et al., 2001; Bellosta et al., 2003; Rentsendorj et al., 2010; Cardelli et al., 2013). In *shox*-deficient zebrafish fins, *cdkn1a* was strongly upregulated, *cdkn1ba* was not affected, and the third family member, *cdkn1ca*, was downregulated. This gene family provides another example of differential regulation depending on the cell and tissue type. CKI family members are well-connected in the SHOX-dependent gene regulatory network (**Figure 5A**), suggesting a role in chondrocyte proliferation, controlled by SHOX-dependent regulation. FGFR3 signaling induces *CDKN1A* expression (Su et al., 1997; Nakajima et al., 2003), so may directly link *SHOX* and *CDKN1A*.

The three members of the cytochrome P450 family 26, *CYP26A1*, *CYP26B1*, and *CYP26C1*, encode retinoic acid metabolizing enzymes involved in chondrogenesis (Pennimpede et al., 2010; Cunningham and Duester, 2015). *CYP26C1* is a genetic modifier of *SHOX* deficiency and downregulates *shox* expression in zebrafish (Montalbano et al., 2016). Moreover, *CYP26C1* variants cause isolated short stature in the absence of *SHOX* deficiency (Montalbano et al., 2018). Here, we show that *shox* knockdown significantly upregulates *cyp26c1* in zebrafish fins. This reciprocal regulation might maintain the delicate balance of retinoic acid levels during fin development. In addition, we observed dysregulation of *CYP26B1*/*cyp26b1* in NHDF cells and zebrafish fins, while *cyp26a1* was not affected by Shox. *Cyp26b1* regulates osteogenesis in the axial skeleton as indicated by the zebrafish *stocksteif* mutant (Spoorendonk et al., 2008). The detailed relationship between *CYP26B1* and *SHOX* deficiency so far remains unclear.

Our tissue-specific validation approach also indicates new roles for Shox during different embryonic developmental processes, including neuronal development and cardiogenesis, similar to/reminiscent of its paralog Shox2 (Yu et al., 2007; Vickerman et al., 2011; Liu et al., 2012; Ha and Dougherty, 2018; Hu et al., 2018). Shox2-regulated targets, such as *Bmp4* and *Nppb*, are involved in various biological processes such as heart and limb development (Yu et al., 2007; Puskaric et al., 2010; Aza-Carmona et al., 2014; Hoffmann et al., 2017).

The differential expression of *sox8a*, *bmp4*, *cyp26c1*, and *cdkn1a* in *shox*-deficient zebrafish hearts was clearly a Shox-specific effect since *shox2* expression was unaffected in this tissue, so did not have any indirect regulatory effects. While *shox* expression has previously been described in the zebrafish heart (Kenyon et al., 2011; Sawada et al., 2015), the role of shox during cardiogenesis remains unclear and requires further analysis in this model.

Shox-regulated gene expression in head tissue of zebrafish embryos also indicated a possible role for SHOX in brain development or neurodevelopmental disease. Microduplications at the pseudoautosomal SHOX locus have already been identified in patients with autism spectrum disorders (ASD) and related neurodevelopmental conditions (Tropeano et al., 2016). It is interesting to note that 17 of the 23 investigated genes are also associated with neuronal phenotypes including neurodegenerative diseases, intellectual disability/ASD, and psychiatric disorders (**Supplementary Figure 2**).

Evidence from both human and animal models has supported the notion that the genetic network involving *SHOX*, *FGFR3*, *NPPC*, among others, is an important regulator of growth. Mutations in these genes have not only been shown to cause rare skeletal malformations but also to contribute to the common forms of height (Rao et al., 1997; Ogata et al., 2000; Toydemir et al., 2006; Bocciardi et al., 2007; Tassano et al., 2013; Estrada et al., 2021). The target genes identified in this study add new members to this network which may contribute to rare skeletal forms or common forms of height and thus represent novel candidates for tall or short stature or other skeletal anomalies. Damaging mutations in these target genes may explain clinical phenotypes, e.g., short stature. As shown in **Figure 5**, some of the novel identified SHOX target genes have already been associated with a skeletal phenotype.

In conclusion, we have identified novel SHOX targets, many of which are consistent with known SHOX functions in limb development, and thereby provide novel insights into the genetic pathways leading to the clinical manifestation of *SHOX* deficiency. In addition, our tissue-specific approach suggests that some target genes may also play a role in other organs, such as heart and brain, indicating a pleiotropic role for SHOX in different phenotypic traits.

DATA AVAILABILITY STATEMENT

The datasets generated and analyzed for this study can be found in the public NCBI GEO database (GSE169732) and can be accessed *via* https://www.ncbi.nlm.nih.gov/geo/query/acc.cgi?acc=GSE169732.

ETHICS STATEMENT

Ethical review and approval was not required for the animal study because only zebrafish embryos at early life stages (55 hpf) were used in this study.

AUTHOR CONTRIBUTIONS

SH and GR designed the study and experimental design and wrote the manuscript. Material preparation, acquisition, and data analysis were performed by SH, RR, SD, JG, DH, and SJ. All authors contributed to the article and approved the submitted version.

FUNDING

This work was funded by the Deutsche Forschungsgemeinschaft (DFG; RA 380/12-1) and University of the Medical Faculty, Heidelberg (9422170). We acknowledge financial support within the funding program Open Access Publishing, by the Baden-Wuerttemberg Ministry of Science, Research and the Arts and by the Ruprecht-Karls-Universität Heidelberg.

ACKNOWLEDGMENTS

We are indebted to Sebastian Bender and Stephan Wolf, who started this project using NHDF cells. We thank the nCounter Core Facility Heidelberg (head: Beate Niesler) for technical support and Claire Bacon for reading the manuscript.

SUPPLEMENTARY MATERIAL

The Supplementary Material for this article can be found online at: https://www.frontiersin.org/articles/10.3389/fgene.2021.688808/full#supplementary-material

REFERENCES

Aza-Carmona, M., Barca-Tierno, V., Hisado-Oliva, A., Belinchon, A., Gorbenko-Del Blanco, D., Rodriguez, J. I., et al. (2014). NPPB and ACAN, two novel SHOX2 transcription targets implicated in skeletal development. *PLoS One* 9:e83104. doi: 10.1371/journal.pone.0083104

Aza-Carmona, M., Shears, D. J., Yuste-Checa, P., Barca-Tierno, V., Hisado-Oliva, A., Belinchon, A., et al. (2011). SHOX interacts with the chondrogenic transcription factors SOX5 and SOX6 to activate the aggrecan enhancer. *Hum. Mol. Genet.* 20, 1547–1559. doi: 10.1093/hmg/ddr032

Beiser, K. U., Glaser, A., Kleinschmidt, K., Scholl, I., Roth, R., Li, L., et al. (2014). Identification of novel SHOX target genes in the developing limb using a transgenic mouse model. *PLoS One* 9:e98543. doi: 10.1371/journal.pone.0098543

Belin, V., Cusin, V., Viot, G., Girlich, D., Toutain, A., Moncla, A., et al. (1998). SHOX mutations in dyschondrosteosis (Leri-Weill syndrome). *Nat. Genet.* 19, 67–69. doi: 10.1038/ng0198-67

Bellosta, P., Masramon, L., Mansukhani, A., and Basilico, C. (2003). p21(WAF1/CIP1) acts as a brake in osteoblast differentiation. *J. Bone Miner. Res.* 18, 818–826. doi: 10.1359/jbmr.2003.18.5.818

Benito-Sanz, S., Thomas, N. S., Huber, C., Gorbenko Del Blanco, D., Aza-Carmona, M., Crolla, J. A., et al. (2005). A novel class of Pseudoautosomal region 1 deletions downstream of SHOX is associated with Leri-Weill dyschondrosteosis. *Am. J. Hum. Genet.* 77, 533–544. doi: 10.1086/449313

Binder, G. (2011). Short stature due to SHOX deficiency: genotype, phenotype, and therapy. *Horm. Res. Paediatr.* 75, 81–89. doi: 10.1159/000324105

Binder, G., Renz, A., Martinez, A., Keselman, A., Hesse, V., Riedl, S. W., et al. (2004). SHOX haploinsufficiency and Leri-Weill dyschondrosteosis: prevalence and growth failure in relation to mutation, sex, and degree of wrist deformity. *J. Clin. Endocrinol. Metab.* 89, 4403–4408. doi: 10.1210/jc.2004-0591

Blaschke, R. J., Hahurij, N. D., Kuijper, S., Just, S., Wisse, L. J., Deissler, K., et al. (2007). Targeted mutation reveals essential functions of the homeodomain transcription factor Shox2 in sinoatrial and pacemaking development. *Circulation* 115, 1830–1838. doi: 10.1161/CIRCULATIONAHA.106.637819

Bobick, B. E., and Cobb, J. (2012). Shox2 regulates progression through chondrogenesis in the mouse proximal limb. *J. Cell Sci.* 125, 6071–6083. doi: 10.1242/jcs.111997

Bocciardi, R., Giorda, R., Buttgereit, J., Gimelli, S., Divizia, M. T., Beri, S., et al. (2007). Overexpression of the C-type natriuretic peptide (CNP) is associated with overgrowth and bone anomalies in an individual with balanced t(2,7) translocation. *Hum. Mutat.* 28, 724–731. doi: 10.1002/humu.20511

Cardelli, M., Zirngibl, R. A., Boetto, J. F., Mckenzie, K. P., Troy, T. C., Turksen, K., et al. (2013). Cartilage-specific overexpression of ERRgamma results in Chondrodysplasia and reduced chondrocyte proliferation. *PLoS One* 8:e81511. doi: 10.1371/journal.pone.0081511

Carnovali, M., Banfi, G., and Mariotti, M. (2019). Zebrafish models of human skeletal disorders: embryo and adult swimming together. *Biomed. Res. Int.* 2019:1253710. doi: 10.1155/2019/1253710

Cunningham, T. J., and Duester, G. (2015). Mechanisms of retinoic acid signalling and its roles in organ and limb development. *Nat. Rev. Mol. Cell Biol.* 16, 110–123. doi: 10.1038/nrm3932

Decker, E., Durand, C., Bender, S., Rodelsperger, C., Glaser, A., Hecht, J., et al. (2011). FGFR3 is a target of the homeobox transcription factor SHOX in limb development. *Hum. Mol. Genet.* 20, 1524–1535. doi: 10.1093/hmg/ddr030

Durand, C., Roeth, R., Dweep, H., Vlatkovic, I., Decker, E., Schneider, K. U., et al. (2011). Alternative splicing and nonsense-mediated RNA decay contribute to the regulation of SHOX expression. *PLoS One* 6:e18115. doi: 10.1371/journal.pone.0018115

Estrada, K., Froelich, S., Wuster, A., Bauer, C. R., Sterling, T., Clark, W. T., et al. (2021). Identifying therapeutic drug targets using bidirectional effect genes. *Nat. Commun.* 12:2224. doi: 10.1038/s41467-021-21843-8

Fukami, M., Seki, A., and Ogata, T. (2016). SHOX haploinsufficiency as a cause of syndromic and nonsyndromic short stature. *Mol. Syndromol.* 7, 3–11. doi: 10.1159/000444596

Ha, N. T., and Dougherty, K. J. (2018). Spinal Shox2 interneuron interconnectivity related to function and development. *eLife* 7:e42519. doi: 10.7554/eLife.42519

Herlofsen, S. R., Hoiby, T., Cacchiarelli, D., Zhang, X., Mikkelsen, T. S., and Brinchmann, J. E. (2014). Brief report: importance of SOX8 for in vitro chondrogenic differentiation of human mesenchymal stromal cells. *Stem Cells* 32, 1629–1635. doi: 10.1002/stem.1642

Hoffmann, S., Berger, I. M., Glaser, A., Bacon, C., Li, L., Gretz, N., et al. (2013). Islet1 is a direct transcriptional target of the homeodomain transcription factor Shox2 and rescues the Shox2-mediated bradycardia. *Basic Res. Cardiol.* 108:339. doi: 10.1007/s00395-013-0339-z

Hoffmann, S., Schmitteckert, S., Griesbeck, A., Preiss, H., Sumer, S., Rolletschek, A., et al. (2017). Comparative expression analysis of Shox2-deficient embryonic stem cell-derived sinoatrial node-like cells. *Stem Cell Res.* 21, 51–57. doi: 10.1016/j.scr.2017.03.018

Hristov, G., Marttila, T., Durand, C., Niesler, B., Rappold, G. A., and Marchini, A. (2014). SHOX triggers the lysosomal pathway of apoptosis via oxidative stress. *Hum. Mol. Genet.* 23, 1619–1630. doi: 10.1093/hmg/ddt552

Hu, W., Xin, Y., Zhao, Y., and Hu, J. (2018). Shox2: the role in differentiation and development of cardiac conduction system. *Tohoku J. Exp. Med.* 244, 177–186. doi: 10.1620/tjem.244.177

Just, S., Berger, I. M., Meder, B., Backs, J., Keller, A., Marquart, S., et al. (2011). Protein kinase D2 controls cardiac valve formation in zebrafish by regulating histone deacetylase 5 activity. *Circulation* 124, 324–334. doi: 10.1161/CIRCULATIONAHA.110.003301

Kenyon, E. J., Mcewen, G. K., Callaway, H., and Elgar, G. (2011). Functional analysis of conserved non-coding regions around the short stature hox gene (shox) in whole zebrafish embryos. *PLoS One* 6:e21498. doi: 10.1371/journal.pone.0021498

Kramer, A., Green, J., Pollard, J. Jr., and Tugendreich, S. (2014). Causal analysis approaches in ingenuity pathway analysis. *Bioinformatics* 30, 523–530. doi: 10.1093/bioinformatics/btt703

Kronenberg, H. M. (2003). Developmental regulation of the growth plate. *Nature* 423, 332–336. doi: 10.1038/nature01657

Lambert, S. A., Jolma, A., Campitelli, L. F., Das, P. K., Yin, Y., Albu, M., et al. (2018). The human transcription factors. *Cell* 175, 598–599. doi: 10.1016/j.cell.2018.01.029

Lin, S., Lin, X., Zhang, Z., Jiang, M., Rao, Y., Nie, Q., et al. (2018). Copy number variation in SOX6 contributes to chicken muscle development. *Gene* 9:42. doi: 10.3390/genes9010042

Liu, H., Espinoza-Lewis, R. A., Chen, C., Hu, X., Zhang, Y., and Chen, Y. (2012). The role of Shox2 in SAN development and function. *Pediatr. Cardiol.* 33, 882–889. doi: 10.1007/s00246-012-0179-x

Lui, J. C., Jee, Y. H., Garrison, P., Iben, J. R., Yue, S., Ad, M., et al. (2018). Differential aging of growth plate cartilage underlies differences in bone length and thus helps determine skeletal proportions. *PLoS Biol.* 16:e2005263. doi: 10.1371/journal.pbio.2005263

Marchini, A., Hacker, B., Marttila, T., Hesse, V., Emons, J., Weiss, B., et al. (2007). BNP is a transcriptional target of the short stature homeobox gene SHOX. *Hum. Mol. Genet.* 16, 3081–3087. doi: 10.1093/hmg/ddm266

Marchini, A., Marttila, T., Winter, A., Caldeira, S., Malanchi, I., Blaschke, R. J., et al. (2004). The short stature homeodomain protein SHOX induces cellular growth arrest and apoptosis and is expressed in human growth plate chondrocytes. *J. Biol. Chem.* 279, 37103–37114. doi: 10.1074/jbc.M307006200

Marchini, A., Ogata, T., and Rappold, G. A. (2016). A track record on SHOX: from basic research to complex models and therapy. *Endocr. Rev.* 37, 417–448. doi: 10.1210/er.2016-1036

Montalbano, A., Juergensen, L., Fukami, M., Thiel, C. T., Hauer, N. H., Roeth, R., et al. (2018). Functional missense and splicing variants in the retinoic acid catabolizing enzyme CYP26C1 in idiopathic short stature. *Eur. J. Hum. Genet.* 26, 1113–1120. doi: 10.1038/s41431-018-0148-9

Montalbano, A., Juergensen, L., Roeth, R., Weiss, B., Fukami, M., Fricke-Otto, S., et al. (2016). Retinoic acid catabolizing enzyme CYP26C1 is a genetic modifier in SHOX deficiency. *EMBO Mol. Med.* 8, 1455–1469. doi: 10.15252/emmm.201606623

Monzani, A., Babu, D., Mellone, S., Genoni, G., Fanelli, A., Prodam, F., et al. (2019). Co-occurrence of genomic imbalances on Xp22.1 in the SHOX region and 15q25.2 in a girl with short stature, precocious puberty, urogenital malformations and bone anomalies. *BMC Med. Genet.* 12:5. doi: 10.1186/s12920-018-0445-8

Nakajima, A., Shimizu, S., Moriya, H., and Yamazaki, M. (2003). Expression of fibroblast growth factor receptor-3 (FGFR3), signal transducer and activator of transcription-1, and cyclin-dependent kinase inhibitor p21 during

endochondral ossification: differential role of FGFR3 in skeletal development and fracture repair. *Endocrinology* 144, 4659–4668. doi: 10.1210/en.2003-0158

Negishi, Y., Ui, N., Nakajima, M., Kawashima, K., Maruyama, K., Takizawa, T., et al. (2001). p21Cip-1/SDI-1/WAF-1 gene is involved in chondrogenic differentiation of ATDC5 cells in vitro. *J. Biol. Chem.* 276, 33249–33256. doi: 10.1074/jbc.M010127200

Ogata, T., Kosho, T., Wakui, K., Fukushima, Y., Yoshimoto, M., and Miharu, N. (2000). Short stature homeobox-containing gene duplication on the der(X) chromosome in a female with 45,X/46,X, der(X), gonadal dysgenesis, and tall stature. *J. Clin. Endocrinol. Metab.* 85, 2927–2930. doi: 10.1210/jcem.85.8.6745

Oliveira, C. S., and Alves, C. (2011). The role of the SHOX gene in the pathophysiology of Turner syndrome. *Endocrinol. Nutr.* 58, 433–442. doi: 10.1016/j.endonu.2011.06.005

Pennimpede, T., Cameron, D. A., Maclean, G. A., Li, H., Abu-Abed, S., and Petkovich, M. (2010). The role of CYP26 enzymes in defining appropriate retinoic acid exposure during embryogenesis. *Birth Defects Res. A Clin. Mol. Teratol.* 88, 883–894. doi: 10.1002/bdra.20709

Pinero, J., Queralt-Rosinach, N., Bravo, A., Deu-Pons, J., Bauer-Mehren, A., Baron, M., et al. (2015). DisGeNET: a discovery platform for the dynamical exploration of human diseases and their genes. *Database* 2015:bav028. doi: 10.1093/database/bav028

Puskaric, S., Schmitteckert, S., Mori, A. D., Glaser, A., Schneider, K. U., Bruneau, B. G., et al. (2010). Shox2 mediates Tbx5 activity by regulating Bmp4 in the pacemaker region of the developing heart. *Hum. Mol. Genet.* 19, 4625–4633. doi: 10.1093/hmg/ddq393

Rao, E., Blaschke, R. J., Marchini, A., Niesler, B., Burnett, M., and Rappold, G. A. (2001). The Leri-Weill and Turner syndrome homeobox gene SHOX encodes a cell-type specific transcriptional activator. *Hum. Mol. Genet.* 10, 3083–3091. doi: 10.1093/hmg/10.26.3083

Rao, E., Weiss, B., Fukami, M., Rump, A., Niesler, B., Mertz, A., et al. (1997). Pseudoautosomal deletions encompassing a novel homeobox gene cause growth failure in idiopathic short stature and Turner syndrome. *Nat. Genet.* 16, 54–63. doi: 10.1038/ng0597-54

Rentsendorj, A., Mohan, S., Szabo, P., and Mann, J. R. (2010). A genomic imprinting defect in mice traced to a single gene. *Genetics* 186, 917–927. doi: 10.1534/genetics.110.118802

Rosilio, M., Huber-Lequesne, C., Sapin, H., Carel, J. C., Blum, W. F., and Cormier-Daire, V. (2012). Genotypes and phenotypes of children with SHOX deficiency in France. *J. Clin. Endocrinol. Metab.* 97, E1257–E1265. doi: 10.1210/jc.2011-3460

Rottbauer, W., Wessels, G., Dahme, T., Just, S., Trano, N., Hassel, D., et al. (2006). Cardiac myosin light chain-2: a novel essential component of thick-myofilament assembly and contractility of the heart. *Circ. Res.* 99, 323–331. doi: 10.1161/01.RES.0000234807.16034.fe

Sawada, R., Kamei, H., Hakuno, F., Takahashi, S., and Shimizu, T. (2015). In vivo loss of function study reveals the short stature homeobox-containing (shox) gene plays indispensable roles in early embryonic growth and bone formation in zebrafish. *Dev. Dyn.* 244, 146–156. doi: 10.1002/dvdy.24239

Schepers, G. E., Bullejos, M., Hosking, B. M., and Koopman, P. (2000). Cloning and characterisation of the Sry-related transcription factor gene Sox8. *Nucleic Acids Res.* 28, 1473–1480. doi: 10.1093/nar/28.6.1473

Schiller, S., Spranger, S., Schechinger, B., Fukami, M., Merker, S., Drop, S. L., et al. (2000). Phenotypic variation and genetic heterogeneity in Leri-Weill syndrome. *Eur. J. Hum. Genet.* 8, 54–62. doi: 10.1038/sj.ejhg.5200402

Schneider, K. U., Marchini, A., Sabherwal, N., Roth, R., Niesler, B., Marttila, T., et al. (2005). Alteration of DNA binding, dimerization, and nuclear translocation of SHOX homeodomain mutations identified in idiopathic short stature and Leri-Weill dyschondrosteosis. *Hum. Mutat.* 26, 44–52. doi: 10.1002/humu.20187

Shears, D. J., Vassal, H. J., Goodman, F. R., Palmer, R. W., Reardon, W., Superti-Furga, A., et al. (1998). Mutation and deletion of the pseudoautosomal gene SHOX cause Leri-Weill dyschondrosteosis. *Nat. Genet.* 19, 70–73. doi: 10.1038/ng0198-70

Spoorendonk, K. M., Peterson-Maduro, J., Renn, J., Trowe, T., Kranenbarg, S., Winkler, C., et al. (2008). Retinoic acid and Cyp26b1 are critical regulators of osteogenesis in the axial skeleton. *Development* 135, 3765–3774. doi: 10.1242/dev.024034

Su, W. C., Kitagawa, M., Xue, N., Xie, B., Garofalo, S., Cho, J., et al. (1997). Activation of Stat1 by mutant fibroblast growth-factor receptor in thanatophoric dysplasia type II dwarfism. *Nature* 386, 288–292. doi: 10.1038/386288a0

Tassano, E., Buttgereit, J., Bader, M., Lerone, M., Divizia, M. T., Bocciardi, R., et al. (2013). Genotype-phenotype correlation of 2q37 deletions including NPPC gene associated with skeletal malformations. *PLoS One* 8:e66048. doi: 10.1371/journal.pone.0066048

Toydemir, R. M., Brassington, A. E., Bayrak-Toydemir, P., Krakowiak, P. A., Jorde, L. B., Whitby, F. G., et al. (2006). A novel mutation in FGFR3 causes camptodactyly, tall stature, and hearing loss (CATSHL) syndrome. *Am. J. Hum. Genet.* 79, 935–941. doi: 10.1086/508433

Tropeano, M., Howley, D., Gazzellone, M. J., Wilson, C. E., Ahn, J. W., Stavropoulos, D. J., et al. (2016). Microduplications at the pseudoautosomal SHOX locus in autism spectrum disorders and related neurodevelopmental conditions. *J. Med. Genet.* 53, 536–547. doi: 10.1136/jmedgenet-2015-103621

Verdin, H., Fernandez-Minan, A., Benito-Sanz, S., Janssens, S., Callewaert, B., De Waele, K., et al. (2015). Profiling of conserved non-coding elements upstream of SHOX and functional characterisation of the SHOX cis-regulatory landscape. *Sci. Rep.* 5:17667. doi: 10.1038/srep17667

Vickerman, L., Neufeld, S., and Cobb, J. (2011). Shox2 function couples neural, muscular and skeletal development in the proximal forelimb. *Dev. Biol.* 350, 323–336. doi: 10.1016/j.ydbio.2010.11.031

Westerfield, M. (2000). *The Zebrafish Book: A Guide for the Laboratory Use of Zebrafish (Danio rerio)*. Eugene: University of Oregon Press.

Yan, Y., Frisen, J., Lee, M. H., Massague, J., and Barbacid, M. (1997). Ablation of the CDK inhibitor p57Kip2 results in increased apoptosis and delayed differentiation during mouse development. *Genes Dev.* 11, 973–983. doi: 10.1101/gad.11.8.973

Yokokura, T., Kamei, H., Shibano, T., Yamanaka, D., Sawada-Yamaguchi, R., Hakuno, F., et al. (2017). The short-stature homeobox-containing gene (shox/SHOX) is required for the regulation of cell proliferation and bone differentiation in zebrafish embryo and human mesenchymal stem cells. *Front. Endocrinol.* 8:125. doi: 10.3389/fendo.2017.00125

Yu, L., Liu, H., Yan, M., Yang, J., Long, F., Muneoka, K., et al. (2007). Shox2 is required for chondrocyte proliferation and maturation in proximal limb skeleton. *Dev. Biol.* 306, 549–559. doi: 10.1016/j.ydbio.2007.03.518

Zhu, D., Yang, D., Li, X., and Feng, F. (2018). Heterogeneous expression and biological function of SOX18 in osteosaroma. *J. Cell. Biochem.* 119, 4184–4192. doi: 10.1002/jcb.26635

Conflict of Interest: The authors declare that the research was conducted in the absence of any commercial or financial relationships that could be construed as a potential conflict of interest.

frontiers in Endocrinology

ORIGINAL RESEARCH
published: 02 July 2021
doi: 10.3389/fendo.2021.695426

Analysis of Mutation Spectra of 28 Pathogenic Genes Associated With Congenital Hypothyroidism in the Chinese Han Population

Miao Huang[1], Xiyan Lu[1], Guoqing Dong[1], Jianxu Li[1], Chengcong Chen[1], Qiuxia Yu[2], Mingzhu Li[1] and Yueyue Su[1]*

[1] Section of Endocrinology, Department of Pediatrics, Shenzhen Maternity and Child Healthcare Hospital, Southern Medical University, Shenzhen, China, [2] Department of Prenatal Diagnostic Center, Guangzhou Women and Children's Medical Center, Guangzhou Medical University, Guangzhou, China

Purpose: Congenital hypothyroidism (CH) is the most common neonatal endocrine disease; its early detection ensures successful treatment and prevents complications. However, its molecular etiology remains unclear.

Methods: We used second-generation sequencing to detect 28 pathogenic genes in 15 Chinese Han patients with CH in Shenzhen, China, and analyzed the genetic pattern of the pathogenic genes through their pedigrees. The pathogenicity assessment of gene mutations was performed based on the American College of Medical Genetics and Genomics (ACMG) classification guidelines, inheritance models, and published evidence.

Results: Mutations in several target genes were identified in 14 of 15 patients (93.33%); these mutations were distributed in eight genes (DUOX2, *DUOXA2, TPO, TG, TSHR, FOXE1, KDM6A*, and *POU1F1*). *DUOX2* exhibited the highest mutation frequency (44%, 11/25), followed by *TPO* (16%, 4/25) and TG (16%, 4/25). *DUOX2* exhibited the highest biallelic mutation (7/15). Eight out of 25 variants verified by the ACMG guidelines were classified as pathogenic (P, category 1) or possibly pathogenic (LP, Type 2), namely six variants of *DUOX2*, and one variant of *TPO* and *DUOXA2*. Five new mutations were detected: one in *DUOX2*, which was located in the splicing region of mRNA (c.1575-1G>A), three new missense mutants, p.A291T, p.R169W, and p. S1237dup, and one new *TPO* missense variant c.2012G>T (p.W671L). The main criteria for determining the genotype–phenotype relationship were a diagnostic detection rate of 53.33% (8/15) and combination of three or more gene mutations.

Conclusions: CH gene mutations in the population may be mainly manifested in genes influencing thyroid hormone synthesis, such as *DUOX2* compound heterozygous mutations, which exhibited a high detection rate. The clinical manifestations are diverse, and mainly include transient CH. Therefore, genetic screening is recommended for CH patients to determine the correlation between clinical phenotypes and gene mutations, which will assist in clinical management.

Keywords: congenital, hypothyroidism, targeted next-generation, sequencing, mutations, DUOX2, Chinese Han population

OPEN ACCESS

Edited by:
Liborio Stuppia, University of Studies G. d'Annunzio Chieti and Pescara, Italy

Reviewed by:
Jean-Pierre Chanoine, University of British Columbia, Canada
Katja Dumic Kubat, University of Zagreb, Croatia

****Correspondence:***
Guoqing Dong
szdonggq@163.com

Specialty section:
This article was submitted to Pediatric Endocrinology, a section of the journal Frontiers in Endocrinology

Received: *15 April 2021*
Accepted: *18 June 2021*
Published: *02 July 2021*

Citation:
Huang M, Lu X, Dong G, Li J, Chen C, Yu Q, Li M and Su Y (2021) Analysis of Mutation Spectra of 28 Pathogenic Genes Associated With Congenital Hypothyroidism in the Chinese Han Population. Front. Endocrinol. 12:695426. doi: 10.3389/fendo.2021.695426

INTRODUCTION

The incidence of congenital hypothyroidism (CH) is 1/2,400 (0.042%), and it is the most commonly detected disease in Chinese newborn screenings (1); early diagnosis and treatment can prevent growth defects and mental retardation (2, 3). The etiology of CH is complicated and its pathogenesis remains unclear. Certain types of CH are familial, suggesting that its pathogenesis may be related to genetic factors (4, 5). Congenital hypothyroidism (CH) can be classified as permanent hypothyroidism (PCH) and transient congenital hypothyroidism (TCH) based on the treatment time. PCH requires permanent treatment, whereas TCH can be treated after a period of time. A study reported that the drug was discontinued after the treatment period (6). Current guidelines recommend that if the serum free T4 (fT4) concentration is reduced and thyroid-stimulating hormone (TSH) is significantly increased, levothyroxine (LT4) treatment should be started immediately (7). However, for CH with elevated serum TSH and normal fT4, the requirement for LT4 treatment remains controversial (8, 9). Currently, better methods to identify such42 conditions do not exist; thus, genetic screening may be helpful (10).

The synthesis, secretion, and action of thyroid hormones are regulated by various genes (11). The genes reported to affect thyroid hormone synthesis and secretion dysfunction comprise of *DUOX2, DUOXA2, IYD, SLC5A5, TG, TPO, SLC26A4*, and *SECISBP2* (12–15); genes that control the biosynthetic pathway of thyroid stimulating hormone include *TSH, THRB, TRHR*, and *IGSF1* (16); pituitary development-related genes *POU1F1, PROP1*, and *HESX1*, and genes that can cause diverse syndromes and abnormal thyroid function, including *GLIS3, GNAS, KDM6A, KMT2D, NKX2-1, NKX2-5*, and *UBR1* (17–19). All the above-mentioned gene mutations can lead to CH. It is important to determine53 whether these genetic mutations or mutation sites may help guide clinical treatment in children.

Most previous studies focus on a certain gene associated with CH (16), and there is a lack of joint screening studies for multiple genes, and related research on CH-related genes and clinical phenotypes. This study employed second-generation sequencing technology to detect 28 candidate genes related to CH, and combined information pertaining to family history and clinical phenotypes to clarify the etiology of CH.61. These results may help guide accurate clinical diagnosis and treatment, and reduce excessive medical treatment.

MATERIALS AND METHODS

Patient Information

From September 2020 to March 2021, 15 CH cases were screened by genetic testing at the Shenzhen Maternal and Child Health Hospital after obtaining parental consent72. The age of the patients at the time of the study ranged from 3 months to 10 years.

The inclusion criteria were as follows: elevated TSH during neonatal screening, venous blood TSH serum level > 10 mIU/L using electrochemiluminescence assay (Cobas 6000, Roche Diagnostics) during follow-up, or CH manifestations (with persistent jaundice, growth and developmental delay, constipation, and feeding difficulties in children with abnormal TSH or thyroid hormone. Patients with acute infection. renal and liver dysfunction, 78 and glucocorticoid users were excluded from the study. When the TSH level was confirmed to be elevated (> 20 μIU/ml), replacement therapy with levothyroxine (LT4) was initiated. When the child turned 3 years old, oral thyroid hormone was stopped, and the thyroid hormone level was monitored regularly to determine whether the treatment should proceed. All patients underwent a thyroid ultrasound examination before treatment. The participants were all Chinese Hans, and the included patients comprised of eight females and seven males. Simultaneously, blood samples from the patient's fathers and mothers were collected for genetic analysis. The parents of all participants signed an informed consent form. The study was approved by the Medical Ethics Committee of Shenzhen Maternal and Child Health Hospital and conducted in accordance with the Declaration of Helsinki.

DNA Extraction and Sequencing

Peripheral blood was collected from the patients and their parents. Genomic DNA was prepared using a salting-out blood DNA extraction kit (Guangzhou Meji Biotechnology, China). The 28 potential pathogenic genes associated with congenital hypothyroidism, *DUOXA2* (NM_207581), *DUOX2* 94 (NM_014080), *FOXE1* (NM_004473), *GLIS3* (NM_152629), *GNAS* (NM_000516), *HESX1* 95 (NM_003865), *IGSF1* (NM_001170961), *IYD* (NM_203395), *KDM6A* (NM_021140), *KMT2D* 96 (NM_003482), *NKX2-1* (NM_001079668), *NKX2-5* (NM_004387), *PAX8* (NM_003466), *POU1F1* 97 (NM_000306), *PROP1* (NM_006261), *SEC077ISBP2* (NM_024_006261), *SLC16A2* (NM_006517), 98 *SLC26A4* (NM_000441), *SLC5A5* (NM_000453), *TG* (NM_003235), *THRA* (NM_199334), *THRB* 99 (NM_000461), *TPO* (NM_000547), *TRH* (NM_007117), *TRHR* (NM_003301, *TSHB* (NM_000549), *TSHR* (NM_000369), and *UBR1* (NM_174916), were selected for sequencing in the present study. The barcode library was established and the hybridization probe of the human exon library was used for hybridization capture using the NextSeq 500 platform (Illumina, San Diego, California, USA) for in-depth sequencing. This gene package-detection range included 28 related genes, 399 coding regions, and a total of 73,686 bases. The average coverage depth was 253 ± 68 ×, which was greater than 10 × coverage. There was a more than 20 × coverage area to account for 100% sequencing coverage. Simultaneously, we identified and analyzed the copy number variation of genes within the detection range.

Analysis of Mutation Data

Sequencing results were analyzed using bioinformatics methods. The annotation range of the original second-generation sequencing data is the variation of each exon, variation in the

10 bp upstream and downstream of the exon, and known pathogenic mutations in the intron region. Variations included missense, nonsense, synonymous, frameshift, whole code, and cut. Quality control was performed on the variant data, and variants with a sequencing coverage depth < 20× were marked as low-quality variants. We performed a search of internal databases, dbSNP, ESP6500, gnomAD, and other population databases and marked SNPs and low-frequency benign variants. Prediction software was then used to predict if the mutations were conserved and the contribution of the mutations CH pathogenesis. We searched the HGMD, PubMed, Clinvar, and other databases and literature related to the variation, and referred to the American College of Medical Genetics and Genomics (ACMG) classification guidelines (20, 21) to classify the variation.

RESULTS

Clinical Characteristics and Mutation Spectrum of Patients

This study included 15 unrelated patients diagnosed with CH with no history of thyroid disease, except for P2 and P3 patients. Ultrasonography of the thyroid revealed two cases of abnormal thyroid morphology — one case of thyroid hypoplasia and one case of ectopic thyroid. There were 13 cases of *in situ* glands (GIS), all of which were of normal sizes (**Table 1**). Fourteen out of 15 patients were identified as having a mutated gene (93.33%). Simultaneously, through copy number and SNP analysis, no variation in copy number potentially related to clinical manifestations was detected. The mutations were distributed among eight genes (*DUOX2, DUOXA2, TPO, TG, TSHR, FOXE1, KDM6A*, and *POU1F1*); the highest mutation frequency was detected in *DUOX2* (44%, 11/25), followed by *TPO* (16%, 4/25) and TG (16%, 4/25). Fourteen patients harbored mutations in at least one thyroid hormone-synthesizing gene (*DUOX2, DUOXA2, TPO, TG*, and *TSHR*). Twelve patients (80%, 12/15) possessed a combination of two gene locus mutations, and six patients (40%, 6/15) possessed a combination of 3 gene locus mutations. A total of 8 patients had double grades in *DUOX2* and *TPO*, and the highest gene mutation rate 127 was observed in *DUOX2* (7/15; see **Table 1** and **Figure 1**).

Patients P3 and P2 were the children of a brother and sister of the same family. Two heterozygous variants of the DUOX2 gene, c.505C>T (p.R169W) and c.3709_3711dup (p.S1237dup), were detected. The verification experiment showed that these two variants were inherited from the candidate's mother and father (both heterozygous). At the same time, no129 copy number variation potentially related to clinical manifestations was detected by copy number and SNP analysis. The clinical manifestations of the siblings included congenital hypothyroidism, but the parents of the candidates showed no corresponding clinical manifestations. The older brother displayed TCH. His131 treatment was discontinued at the age of 3, however he was short in height.

Evaluation of the Pathogenicity of Mutant Genes

As shown in **Table 2**, 14 patients harbored a total of 25 gene mutation sites. According to ACMG guidelines, only variants classified as pathogenic or potentially pathogenic are considered to be determinants of "genetic134 diagnosis". Of the 25 validated variants, eight were classified as pathogenic (P, category 1) or potentially pathogenic (LP, category 2), namely six *DUOX2* genes, and one *TPO* and *DUOXA2* gene. A total of 18 variants were classified as variants of uncertain importance (category 3). Among the five new variants, one was classified as potentially pathogenic (mRNA splicing region mutant c.1575-1G>A in *DUOX2*), and the others were classified as VUS.

Eleven *DUOX2* mutants were found in 11 individuals (**Table 2**). The detected *DUOX2* mutants included seven previously reported missense mutants, (p.K530*), (p.R625*), (p. G702del), (p.R885L), (p.R1470W), (p.R1110Q), and (p.E879K), a new mutant located in the splicing region of mRNA (c.1575-1G>A), and three new missense mutants p.A291T, p.R169W, and p. S1237dup. Among them, p.R169W and p.S1237dup were detected in siblings from the same family and from the mother and father, respectively, and none of them have been reported in related clinical cases. A new missense variant, c.2012G>T (p.W671L), was found to be associated with *TPO*.

The Relationship Between Genotype and Phenotype

Through family verification and pathogenicity assessment, seven cases (patients 2, 3, 4, 6, 9, 11, 13) were considered "resolved", and the diagnostic detection rate was 46.67% (**Table 1**). These "resolved" cases refer to the presence of at least two pathogenic variants in the same gene. These variants are from paternal or maternal lines, but not from a single parent. Due to the weak association between genotype and phenotype, a total of six cases (40%) were considered "ambiguous". Moreover, one case of P10 was considered "unresolved" because it did not carry any genetic mutations, but a color Doppler ultrasound revealed hypoplasia of the left lobe. Among the resolved cases, three were monogenic, whereas four were polygenic. The distribution of genes in all the resolved cases showed a *DUOX2* heterozygous mutation. Notably, all "resolved" cases included patients with normal thyroid morphology. Therefore, the155 diagnosis rate of patients with normal thyroid morphology was 53.84% (**Table 1**).

In these "resolved" cases, oral eumethal therapy for patients P2, P3, P4, and P6 could not be stopped at 2 years of age, but the oral LT4 level was < 3 Ug/Kg·d. Patient P13 is now 10 years old. Genetic screening revealed a heterozygous mutation in *DUOX2* in this patient, which manifested as PCH, but was maintained by a low 157 dose of T4 (1 Ug/Kg·d). The patient's height and intelligence were normal.

DISCUSSION

Second-generation sequencing was used to screen 28 pathogenic genes associated with CH. The screening showed that the gene

TABLE 1 | Clinical Information, detected variants, and results of family segregation analysis of studied patients with CH.

Neonatal Period													
Patients ID	**Sex**	**Birth weight (g)**	**Gestational age (week+ day)**	**Thyroid morphology**	**L-T4 (μg/kg/ day) initial/ current**	**Clinical phenotype**	**Development/ age (y)**	**TSH (uIU/ml)**	**FT4 (pmol/l)**	**Detected variant**	**Father**	**Mother**	**Solved/ ambiguous/ unsolved**
1	M	3000	39	N	8/0	TCH	Ht(-1 SD)/3	21.53	15.81	**TSHR** c.2272G>A(p.E75 8K) **TG**c.958C>T (p.R320C) **TPO**c.2748+5_2748+6insG	NA	G/A	Ambiguous
2*	F	3350	38	N	10/1	CH	N/2.3	35.65	8.75	**DUOX2c.505C> T(p.R169W)/ c.3709_3711dup(p .S1237dup)**	c.3709_3 711dup	c.505 C>T	Solved
3*	M	2850	37+3	N	10/0	TCH	N/4.1	56.47	6.45	**DUOX2**c.505C>T(p.R169W)/ c.3709_3711dup(p .S1237dup)	c.3709_3711dup	c.505 C>T	Solved
4	F	1500	33+3	N	10/4	CH	Ht(-1 SD)/2	>100	3.31	**DUOX2**c.1588A> T(p.K530*)/ c.1873C>T(p.R625*)	c.1873C >T	c.158 8A>T	Solved
5	F	3100	39	undetected	7/2.5	CH	N/1.2 5	37.48	17.53	**DUOX2**c.2104_21 06del(p.G702del) **TG** c.4859C>T(p.T162 0M)	NA	NA	ambiguous
6	F	3200	39	N	10/2	PCH	Ht(-1 SD)/3	64.25	4.73	**DUOX2**c.1588A> T(p.K530*)/c.2654 G>T(p.R885L) **FOXE1**c.412G>C(p.E138Q)	c.2654G >T	c.158 8A>T/ G>C	Solved
7	M	3500	40	N	10/0	TCH	N/3	32.83	13.1	**DUOX2**c.4408C>T(p.R14 70W)	C>T	NA	ambiguo us
8	M	3050	40	N	10/1	CH	N/2	>100	5.81	**DUOX2** c.3329G>A(p.R11 10Q) **TG**c.3035C>T(p.P 1012L)	NA	G>A	ambiguous
9	F	3900	40	N	10/5	CH	N/0.2	>100	6.37	**DUOX2**c.2654G> T(p.R885L)/ c.3329G>A(p.R11 10Q) ***DUOXA2***c.769+5G>A	c.3329G >A	c.265 4G>T	Solved
10	M	3024	39+6	The left lobe is absent	10/2.5	PCH	N/3.8	53.26	7.12	NA	–	–	unsolved
11	M	2790	40	N	10/8	CH	N/0.3	57.54	8.13	**DUOX2**c.2654G> T(p.R885L)/ **c.871G>A(p.A291 T)** **POU1F1**c.302C>A (p.T101N)	G>T	G>A	Solved
12	F	2965	39+5	N	10/0	TCH	Ht(-1 SD)/3	63.79	4.22	**TG** c.7753C>T(p.R25 85W) **TPO**c.1082G>T	NA	NA	ambiguous

(Continued)

TABLE 1 | Continued

Patients ID	Sex	Birth weight (g)	Gestational age (week+ day)	Thyroid morphology	L-T4 (μg/kg/day) initial/current	Clinical phenotype	Development/age (y)	TSH (uIU/ml)	FT4 (pmol/l)	Detected variant	Father	Mother	Solved/ambiguous/unsolved
							Neonatal Period						
13	M	3300	40+1	N	10/1	PCH	N/10	83.43	3.12	(p.R361L) **DUOX2c.1575-1 G>A**/c.3329G>A(p.R1110Q) **KDM6A** c.1835G>T (p.R612L)	G>A	c.3329 G>A	Solved
14	M	3026	39+7	N	10/2.5	PCH	N/8.9	43.85	7.53	**TPO**c.2268dup(p.E757*)/**c.2012G>T(p.W671L) DUOX2**c.2635G>A(p.E879K)	NA	NA	Solved
15	F	2750	38+2	N	0/5	CH	N/0.3	479	0.37	**DUOXA2**c.738C>	NA	C>G	ambiguous

*CH, congenital hypothyroidism; m, month; d, day; y, year; F, female; M, male; TSH, thyroid-stimulating hormone; FT4, free tetraiodothyronine; *, P2 and P3 are siblings of the same family; NA, data not available. PCH, permanent CH; TCH, transient CH; NC, not to time to make sure the clinical phenotype; NA, data not available; N, normal; age; the time for genetic testing.*

mutation detection rate was 93.33%, and was mainly detected in genes that affect thyroid hormone synthesis, such as *DUOX2*, *TPO*, and *TG*. Previous studies have shown that the detection rate of *DUOX2* mutations in children with CH in China is as high as 28%-44%, whereas the detection rate obtained in this study was 44%, suggesting that *DUOX2* mutations may be the160 main cause of CH in the Chinese population (22–24). *DUOX2* is mainly involved in the production of peroxide protein complexes and catalyzes the synthesis of thyroid hormones in thyroid follicular cells (25). Studies have found that mutations in *DUOX2* can initiate CH, but the clinical phenotype, primarily the manifestation of TCH, is variable (26, 27). In this study, except for the mutations observed in patients P1, P10, and P12, all genes merged with one or two *DUOX2* mutations. These children exhibited various clinical manifestations, including severe CH, mild CH, hyper-TSH-emia, and permanent CH (28). In the resolved cases, compound heterozygous mutations in *DUOX2* were combined, and the oral LT4 dosage at the age of 2 years was less than 3 Ug/Kg·d. It is suggested that CH combined with compound heterozygous mutations of *DUOX2* is primarily the outcome of TCH. The small sample size in this study requires the165 correlation between gene mutations and clinical phenotypes to be further confirmed by studies with a larger sample size.

TPO encodes thyroid peroxidase (TPO), which catalyzes a key reaction in the synthesis of thyroid hormones and is inherited in an autosomal recessive manner (29). In this study, we detected a heterozygous mutation of P1 and P12 combined with the *TPO* gene, which was manifested as TCH. P14 combined with the *TPO* gene c.2012G>T (p.W671L) and c.2268dup (p.E757*) compound heterozygous mutations manifested as PTH at 10 years of age, wherein a thyroid color Doppler ultrasound171 indicated mild goiter. The rare missense mutation in *TPO* c.2012G>T (p.W671L) has not been reported in related clinical cases, but numerous clinical cases related to thyroid hormone production disorders have reported a rare variant of *TPO* c.2268dup (p.E757*). It is a homozygous mutation or forms a compound heterozygous state with other variants. Here, the patient's 174 clinic al manifestations were as follows: the level of TSH increased in the neonatal period, that of thyroid hormone decreased, and goiter occurred during adolescence (13, 30). Moreover, functional experiments have shown that this mutation can cause reduced expression of176 TPO and loss of enzyme activity (31).

Zamproni (32) reported that a Chinese patient born to parents of unrelated descent was homozygous for a nonsense mutation (p.Y246X) and produced a truncated DUOXA2 protein with a missing transmembrane helix 5 and C-terminal cytoplasmic domains. DUOX2 cannot be recombined *in vitro*, thereby affecting the synthesis of thyroid hormones. Patient P15 harbored only one mutation in DUOXA2c.738C>G (p.Y246*), which originated from a mother with a normal phenotype. The clinical manifestations of TSH screening at birth were normal. Due to repeated jaundice, the altered blood thyroid hormone [TSH 479 (uIU/ml) and fT4 0.37 (pmol/l)] was associated with abdominal distension, constipation, low crying, weight loss, and other severe hypothyroidism. Patient P7 only

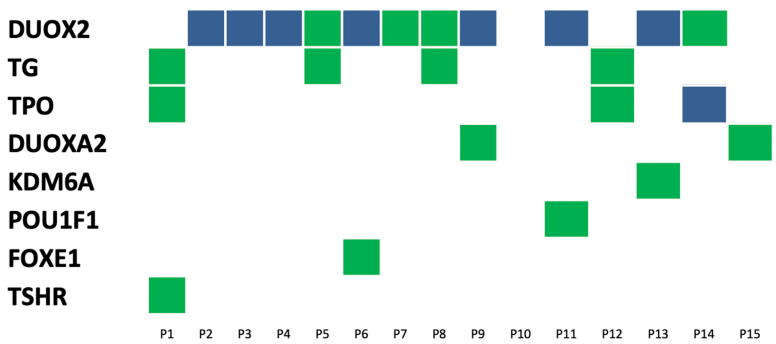

FIGURE 1 | Distribution of variants in15 congenital hypothyroidism. The left side was 8 detected genes with variants, and the number on top of each box is the patient ID. Each column represents a patient and each row represents a gene. Blue blocks represent biallelic variants and green blocks represent monoallelic variants. Such as patient 9 carries variants on two genes: biallelic variants in the DUOX2 gene and monoallelic variant in DUOXA2.

TABLE 2 | Potential pathological variants detected in the present study.

Gene	cDNA change	Amino Acids change	GnomAD east asian	Status[a]	ACMG classificationa
DUOX2	c.505C>T	p.R169W	0·002	Novel	VUS
DUOX2	c.3709_3711dup	p.S1237dup	0·002	Novel	VUS
DUOX2	c.1588A>T	p.K530*	0·009	Known	P
DUOX2	c.1873C>T	p.R625*	<0.001	Known	P
DUOX2	c.2104_2106del	p.G702del	<0.001	Known	VUS
DUOX2	c.2654G>T	p.R885L	<0.001	Known	LP
DUOX2	c.4408C>T	p.R1470W	0.002	Known	VUS
DUOX2	c.3329G>A	p.R1110Q	0.003	Known	LP
DUOX2	c.1575-1G>A	–	–	Novel	LP
DUOX2	c.871G>A	p.A291T	–	Novel	VUS
DUOX2	c.2635G>A	p.E879K	<0.001	Known	LP
TG	c.4859C>T	p.T1620M	0.016	Known	VUS
TG	c.3035C>T	p.P1012L	0.028	Known	VUS
TG	c.7753C>T	p.R2585W	0.005	Known	VUS
TG	c.958C>T	p.R320C	<0.001	Known	VUS
TPO	c.2268dup	p.E757*	0.002	Known	P
TPO	c.1082G>T	p.R361L	0.009	Known	VUS
TPO	c.2012G>T	p.W671L	<0.001	Novel	VUS
TPO	c.2748+5_2748+6insG	–	–	Known	VUS
DUOXA 2	c.769+5G>A	–	–	Known	VUS
DUOXA 2	c.738C>G	p.Y246*	0.002	Known	LP
KDM6A	c.1835G>T	p.R612L	–	Known	VUS
POU1F 1	c.302C>A	p.T101N	0.006	Known	VUS
FOXE1	c.412G>C	p.E138Q	–	Known	VUS
TSHR	c.2272G>A	p.E758K	<0.001	Known	VUS

P, pathogenic; LP, likely pathogenic; VUS, variants of uncertain significance.
**Premature termination of encoded amino acid.*

revealed that *DUOX2* c.4408C>T (p.R1470W) harbored a gene mutation from a father with a normal phenotype, showing temporary hyper-TSH-emia, and the drug was discontinued at the age of 3. This rare variant has been reported in disorders of thyroid hormone synthesis, and the patient harbored a compound heterozygous mutation (33). The above two cases do not conform to the rules of Mendelian inheritance. We speculated that these cases were caused by other genes, which are excluded from the scope of this analyses, or there may be other genes that function in collaboration with these mutations to cause the disease, which requires further181 follow-up functional studies.

Herein, 8 of the 25 variants verified based on the ACMG guidelines were classified as pathogenic (P,183 category 1) or potentially pathogenic (LP, category 2), namely six variants of *DUOX2* (p.K530 *, p.R625*, p.R885L, p.R1110Q, c.1575-1G>A, p.E879K), and one variant of *TPO* (p.E757*) and *DUOXA2* (p.Y246*). These results indicated that that *DUOX2* mutations are the main pathogenic genes associated with CH in the Han population in China. Five new mutations were found, one

DUOX2 mutation, which was located in the splicing region of mRNA (c.1575-1G>A), three new missense mutants, p.A291T, p.R169W, and p.S1237dup, and one new *TPO* missense variant c.2012G>T (p.W671L). To date, these variants exhibit a low frequency in the reference population gene database. The region where the mutation is located is an important part of this protein, and the amino acid sequences of different species are highly conserved. Computer-aided analysis predicts that this mutation is more likely to affect protein structure and function. In this study, patients P2 and P3 represented two siblings. New rare variants that may be related to clinical manifestations were detected, which included two heterozygous variants of *DUOX2*, c.505C>T (p.R169W) and c.3709_3711dup (p.S1237dup). Family verification showed that these two variants were inherited from the mother and father of the candidate (both are heterozygous). The clinical manifestations included high TSH and low FT4 levels after birth. For the elder brother, thyroid hormone therapy can only be stopped at 4 years of age, whereas the younger sister is currently 2 years old and still requires oral thyroid hormone therapy. These two rare variants, c.505C>T and (p.R169W), have not been reported in relevant242 clinical cases. However, their relevance requires further clarification.

This study has some limitations. First, the sample size was relatively small; most of the patients had a short follow-up period, and the clinical phenotype data were not comprehensive. Therefore, it is not analytically conducive to determine the correlation between the detected mutation and clinical phenotype. Simultaneously, there is a lack of *in vitro* functional studies of new variants identified in the current study.

In summary, the mutation profiles of 15 Han patients with CH in Shenzhen, China were determined using second-generation sequencing targeting 28 known disease-causing genes. It is mainly manifested in genes that affect thyroid hormone synthesis—primarily compound heterozygous mutations in253 *DUOX2*. Moreover, the gene mutation detection rate was as high as 93.33%, and the new gene mutation rate was 5/25 (20%). Therefore, pathogenic gene screening for patients with CH, enriching the mutation spectrum, and identifying the relationship between gene mutations and phenotypes are the recommended steps to achieve accurate clinical diagnosis256 and treatment of CH.

DATA AVAILABILITY STATEMENT

The variation data reported in this paper have been deposited in the Genome Variation Map (GVM) [1] in Big Data Center [2], Beijing Institute of Genomics (BIG), Chinese Academy of Science, under accession numbers GVM000180 at http://bigd.big.ac.cn/gvm/getProjectDetail?project=GVM000180.

ETHICS STATEMENT

The studies involving human participants were reviewed and approved by the Medical Ethics Committee of Shenzhen Maternal and Child Health Hospital. Written informed consent to participate in this study was provided by the participants' legal guardian/next of kin.

AUTHOR CONTRIBUTIONS

MH and XL conceptualized and designed the study, and drafted the initial manuscript. GD conceptualized and designed the study. JL and CC performed the initial analyses, reviewed and revised the manuscript, and approved the final manuscript. QY performed the initial analyses and approved the final manuscript. ML and YS coordinated and supervised data collection, critically reviewed the manuscript and approved the final manuscript. All authors contributed to the article and approved the submitted version.

FUNDING

This study was supported by Sanming Project of Medicine in Shenzhen (SZSM201812056).

ACKNOWLEDGMENTS

We thank all subjects for their collaborative participation in our study. Thanks to Guangzhou Jiajian Medical Testing Co., Ltd. for gene sequencing.

REFERENCES

1. Deng K, He C, Zhu J, Liang J, Li X, Xie X, et al. Incidence of Congenital Hypothyroidism in China: Data From the National Newborn Screening Program, 2013-2015. *J Pediatr Endocrinol Metab* (2018) 31:601–8. doi: 10.1515/jpem-2017-0361
2. Cherella CE, Wassner AJ. Update on Congenital Hypothyroidism. *Curr Opin Endocrinol Diabetes Obes* (2020) 27:63–9. doi: 10.1097/MED.0000000000000520
3. Nilsson M, Fagman H. Development of the Thyroid Gland. *Development (Cambridge Engl)* (2017) 144:2123–40. doi: 10.1242/dev.145615
4. Hannoush ZC, Weiss RE. Defects of Thyroid Hormone Synthesis and Action. *Endocrinol Metab Clinics North Am* (2017) 46:375–88. doi: 10.1016/j.ecl.2017.01.005
5. Kostopoulou E, Miliordos K, Spiliotis B. Genetics of Primary Congenital Hypothyroidism-A Review. *Horm (Athens Greece)* (2021):225–36. doi: 10.1007/s42000-020-00267-x
6. Park IS, Yoon JS, So CH, Lee HS, Hwang JS. Predictors of Transient Congenital Hypothyroidism in Children With Eutopic Thyroid Gland. *Ann Pediatr Endocrinol Metab* (2017) 22:115–8. doi: 10.6065/apem.2017.22.2.115
7. Léger J, Olivieri A, Donaldson M, Torresani T, Krude H, van Vliet G, et al. European Society for Paediatric Endocrinology Consensus Guidelines on Screening, Diagnosis, and Management of Congenital Hypothyroidism. *J Clin Endocrinol Metab* (2014) 99:363–84. doi: 10.1210/jc.2013-1891
8. Park ES, Yoon JY. Factors Associated With Permanent Hypothyroidism in Infants With Congenital Hypothyroidism. *BMC Pediatr* (2019) 19:453. doi: 10.1186/s12887-019-1833-8
9. Salerno M, Improda N, Capalbo D. MANAGEMENT OF ENDOCRINE DISEASE Subclinical Hypothyroidism in Children. *Eur J Endocrinol* (2020) 183:R13–28. doi: 10.1530/EJE-20-0051
10. van Trotsenburg P, Stoupa A, Léger J, Rohrer T, Peters C, Fugazzola L, et al. Congenital Hypothyroidism: A 2020-2021 Consensus Guidelines Update-An

ENDO-European Reference Network Initiative Endorsed by the European Society for Pediatric Endocrinology and the European Society for Endocrinology. *Thyroid: Off J Am Thyroid Assoc* (2021) 31:387–419. doi: 10.1089/thy.2020.0333
11. Stoupa A, Kariyawasam D, Muzza M, de Filippis T, Fugazzola L, Polak M, et al. New Genetics in Congenital Hypothyroidism. *Endocrine* (2021) 71:696–705. doi: 10.1007/s12020-021-02646-9
12. Fu C, Luo S, Zhang S, Wang J, Zheng H, Yang Q, et al. Next-Generation Sequencing Analysis of DUOX2 in 192 Chinese Subclinical Congenital Hypothyroidism (SCH) and CH Patients. *Clinica Chimica Acta; Int J Clin Chem* (2016) 458:30–4. doi: 10.1016/j.cca.2016.04.019
13. Lee CC, Harun F, Jalaludin MY, Heh CH, Othman R, Junit SM, et al. Prevalence of C.2268dup and Detection of Two Novel Alterations, C.670_672del and C.1186C>T, in the TPO Gene in a Cohort of Malaysian-Chinese With Thyroid Dyshormonogenesis. *BMJ Open* (2015) 5:e006121. doi: 10.1136/bmjopen-2014-006121
14. Tan MY, Huang YL, Li B, Jiang X, Chen QY, Jia XF, et al. Characteristics of DUOXA2 Gene Mutation in Children With Congenital Hypothyroidism. *Zhongguo dang dai er ke za zhi = Chin J Contemp Pediatr* (2017) 19:59–63. doi: 10.7499/j.issn.1008-8830.2017.01.009
15. Targovnik HM, Citterio CE, Rivolta CM. Iodide Handling Disorders (NIS, TPO, TG, IYD). *Best Pract Res Clin Endocrinol Metab* (2017) 31:195–212. doi: 10.1016/j.beem.2017.03.006
16. Stephenson A, Lau L, Eszlinger M, Paschke R. The Thyrotropin Receptor Mutation Database Update. *Thyroid: Off J Am Thyroid Assoc* (2020) 30:931–5. doi: 10.1089/thy.2019.0807
17. Chen XY, Liu Y, Liu JH, Qin XS. An Analysis of GNAS and THRA Gene Mutations in Children With Congenital Hypothyroidism. *Zhongguo dang dai er ke za zhi= Chin J Contemp Pediatr* (2019) 21:680–4. doi: 10.7499/j.issn.1008-8830.2019.07.012
18. Dimitri P, Habeb AM, Gurbuz F, Millward A, Wallis S, Moussa K, et al. Expanding the Clinical Spectrum Associated With GLIS3 Mutations. *J Clin Endocrinol Metab* (2015) 100:E1362–E69. doi: 10.1210/jc.2015-1827
19. Shinohara H, Takagi M, Ito K, Shimizu E, Fukuzawa R, Hasegawa T, et al. A Novel Mutation in NKX2-1 Shows Dominant-Negative Effects Only in the Presence of PAX8. *Thyroid: Off J Am Thyroid Assoc* (2018) 28:1071–3. doi: 10.1089/thy.2017.0481
20. Richards S, Aziz N, Bale S, Bick D, Das S, Gastier–Foster J, et al. Standards and Guidelines for the Interpretation of Sequence Variants: A Joint Consensus Recommendation of the American College of Medical Genetics and Genomics and the Association for Molecular Pathology. *Genet Med: Off J Am Coll Med Genet* (2015) 17:405–24. doi: 10.1038/gim.2015.30
21. Riggs ER, Andersen EF, Cherry AM, Kantarci S, Kearney H, Patel A, et al. Technical Standards for the Interpretation and Reporting of Constitutional Copy-Number Variants: A Joint Consensus Recommendation of the American College of Medical Genetics and Genomics (ACMG) and the Clinical Genome Resource (ClinGen). *Genet Med: Off J Am Coll Med Genet* (2020) 22:245–57. doi: 10.1038/s41436-019-0686-8
22. Sun F, Zhang JX, Yang CY, Gao GQ, Zhu WB, Han B, et al. The Genetic Characteristics of Congenital Hypothyroidism in China by Comprehensive Screening of 21 Candidate Genes. *Eur J Endocrinol* (2018) 178:623–33. doi: 10.1530/EJE-17-1017
23. Wang F, Zang Y, Li M, Liu W, Wang Y, Yu X, et al. DUOX2 and DUOXA2 Variants Confer Susceptibility to Thyroid Dysgenesis and Gland-In-Situ With Congenital Hypothyroidism. *Front Endocrinol* (2020) 11:237. doi: 10.3389/fendo.2020.00237
24. Yu B, Long W, Yang Y, Wang Y, Jiang L, Cai Z, et al. Newborn Screening and Molecular Profile of Congenital Hypothyroidism in a Chinese Population. *Front Genet* (2018) 9:509. doi: 10.3389/fgene.2018.00509
25. De Deken X, Wang D, Many MC, Costagliola S, Libert F, Vassart G, et al. Cloning of Two Human Thyroid cDNAs Encoding New Members of the NADPH Oxidase Family. *J Biol Chem* (2000) 275:23227–33. doi: 10.1074/jbc.M000916200
26. Long W, Zhou L, Wang Y, Liu J, Wang H, Yu B, et al. Complicated Relationship Between Genetic Mutations and Phenotypic Characteristics in Transient and Permanent Congenital Hypothyroidism: Analysis of Pooled Literature Data. *Int J Endocrinol* (2020) 2020:6808517. doi: 10.1155/2020/6808517
27. Wang H, Wang X, Kong Y, Pei X, Cui Y, Zhu Z, et al. Mutation Spectrum Analysis of 29 Causative Genes in 43 Chinese Patients With Congenital Hypothyroidism. *Mol Med Rep* (2020) 22:297–309. doi: 10.3892/mmr.2020.11078
28. Maruo Y, Nagasaki K, Matsui K, Mimura Y, Mori A, Fukami M, et al. Natural Course of Congenital Hypothyroidism by Dual Oxidase 2 Mutations From the Neonatal Period Through Puberty. *Eur J Endocrinol* (2016) 174:453–63. doi: 10.1530/EJE-15-0959
29. Park SM, Chatterjee VK. Genetics of Congenital Hypothyroidism. *J Med Genet* (2005) 42:379–89. doi: 10.1136/jmg.2004.024158
30. Ma SG, Qiu YL, Zhu H, Liu H, Li Q, Ji CM, et al. Novel Genetic Variants in the TPO Gene Cause Congenital Hypothyroidism. *Scand J Clin Lab Invest* (2015) 75:633–7. doi: 10.3109/00365513.2015.1055789
31. Lee CC, Harun F, Jalaludin MY, Lim CY, Ng KL, Mat Junit S, et al. Functional Analyses of C.2268dup in Thyroid Peroxidase Gene Associated With Goitrous Congenital Hypothyroidism. *BioMed Res Int* (2014) 2014:370538. doi: 10.1155/2014/370538
32. Zamproni I, Grasberger H, Cortinovis F, Vigone MC, Chiumello G, Mora S, et al. Biallelic Inactivation of the Dual Oxidase Maturation Factor 2 (DUOXA2) Gene as a Novel Cause of Congenital Hypothyroidism. *J Clin Endocrinol Metab* (2008) 93:605–10. doi: 10.1210/jc.2007-2020
33. Jiang H, Wu J, Ke S, Hu Y, Fei A, Zhen Y, et al. High Prevalence of DUOX2 Gene Mutations Among Children With Congenital Hypothyroidism in Central China. *Eur J Med Genet* (2016) 59:526–31. doi: 10.1016/j.ejmg.2016.07.004

Conflict of Interest: The authors declare that the research was conducted in the absence of any commercial or financial relationships that could be construed as a potential conflict of interest.

frontiers in Genetics

ORIGINAL RESEARCH
published: 20 July 2021
doi: 10.3389/fgene.2021.616761

Variants in *LAMC3* Causes Occipital Cortical Malformation

Xiaohang Qian[1†], Xiaoying Liu[1†], Zeyu Zhu[1], Shige Wang[1], Xiaoxuan Song[1], Guang Chen[1], Jingying Wu[1], Yuwen Cao[1], Xinghua Luan[1,2], Huidong Tang[1] and Li Cao[1,2]**

[1] Department of Neurology and Institute of Neurology, Rui Jin Hospital, Shanghai Jiao Tong University School of Medicine, Shanghai, China, [2] Department of Neurology, Shanghai Jiao Tong University Affiliated Sixth People's Hospital, Shanghai, China

Occipital cortical malformation (OCCM) is a disease caused by malformations of cortical development characterized by polymicrogyria and pachygyria of the occipital lobes and childhood-onset seizures. The recessive or complex heterozygous variants of the *LAMC3* gene are identified as the cause of OCCM. In the present study, we identified novel complex heterozygous variants (c.470G > A and c.4030 + 1G > A) of the *LAMC3* gene in a Chinese female with childhood-onset seizures. Cranial magnetic resonance imaging was normal. Functional experiments confirmed that both variant sites caused premature truncation of the laminin γ3 chain. Bioinformatics analysis predicted 10 genes interacted with *LAMC3* with an interaction score of 0.4 (*P* value = 1.0e–16). The proteins encoded by these genes were mainly located in the basement membrane and extracellular matrix component. Furthermore, the biological processes and molecular functions from gene ontology analysis indicated that laminin γ3 chain and related proteins played an important role in structural support and cellular processes through protein-containing complex binding and signaling receptor binding. KEGG pathway enrichment predicted that the *LAMC3* gene variant was most likely to participate in the occurrence and development of OCCM through extracellular matrix receptor interaction and PI3K-Akt signaling pathway.

Keywords: occipital cortical malformation, *Lamc3*, childhood-onset seizures, ECM-receptor interaction, PI3K-Akt signaling pathway

OPEN ACCESS

Edited by:
Liborio Stuppia, University of Studies G. D'Annunzio Chieti and Pescara, Italy

Reviewed by:
Muhammad Umair, King Abdullah International Medical Research Center (KAIMRC), Saudi Arabia
Murim Choi, Seoul National University, South Korea

****Correspondence:***
Huidong Tang
thd10495@rjh.com.cn
Li Cao
caoli2000@yeah.net

† These authors share first authorship

Specialty section:
This article was submitted to Genetics of Common and Rare Diseases, a section of the journal Frontiers in Genetics

Received: *13 October 2020*
Accepted: *21 June 2021*
Published: *20 July 2021*

Citation:
Qian X, Liu X, Zhu Z, Wang S, Song X, Chen G, Wu J, Cao Y, Luan X, Tang H and Cao L (2021) Variants in LAMC3 Causes Occipital Cortical Malformation. Front. Genet. 12:616761. doi: 10.3389/fgene.2021.616761

INTRODUCTION

Malformations of cortical development (MCD) are a series of disrupted cerebral cortex formation disorders caused by multiple etiologies, including genetic, metabolic, vascular, and other factors (Severino et al., 2020). MCD usually occur in early childhood or early adulthood (Raybaud and Widjaja, 2011; Barkovich et al., 2012). It is characterized by developmental delays, intellectual disability, epilepsy, and even cerebral palsy. Occipital cortical malformation (OCCM; MIM: 614115) is a form of MCD characterized by polymicrogyria and pachygyria limited to the occipital lobe. Besides, the seizures, developmental, and cognitive delays can also be observed in affected individuals (Zambonin et al., 2018). A recent study found that impaired visual function was another clinical feature of OCCM due to compromised cortical architecture (Urgen et al., 2019). In 2011, Barak et al. applied whole-exome capture and sequencing technology to identify the recessive or complex heterozygous variants of the gamma-3 chain isoform of laminin (*LAMC3*) caused OCCM

(Barak et al., 2011). Thus far, five unrelated families of OCCM caused by *LAMC3* variants have been reported worldwide (Barak et al., 2011; Afawi et al., 2016; Zambonin et al., 2018). Total six variants of *LAMC3* gene were identified in these unrelated families. The clinical features of patients with OCCM caused by *LAMC3* gene variants includes seizures, developmental delay or degeneration and pachygyria and polymicrogyria.

LAMC3 gene, cloned by Koch et al. (1999), was found to be located on chromosome 9 at q31-34. The *LAMC3* gene encodes the laminin gamma-3 chain, which is made up of 1575 amino acids (Barak et al., 2011). The laminin γ3 chain is widely distributed in different tissue, including the placenta, spleen, skin, reproductive tract, heart, kidney, and brain (Koch et al., 1999; Barak et al., 2011). However, the distribution of the laminin γ3 chain in different organizations has temporal and spatial characteristics. On the one hand, the laminin γ3 chain is located primarily in the skin's basement membrane, while it is located primarily on the surface of ciliated epithelial cells in the seminiferous tubes and lung (Koch et al., 1999). On the other hand, the expression level of the laminin γ3 chain in the human cortex peaks from late fetal development to late infancy (Barak et al., 2011). However, the study on biological functions and molecular regulatory mechanisms of the laminin γ3 chain in mammals is very limited. For example, the laminin γ3 chain was shown to participate in retinal angiogenesis by regulating astrocyte migration (Gnanaguru et al., 2013).

Here we identified novel compound heterozygous variants in the *LAMC3* gene in a Chinese OCCM patient. Based on thorough clinical and genetic analysis, we further verified the function of the variants *in vitro*. To further explore the molecular mechanisms involved in *LAMC3*, we applied bioinformatics to analyze and predict the pathogenic mechanism of *LAMC3* gene variant. Finally, we summarized the clinical and genetic characteristics of currently reported patients with OCCM due to the *LAMC3* gene variants.

MATERIALS AND METHODS

Genetic Analysis

The genomic DNA of the proband and her parents were extracted using a standardized phenol/chloroform extraction method. Whole exome sequencing was performed as previously described (Zhu et al., 2019). Sanger sequencings was applied to validate variants of the *LAMC3* gene in the proband and her parents. One thousand unaffected individuals of matched geographic ancestry were used as normal controls.

Cell Culture

HEK 293T cells were cultured in Dulbecco's Modified Eagle Medium (DMEM) containing 10% fetal bovine serum (FBS) and 1% penicillin/streptomycin (PS) at 37°C with 5% CO2 and 95% O2. *LAMC3* wild-type (*LAMC3*-WT) or variant (c.470G > A) plasmid, synthesized by Gene Create (Wuhan, China), with spliced GFP labels on the N-terminal. Before transfection, cells were plated at 150,000 cells per well in 6-well culture dishes. After 24 h, HEK 293T cells were transfected with 2.5 μg *LAMC3*-WT or variant (c.470G > A) plasmid DNA through Lipofectamine 3000 transfection reagent (Invitrogen). 36 h later, the cells were used for immunofluorescence and western blotting.

Western Blotting

The concentration of protein samples was determined using a BCA kit. Protein samples were diluted in 5X SDS-PAGE and boiled at 100°C for 10 min. 30 μg of protein sample was resolved by 8% SDS polyacrylamide gels. After being transferred to polyvinylidene fluoride membrane, the blots were incubated at 4°C for 12 h with the anti-GFP antibody (1:1000, Cell Signal Technology) and α-tubulin primary antibody (1:1000, Cell Signaling Technology). Finally, after incubation with secondary antibodies (1:5000, Beyotime), blots were analyzed by Kodak Digital Science1D software (East-man Kodak Co., New Haven, CT, United States).

Immunofluorescence

After transfection, PBS containing 4% paraformaldehyde was used to fix the cells for 30 min. Cells were blocked using a blocking solution, containing 0.3% Triton X-100 and 5% bovine serum albumin (BSA) in PBS for 30 min. DAPI (1:10,000, Cell Signal technology) was then applied for 5 min to stain nucleic acid staining. Finally, A Zeiss 710 confocal microscope was used for image collection.

Minigene Reporter Assay

BDGP: Splice Site Prediction by Neural Network,[1] NetGene2 Sever[2] and HSF: Human Splicing Finder Version 3.1[3] were used to evaluate the effects of variants on splice sites. PCR amplified the LAMC3 exons relevant to 1 novel splicing variant (c.4030 + 1G > A) along with flanking intronic sequences from patients P3672 with gDNA. The PCR products of c.4030 + 1G > A were cloned into the pcDNA3.1 vector and the pcMINI vector. Then the minigenes were transfected into HeLa cells and HEK 293T cells, respectively. The RNAiso Plus kit (Takara, Japan) was used for total RNA extraction, followed by RT-PCR using the PrimeScript RT reagent kit (Takara, Japan) to generate related cDNA. Electrophoresis on 2% agarose gels and Sanger sequencing were used for splicing pattern analysis.

Bioinformatic Analysis

The signal peptide sequence of *LAMC3* was predicted by SignalP-5.0.[4] The Search Tool for the Retrieval of Interacting Genes database (STRING) online database[5] database was applied to predict genes potentially associated with *LAMC3*. Protein-protein interaction network (PPI) network and functional enrichment analysis including the cellular component, biological process, molecular function, and KEGG were exported as tables. Sangerbox[6] and Cytoscape software were used to construct

[1]http://www.fruitfly.org/seq_tools/splice.html
[2]http://www.cbs.dtu.dk/services/NetGene2/
[3]http://www.umd.be/HSF3/HSF.shtml
[4]http://www.cbs.dtu.dk/services/SignalP/
[5]https://www.string-db.org/
[6]http://sangerbox.com/

the visualized PPI network diagram and functional enrichment analysis bubble diagram, respectively.

Ethics

According to the Declaration of Helsinki principles, this study was approved by the Ethics Committee of the Ruijin Hospital affiliated with Shanghai Jiao Tong University School of Medicine. The patient, her parents, and the healthy controls signed informed consent.

RESULTS

Case Report

A 24 years old female patient, born from non-consanguineous healthy parents with normal development, had epilepsy for 11 years. The patient's two younger siblings were both unaffected (**Figure 1B**). According to the parents' recollection, high fever convulsions for 4–5 min occurred at 9 months and 2 years of age. At the age of 13, the patient first had an absence seizure accompanied by incontinence without obvious inducement. The absence seizure lasted a few minutes and occurred once or twice a month. In addition, generalized tonic-clonic seizures also occurred five times. After each seizure, the patient felt pain on the right side of the head. The patient was treated with valproate at age 20 (500 mg, three times daily). The frequency of absence seizures decreased but still occurred. At the age of 22, the dose of valproate was adjusted to two dose (1000 mg) twice daily. At the same time, the electroencephalogram (EEG) showed 8–9 Hz alpha waves companying with 5–7 Hz theta waves. Cranial magnetic resonance imaging (MRI) was normal (**Figure 1A**). 3 months later, due to the poor effect of valproate on epilepsy control, the patient was treated with levetiracetam twice a day reducing the dosage of valproate to 500 mg twice daily. After half a year, valproate was discontinued. The most recent follow-up was at age 24. The patient suffered from an absence of seizures twice in the past 2 years. An EEG showed 8–10 Hz alpha waves and 4–7 Hz slow waves.

Genetic Findings

The patient was revealed to have compound heterozygous variants in the *LAMC3* (NG_029800.1, NM_006059, NP_006050.3) exon 2 c.470G > A/p.Trp157* and exon 24 c.4030 + 1G > A by whole exome sequencing. Direct polymerase chain reaction and Sanger sequencing were used to verify these variants in the patient and her parents (**Figure 1C**). A heterozygous variant c.4030 + 1G > A on exon 24 of the father's *LAMC3* gene, and a heterozygous variant c.470G > A on exon 2 of the mother's *LAMC3* gene. c.470G > A was found in the Human Mutation Database (HGMD).[7] c.4030 + 1G > A was not found in the Genome Aggregation Database (gnomAD), 1000 Genome Project, or 1000 healthy controls. The pathogenicity prediction of the two variants was disease-causing for both using Mutation Taster (probability score: 1.0, range: 0–1.0 for both). In addition, c.470G > A was predicted to be damaging in PolyPhen2 and SIFT. Pathogenicity assessment according to the American College of Medical Genetics and Genomics (ACMG), revealed that both the c.470G > A and c.4030 + 1G > A were pathogenic (Richards et al., 2015).

[7]http://www.hgmd.cf.ac.uk/ac/index.php as ID, CM113688.

Functional Analysis

A truncated protein with a molecular weight of 47 kDa was found in *LAMC3* variant (c.470G > A) transfected cells, while a normal protein with a molecular weight of 198 kDd was found in the WT group (**Figure 2A**). However, the variant and WT group were both localized in the cytoplasm, and no significant difference was found (**Figure 2B**). To analyze of the variant c.4030 + 1G > A, three bioinformatics databases (BDGP, NetGene2, and HSF) were adopted to predict the effect of this variant on splicing, and all suggested that the variant would destroy the original Donor and affect the splicing. Then, the minigene comprising intron 23, exon 24, and intron 24 of the WT or variant (c.4030 + 1G > A) were constructed. Both the WT and mutated minigenes were transfected into HEK 293T and HeLa cells to verify this result, respectively (**Figures 2C,D**). The length of the product detected by RT-PCR in the WT group was consistent with the expected value in both HEK 293T and HeLa cells. However, a similar length of the product was observed in the variant group (**Figure 2E**). Furthermore, Sanger sequencing of RT-PCR products showed that the variant c.4030 + 1G > A affected the normal splicing of *LAMC3* mRNA, resulting in 4 bp base (ATAC) retention at the left of intron 24 (**Figure 2F**). The retention of these 4 bp bases further resulted in the production of a truncated protein consisting of 1,367 amino acids.

Prediction of the Pathogenic Mechanism

Currently, the mechanism of OCCM caused by *LAMC3* gene variants remained unclear. Therefore, this study intended to explore the pathogenic mechanism through bioinformatic methods. Firstly, online analysis software predicted that the first 19 amino acids of the laminin γ3 chain were the signal peptide sequences of the protein (**Figure 3A**), which was consistent with reported results (Koch et al., 1999). The STRING online database predicted ten genes (*DAG1*, *LAMA1*, *LAMA3*, *LAMA5*, *LAMB1*, *LAMB2*, *LAMB3*, *NID1*, *NID2*, and *NTN4*) associated with *LAMC3* at the interaction score of 0.4 (*P* value = 1.0e–16) (**Figure 3B**). The cellular component of gene ontology analysis indicated that *LAMC3* and its interacting proteins were mainly located in the basement membrane, extracellular matrix organization, laminin complex (**Figure 3C**). In addition, the biological processes of these proteins were involved in extracellular matrix organization, cell adhesion, cellular component organization, and anatomical structure morphogenesis (**Figure 3D**). Furthermore, the molecular function of gene ontology analysis showed that these proteins were primarily associated with structural molecule activity, protein-containing complex binding, signaling receptor binding, and laminin-1 binding (**Figure 3E**). Finally, KEGG pathway enrichment showed that ECM-receptor interaction was the most significant pathway and the other pathways contained amoebiasis, small cell lung cancer, toxoplasmosis, focal adhesion,

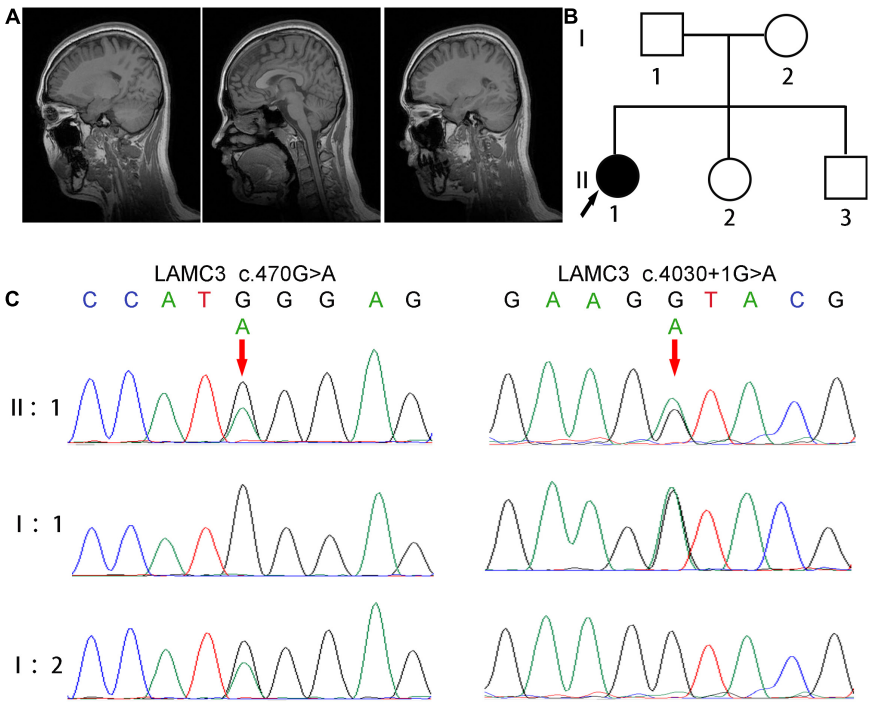

FIGURE 1 | Clinical and genetic characterizations. **(A)** Cranial MRI showed normal brain structure without abnormal signal and lateral ventricular dilation. **(B)** The pedigree of this family shows only the patient had epilepsy, and her parents and two younger siblings were both unaffected. **(C)** Direct polymerase chain reaction sequencing revealed a heterozygous variant c.4030 + 1G > A on exon 24 of the father's *LAMC3* gene, and a heterozygous variant c.470G > A on exon 2 of the mother's LAMC3 gene.

human papillomavirus infection, PI3K-Akt signaling pathway, and pathways in cancer (**Figure 3F**).

Literature Review

In 2011, Barak et al. first identified *LAMC3* gene variants as pathogenic variants in three unrelated Turkish families with occipital polymicrogyria and epileptic patients through whole-exome sequencing. Thus far, a total of 12 patients from six unrelated families worldwide (including our patients) have been reported with occipital cortical malformations due to *LAMC3* variants. Genetic and clinical characteristics were summarized in **Supplementary Table 1**. Firstly, there were seven variants in the *LAMC3* gene that have been identified, including one missense variant, five non-sense variants, and one frameshift variant. The patients in this study carried two variant sites in the *LAMC3* gene: one was c.470G > A, which has been reported by Barak et al. (Barak et al., 2011), and the other was the frameshift variant (c.4030 + 1G > A). This was the first time this frameshift variant has been reported. Seizure was the most common clinical feature of patients with OCCM caused by *LAMC3* gene variants. However, different patients suffered from different types of seizures, including myoclonic-astatic, atypical absence, complex partial, and vision loss. The patient in this study had an absence seizure as the main type of seizure, and had several generalized tonic-clonic seizures. The median age of seizure onset was 10 years old with a range of 2–13 years. In addition, developmental delay or degeneration was another typical clinical feature, including intellectual impairment, speech, fine motor skills delay, and language regression. However, the patient in this study had a normal developmental process with normal cognitive, language, and motor skills. Finally, pachygyria and polymicrogyria were the most representative imaging feature of patients with the *LAMC3* gene variant. The occipital cortex was the most important accumulation site, and the frontal, temporal, and parietal cortex were also reported. Pachygyria and polymicrogyria were not observed in this patient.

DISCUSSION

OCCM was one kind of MCD characterized by polymicrogyria and pachygyria confined to the occipital lobe and childhood-onset seizures. Studies have found that complex heterozygous or homozygous variants of the LAMC3 gene were responsible for OCCM. This study reported a Chinese female patient with recurrent seizures due to a novel complex heterozygous variant of the *LAMC3* gene. Among them, the non-sense variant (c.470G > A) has been reported by Barak et al. (Barak et al., 2011), while another the frameshift variant (c.4030 + 1G > A) was the first to be identified. Childhood-onset seizures, the most common clinical manifestation of OCCM, were also observed in this patient. However, what was remarkable about this patient was that cranial MRI did not show polymicrogyria and pachygyria in the occipital cortex or other areas. Furthermore,

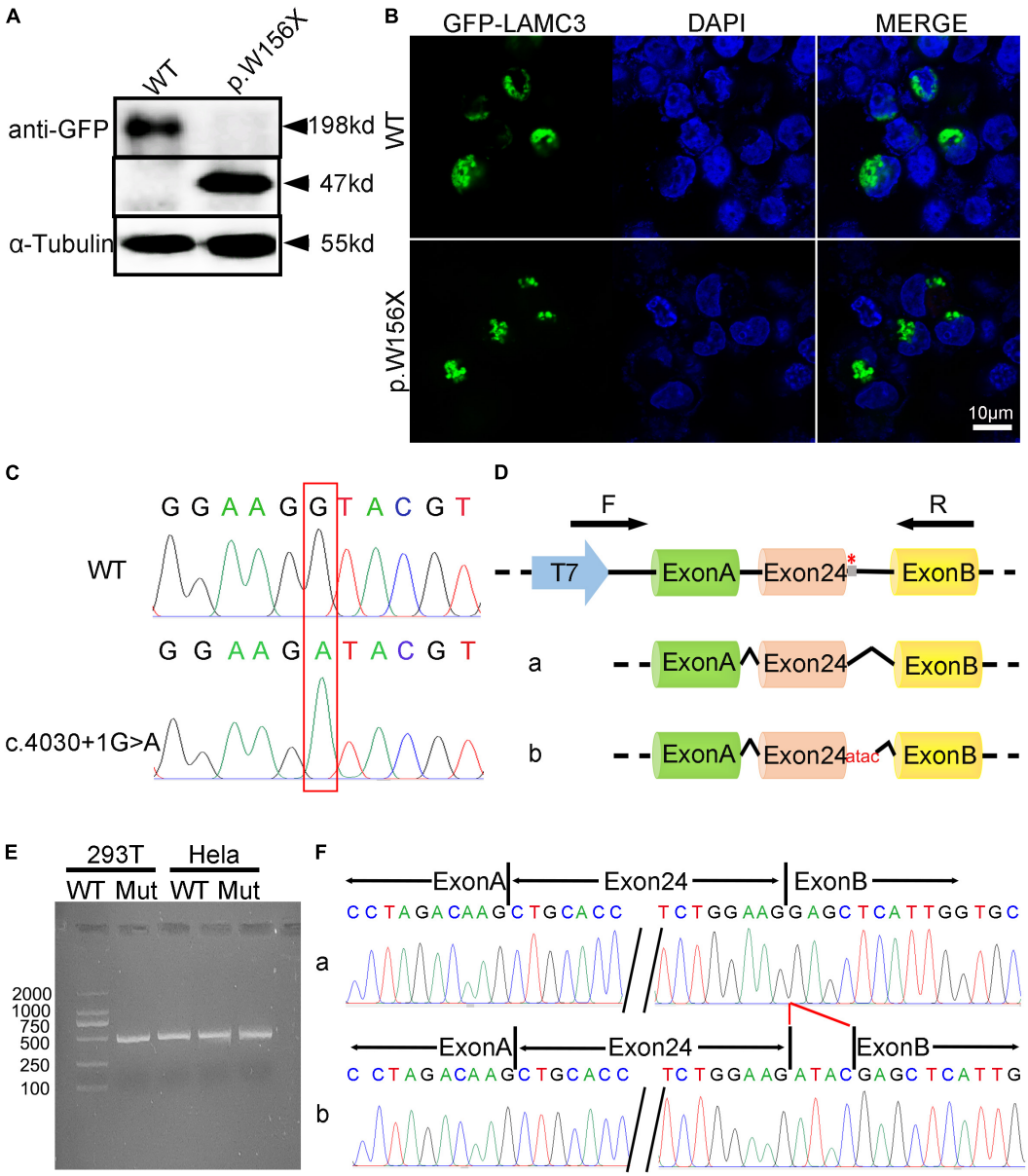

FIGURE 2 | The functional analysis of complex heterozygous variants in *LAMC3* gene. **(A)** The *LAMC3* WT group expressed a normal protein with a molecular weight of 198 kDd and a truncated protein with a molecular weight of 47 kDd in *LAMC3* variant group (c.470G > A). **(B)** The cellular localization of *LAMC3* in WT and variant group was in the cytoplasm without significant morphological difference. **(C)** Sanger sequence of minigene in in WT (above) and variant (below) group (c.4030 + 1G > A). **(D)** The schematic diagrams showed the minigene comprising intron 23, exon 24, and intron 24 of the WT or variant (c.4030 + 1G > A). The variant c.4030 + 1G > A affected the normal splicing of *LAMC3* mRNA, resulting in 4 bp base (ATAC) retention at the left of intron 24, "*" represents variant location. **(E)** Agarose gel electrophoresis of RT-PCR fragments showed a similar length of the product between the WT and variant group. **(F)** The Sanger sequences showed a 4 bp base (ATAC) retention at the left of intron 24 in the variant group.

the patient had no developmental delay, including language, motor, and cognitive ability. In terms of treatment, valproate could not control the occurrence of epilepsy in this patient, and levetiracetam achieved better control. This also provides a reference for the treatment of recurrent seizures caused by *LAMC3* variant.

The laminins, major components of basement membranes, are heterotrimeric molecules composed of a combination of different α, β, and γ chains (Durbeej, 2010).Until now, five α chains (α1-α5), three β chains (β1-β3), and three γ chains (γ1-γ3) have been recognized to correspond to different gene products (Tunggal et al., 2000; Durbeej, 2010). The LAMC3 gene (NG_029800.1, NM_006059, NP_006050.3) contains a total of 28 exons, which encodes a laminin gamma-3 chain protein with 1575 amino acids. Thus far, one missense variant, five non-sense variants, and one frameshift variant of the *LAMC3* gene have

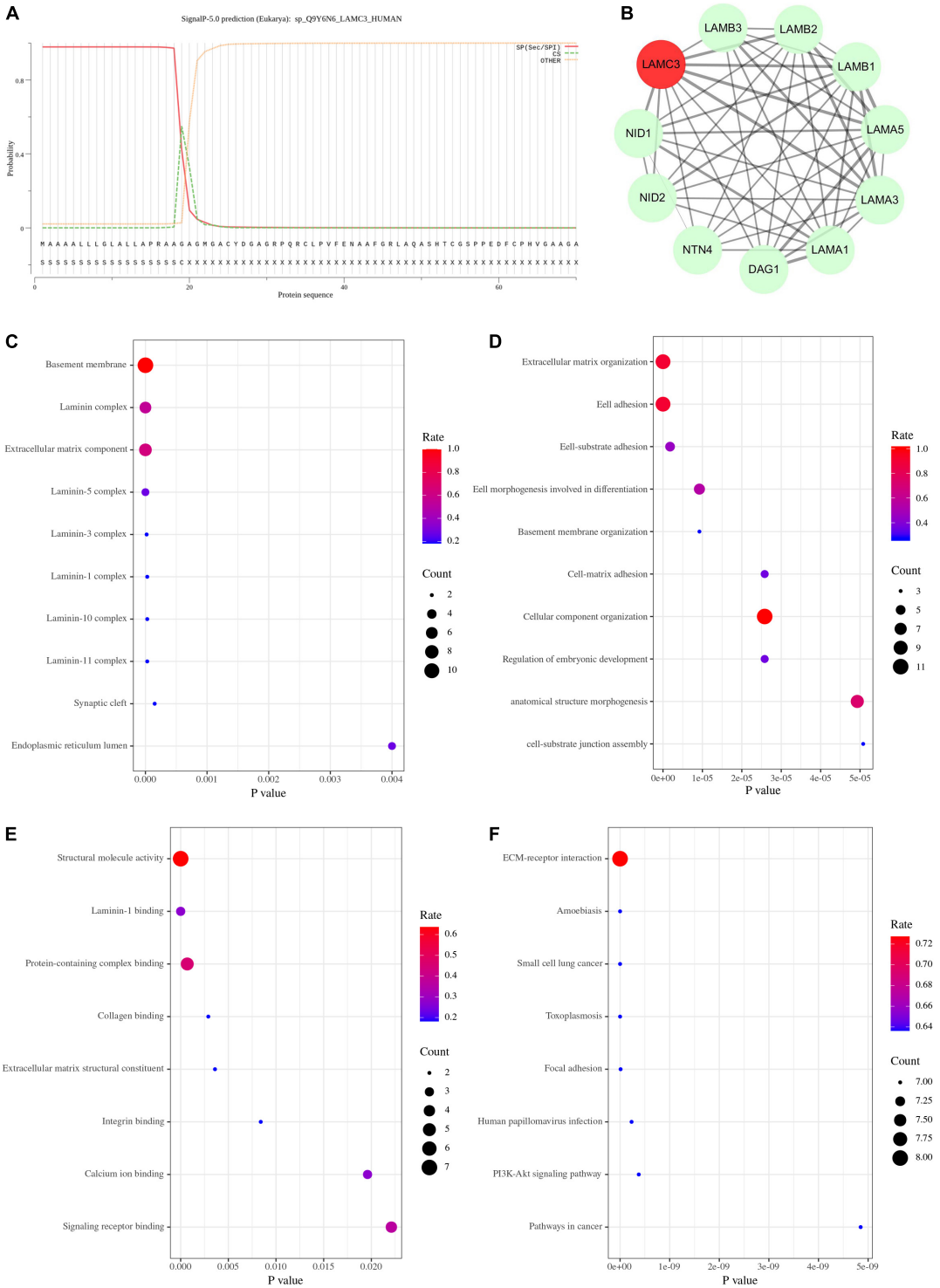

FIGURE 3 | The bioinformatics analysis of LAMC3 gene. **(A)** The first 19 amino acids of the laminin γ3 chain were predicted as a signal peptide. **(B)** The protein-protein interaction network showed 10 genes (*DAG1*, *LAMA1*, *LAMA3*, *LAMA5*, *LAMB1*, *LAMB2*, *LAMB3*, *NID1*, *NID2*, and *NTN4*) that have potential interactions with *LAMC3*. **(C)** The cellular component of gene ontology showed *LAMC3* and its interacting genes were mainly located in the basement membrane, extracellular matrix organization, laminin complex. **(D)** The biological process of gene ontology indicated these genes were mainly associated with extracellular matrix organization, cell adhesion, cellular component organization, and anatomical structure morphogenesis. **(E)** The molecular function of these genes were primarily involved in structural molecule activity, protein-containing complex binding, signaling receptor binding, and laminin-1 binding. **(F)** The KEGG pathway enrichment analysis showed eight potential signal pathways of these genes, including ECM-receptor interaction, amoebiasis, small cell lung cancer, toxoplasmosis, focal adhesion, human papillomavirus infection, PI3K-Akt signaling pathway, and pathways in cancer.

been identified including the two we found. More importantly, functional experiments demonstrated that both variant sites could cause premature truncation of the laminin γ3 chain. This is consistent with the previously reported effect of variants in the *LAMC3* gene, suggesting the importance of the loss of function caused by premature truncation of laminin γ3 chain in OCCM.

To explore the pathogenic mechanism of the *LAMC3* gene variant, we constructed a protein-protein interaction network with the *LAMC3* gene using bioinformatics. The top ten genes (*DAG1*, *LAMA1*, *LAMA3*, *LAMA5*, *LAMB1*, *LAMB2*, *LAMB3*, *NID1*, *NID2*, and *NTN4*) were predicted to be associated with *LAMC3*. *LAMA1*, *LAMA2*, *LAMC3*, *LAMB1*, and *LAMB2* genes can form different types of laminins through different permutations and combinations with *LAMC3*, such as laminin 213, 323, and 333 trimers (Li et al., 2012). In addition, *LAMC3* was predicted to be related to *NID1* and *NID2*, which was consistent with the previous study. The previous study demonstrated that the laminin γ3 chain was co-located with nidogen-1 and nidogen-2 (Iivanainen et al., 1999; Gersdorff et al., 2005). Furthermore, laminins are the major component of basement membranes, which together with the connective tissue matrix constituted the extracellular matrix (ECM) (Bonnans et al., 2014). The ECM has been shown to play role in structural support, cell differentiation, proliferation, adhesion, migration, and morphogenes (Frantz et al., 2010; Hynes, 2014; Pozzi et al., 2017). Therefore, the laminin γ3 chain, as an integral part of the ECM, plays an important role in these functions. In addition, recent studies on the distribution and function of the laminin γ3 chain in the CNS have found that the laminin γ3 chain was also expressed in the cell body and apical dendrites of the pyramidal neurons on the human temporal occipital region from late fetal development to late infancy (Barak et al., 2011; Zambonin et al., 2018). In the KEGG pathway enrichment analysis, the ECM-receptor interaction was the most significant pathway, which was consistent with the distribution and function of the laminin γ3 chain. Furthermore, the PI3K-AKT signal pathway was predicted as a candidate effector pathway and was activated by growth factors including fibroblast growth factor 2 (FGF2) and insulin-like growth factor 2 (IGF2) to mediate the cell proliferation and growth in the developing brain (Hevner, 2015). However, whether the laminin γ3 chain was involved in the regulation of this pathway remains unclear. It should be noted that studies have shown that the PI3K/AKT pathway was critical in MCD (Iffland and Crino, 2016; Benova and Jacques, 2019). For example, the mutation of the PI3K/AKT pathway was responsible for focal cortical dysplasias (FCDs), hemimegalencephaly (HMEG), and epileptogenic brain malformations (Jansen et al., 2015; Iffland and Crino, 2017). Therefore, the PI3K-AKT signal pathway may be a key pathogenic pathway in OCCM caused induced by the *LAMC3* gene variants. Animal model studies using *LAMC3* gene knockout mice have shown only mild abnormalities. In the nervous system, ectopia of granule cells in the cerebellum, and increased branching of capillaries in the outer retina were observed (Li et al., 2012). In zebrafish embryos, *LAMC3* knockdown resulted in defects in motor neuron guidance (Eve and Smith, 2017). Taken together, these studies suggest that *LAMC3* plays a unique role in the nervous system.

CONCLUSION

This work identified novel compound heterozygous variants in the *LAMC3* gene that causes OCCM with recurrent seizures without polymicrogyria and pachygyria. The administration of levetiracetam may be a relatively effective method to control epilepsy associated with *LAMC3* variants. In addition, both variant sites in the *LAMC3* gene could cause premature truncation of the laminin γ3 chain to loss of function. Finally, the extracellular matrix and the ECM-receptor interaction were the main location and signal transduction pathways of the laminin γ3 chain, respectively.

DATA AVAILABILITY STATEMENT

The raw data supporting the conclusions of this article will be made available by the authors, without undue reservation.

ETHICS STATEMENT

The studies involving human participants were reviewed and approved by the Ethics Committee of Ruijin Hospital affiliated with Shanghai Jiao Tong University School of Medicine. The patients/participants provided their written informed consent to participate in this study. Written informed consent was obtained from the individual(s) for the publication of any potentially identifiable images or data included in this article.

AUTHOR CONTRIBUTIONS

LC and HT proposed the idea and designed the study. XQ, XLi, and ZZ completed the experiments. XQ wrote the first draft of the manuscript. XLu provided the clinical patient information. SW, XS, and GC completed part of the manuscript. All authors contributed to manuscript revisions and approved the final version.

FUNDING

This work was supported by the grants from the National Natural Science Foundation of China (Nos. 81870889, 81571086, and 82071258) and National Key R&D Program of China (Nos. 2017YFC1310200 and 2016YFC1305804).

ACKNOWLEDGMENTS

We wish to thank the patient and her family for their cooperation.

SUPPLEMENTARY MATERIAL

The Supplementary Material for this article can be found online at: https://www.frontiersin.org/articles/10.3389/fgene.2021.616761/full#supplementary-material

REFERENCES

Afawi, Z., Oliver, K. L., Kivity, S., Mazarib, A., Blatt, I., Neufeld, M. Y., et al. (2016). Multiplex families with epilepsy: success of clinical and molecular genetic characterization. *Neurology* 86, 713–722. doi: 10.1212/WNL.0000000000002404

Barak, T., Kwan, K. Y., Louvi, A., Demirbilek, V., Saygı, S., Tüysüz, B., et al. (2011). Recessive LAMC3 mutations cause malformations of occipital cortical development. *Nat. Genet.* 43, 590–594. doi: 10.1038/ng.836

Barkovich, A. J., Guerrini, R., Kuzniecky, R. I., Jackson, G. D., and Dobyns, W. B. (2012). A developmental and genetic classification for malformations of cortical development: update 2012. *Brain* 135, 1348–1369. doi: 10.1093/brain/aws019

Benova, B., and Jacques, T. S. (2019). Genotype-phenotype correlations in focal malformations of cortical development: a pathway to integrated pathological diagnosis in epilepsy surgery. *Brain Pathol.* 29, 473–484. doi: 10.1111/bpa.12686

Bonnans, C., Chou, J., and Werb, Z. (2014). Remodelling the extracellular matrix in development and disease. *Nat. Rev. Mol. Cell Biol.* 15, 786–801. doi: 10.1038/nrm3904

Durbeej, M. (2010). Laminins. *Cell Tissue Res.* 339, 259–268. doi: 10.1007/s00441-009-0838-2

Eve, A. M. J., and Smith, J. C. (2017). Knockdown of Laminin gamma-3 (Lamc3) impairs motoneuron guidance in the zebrafish embryo. *Wellcome Open Res.* 2:111. doi: 10.12688/wellcomeopenres.12394.1

Frantz, C., Stewart, K. M., and Weaver, V. M. (2010). The extracellular matrix at a glance. *J. Cell Sci.* 123, 4195–4200. doi: 10.1242/jcs.023820

Gersdorff, N., Kohfeldt, E., Sasaki, T., Timpl, R., and Miosge, N. (2005). Laminin gamma3 chain binds to nidogen and is located in murine basement membranes. *J. Biol. Chem.* 280, 22146–22153. doi: 10.1074/jbc.M501875200

Gnanaguru, G., Bachay, G., Biswas, S., Pinzón-Duarte, G., Hunter, D. D., and Brunken, W. J. (2013). Laminins containing the β2 and γ3 chains regulate astrocyte migration and angiogenesis in the retina. *Development* 140, 2050–2060. doi: 10.1242/dev.087817

Hevner, R. F. (2015). Brain overgrowth in disorders of RTK-PI3K-AKT signaling: a mosaic of malformations. *Semin. Perinatol.* 39, 36–43. doi: 10.1053/j.semperi.2014.10.006

Hynes, R. O. (2014). Stretching the boundaries of extracellular matrix research. *Nat. Rev. Mol. Cell Biol.* 15, 761–763. doi: 10.1038/nrm3908

Iffland, P. H. II, and Crino, P. B. (2016). Sending Mixed Signals: the Expanding Role of Molecular Cascade Mutations in Malformations of Cortical Development and Epilepsy. *Epilepsy Curr.* 16, 158–163. doi: 10.5698/1535-7511-16.3.158

Iffland, P. H. II, and Crino, P. B. (2017). Focal Cortical Dysplasia: gene Mutations, Cell Signaling, and Therapeutic Implications. *Annu. Rev. Pathol.* 12, 547–571. doi: 10.1146/annurev-pathol-052016-100138

Iivanainen, A., Morita, T., and Tryggvason, K. (1999). Molecular cloning and tissue-specific expression of a novel murine laminin gamma3 chain. *J. Biol. Chem.* 274, 14107–14111. doi: 10.1074/jbc.274.20.14107

Jansen, L. A., Mirzaa, G. M., Ishak, G. E., O'Roak, B. J., Hiatt, J. B., Roden, W. H., et al. (2015). PI3K/AKT pathway mutations cause a spectrum of brain malformations from megalencephaly to focal cortical dysplasia. *Brain* 138, 1613–1628. doi: 10.1093/brain/awv045

Koch, M., Olson, P. F., Albus, A., Jin, W., Hunter, D. D., Brunken, W. J., et al. (1999). Characterization and expression of the laminin gamma3 chain: a novel, non-basement membrane-associated, laminin chain. *J. Cell Biol.* 145, 605–618. doi: 10.1083/jcb.145.3.605

Li, Y. N., Radner, S., French, M. M., Pinzón-Duarte, G., Daly, G. H., Burgeson, R. E., et al. (2012). The γ3 chain of laminin is widely but differentially expressed in murine basement membranes: expression and functional studies. *Matrix Biol.* 31, 120–134. doi: 10.1016/j.matbio.2011.12.002

Pozzi, A., Yurchenco, P. D., and Iozzo, R. V. (2017). The nature and biology of basement membranes. *Matrix Biol.* 5, 1–11. doi: 10.1016/j.matbio.2016.12.009

Raybaud, C., and Widjaja, E. (2011). Development and dysgenesis of the cerebral cortex: malformations of cortical development. *Neuroimaging Clin. N. Am.* 21, 483–543,vii. doi: 10.1016/j.nic.2011.05.014

Richards, S., Aziz, N., Bale, S., Bick, D., Das, S., Gastier-Foster, J., et al. (2015). Standards and guidelines for the interpretation of sequence variants: a joint consensus recommendation of the American College of Medical Genetics and Genomics and the Association for Molecular Pathology. *Genet. Med.* 17, 405–424. doi: 10.1038/gim.2015.30

Severino, M., Geraldo, A. F., Utz, N., Tortora, D., Pogledic, I., Klonowski, W., et al. (2020). Definitions and classification of malformations of cortical development: practical guidelines. *Brain* 143, 2874–2894. doi: 10.1093/brain/awaa174

Tunggal, P., Smyth, N., Paulsson, M., and Ott, M. C. (2000). Laminins: structure and genetic regulation. *Microsc. Res. Tech.* 51, 214–227.

Urgen, B. M., Topac, Y., Ustun, F. S., Demirayak, P., Oguz, K. K., Kansu, T., et al. (2019). Homozygous LAMC3 mutation links to structural and functional changes in visual attention networks. *Neuroimage* 190, 242–253. doi: 10.1016/j.neuroimage.2018.03.077

Zambonin, J. L., Dyment, D. A., Xi, Y., Lamont, R. E., Hartley, T., Miller, E., et al. (2018). A novel mutation in LAMC3 associated with generalized polymicrogyria of the cortex and epilepsy. *Neurogenetics* 19, 61–65. doi: 10.1007/s10048-017-0534-4

Zhu, Z., Zhang, C., Zhao, G., Liu, Q., Zhong, P., Zhang, M., et al. (2019). Novel mutations in the SPAST gene cause hereditary spastic paraplegia. *Parkinsonism. Relat. Disord.* 69, 125–133. doi: 10.1016/j.parkreldis.2019.11.007

Conflict of Interest: The authors declare that the research was conducted in the absence of any commercial or financial relationships that could be construed as a potential conflict of interest.

frontiers in Pediatrics

CASE REPORT
published: 29 July 2021
doi: 10.3389/fped.2021.675934

Case Report: Improved Height in a Patient With Myhre Syndrome Using a Combination of Growth Hormone and Letrozole

Hui Wu, Xinli Wang, Yunpu Cui and Xuemei Wang*

Department of Pediatrics, Peking University Health Science Center, Peking University Third Hospital, Beijing, China

Myhre syndrome is a rare disorder caused by a heterozygous mutation in the *SMAD4* gene. Affected patients may exhibit dysmorphic facial features, intrauterine growth retardation, short stature, obesity, muscle hypertrophy, thickened skin, limited joint movement, hearing impairment, and varying degrees of psychomotor developmental disorder. Serious complications of the cardiovascular and respiratory system may be seen later in life. We report the case of a Chinese boy with Myhre syndrome presenting with a novel symptom of giant testicles where treatment with growth hormone combined with letrozole successfully improved his short stature. This case shows that letrozole combined with growth hormone can improve height in children with Myhre syndrome without adverse effects.

Keywords: Myhre syndrome, growth hormone, letrozole, testicles, short stature

OPEN ACCESS

Edited by:
Liborio Stuppia,
University of Studies G. d'Annunzio Chieti and Pescara, Italy

Reviewed by:
Giorgio Radetti,
Ospedale di Bolzano, Italy
Yongyi Yuan,
PLA General Hospital, China

****Correspondence:***
Xinli Wang
obesity530@126.com

Specialty section:
This article was submitted to Pediatric Endocrinology, a section of the journal Frontiers in Pediatrics

Received: *04 March 2021*
Accepted: *05 July 2021*
Published: *29 July 2021*

Citation:
Wu H, Wang X, Cui Y and Wang X (2021) Case Report: Improved Height in a Patient With Myhre Syndrome Using a Combination of Growth Hormone and Letrozole. Front. Pediatr. 9:675934. doi: 10.3389/fped.2021.675934

INTRODUCTION

Myhre syndrome (MS, MIM 139210) is a rare autosomal, dominant, and hereditary disease caused by a mutation in the SMAD4 gene (1). The first case of MS was reported in 1981 (2). To date, 90 confirmed cases have been reported, with the youngest patient being 23 months old (3). Clinical manifestations include short stature, intrauterine growth restriction, dysmorphic facial features (blepharoptosis, prognathism, and small ears among others), varying degrees of cognitive impairment, decreased joint mobility, skin stiffness, and hearing impairment. Moreover, the common complications include hypertension, recurrent pericarditis, airway stenosis, and respiratory disorders. Few patients exhibit abnormal sexual development, such as premature puberty, cryptorchidism, secondary amenorrhea, and delayed sexual development (4). Additionally, skeletal abnormalities have been reported. Genetic testing has confirmed that almost all patients diagnosed with MS to date had de novo mutations in the SMAD4 gene, with only three cases resulting from an Arg496 residue mutation (5).

We report a case of a Chinese child with MS who was treated with growth hormone combined with letrozole and a yoga program.

CASE DESCRIPTION

The patient was the first child of healthy non-consanguineous parents, with no relevant family history. He was delivered by cesarean section for oligohydramnios at 38 weeks' gestation. His birth weight was 2,250 g (<P3), and his birth height was 45 cm (P3). Since birth, he had a slow growth rate

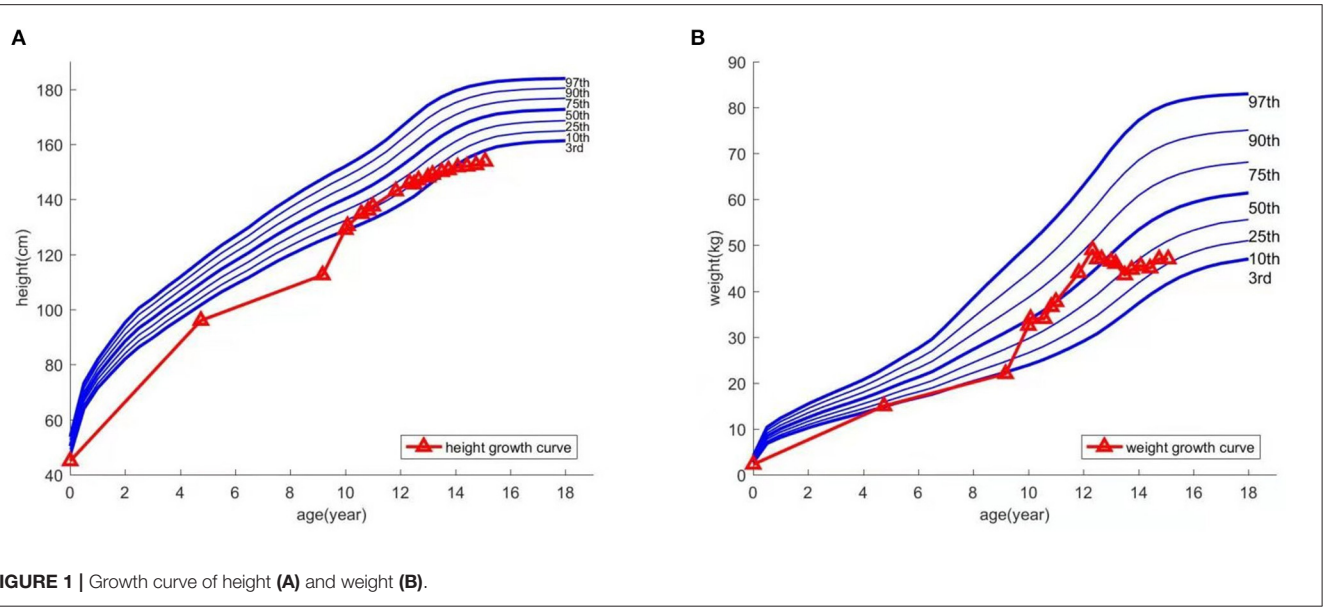

FIGURE 1 | Growth curve of height **(A)** and weight **(B)**.

and displayed difficulty squatting at age 3. At age 4 years and 9 months, he was 96 cm tall (<P3) and weighed 15 kg (P3); he was referred to a local hospital for growth retardation. His growth hormone level was normal, and no treatment was given at this time. At age 6, while his growth hormone level was still normal, he received growth hormone treatment for 1 year and his height increased by 10 cm; his parents then decided to stop the treatment.

At age 9, the patient experienced an abnormally large testicular growth. Examination showed a testicular volume of 6 ml, Tanner stage of pubic hair stage III, and bone age of 12 years and 1 month. A gonadotropin-releasing hormone (GnRH) provocation test showed a peak luteinizing hormone (LH) of 12 mIU/ml, with no abnormalities observed on pituitary magnetic resonance imaging and adrenal ultrasound. He was diagnosed with central precocious puberty and received triptorelin for 8 months, which was then discontinued due to his increasing bone age. Furthermore, the patient resumed growth hormone treatment. During the course, hyperinsulinemia developed intermittently and was controlled after growth hormone withdrawal. The patient was hyperactive and inattentive from an early age; his Intelligence Quotient test score was 85. Integrated visual and auditory continuous performance tests indicated severe sensory integration disorder. Height and weight growth are shown in the growth curve (**Figure 1**).

At age 12, he was referred to our outpatient clinic with the aim to further increase his height. His height and weight were 145.5 cm (P10) and 47 kg (P50-P75), respectively. Physical examination revealed abnormal facial features (short palpebral fissures, low nose bridge, small ears, short philtrum, prognathism) and a large body size. Short fingers, valgus elbows, and thick and rigid skin were observed (**Figure 2**). His testicular volume was 25–30 ml. His penis was 7 cm long, with a circumference of 9 cm. The Tanner stage of pubic hair was stage V.

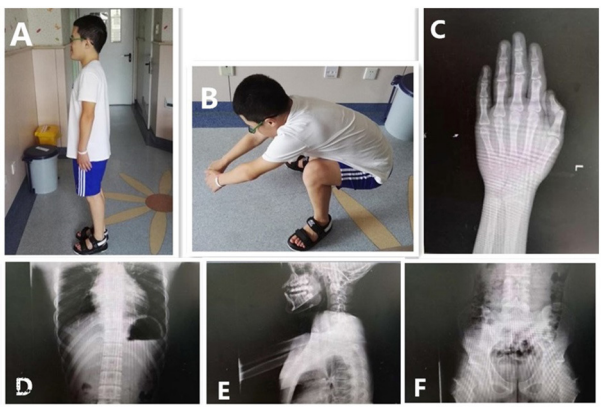

FIGURE 2 | Clinical features and radiographs of the proband at 12.5 years. Special facial features: small ears, prognathism, and short fingers **(A)**. Difficulty in squatting **(B)**. The bone age in the image of the left hand was 16.5 years old; the phalanges were short **(C)**. Anteroposterior and lateral images of the spine showed wide ribs, flat vertebral bodies, large pedicles, and small and hypoplastic iliac wings **(D–F)**.

Radiographic assessment indicated a bone age 16.5 years; his phalanges were short. No obvious abnormalities of the knees or spine were found; however, the vertebral bodies were flat with large pedicles. Wide ribs, hypoplastic iliac wings, and a small pelvis were noted. Echocardiogram, urinary ultrasound, and ultrasonography of the testicles and epididymis showed no abnormalities (**Figure 2**).

Laboratory tests revealed a slightly elevated glycosylated hemoglobin level A1c (HbA1c, 6.2%); the glucose tolerance and fasting insulin tests showed normal findings. Whole exome

sequencing detected a heterozygous mutation in the SMAD4 gene (NM-005359.5, c.1498A > G).

Due to the wishes of the parents to increase the boy's height, and after full disclosure of the potential risks and uncertainties of treatment, growth hormone (7 IU/day), letrozole (2.5 mg/day), and metformin (250 mg/day, 3 times a day) were administered for 31 months. Over the treatment course, the boy's height increased by 9 cm. Blood pressure; thyroid, liver, and kidney function; glucose; fasting insulin; 25-hydroxyvitamin D3; HbA1c and blood lipid levels were normal. The LH and FSH levels slightly increased compared to the child's basal levels; however, they returned to normal 1 year later. Testosterone (T) increased transiently at treatment initiation and then decreased to normal. Following yoga, the child was able to squat normally.

The child was followed up until he was 15 years old, at which time he was 153.8 cm tall (<P3) and weighed 47 kg (P10–P25). There were no pulmonary or abdominal abnormalities observed during his last physical examination; his bone age had remained the same (16.5 years). Considering the side effects of long-term medication, the child's parents agreed to stop the treatment. Timeline of the patient's treatment process was showed in **Figure 3**. Informed consent and full permission for publication of this case report were obtained from the parents.

DISCUSSION

We reviewed more than 90 cases of patients with MS reported so far, and more than 80% had short stature. Unfortunately, short stature treatment was described in detail in few cases. Only seven cases were treated with growth hormone with diverse results, of which only three had good outcomes (6, 7). However, to the best of our knowledge, none have used growth hormone combined with letrozole treatment.

Letrozole is an aromatase inhibitor, which catalyzes the conversion of androgen to estrogen. Excessive estrogen can cause premature epiphyseal closure, and aromatase inhibitors may be used to delay epiphyseal closure, thereby increasing adult height. However, a main problem with aromatase inhibition is the possible adverse effects on bone mineralization, which was only described as transitory in children. Vertebral deformities were observed in boys treated for delayed puberty onset (8). Further, aromatase-induced hyperandrogenemia may reduce high-density lipoprotein and increase hemoglobin levels (9). Treatment with growth hormone and letrozole has been used previously to improve the height of boys with idiopathic short stature. This case also showed vertebral changes, but it was in line with the typical manifestations of MS, and it had appeared before letrozole treatment. This is the first report of successful treatment using this regime in a patient with MS. Our results indicate that letrozole therapy is a safe and effective option in patients with MS and is free from any adverse side effects such as increased bone age. However, the long-term safety and efficacy of treatment with aromatase inhibitors in males is not well-established and should therefore be used with caution.

Increased testicular volume was observed throughout the course of this patient's treatment, a finding not previously reported. Earlier reports on sexual dysplasia associated with MS include precocious puberty, cryptorchidism, secondary amenorrhea, and delayed sexual development (10). We speculate that MS may cause dysfunction of the hypothalamic-pituitary-gonadal axis; however, the underlying mechanisms need to be further investigated.

In summary, we describe a case of MS in a child from mainland China. Following the wishes of the boy and his family,

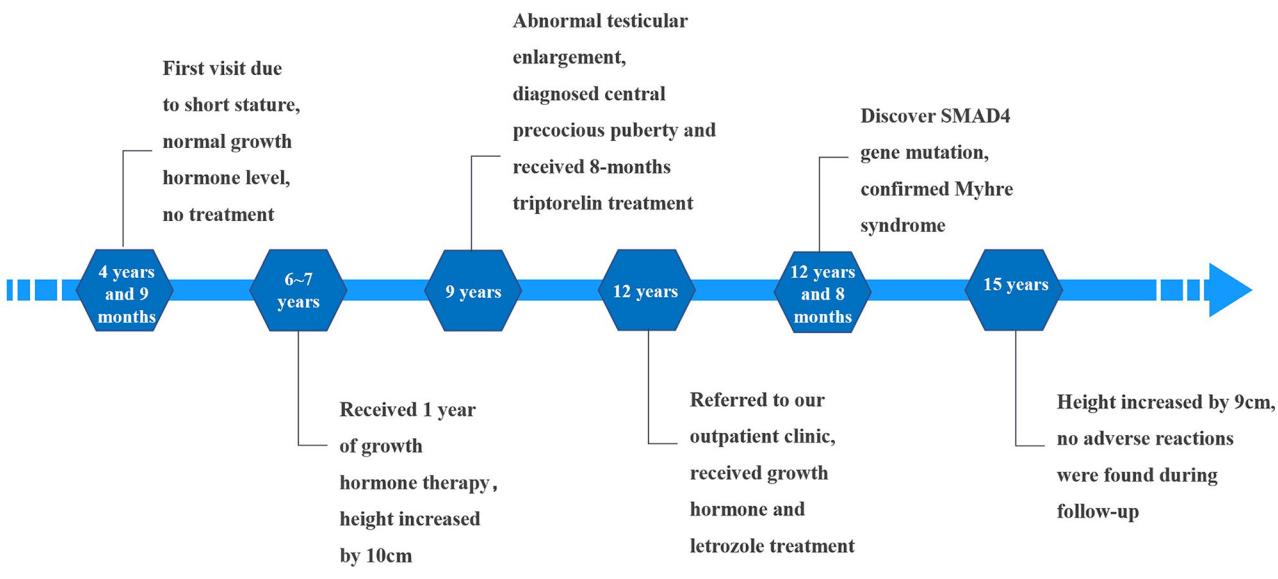

FIGURE 3 | Timeline of the patient's treatment process.

we treated him with growth hormone combined with letrozole and advised him to practice yoga. Following treatment, the boy's height increased, and he was able to squat better. Previous reports on MS focus on the clinical manifestations; however, we suggest using safe and appropriate individualized treatment considering the wishes of patients to improve their quality of life.

DATA AVAILABILITY STATEMENT

The raw data supporting the conclusions of this article will be made available by the authors, without undue reservation.

ETHICS STATEMENT

Ethical review and approval was not required for the study on human participants in accordance with the local legislation and institutional requirements. Written informed consent to participate in this study was provided by the participants' legal guardian/next of kin. Written informed consent was obtained from the individuals, and minors' legal guardian/next of kin, for the publication of any potentially identifiable images or data included in this article.

AUTHOR CONTRIBUTIONS

XW and HW were attending physicians of the patient. HW performed the literature review, and wrote the first draft of the manuscript. YC and XW assisted in the patient's treatment. XW critically revised the paper. All authors contributed to the article and approved the submitted version.

ACKNOWLEDGMENTS

We thank the patient and his family for their contribution to this work. We thank Mr. Li Jun from the School of Medical Humanities of Peking University for his polish and suggestions on the language of the article.

REFERENCES

1. Le Goff C, Mahaut C, Abhyankar A, Le Goff W, Serre V, Afenjar A, et al. Mutations at a single codon in Mad homology 2 domain of SMAD4 cause Myhre syndrome. *Nat Genet.* (2012) 44:85–8. doi: 10.1038/ng.1016
2. Myhre SA, Ruvalcaba RH, Graham CB. A new growth deficiency syndrome. *Clin Genet.* (1981) 20:1–5. doi: 10.1111/j.1399-0004.1981.tb01798.x
3. Hawkes L, Kini U. Myhre syndrome with facial paralysis and branch pulmonary stenosis. *Clin Dysmorphol.* (2015) 24:84–5. doi: 10.1097/MCD.0000000000000068
4. Asakura Y, Muroya K, Sato T, Kurosawa K, Nishimura G, Adachi M. First case of a Japanese girl with Myhre syndrome due to a heterozygous SMAD4 mutation. *Am J Med Genet A.* (2012) 158:1982–6. doi: 10.1002/ajmg.a.35440
5. Michot C, Le Goff C, Mahaut C, Afenjar A, Brooks AS, Campeau PM, et al. Myhre and LAPS syndromes: clinical and molecular review of 32 patients. *Eur J Hum Genet.* (2014) 22:1272–7. doi: 10.1038/ejhg.2013.288
6. Starr LJ, Grange DK, Delaney JW, Yetman AT, Hammel JM, Sanmann JN, et al. Myhre syndrome: clinical features and restrictive cardiopulmonary complications. *Am J Med Genet A.* (2015) 167:2893–901. doi: 10.1002/ajmg.a.37273
7. Le Goff C, Michot C, Cormier-Daire V. Myhre syndrome. *Clin Genet.* (2014) 85:503–13. doi: 10.1111/cge.12365
8. Hero M, Toiviainen-Salo S, Wickman S, Mäkitie O, Dunkel L. Vertebral morphology in aromatase inhibitor treated males with idiopathic short stature or constitutional delay of puberty. *J Bone Miner Res.* (2010) 25:1536-43. doi: 10.1002/jbmr.56
9. de Ronde W, de Jong FH. Aromatase inhibitors in men: effects and therapeutic options. *Reprod Biol Endocrinol.* (2011) 9:93. doi: 10.1186/1477-7827-9-93
10. Burglen L, Heron D, Moerman A, Dieux-Coeslier A, Bourguignon JP, Bachy A, et al. Myhre syndrome: new reports, review, and differential diagnosis. *J Med Genet.* (2003) 40:546–51. doi: 10.1136/jmg.40.7.546

Conflict of Interest: The authors declare that the research was conducted in the absence of any commercial or financial relationships that could be construed as a potential conflict of interest.

Publisher's Note: All claims expressed in this article are solely those of the authors and do not necessarily represent those of their affiliated organizations, or those of the publisher, the editors and the reviewers. Any product that may be evaluated in this article, or claim that may be made by its manufacturer, is not guaranteed or endorsed by the publisher.

frontiers in Genetics

CASE REPORT
published: 12 August 2021
doi: 10.3389/fgene.2021.708864

Retrospective Diagnosis of a Novel *ACAN* Pathogenic Variant in a Family With Short Stature: A Case Report and Review of the Literature

Valentina Mancioppi[1], Flavia Prodam[1,2,3], Simona Mellone[4], Roberta Ricotti[1], Enza Giglione[1], Nicolino Grasso[1], Denise Vurchio[4], Antonella Petri[1], Ivana Rabbone[1], Mara Giordano[4,5] and Simonetta Bellone[1,3]*

[1] Division of Pediatrics, Department of Health Sciences, University of Piemonte Orientale, Novara, Italy, [2] Endocrinology, Department of Translational Medicine, University of Piemonte Orientale, Novara, Italy, [3] Interdisciplinary Research Center of Autoimmune and Allergic Diseases, University of Piemonte Orientale, Novara, Italy, [4] Laboratory of Genetics, SCDU Biochimica Clinica, Ospedale Maggiore della Carità, Novara, Italy, [5] Department of Health Sciences, University of Piemonte Orientale, Novara, Italy

OPEN ACCESS

Edited by:
Massimo Zeviani, University of Padua, Italy

Reviewed by:
Saadullah Khan, Kohat University of Science and Technology, Pakistan
Liang-Liang Fan, Central South University, China

***Correspondence:**
Flavia Prodam
flavia.prodam@med.uniupo.it

Specialty section:
This article was submitted to Genetics of Common and Rare Diseases, a section of the journal Frontiers in Genetics

Received: *12 May 2021*
Accepted: *19 July 2021*
Published: *12 August 2021*

Citation:
Mancioppi V, Prodam F, Mellone S, Ricotti R, Giglione E, Grasso N, Vurchio D, Petri A, Rabbone I, Giordano M and Bellone S (2021) Retrospective Diagnosis of a Novel ACAN Pathogenic Variant in a Family With Short Stature: A Case Report and Review of the Literature. Front. Genet. 12:708864. doi: 10.3389/fgene.2021.708864

Short stature is a frequent disorder in the pediatric population and can be caused by multiple factors. In the last few years, the introduction of Next Generation Sequencing (NGS) in the molecular diagnostic workflow led to the discovery of mutations in novel genes causing short stature including heterozygous mutations in *ACAN* gene. It encodes for aggrecan, a primary proteoglycan component specific for the structure of the cartilage growth plate, articular and intervertebral disc. We report a novel *ACAN* heterozygous pathogenic variant in a family with idiopathic short stature, early-onset osteoarthritis and osteoarthritis dissecans (SSOAOD). We also performed a literature review summarizing the clinical characteristic of *ACAN*'s patients. The probands are two Caucasian sisters with a family history of short stature and osteoarthritis dissecans. They showed dysmorphic features such as mild midface hypoplasia, brachydactyly and broad thumbs, especially the great toes. The same phenotype was presented in the mother who had had short stature and suffered from intervertebral disc disease. DNA sequencing identified a heterozygous pathogenic variation (c.4390delG p.Val1464Ter) in the sisters, with a maternal inheritance. The nonsense mutation, located on exon 12, results in premature truncation and presumed loss of protein function. In terms of treatment, our patients underwent recombinant human growth hormone replacement therapy, associated with gonadotropin releasing hormone therapy, in order to block early growth cessation and therefore reach a better final height. Our case suggests that SSOAOD *ACAN* related should be considered in the differential diagnosis of children with autosomal dominant short stature and family history of joints disease.

Keywords: short stature, *ACAN*, mutation, aggrecans, osteoarthritis dissecans

INTRODUCTION

Short stature is defined as a height of at least two standard deviations below the average observed in age and sex control population (Hauer et al., 2017). It's a frequent disorder affecting 3% of the pediatric population and one of the most common causes of pediatric endocrinologist evaluation (Stavber et al., 2020). According to its etiology, short stature can be classified into primary growth disorder, secondary growth disorder and idiopathic short stature (ISS) (Xu et al., 2018). In addition to forms determined by common variants with polygenic inheritance, recent studies have highlighted that monogenic defects could be the cause of the growth disorder observed in non-syndromic children (Grunauer and Jorge, 2018; Vasques et al., 2019). More than 700 genes are associated with growth failure, with SHOX haploinsufficiency as the most frequent form, estimated to cause 2–3% of idiopathic short stature (ISS) cases (Fukami et al., 2016).

The introduction of NGS in the molecular diagnostic workflow led to the discovery of mutations in novel genes causing short stature including heterozygous mutations in *ACAN* gene (*ACAN*, OMIM:*155760) (Sentchordi-Montané et al., 2018). *ACAN* is located on chromosome 15q26 and consists of 19 exons, ranging in size from 77 to 4224 bp. It encodes for aggrecan, a primary proteoglycan component specific for the structure of the cartilage growth plate, articular and intervertebral disc (Uchida et al., 2020). Aggrecan is fundamental in articular cartilage, providing the hydrated gel structure necessary for the load-bearing properties of joints (Dateki, 2017) as well as chondrocyte and bone morphogenesis (Quintos et al., 2015). The core protein consists of three globular domains (G1, G2, and G3), interglobular domain (IGD), and centrally located glycosaminoglycan attachment region (GAG), consisting of chondroitin sulfate attachment domains (CS1 and CS2) and keratan sulfate attachment domain (KS) (**Figure 1**). G1 domain forms interactions with hyaluronan, G2 biological function is still not known whereas the G3 domain binds to different extracellular proteoglycans (i.e., tenascin and fibulin) via its C-type lectin repeat domain (CLD) (Gkourogianni et al., 2017). *ACAN* biallelic mutations are related to spondyloepimetaphyseal dysplasia, aggrecan type (SEMD, OMIM#612813) (Tompson et al., 2009), while mutations at the heterozygous state can cause spondyloepiphyseal dysplasia, Kimberley type (SEDK, OMIM#608361) (Gleghorn et al., 2005), short stature associated with or without accelerated bone age (BA), early-onset osteoarthritis (OA) and/or osteoarthritis dissecans (SSOAOD, OMIM#165800) and various idiopathic short stature phenotypes (Stattin et al., 2010; Quintos et al., 2015; Tatsi et al., 2017; Van der Steen et al., 2017).

Here we report two sisters from a family with idiopathic short stature, early-onset osteoarthritis and osteoarthritis dissecans caused by novel heterozygous *ACAN* variant.

CASE PRESENTATION

The probands are two caucasian sisters (III-1 and III-2, **Figures 2A,B**), previously referred to another hospital for persistent short stature.

III-1 was born full-term after an uncomplicated pregnancy and delivery. At birth, her weight was 3.3 kg (−0.05 SD), length of 46 cm (−2.12 SD), head circumference of 36 cm (+1.68 SD) and she presented normal psychomotor development (**Table 1**). Growth rate has been below normal during most of her childhood. At our first evaluation, she was 10.8 years old, her height was 125.8 cm (−2.5 SD) with a genetic target of 150.4 cm (−2 SD). The previous year her physical examination revealed bilateral breast development (Tanner stage B2) and gonadotropin releasing hormone stimulation test was performed (peak FSH value of 18.6 mU/ml, peak PH 7.3 mU/ml). She started Gonadotropin-releasing hormone (GnRH) treatment for precocious puberty with Triptorelin 11.25 mg i.m. every 4 weeks. The father's height (II-2) was 165.4 cm (−1.84 SD) while maternal height (II-1) was 147.3 cm (−2.6 SD). Maternal family history of short stature was described:

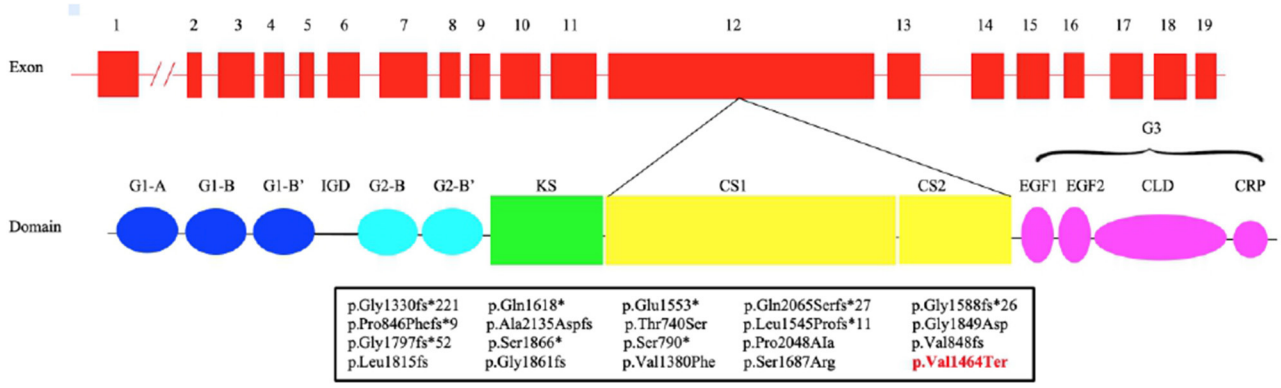

FIGURE 1 | Structure of ACAN gene and aggrecan protein. Pathogenic variants in exon 12 (bottom) with respective predicted changes in the amino acid sequence are shown. The mutations identified in previous studies are shown in black, while our is in red. CLD, C-type lectin domain; CRP, complement regulatory protein-like domain; CS1, chondroitin sulfate 1; CS2, chondroitin sulfate 2; EGF1, 2, epidermal growth factor–like domain 1, 2; G1, globular domain 1; G2, globular domain 2; G3, globular domain 3; IGD, interglobular domain; KS, keratan sulfate.

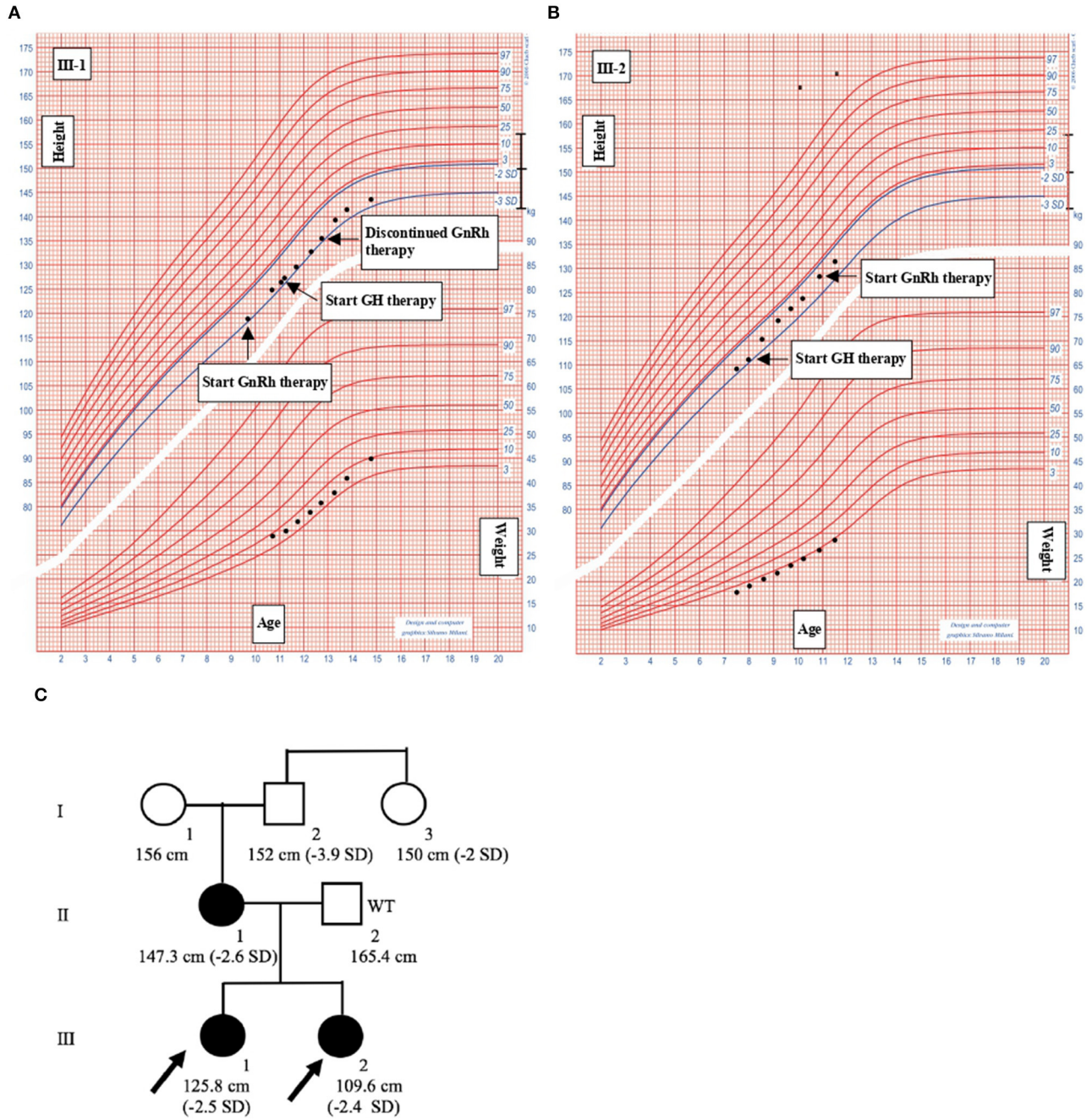

FIGURE 2 | Clinical informations of the family members. **(A)** III-1. **(B)** III-2. Growth charts of the probands. Heights and weights are shown as black points. GH, Growth hormone; GnRH, gonadotropin-releasing hormone. **(C)** Pedigree of the family with familiar short stature. Shaded symbols indicate patients with stature below 2 SD; empty symbols with "WT" (Wild Type) are family members without mutations; empty symbols indicate family members who have not undergone ACAN sequencing.

the grandfather's height (I-2) was 152 cm (−3.9 SD), the grandmother's height (I-1) was 156 cm (−1.12 SD) and the height of the grandfather's sister (I-3) was 150 cm (−2 SD) (**Figure 2C**). They had all the same phenotype characterized by short stature, macrocephaly, short neck, barrel chest, muscle hypertrophy and severe osteoarthritis. III-1 showed dysmorphic features such as macrocephaly, frontal bossing, low-set rotated ears, flat nasal filter, brachydactyly and broad thumbs, especially the great toes. Growth hormone (GH) stimulation test (arginine) produced a peak GH value of 25.6 ng/ml. Additional laboratory and endocrine assessment revealed normal complete blood count, chemistry panel, inflammatory markers, celiac screening, epatic-renal-thyroid function test, insulin-like growth factor-1 (IGF-1) (**Table 1**). The hand and wrist radiography showed no

TABLE 1 | Phenotype of our two patients with ACAN mutations.

Patient	III-1	III-2
Birth characteristics		
Weight (kg)	3.3	3.1
Length (cm)	46	46
HC (cm)	36	35.5
First visit		
Age (years)	10.8	7.6
Weight (kg)	28.9	18.6
Height (cm)	125.8	109.6
Target Height	150.4	150.4
Arm Span (cm)	131.5	108
Sit Height (cm)	64.5	58.9
Arm Span/height (cm)	1.04	0.99
Sit Height/height (cm)	0.51	0.54
Endocrine evaluation		
GH Peak at GH stimulation test (ng/ml)	25.6	27.9
IGF-1 (ng/ml)	275	132
Skeletal system		
Chronologic age (y)	10.6	7.6
Bone age (Greulich/Pyle)	11	7.6

HD, head circumference; GH, growth hormone.

characteristic signs of skeletal dysplasia, other than shortening of the 1st distal phalanx. According to the Greulich and Pyle method, her bone age (BA) was 0.6 years advanced relative to the calendar age (CA). She started recombinant human GH (rhGH) replacement therapy at a dose of 0.25 mg/kg/week when she was 11 year old. At 12.6 years of age, the treatment with GnRH was discontinued and menarche occurred at 14.5 years of age. Moreover in the last two years, she had a history of persistent pain in both knees: x-ray and magnetic resonance imaging detected multiple osteochondral lesions consistent with osteochondritis dissecans and she underwent a surgical operation. At her latest visit (age 14.7 years) her height was 143 cm (−2.3 SD) with a growth velocity of 2 cm/year (+0.6 SD).

The younger sister (III-2) was born full-term after an uncomplicated pregnancy with a birth weight of 3.1 kg (−0.85 SD), birth length of 46 cm (−2.34 SD), head circumference of 35.5 cm (+0.97), normal mental and motor development (**Table 1**). Short stature developed in early childhood, with appropriate weight for height. At our first visit, she was 7.6 years old, her height was 109.6 cm (−2.4 SD) and she was prepubertal. She had the same dysmorphic features as the older sister, bone age corresponding to chronological age, no signs of skeletal dysplasia. Growth hormone (GH) stimulation test (arginine) produced a peak GH value of 27.9 ng/ml. She had normal screening laboratory evaluation including complete blood count, inflammatory markers, celiac screening, epatic-renal-thyroid function test, insulin-like growth factor-1 (IGF-1) or other systemic explanation for her short stature (**Table 1**). At 8.2 years of age, she started GH therapy at a dose of 0.27 mg/kg/week. Thelarche occurred at approximately 11 years of age (height-−2.3 SD) and she was started on GnRH agonist (Triptorelin 11.25 mg i.m. every 4 weeks, still ongoing). She also suffered from persistent ankles' pain (especially the right), with the magnetic resonance imaging revealing mild osteochondritis dissecans. She didn't need to perform any surgical procedure but had to use bilateral ankle braces. At her latest visit (age 11.6 years) her height was 131.1 cm (−2.1 SD) with a growth rate of 5.3 cm/year (+1.4 SD).

After starting GH's therapy, both sisters were seen every 6 months for monitoring their growth and pubertal development but also for undergoing laboratory and endocrine assessment for glucose and lipid metabolism, epatic-renal-thyroid and corticotrope function test. All the evaluations were always normal; the dose adjustment for GH therapy was based on IGF-I levels. No side effects were registered for both GH and GnRH therapy. Clinical, anthropometric, and metabolic features during GH treatment are summarized in **Table 2**.

The mother had the same phenotype, characterized by short stature, macrocephaly, short neck, frontal bossing, flat nasal filter, brachydactyly and broad thumbs, especially the great toes. Despite having a stature < 2.6 SD, she was never referred to an endocrinologist or didn't undergo any endocrine assessment. From 35–40 years, she started suffering from severe intervertebral disc disease but didn't need to perform any surgical procedure.

METHODS

Genetic Analysis

Following written informed consent, the genomic DNA of the patients was extracted from peripheral blood through the ReliaPrep Blood gDNA Miniprep System (Promega), according to the manufacturer's recommendation. The GenetiSure Dx Postnatal Array 4x180K + SNP (Agilent Technologies, USA) was used following standard protocols.

The entire coding region of the *SHOX* gene (exon 1–exon 6a/6b) and intron–exon boundaries were amplified by PCR and sequenced by Big Dye Terminator Kit (Applied Biosystems, Foster City, CA) through the automatic sequencer ABI PRISM 3100 Genetic Analyzer (Applied Biosystems). Search for deletions/duplications was performed by an MLPA assay using an MLPA Commercial Kit (SALSA MLPA Kit P018-G1 SHOX; MRC-Holland, Amsterdam, Netherlands) following the manufacturer's instructions.

A custom-designed NGS panel including 67 genes [*A2ML1, ACAN, ANKRD11, BRAF, CBL, CHD7, COL2A1, COMP, CUL7, FGD1, FGF8, FGFR1, FGFR3, FLNB GH1, GHR, GHRH, GHRHR, GHSR, GLI2, GLI3, GNAS, HDAC6, HESX1, HMGA2, HRAS, IGF1, IGF1R, IGFALS, IHH, KAT6B, KDM6A, KRAS, LHX3, LHX4, LIG4, LZTR1, MATN3, MEK1, MEK2, NF1, NPPC, NPR2, NRAS, OTX2, PCNT, PDE3A, PDE4D, POC1A, POU1F1, PROK2, PROKR2, PROP1, PTPN11, RAF1, RIT1, SHH, SHOC2, SLC26A2, SOS1, SOS2, SOX2, SOX3, SOX9, SPRED1, STAT5B, TRIM37*] involved in bone growth plate development, hypothalamic-pituitary IGF-1 axis and reported mutated in syndromic short stature was used to investigate the presence of pathogenic variants in the two sibs. An

TABLE 2 | Clinical, anthropometric, and metabolic features at baseline and during GH treatment.

Clinical, anthropometric, and metabolic features	Baseline		1th year		2th year		3th year		4th year
	III-1	III-2	III-1	III-2	III-1	III-2	III-1	III-2	III-1
Age (years)	10.8	8.2	11.7	9.1	12.7	10.1	13.8	11.6	14.7
Height (cm)	125.8	112.5	130.3	117.7	133.7	123.6	140.7	131.1	143
Weight (kg)	28.9	19.7	31.9	22.2	35.7	24.8	38.3	29.4	45.5
Tanner Stage	B1 PH1	B1 PH1	B2 PH3	B1 PH1	B2 PH3	B2 PH1	B3 PH3	B2 PH1	B4 PH4
Growth velocity (cm/year)	–	–	5.7	6.1	3.9	6.1	4.6	5.3	2.0
GH dose (mg/day)	1.0	0.7	1.0	0.8	1.3	0.8	1.3	1.0	1.6
Side effects GH therapy	N.T.	N.T.	No	no	No	no	No	no	no
IGF-1 (ng/ml)	260.2	112	419.3	300.5	589.5	294.2	678.7	304.6	480.8
HbA1c (%)	5.2	5.2	5.3	5.0	5.5	5.0	5.2	4.7	5.0
Side effects GnRH therapy	No	N.T.	No	N.T.	Therapy discontinued	N.T.	N.T.	in therapy	N.T.

HbA1c, glycosylated hemoglobin; GH, growth hormone; IGF-1, Insulin-like growth factor-1; GnRH, gonadotropin-releasing hormone; N.T., not therapy.

Agilent SureSelectQXT target capture method was utilized with a panel size corresponding to 1.3 Mb. The sequencing probes were designed to cover all coding exons of the 67 genes and the 20 bp flanking sequence from the intron-exon boundary. Sequencing reaction was performed using an Illumina MiSeq and MiSeq v2 300 Cycle Reagent Kits. Variant calling was performed with the SureCall v3.5 software (Agilent Technologies) and VCF files were annotated with the wANNOVAR tool. Finally post aligned, annotated, and categorized sequence data was analyzed using a personalized bioinformatics pipeline: variants were filtered by frequency, excluding those with a MAF $\geq$0.01 in the public databases: 1000 Genome project (https://www.internationalgenome.org/) and gnomAD (https://gnomad.broadinstitute.org/). We prioritized variants causing frameshift, stop codon, splicing or aminoacidic changes predicted as pathogenic by at least four in silico prediction software (SIFT, Polyphen-2, Mutation Taster, CADD). Classification of variants was evaluated using the consensus guidelines as set out by the American College of Medical Genetics and Genomics (ACMG) guidelines (https://www.acmg.net/ACMG). Sanger sequencing was performed to confirm the presence or absence of these mutations in all the family members.

RESULTS

In the two sisters (III-1 and III-2) the aCGH revealed a normal female Karyotype and *SHOX* molecular analysis excluded any form of SHOX-haploinsufficiency. A targeted NGS panel containing 67 genes involved in syndromic and non-syndromic short stature detected in both sibs the presence of a heterozygous pathogenic variation in exon 12, namely c.4390delG that causes the changing of the reading frame from GTA encoding Valine at position 464 to stop codon (p.Val1464Ter). The variant, validated by Sanger sequencing, was inherited from the short stature mother (**Figure 3**).

DISCUSSION AND CONCLUSION

The etiology of short stature is complex and can be related to multiple factors such as GH deficiency, ISS, genetic inheritance, malnutrition, chronic disease (such as hypothyroidism, chronic liver and kidney diseases), constitutional delay of growth and puberty, intrauterine growth retardation, skeletal dysplasia, psychosocial stress and environmental factors (Liang et al., 2020; Wang et al., 2020). Based on new gene sequencing techniques, it is now possible to identify the cause of some short stature cases previously diagnosed as ISS.

We report a novel heterozygous mutation in *ACAN* (c.4390delG; p.Val1464Ter), located in exon 12, in a family with short stature associated with early-onset osteoarthritis and osteoarthritis dissecans (SSOAOD). Nilsson et al. (2014) reported for the first time that heterozygous *ACAN* mutations could be the cause of short stature and accelerated bone age (Nilsson et al., 2014). Since than an increasing number of *ACAN* pathogenic variants have been identified. To date, 93 mutations in this gene have been reported in HGMD (http://www.hgmd.cf.ac.uk/ac/index.php), with the majority of the variants (81/93) associated with ISS. Among them, 87.9% were inherited whereas the remaining arose *de novo*. Up to now 18 different mutations in exon 12 have been described (**Figure 1**; **Table 3**) (Gleghorn et al., 2005; Quintos et al., 2015; Gkourogianni et al., 2017; Hattori et al., 2017; Hauer et al., 2017; Tatsi et al., 2017; Van der Steen et al., 2017; Sentchordi-Montané et al., 2018; Zeng et al., 2018; Fukuhara et al., 2019; Uchida et al., 2020; Lin et al., 2021). This represents the exon with the highest number of mutations, accounting for the 19% of *ACAN* alterations (Liang et al., 2020; Lin et al., 2021). Exon 12 encodes for the chondroitin sulfate attachment domains (CS1 and CS2) and along with exon 11, for the keratan sulfate attachment domain (KS). Thanks to the sulfation of these domains (KS, CS1 and CS2) and the aggregation with hyaluronan, a fixed negative charge is generated (Dateki, 2017). This process is fundamental to cartilage because it attracts ions and water molecules, letting the cartilage bear the high mechanical load found in the skeletal joint (Gibson

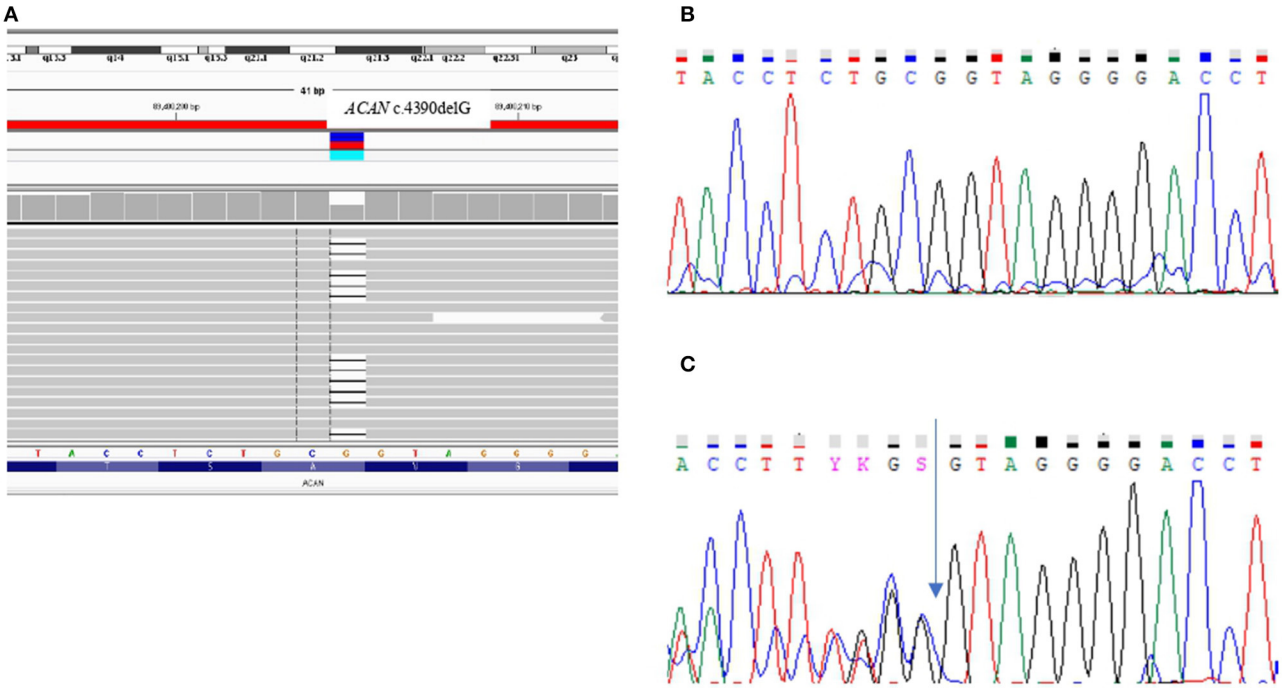

FIGURE 3 | Genetic analysis. **(A)** NGS file and **(B,C)** Sanger sequencing chromatograms reporting the wild-type **(B)** and the c.4390delG variant identified in the patients **(C)** in exon 12 (NM_013227) of the ACAN gene.

and Briggs, 2016). All heterozygous aggrecan mutations known so far cause short stature of similar severity, indicating that they similarly affect growth plate cartilage. Nevertheless, not all of them cause involve the articular cartilage and, therefore, determine early-onset osteoarthritis. Early-frameshift or splice-site mutations are likely to cause early truncation of the protein and may therefore functionally represent haploinsufficiency of *ACAN*. Patients with these types of mutations have short stature but no evidence of early-onset osteoarthritis, suggesting that *ACAN* haploinsufficiency primarily affects growth plate cartilage. Previously reported familial osteochondritis dissecans family and our family have missense or non-sence mutations in the C-type lectin domain and articular disease, suggesting that the presence of aggrecan protein with a dysfunctional C-type lectin domain causes a more severe phenotype affecting both growth plate and articular cartilage function (Nilsson et al., 2014). The nonsense mutation found in the present patients results in premature truncation and presumed loss of protein function. Ten frameshift variants, four missense variants and four nonsense variants (**Table 3**) had been previously identified in exon 12, causing a premature termination codon and the loss of the C-terminal globular domains (G3) (**Figure 1**; **Table 3**). G3 is fundamental for the proper protein function, contributing to the interaction between the aggrecan molecule and various components of the extracellular matrix (ECM) (Aspberg, 2012; Quintos et al., 2015). Nevertheless, numerous authors reiterate the importance of performing additional studies to determine whether these variants cause mRNA nonsense-mediated decay (NMD) or allow translation of a truncated aggrecan protein into the cartilage extracellular matrix (Gibson and Briggs, 2016; Stavber et al., 2020). To date, the few functional studies on the consequences of mutations in the G3 domain conducted showed the secretion of a truncated aggrecan, ruining cartilage structure and function with a dominant-negative effect (Tompson et al., 2009; Stattin et al., 2010; Gibson and Briggs, 2016).

The heterozygous variant detected in III-1 and III-2 was maternally inherited and their similar phenotype is consistent with that described in previous reports (**Table 3**), with short stature below −2.4/−2.5 SD, prognathia, flat nasal bridge, midfacial hypoplasia, posteriorly rotated ears, broad forehead, relative macrocephaly, brachydactyly, broad great toes, short thumbs, lordosis, genu valgum, joint problems (Dateki, 2017; Dateki et al., 2017; Hu et al., 2017; Van der Steen et al., 2017; Kim et al., 2020; Nilsson, 2020). The same characteristics can be detected, also, among patients carrying *ACAN* mutations located on other domains, underlying the absence of a genotype-phenotype correlation. The three most frequent features described among all *ACAN*'s patients were short neck, mild midface hypoplasia (frontal bossing, flat nasal bridge, and long philtrum), and brachydactyly, secondly osteoarthritis, spine malformation, short limbs, thoracic deformity (Liang et al., 2020). Both the sibs developed early-onset osteoarthritis (II-1 in the knee, while the III-2 in the ankle) and, subsequently, osteochondritis dissecans. While these clinical presentations are relatively common in patients carrying *ACAN* mutations, in the other cases with truncating mutations in the G3 domain there

TABLE 3 | Clinical findings of patients with ACAN mutation in exon 12 in this study and the literatures.

Subject	Mutation	Protein	Type	Sex/Age	Height (SDS)	Phenotype	Patterns of inheritance/affected family members (n)	References
1	c.3986dupC	p.Gly1330fs*221	Frameshift	NA	NA	SEDK	NA	Gleghorn et al. (2005)
2	c.4657G>T	p.Glu1553*	Nonsense	F/NA	−3.20	ISS, midface hypoplasia, flat nasal bridge, short thumbs, OA, familiar short stature with intervertebral disc disease	Mother/(7)	Gkourogianni et al. (2017)
3	c.4762_4765del	p.Gly1588fs*26	Frameshift	M/12.3 yr	−2.70	ISS, midface hypoplasia, broad great toes, posteriorly rotated ears, familiar short stature with hip joint problems, advanteg BA (13.3 yr)	Father/(2)	Van der Steen et al. (2017)
4a	c.5391delG	p.Gly1797fs*52	Frameshift	M/5.6 yr	−2.80	ISS, midface hypoplasia, flat nasal bridge, familiar short stature with hip joint problems, advanteg BA (8 yr)	Mother/(3)	Quintos et al. (2015)
4b	c.5391delG	p.Gly1797fs*52	Frameshift	M/NA	−2.60	ISS, midface hypoplasia, flat nasal bridge, short thumbs, markedly advanteg BA, familiar short stature	Mother/(3)	Gkourogianni et al. (2017)
5	c.5597C>A	p.Ser1866*	Nonsense	M/NA	−2.00	ISS, prominent forehead, short neck, barrel-shaped chest, brachydactyly, advanteg BA	*De novo* mutation	Hauer et al. (2017)
6	c.2218A>T	p.Thr740Ser	Missense	M/3.0 yr	−3.20	ISS, frontal bossing, midface hypoplasia, high arched palate, triangular face, brachydactyly, BA equal to CA, familiar short stature	NA/(1)	Sentchordi-Montané et al. (2018)
7	c.2369C>G	p.Ser790*	Nonsense	M/14.5 yr	−2.20	ISS, frontal bossing, broad nose and philtrum, hypertelorism, brachydactyly, hyperlordosis, advanteg BA (16.5 yr), no familiar short stature,	NA/(0)	Sentchordi-Montané et al. (2018)
8	c.6142C>G	p.Pro2048Ala	Missense	F/12.5 yr	−2.20	ISS, brachydactyly, BA equal to CA, familiar short stature	NA/(1)	Sentchordi-Montané et al. (2018)
9	c.463delT	p.Leu1545Profs*11	Frameshift	F/7.8 yr	−3.60	ISS, midface hypoplasia, short left 4th toe, broad 5th toes, short 1st distal phalanx, advanteg BA (8.10 yr), familiar short stature with early-onset invertebral disc disease	Mother/(3)	Uchida et al. (2020)
10	c.2535_2536 insTTCA	p.Pro846Phefs*9	Frameshift	M/4.9 yr	−2.47	ISS, BA equal to CA, no familiar short stature	*De novo* mutation	Hattori et al. (2017)

(Continued)

TABLE 3 | Continued

Subject	Mutation	Protein	Type	Sex/Age	Height (SDS)	Phenotype	Patterns of inheritance/affected family members (n)	References
11	c.6404delC	p.Ala2135Aspfs	Frameshift	M/6.9 yr	−3.20	Disproportionate short stature, midface hypoplasia, advanteg BA (9.9 yr), no familiar short stature	*De novo* mutation	Tatsi et al. (2017)
12	c.4852C>T	p.Gln1618*	Nonsense	M/11.7 yr	−4.00	ISS, attention deficit hyperactivity disorder, mild dysmorphic facial features as retrognathia and midface hypoplasia, BA equal to CA, familiar short stature with OA and invertebral disc disease	Father/(12)	Tatsi et al. (2017)
13a	c.6193delC	p.Gln2065Serfs*27	Frameshift	M/9.10 yr	NA	ISS, familiar short stature	Father/(3)	Zeng et al. (2018)
13b	c.6193delC	p.Gln2065Serfs*27	Frameshift	M/7 yr	NA	ISS, familiar short stature	Father/(3)	Zeng et al. (2018)
14	c.5443delC	p.Leu1815fs	Frameshift	M/4 yr	−4.38	ISS, BA equal to CA	NA	Lin et al. (2021)
15	c.5579delC	p.Gly1861fs	Frameshift	F/9.4 yr	−2.91	ISS, advanteg BA (10.7 yr),	NA	Lin et al. (2021)
16	c.4138G>T and c.5061T>A	p.Val1380Phe and p.Ser1687Arg	Missense	M/ 45 yr	−9.1	SEMD, diagnosis of osteogenesis imperfecta at 6 years of age	NA	Fukuhara et al. (2019)
17	c.2541del	p.Val848fs	Frameshift	NA	NA	ISS, OA, OCD	NA	-
18	c.5546G>A	p.Gly1849Asp	Missense	NA	NA	NA	NA	-
19a	c.4390delG	p.Val1464Ter	Nonsense	F/10.8 yr	−2.50	ISS, macrocephaly, frontal bossing, low-set rotated ears, flat nasal filter, brachydactyly and broad thumbs, OA, OCD, familiar short stature with early-onset invertebral disc disease, BA equal to CA	Mother/(3)	III-1 (current study)
19b	c.4390delG	p.Val1464Ter	Nonsense	F/7.6 yr	−2.40	ISS, macrocephaly, frontal bossing, low-set rotated ears, flat nasal filter, brachydactyly and broad thumbs, OA, OCD, familiar short stature with early-onset invertebral disc disease, BA equal to CA	Mother/(3)	III-2 (current study)

NA, not available; Yr, year; SEDK, spondyloepiphyseal dysplasia Kimberley type; ISS, idiopathic short stature; OA, osteoarthritis; OCD, osteochondritis dissecans; SEMD, spondyloepimetaphyseal dysplasia, aggrecan type.

were only two cases of early-onset osteoarthritis (Gleghorn et al., 2005; Gkourogianni et al., 2017) but no other osteochondritis dissecans. The two sibs presented joint problems at a young age (between 10–12 years), in contrast to previous reports where the common start was late adolescence or even later (Gkourogianni et al., 2017). Their affected mother (II-1) suffered from severe intervertebral disc disease, starting at 35–40 years, indicating wide phenotype variability within this family.

In terms of treatment, although the two sisters didn't develop precocious puberty, they underwent gonadotropin releasing hormone (GnRH) therapy, to block early growth cessation and therefore reached a better final height. Several studies evaluated the effectiveness of combined GH and GnRH analog treatment for achieving a proper final height in patients with *ACAN* mutations (Dateki, 2017; Van der Steen et al., 2017; Zeng et al., 2018; Stavber et al., 2020). Gkourogianni et al. (2017) found that the mean height SD for *ACAN* adult patients previously treated with GH was −2.5, while that of untreated adult individuals was −3.0 (Gkourogianni et al., 2017). Furthermore, Van der Steen et al. (2017) reported that GH-treated adult individuals, who received in addition GnRH analog treatment for two years from puberty (mean age of GnRH treatment's start between 10–12 years, with normal timing of puberty), gain 5–8 cm at their adult height compared to their family members, with the same sex and *ACAN* mutation (Van der Steen et al., 2017). Stavber et al. (2020) described the cases of three children who, in addition to GH treatment, received treatment with GnRHa during puberty after 10 years of age. During the combined therapy there was a significant improvement in SD height and growth velocity increased significantly. Nevertheless, the author underlines that it's not possible to establish the efficacy of the therapy since none of the patients have already achieved the final height at the time of publication (Stavber et al., 2020). Therefore, it is still controversial if *ACAN* patients need to undergo GH therapy with or without GnRHa to achieve a proper final height and further studies are needed (Dateki, 2017).

In conclusion we identified a novel heterozygous *ACAN* mutation causing SSOAOD in the family. SSOAOD *ACAN* related should be considered in the differential diagnosis of children with autosomal dominant short stature and family history of joints disease, even in patients in which BA is equal to CA. Diagnosis of the condition is difficult, and genetic testing may help. As for treatment, growth therapies could be beneficial for improving affected individuals' adult height.

DATA AVAILABILITY STATEMENT

The datasets for this article are not publicly available due to concerns regarding participant/patient anonymity. Requests to access the datasets should be directed to the corresponding author.

AUTHOR CONTRIBUTIONS

VM collected the anamnestic as well as the biochemical data for the patients. VM performed the literature search, reviewed and extracted data from the papers. MG and SM performed the genetic analysis. VM performed the figures and table designing and the manuscript writing with the assistance of MG, SB, and FP. All authors discussed the results and contributed to the final manuscript.

ACKNOWLEDGMENTS

We would like to thank the patients for their participation in this work.

REFERENCES

Aspberg, A. (2012). The different roles of aggrecan interaction domains. *J. Histochem. Cytochem.* 60, 987–996. doi: 10.1369/00221554124 64376

Dateki, S. (2017). ACAN mutations as a cause of familial short stature. *Clin. Pediatr. Endocrinol.* 26, 119–125. doi: 10.1297/cpe.26.119

Dateki, S., Nakatomi, A., Watanabe, S., Shimizu, H., Inoue, Y., Baba, H., et al. (2017). Identification of a novel heterozygous mutation of the Aggrecan gene in a family with idiopathic short stature and multiple intervertebral disc herniation. *J. Hum. Genet.* 62, 717–721. doi: 10.1038/jhg.2017.33

Fukami, M., Seki, A., and Ogata, T. (2016). SHOX Haploinsufficiency as a cause of syndromic and nonsyndromic short stature. *Mol. Syndromol.* 7, 3–11. doi: 10.1159/000444596

Fukuhara, Y., Cho, S. Y., Miyazaki, O., Hattori, A., Seo, J. H., Mashima, R., et al. (2019). The second report on spondyloepimetaphyseal dysplasia, aggrecan type: a milder phenotype than originally reported. *Clin. Dysmorphol.* 28, 26–29. doi: 10.1097/MCD.0000000000000241

Gibson, B. G., and Briggs, M. D. (2016). The aggrecanopathies; an evolving phenotypic spectrum of human genetic skeletal diseases. *Orphanet J. Rare Dis.* 11:86. doi: 10.1186/s13023-016-0459-2

Gkourogianni, A., Andrew, M., Tyzinski, L., Crocker, M., Douglas, J., Dunbar, N., et al. (2017). Clinical characterization of patients with autosomal dominant short stature due to aggrecan mutations. *J. Clin. Endocrinol. Metab.* 102, 460–469. doi: 10.1210/jc.2016-3313

Gleghorn, L., Ramesar, R., Beighton, P., and Wallis, G. (2005). A mutation in the variable repeat region of the aggrecan gene (AGC1) causes a form of spondyloepiphyseal dysplasia associated with severe, premature osteoarthritis. *Am. J. Hum. Genet.* 77, 484–490. doi: 10.1086/444401

Grunauer, M., and Jorge, A. A. L. (2018). Genetic short stature. *Growth Horm. IGF Res.* 38, 29–33. doi: 10.1016/j.ghir.2017.12.003

Hattori, A., Katoh-Fukui, Y., Nakamura, A., Matsubara, K., Kamimaki, T., Tanaka, H., et al. (2017). Next generation sequencing-based mutation screening of 86 patients with idiopathic short stature. *Endocr. J.* 64(10), 947–954. doi: 10.1507/endocrj.EJ17-0150

Hauer, N. N., Sticht, H., Boppudi, S., Büttner, C., Kraus, C., Trautmann, U., et al. (2017). Genetic screening confirms heterozygous mutations in ACAN as a major cause of idiopathic short stature. *Sci Rep.* 22:12225. doi: 10.1038/s41598-017-12465-6

Hu, X., Gui, B., Su, J., Li, H., Li, N., Yu, T., et al. (2017). Novel pathogenic ACAN variants in non-syndromic short stature patients. *Clin. Chim. Acta* 469, 126–129. doi: 10.1016/j.cca.2017.04.004

Kim, Y. T., Jang, K. M., Keum, C. W., Oh, S. H., and Chung, W. Y. (2020). Identification of a heterozygous ACAN mutation in a 15-year-old boy with short stature who presented with advanced bone age: a case report and review of the literature. *Ann. Pediatr. Endocrinol. Metabol.* 25, 272–276. doi: 10.6065/apem.1938198.099

Liang, H., Miao, H., Pan, H., Yang, H., Gong, F., Duan, L., et al. (2020). Growth-promoting therapies may be useful in short stature patients with nonspecific skeletal abnormalities caused by Acan heterozygous mutations:

six Chinese cases and literature review. *Endocr. Pract.* 26, 1255–1268. doi: 10.4158/EP-2019-0518

Lin, L., Li, M., Luo, J., Li, P., Zhou, S., Yang, Y., et al. (2021). A high proportion of novel ACAN mutations and their prevalence in a large cohort of Chinese short stature children. *J. Clin. Endocrinol. Metab.* 106(7):e2711–e2719. doi: 10.1210/clinem/dgab088

Nilsson, O. (2020). Aggrecanopathies highlight the need for genetic evaluation of ISS children. *Eur J. Endocrinol.* 183:C9–C10. doi: 10.1530/EJE-20-0420

Nilsson, O., Guo, M. H., Dunbar, N., Popovic, J., Flynn, D., Jacobsen, C., et al. (2014). Short stature, accelerated bone maturation, and early growth cessation due to heterozygous aggrecan mutations. *J. Clin. Endocrinol. Metab.* 99, E1510–E1518. doi: 10.1210/jc.2014-1332

Quintos, J. B., Guo, M. H., and Dauber, A. (2015). Idiopathic short stature due to novel heterozygous mutation of the aggrecan gene. *J. Pediatr. Endocrinol. Metab.* 28, 927–932. doi: 10.1515/jpem-2014-0450

Sentchordi-Montané, L., Aza-Carmona, M., Benito-Sanz, S., Barreda-Bonis, A. C., Sánchez-Garre, C., Prieto-Matos, P., et al. (2018). Heterozygous aggrecan variants are associated with short stature and brachydactyly: description of 16 probands and a review of the literature. *Clin. Endocrinol. (Oxf).* 88, 820–829. doi: 10.1111/cen.13581

Stattin, E. L., Wiklund, F., Lindblom, K., Onnerfjord, P., Jonsson, B. A., Tegner, Y., et al. (2010). A missense mutation in the aggrecan C-type lectin domain disrupts extracellular matrix interactions and causes dominant familial osteochondritis dissecans. *Am. J. Hum. Genet.* 86, 126–137. doi: 10.1016/j.ajhg.2009.12.018

Stavber, L., Hovnik, T., Kotnik, P., Lovrečić, L., Kovač, J., Tesovnik, T., et al. (2020). High frequency of pathogenic ACAN variants including an intragenic deletion in selected individuals with short stature. *Eur. J. Endocrinol.* 182, 243–253. doi: 10.1530/EJE-19-0771

Tatsi, C., Gkourogianni, A., Mohnike, K., DeArment, D., Witchel, S., Andrade, A. C., et al. (2017). Aggrecan mutations in nonfamilial short stature and short stature without accelerated skeletal maturation. *J. Endocr. Soc.* 1, 1006–1011. doi: 10.1210/js.2017-00229

Tompson, S. W., Merriman, B., Funari, V. A., Fresquet, M., Lachman, R. S., Rimoin, D. L., et al. (2009). A recessive skeletal dysplasia, SEMD aggrecan type, results from a missense mutation affecting the C-type lectin domain of aggrecan. *Am. J. Hum. Genet.* 84, 72–79. doi: 10.1016/j.ajhg.2008.12.001

Uchida, N., Shibata, H., Nishimura, G., and Hasegawa, T. (2020). A novel mutation in the ACAN gene in a family with autosomal dominant short stature and intervertebral disc disease. *Hum. Genome Var.* 7:44. doi: 10.1038/s41439-020-00132-8

Van der Steen, M., Pfundt, R., Maas, S. J. W. H., Bakker-van Waarde, W. M., Odink, R. J., and Hokken-Koelega, A. C. S. (2017). ACAN gene mutations in short children born SGA and response to growth hormone treatment. *J. Clin. Endocrinol. Metab.* 102, 1458–1467. doi: 10.1210/jc.2016-2941

Vasques, G. A., Andrade, N. L. M., and Jorge, A. A. L. (2019). Genetic causes of isolated short stature. *Arch. Endocrinol. Metab.* 63, 70–78. doi: 10.20945/2359-3997000000105

Wang, Y., Ge, J., Ma, J., Qiao, L., and Li, T. (2020). Short stature with precocious puberty caused by aggrecan gene mutation: a case report. *Medicine (Baltimore)* 99:e21635. doi: 10.1097/MD.0000000000021635

Xu, D., Sun, C., Zhou, Z., Wu, B., Yang, L., Chang, Z., et al. (2018). Novel aggrecan variant, p. Gln2364Pro, causes severe familial nonsyndromic adult short stature and poor growth hormone response in Chinese children. *BMC Med. Genet.* 19:79. doi: 10.1186/s12881-018-0591-z

Zeng, T., Liao, L. Y., Li, N., Wang, J., Peng, J., Guo, Y., et al. (2018). Familial short stature caused by ACAN gene mutation: a familial case report [in Chinese]. *J. Clin. Pediatr.* 36, 463–466. doi: 10.3969/j.issn.1000-3606.2018.06.015

Conflict of Interest: The authors declare that the research was conducted in the absence of any commercial or financial relationships that could be construed as a potential conflict of interest.

Publisher's Note: All claims expressed in this article are solely those of the authors and do not necessarily represent those of their affiliated organizations, or those of the publisher, the editors and the reviewers. Any product that may be evaluated in this article, or claim that may be made by its manufacturer, is not guaranteed or endorsed by the publisher.

frontiers in Endocrinology

ORIGINAL RESEARCH
published: 30 September 2021
doi: 10.3389/fendo.2021.604500

A Chinese Case of Cornelia de Lange Syndrome Caused by a Pathogenic Variant in *SMC3* and a Literature Review

Ran Li[1], *Bowen Tian*[2], *Hanting Liang*[1], *Meiping Chen*[1], *Hongbo Yang*[1], *Linjie Wang*[1], *Hui Pan*[1] *and Huijuan Zhu*[1]*

[1] *Key Laboratory of Endocrinology of National Health Commission, Department of Endocrinology, Peking Union Medical College Hospital, Chinese Academy of Medical Science and Peking Union Medical College, Beijing, China,* [2] *Department of Internal Medicine, Peking Union Medical College Hospital, Chinese Academy of Medical Science and Peking Union Medical College, Beijing, China*

OPEN ACCESS

Edited by:
Liborio Stuppia, University of Studies G. d'Annunzio Chieti and Pescara, Italy

Reviewed by:
Paolo Guanciali-Franchi, University of Studies G. d'Annunzio Chieti and Pescara, Italy
Feliciano J. Ramos, University of Zaragoza, Spain

***Correspondence:**
Huijuan Zhu
shengxin2004@163.com

Specialty section:
This article was submitted to Pediatric Endocrinology, a section of the journal Frontiers in Endocrinology

Received: *09 September 2020*
Accepted: *06 September 2021*
Published: *30 September 2021*

Citation:
Li R, Tian B, Liang H, Chen M, Yang H, Wang L, Pan H and Zhu H (2021) A Chinese Case of Cornelia de Lange Syndrome Caused by a Pathogenic Variant in SMC3 and a Literature Review. Front. Endocrinol. 12:604500. doi: 10.3389/fendo.2021.604500

Purpose: Cornelia de Lange syndrome (CdLS) is a rare congenital developmental disorder, and cases caused by variants in *SMC3* are infrequent. This article describes a case of CdLS related to a pathogenic variant in *SMC3* and performs a literature review.

Methods: We collected clinical data and biological samples from a 12-year-old boy with "short stature for 11 years". Gene variants in the proband were detected by whole-exome sequencing, and the variants in his parents were verified by Sanger sequencing. All *SMC3*-related CdLS patients from the PubMed and Web of Science databases were collected and summarized using the available data.

Results: A pathogenic variant in *SMC3* in the proband, c.1942A>G, was identified. Neither of his parents carried the same variant. Twenty-eight patients were diagnosed with CdLS with variants in *SMC3*, including the cases in this study and those reported in the literature, where half of the variant types were missense, followed by 32% (9/28) with a deletion and 11% (3/28) with a duplication. All patients showed symptoms of verbal development delay and intellectual disability to different degrees, and 90% patients had long eyelashes while 89% patients had arched eyebrows.

Conclusion: This study summarized different gene variants in *SMC3* and the frequencies of the various clinical manifestations according to the reported literature. For CdLS caused by *SMC3* variants, short stature and facial dysmorphic features are the two most important clinical clues. Definite diagnosis of this rare disease may be challenging clinically; thus, it is significant to use molecular diagnosis.

Keywords: *SMC3*, Cornelia de Lange syndrome, short stature, growth disorders, heterozygous pathogenic variants

INTRODUCTION

Cornelia De Lange syndrome (CdLS) is a rare multisystem congenital developmental disorder inherited in an autosomal dominant manner or X-linked manner (1). Its predominant features include craniofacial malformations, stunted growth, cognitive impairment, behavioral abnormalities, limb deformities and internal organ changes such as gastroesophageal reflux. CdLS was first reported in two infants by Dutch pediatrician Cornelia de Lange in 1933 (2). The reports of its global prevalence are inconsistent. Kline reported it affected approximately 1~3/10000 (3), while Barisic revealed that its prevalence is approximately 1.6~2.2/100000 (4). To some extent, not all individuals with CdLS exhibit the abovementioned typical clinical characteristics, which are complex and diverse, with varying degrees of severity, so the exact incidence and prevalence still need further study (5).

The cohesin complex is a protein consisting of four core subunits, namely, *SMC1A, SMC3, RAD21*, and *STAG*, which form a circular structure that encircles chromatin (6). The complex remains evolutionarily conserved from prokaryotes to eukaryotes. The cohesin complex is mainly involved in the regulation of gene expression, forming DNA loops with CCCTC binding factor (CTCF) and maintaining the normality of chromosomal domains (6). In addition, in the cell cycle, factors such as *NIPBL* and *HDAC8* assist the cohesin complex in maintaining its normal function. In addition, it is responsible for the stability of the genome by participating in the DNA double-strand mismatch repair mechanism, ensuring proper chromosome separation during mitosis and meiosis (7).

Due to the continuous development of gene sequencing technology, the pathogenesis of CdLS has been attributed to variants of genes that encode the structure and regulatory factors of the cohesin complex. Some of the CdLS-related genes have been identified, including *SMC1A*, *SMC3*, *RAD21*, *NIPBL*, *HDAC8*, *BRD4* and *ANKRD11* (8). According to related studies, CdLS has obvious genetic heterogeneity. All of the previously mentioned genetic variants can only explain a small proportion of the clinical cases (3). There are also some typical CdLS patients who do not have the previously mentioned gene variants. In addition, some studies have concluded that the clinical manifestations of CdLS are related to the different kinds of genetic variants that cause the disease. Among them, truncated pathogenic variants in the *NIPBL* gene cause the most serious phenotype, and the phenotype associated with missense variants in *NIPBL* and *SMC3* is relatively milder (6).

This study reported a case of CdLS and summarized all reported cases caused by SMC3 variants to obtain an in-depth comprehension of this rare disease.

PATIENT AND METHODS

Patient

The patient was 11.7 years old and was admitted to Peking Union Medical College Hospital with the main complaint of "short stature". Because of his special physical signs, he underwent whole-exome sequencing (WES) after a routine evaluation of thyroid function, growth hormone and bone age. He was found to carry a pathogenic variant in SMC3 and was thus diagnosed with CdLS. The parents signed informed consent forms regarding the research conducted on this boy. This study was performed with the approval of the Ethics Committee of Peking Union Medical College Hospital (JS-1663) and was conducted in accordance with the Declaration of Helsinki.

DNA Extraction and Whole-Exome Sequencing

We collected approximately 2~3 ml of peripheral blood from the boy (EDTA anticoagulation), and then peripheral blood DNA was extracted by using a Blood DNA Midi Kit (Omega D3494-04, Biotek, USA). To make a precise diagnosis, we performed WES on the proband. Using 3 μg of genomic DNA from each subject for detection, we sheared the DNA into 100~500 base pairs (bp) with a Covaris LE220 ultrasonicator (Massachusetts, USA), and then fragments measuring 150 to 200 bp were picked out by magnetic beads. An adaptor-ligated library that was quality controlled by an Agilent 2100 Bioanalyzer was set up for each individual subject. The cyclized library was continuously sequenced for 50 cycles by a BGISEQ-500 high-throughput sequencer (BGI, Shenzhen, China), and the raw sequencing data were read. Sequencing reads were aligned to a reference human genome (HG19/HG20) using Burrows-Wheeler Aligner (BWA) software, and single nucleotide variants and insertions and deletions were detected by Genome Analysis Toolkit 4.0 (GATK) software, followed by alignment of the database (NCBI dbSNP, HapMap, the 1000 Genomes dataset and a database of 100 healthy Chinese adults) screened for suspicious variants.

Verification of the *SMC3* Pathogenic Variant by Sanger Sequencing

Primers for our patient's *SMC*3 variant located in exon 18 were designed by the online tool 'Primer-BLAST' (https://www.ncbi.nlm.nih.gov/tools/primer-blast/) based on the *SMC3* reference sequence (NG_012217.1) obtained from NCBI. Forward and reverse primers for *SMC3* (c.1942A>G) were 5'-CAGGG AAAACGCCAATCGTT-3' and 5'-TGCATACAGCTCAA CTGACA-3'.

Total polymerase chain reaction systems containing 10 μl of Taq SuperMix (2X reaction buffer, Taq DNA polymerase dNTPs), 6 μl of double-distilled water, 2 μl of genomic DNA, and 1 μl of forward and reverse primers (10 μmol/L) were amplified. The cycling conditions were 94°C for 4 minutes; 35 cycles of 94°C for 30 seconds, appropriate annealing temperatures for 30 seconds and 72°C for 30 seconds; and one cycle at 72°C for 4 minutes followed by storage at 4°C. The pathogenicity of the *SMC3* variant in this boy was graded according to the American College of Medical Genetics and Genomics (ACMG) guidelines (9).

Literature Review and Statistical Analysis

All cases of CdLS (up to February 1st, 2020) were collected from the PubMed and Web of Science databases using the keywords

"Cornelia de Lange syndrome", and the identified papers were carefully reviewed to include all relevant papers (9–16). The clinical manifestations and genetic results of all cases reported were analyzed and summarized by using SPSS version 25.0.

RESULTS

Case Report

An 11.7-year-old boy was admitted to our hospital with the chief complaint of short stature. His birth weight was 2.45 kg (-2.15 standard deviation score, SDS), and his birth length was 49 cm (-0.79 SDS). He underwent full-term natural delivery and lived in a neonatal incubator for a week due to pyloric spasm. The maternal pregnancy history was unremarkable. In his daily life, he had hyperactivity disorder and poor academic performance, and his pronunciation was vague. He often had enuresis at night.

One year after birth, his height was found to be shorter than normal without detailed records. At the age of 5.5 years, he underwent a growth hormone stimulating test, and the results showed that his growth hormone (GH) baseline was 3.54 ng/ml, and the GH peak value was 8.49 ng/ml. His results of insulin-like growth factor-1 (IGF-1) and insulin-like growth factor binding protein-3 (IGFBP-3) were all within the normal ranges. Therefore, he was diagnosed with partial growth deficiency and was treated with recombinant human growth hormone (rhGH) (unknown dosage). The treatment lasted for 3 months, which resulted in a height increase of 3 cm but it was stopped due to the high cost of the therapy. His pronunciation was nebulous.

The physical examination results when visiting our outpatient clinic were as follows: his height was 125.4 cm (-3.3 SDS), and his weight was 21 kg (-3.2 SDS). The growth curve of the patient is shown in **Figure 1A**. His dentition was very disorderly (**Figure 1B**). He had a thin body, slender limbs, a head circumference of 48 cm, an armspan of 132 cm, and clinodactyly of the 5th finger. HbA1c, thyroid function tests, liver and renal function tests and routine blood tests were normal. His IGF1 level was 133 ng/ml (reference range, RR: 111~551 ng/m, -1.8 SDS). His bone age was approximately 7 years old while his chronological age was 11.7 years (**Figure 1C**).

The parents denied consanguinity. His father was 180 cm tall, and his mother was 155 cm tall. The height of his 18-year-old brother was 176 cm.

Genetic Study

His karyotype was normal (46,XY). The WES results of the proband were as follows: a heterozygous variant in exon 18 of *SMC3*, c.1942A>G (p. Met648Val), was detected. This pathogenic variant of *SMC3* is a missense variant that causes CdLS-3 (MIM 610759). After receiving the genetic results of the proband, the corresponding variant sites of the parents were checked. The results of *SMC3* gene Sanger sequencing showed that neither of his parents carried the same variant in *SMC3* (**Figure 2**).

Literature Review

Due to the rapid development of genetic testing technology, CdLS has been reported in many cases with variants in various genes and different sites since the first case of CdLS was reported in 1933 (2). To date, it is widely believed that CdLS is primarily caused by variants in seven genes, including *NIPBL*, *SMC1A*, *SMC3*, *RAD21*, *BRD4*, *HDAC8* and *ANKRD11*. Through February 1, 2020, 27 cases of CdLS with definite variants of

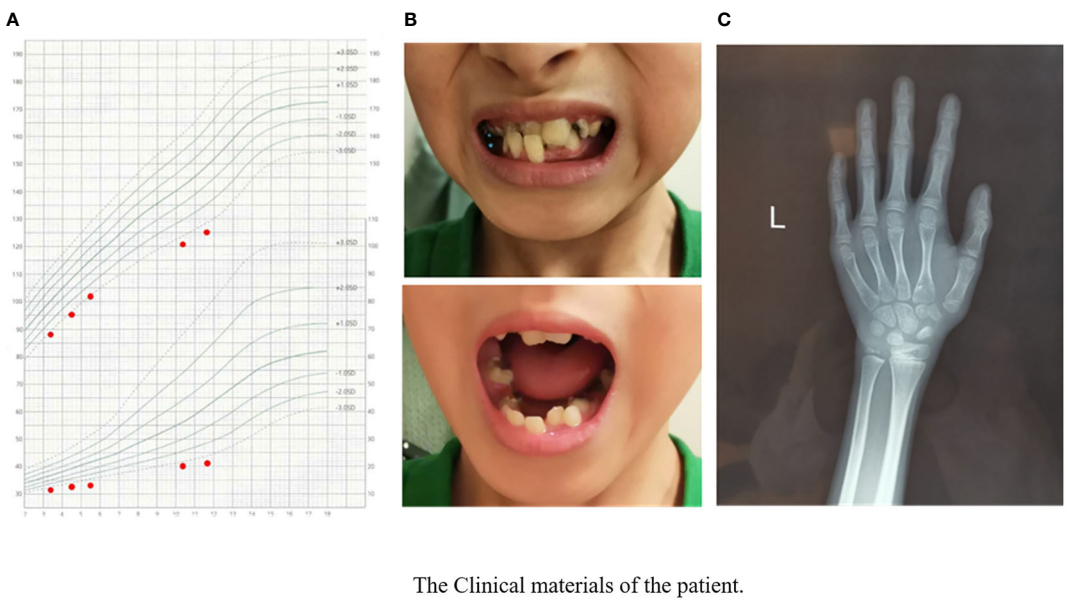

FIGURE 1 | The clinical materials of the patient's growth chart. **(A)** The manifestation of the patient's teeth. **(B)** X-ray of the patient's left hand and wrist. **(C)** Bone age was approximately 7 years when the patients' chronological age was 11 years 8 months.

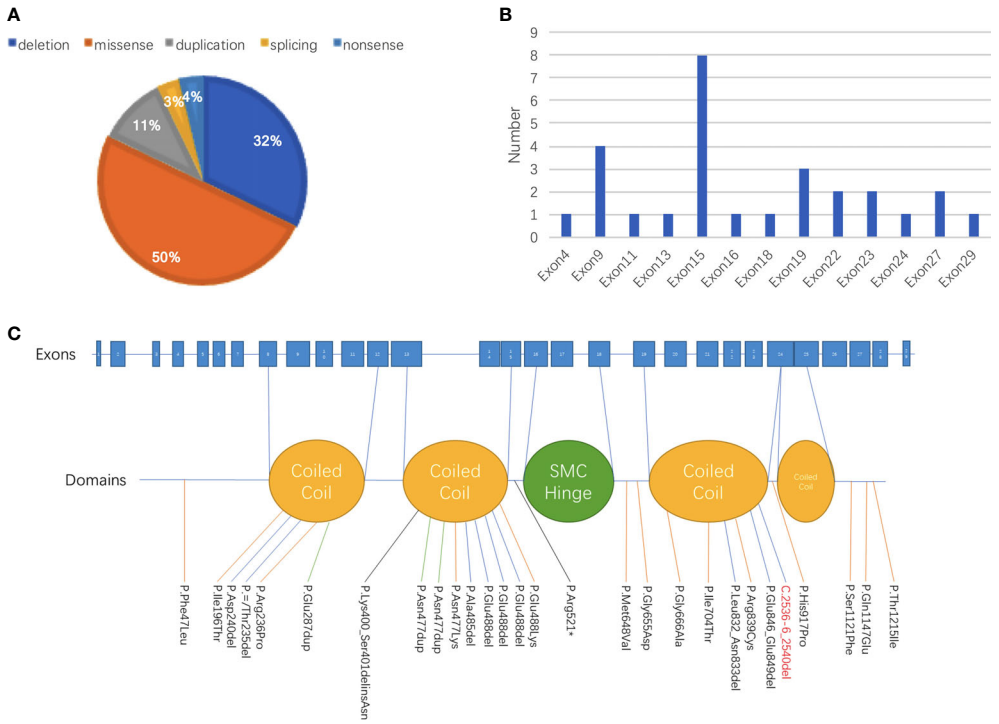

FIGURE 2 | Summary of genetic abnormalities in patients with CdLS carrying *SMC3* pathogenic variants. **(A)** Among all 28 patients with records of genetic alterations, half of the variant types were missense, followed by deletion (32% [9/28]) and duplication (11% [3/28]). One patient was discovered carrying a splicing variant, and one patient was detected with a nonsense variant. **(B)** The site with the largest proportion of variants in *SMC3* was exon 15, which was 28.6%, followed by variants that occurred in exon 9, exon 19, exon 22, exon 23, and exon 27. **(C)** The proportion of patients whose variants were in the domain named coiled coil was 60% (12/20), and 40% (8/20) of patients had alterations in other parts.

SMC3 were reported (**Tables 1** and **2**), including 22 cases with detailed clinical data including sex and age. None of these cases were reported in a consanguineous family. The male to female ratio was 1.44 (13:9) from the available data. In regard to the age distribution of the patients, 6 of 21 (28.6%) people with a recorded age were adults, and 8 of 21 (38.1%) were infants whose ages were between one and three. The remaining 7 patients ranged from 3 to 18 years old. The patients' mean age when they were diagnosed was 10.8 ± 9.7 years old. For the recorded gestational weeks of 18 patients, including the case reported in our center, 14 patients were full-term deliveries, and 4 patients were premature, of which two had the shortest gestational weeks, only 35 weeks. One article reported that among patients with prenatal CdLS, symmetric intrauterine growth restriction (IUGR) with onset in the second trimester was the most common finding significant for the diagnosis of CdLS (17). However, there were no records about the birth weight or length of these patients, which suggests that we need to pay extra attention to such infants.

Detailed clinical characteristics of all of the patients are listed in **Table 2**. Verbal developmental delay and intellectual disability were found in all patients. Other clinical manifestations with relatively higher frequencies include long eyelashes (90% [18/20]), arched eyebrows (89% [17/19]), hirsutism (84% [16/19]), feeding problems in infancy (80% [12/15]), syndactyly of toes (78% [14/18]), broad/bulbous nasal tip (76% [13/17]), synophrys (74% [14/19]), short fifth finger (71% [12/17]), thick eyebrows (71% [12/17]), proximally set thumbs (70% [14/20]) and thin upper lip vermilion (70% [14/20]). In the current case, our patient showed a suspected condition of chronic constipation, which has been reported in the previous literature (5). However, there was no available information about constipation in other cases of patients with *SMC3* variants. According to the evaluation standard stated in a previous study, 20 patients with detailed records of their clinical manifestations were rated. According to the classification of the disease's severity raised by Kline et al., only 3 of them reached severe levels, 10 of them reached moderate levels, and 7 of them were regarded as mild levels (18). However, among the clinical data we obtained thus far, biochemical data and imaging auxiliary examination data are extremely limited.

Except for a baby girl whose variant was inherited from her mother, there were 18 patients with *de novo* variants as confirmed by parental verification. The proportions of different types of variants are shown in **Figure 2**. Among all 28 patients with records of genetic alterations, half of the variant types were missense (50% [14/28]), followed by deletion (32% [9/28]) and duplication (11% [3/28]). Additionally, there was one patient

TABLE 1 | Frequency of Clinical Features in Individuals with *SMC3* variants.

Clinical Characteristics	Frequency
Brachycephaly	58% (11/19)
Low anterior hairline	50% (9/18)
Microcephaly	47% (9/19)
Arched eyebrows	89% (17/19)
Synophrys	74% (14/19)
Thick eyebrows	71% (12/17)
Long eyelashes	90% (18/20)
Depressed nasal bridge	44% (8/18)
Anteverted nostrils	53% (9/17)
Long and/or featureless philtrum	56% (10/18)
Broad/bulbous nasal tip	76% (13/17)
Thin upper lip vermilion	70% (14/20)
Downturned corners of mouth	53% (10/19)
Micrognathia/retrognathia	53% (10/19)
Small hands	67% (12/18)
Proximally set thumbs	70% (14/20)
Short first metacarpal	61% (11/18)
Clinodactyly fifth finger	61% (11/18)
Short fifth finger	71% (12/17)
Hirsutism	84% (16/19)
Small feet	69% (11/16)
Syndactyly of toes	78% (14/18)
Restriction of elbow movements	50% (6/12)
Cardiac defects	61% (11/18)
Feeding problems in infancy	80% (12/15)
Hearing loss	53% (8/15)
Verbal developmental delay	100% (19/19)
Intellectual disability	100% (13/13)

with splicing variant and one patient with nonsense variant. At the same time, we have an idea of the number of variants in each exon as shown in **Figure 2B**. The number of variants that occurred in exon 15 accounted for the largest proportion (28.6%), followed by variants that occurred in exon 9, exon 19, exon 22, exon 23, and exon 27. Different variants corresponding to different protein domains are listed in **Figure 2C**. The proportion of patients whose variants were located in the coiled-coil domain was 60% (12/20), and patients whose alterations were located in other parts accounted for 40% (8/20).

DISCUSSION

When a short stature patient has multisystem involvement, such as limb deformities, organ dysplasia, and cognitive and behavioral defects, it is necessary to pay attention to possible genetic diseases. With the development of gene sequencing technology, Sanger sequencing, panel detection and WES will help us identify the underlying genetic abnormalities and make a molecular diagnosis of a specific genetic disease. As an important type of dwarfism caused by a single gene variant, CdLS is relatively rare, but if the patient has typical facial features, poor language and mental development, or various hand deformities, we ought to consider its possibility.

In this case, the patient's long arms attracted our attention. Although his height was 125.4 cm, he had a 132 cm armspan at that time. To our knowledge, symptoms of a significantly longer armspan than height have never been reported in patients carrying variants in *SMC3*; therefore, careful physical examination provides valuable clues in diagnosing genetic disease. Additionally, this patient had a unique manifestation of his dental abnormalities; although there was wide space between his teeth, some teeth overlapped and squeezed together, which might be related to his micrognathia. Based on the data we collected, verbal development delay and intellectual disability were the two most common symptoms of this condition, which were found in all of the patients to varying degrees. There was one patient who had not spoken for decades, and some patients only showed a certain degree of slurring. Therefore, an evaluation of intellectual development and language development should be given special attention in clinical settings. If necessary, development-related tests such as systematic intelligence tests can be performed instead of simple evaluations. In addition, changes in the facial characteristics of patients with CdLS, such as arched eyebrows, long eyelashes, and synophrys, have a high incidence, occurring in 90% of the patients, and micrognathia is another common feature. Since approximately 50% of patients with micrognathia can be detected by prenatal ultrasound examinations (19), this feature should be given extra attention during prenatal examinations by clinicians. Additionally, hirsutism, syndactyly of the toes, and feeding problems in infancy are also symptoms that can be seen frequently and need to be called out for special attention.

On the basis of reviewed data, it was obvious that *SMC3* variants occurred mostly in exon 15, accounting for 28.5% (8/28) in all of the *SMC3* variants reported, followed by variants that occurred in exon 9, exon 19, exon 22, exon 23, and exon 27 (**Figure 2**). The c.1942A>G (p.Met648Val) variant in the current case was the first variant occurred in exon 18, which was never been reported before. Three unrelated cases were found to have variants in the same position (c.1464_1466del). Two of these three patients had detailed information: one was evaluated as moderate, and the other was graded as mild. Patients carrying the same *SMC3* variant presented with various degrees of severity, demonstrating the phenotypic heterogeneity caused by *SMC3* variants. Heterogeneity appears not only in *SMC3* but also in *NIPBL*. One study pointed out that unrelated probands with a similar *NIPBL* variant can have a phenotype ranging from severe to mild (20).

The cohesin complex plays a crucial role in regulating gene expression (21, 22). Cohesin combines with the sequence-specific DNA binding protein CTCF and forms structural topologically associated domains (TADs), chromatin loops and contact domains, which can bring together distant enhancers with promoter sequences to regulate gene expression. Disruption of the cohesin complex leads to abnormal DNA domain topology, resulting in gene expression dysregulation. CdLS is predominantly caused by pathogenic variants of genes that encode the structure and regulatory factors of the cohesin complex. The data show that *NIPBL* variants can be detected in nearly 70% of CdLS patients. Meanwhile, the proportion of patients carrying *HDAC8* variants was approximately 5%, and 5% of patients carried variants in *SMC1A*. CdLS caused by *SMC3* and *RAD21* each accounted for less than 1% of cases (7).

TABLE 2 | Summaries of clinical phenotype and *SMC3* variants of the 28 patients with Cornelia de Lange syndrome.

	Num	Age	Gender	Severity	Birth weight (kg)	Birth length (cm)	Weight kg (SDS)	Height cm (SDS)	Head	Nose	Eyes	Mouth	Hand	Feet	Developmental delay	Variant site	Type of variant	Exons
Yuan et al. (15)	P1	17y	M	moderate	/	/	/	/	+(microcephaly)	/	+(TE、Sy、long curly eyelashes、strabismus)	+(TUL、M/R)	+(moderate brachydactyly, C5F)	/	+	c.2536-2547del	deletion	23
Kaur et al. (12)	P2	/	M	/	/	/	/	/	/	/	/	/	/	/	/	c.1464_1466del	deletion	15
Yuan et al. (15)	P3	/	/	/	/	/	/	/	/	/	/	/	/	/	/	c.587T>C	missense	9
	P4	/	/	/	/	/	/	/	/	/	/	/	/	/	/	c.1453-1455del	deletion	15
	P5	/	/	/	/	/	/	/	/	/	/	/	/	/	/	c.2111T>C	missense	19
	P6	/	/	/	/	/	/	/	/	/	/	/	/	/	/	c.3362C>T	missense	27
	P7	/	/	/	/	/	/	/	/	/	/	/	/	/	/	c.2536-6_2540del: splicing	splicing	23
	P8	/	/	/	/	/	/	/	/	/	/	/	/	/	/	c.717_719del	deletion	9
Dowsett et al. (11)	P9	2y	M	/	/	/	/	/	/	/	/	/	/	/	+	c.1431T>A/G	missense	15
Infante et al. (10)	P10	7m	F	/	2.24	47	5.89(1st %)*	62(<1st %)*	+(microcephaly、bitemporal narrowing of forehead, LAH)	+(DNB, AN)	+(AE, Sy, TE, LE, HOL, P, bilateral epicanthal folds)	+(DCOM, micrognathia, SN)	+(PST, C5F, S5F)	+(SOT)	+	c.1433-1435dup	duplication	15
	P11	22y	F	/	3.17	/	95.25	170.6	+(narrow forehead, LAH)	+(BNT)	+(AE, Sy, TE, LE, P, M, bilateral epicanthal folds)	+(DA-small widely spaced teeth, micrognathia)	+(SH, PST, S5F)	+(SOT)	+	c.1433-1435dup	duplication	15
Gil-Rodriguez et al. (13)	P12	26y	F	mild	2.8 (-1.40)	/	58 (-1.80)	150 (-2.20)	+(B, LAH)	+(L/FP, BNT)	'+(AE, Sy,LE)	+(TUL, DCOM, DA, SN)	+(SH, C5F, S5F)	+(SF, SOT)	+	c.139T>C	missense	4
	P13	2.5y	F	moderate	2.865 (-1.23)	/	11 (-1.46)	86 (-1.10)	+(B, microcephaly)	+(DNB, AN-mild, BNT-mild)	+(AE, Sy, LE, M, HOL-mild)	+(TUL, DCOM, PHA, M/R, SN)	+(PST, SFM-mild, C5F-mild, S5F)	/	+	c.[=/703_705del] mosaic	deletion	9
	P14	4.5y	M	mild	2.67 (-1.98)	49.5 (-0.8)	14.5 (-1.6)	104 (-0.33)	'+(B, M, posterior hair whorl on left side)	/	+(AE,LE)	+(TUL, caries)	+(PST, SPC- right interruped palmar crease)	/	+	c.707G>C	missense	9
	P15	2m	M	moderate	2.27 (-2.91)	44.5 (-3.84)	3.6 (-3.02)	50.3 (-3.6)	+(LAH)	+(AN, L/FP, BNT)	+(AE, Sy, TE, LE),	+(TUL, DCOM,M/R)	+(SH, PST, SFM)	/	+	c.859_861dup	dup	11
	P16	23y	F	severe	2.14 (-2.2)	44 (-2.81)	42(-5.3)	137 (-4.40)	+(LAH)	+(AN, L/FP, BNT)	+(AE, TE, LE, P, M, lateral extension eyebrows)	+(TUL, DCOM, SN-Klippel-Feil, lowset anteverted ears)	+(SH, PST, SFM, C5F, S5F, SPC)	+(SF, SOT-2–3)	+	c.1200_1202delGTC	deletion	13
	P17	29y	M	mild	2.19 (-2.31)	48 (-0.8)	37(-6.8)	147 (-4.5)	/	+(BNT)	+(AE, Sy, TE, LE, M)	+(TUL, PHA),	+(SH, PST, SFM, C5F, S5F, SPC)	+(SF, SOT-2–3)	+	c.1464_1466delAGA	deletion	15
	P18	21y	M	moderate	2.57 (-2.23)	/	39.5 (-5.6)	150.8 (-3.8)	+(Sh-thick)	+(DNB, AN, BNT)	+(AE, Sy, TE, LE, deepest eyes)	+(DCOM?, Prognathism)	/	'+(SF)	+	c.1464_1466delAGA	deletion	15
	P19	11y6m	M	mild-moderate	2.39 (-0.1)	44 (-1.1)	26 (-1.74)	136 (-1.74)	+(B, LAH, M, Low, frontal hairline, Sh-thick)	+(DNB, AN, L/FP, BNT)	+(AE,TE,LE)	+(TUL, PHA, DA, SN, Facial asymmetry, low-set ears)	+(SH, PST, SFM, C5F)	+(SF)	+	c.1462G>A	missense	15
	P20	8y7m	F	mild	2.94 (0.72)	/	24 (-0.85)	120 (-1.80)	/	+(DNB, L/FP)	+(Sy, LE)	+(M/R)	/	/	+	c.1561C>T	nonsense	16
	P21	33m	F	moderate	2.1 (-1.79)	42 (-2.2)	10.22 (-2.56)	79(-3.7)	+(B, microbrachycephaly)	+(AN, L/FP, BNT)	+(AE, LE, LDO, astigmatism)	+(TUL, PC)	+(SH, SFM, C5F)	+(SF)	+	c.1964G>A	missense	19
	P22	22y	M	mild-moderate	3.21 (-2.48)	49 (-0.83)	63 (-1.02)	163 (-2.26)	+(B)	+(L/FP, BNT)	+(AE, LE, Sy, LE, M, Exotropia)	+(TUL, DCOM, PC-soft, palate, DA-widely spaced)	+(SH, PST, SFM, C5F)	+(SF)	+	c.1997G>C	missense	19
	P23	11m	M	moderate	2.985 (-1.22)	49 (-0.83)	7.5 (-2.27)	71 (-0.68)	+(B, LAH)	+(AND, AN, L/FP)	+(AE, LE, P, M, LDO)	+(TUL, DCOM, PHA, DA-delay, M/R, SN-low, posterior hairline)	+(SH, PST, SFM, C5F, S5F-bilateral dysplasia of the middle phalanx of the fifth finger)	+(SF)	+	c.2494_2499del	deletion	22
	P24	6y	M	severe		/				+(BNT)				+(SF)	+	c.2515C>T	missense	22

(Continued)

TABLE 2 | Continued

	Num	Age	Gender	Severity	Birth weight (kg)	Birth length (cm)	Weight kg (SDS)	Height cm (SDS)	Head	Nose	Eyes	Mouth	Hand	Feet	Developmental delay	Variant site	Type of variant	Exons
					3.005 (-1.17)		18 (-1.19)	104 (-2.46)	+(B, plagiocephaly, frontal bossing)		+(AE, TE, LDO),)	+(DA-dysmorphic teeth, pegged incisors, caried, mild low-set and posteriorly rotated ears, small mouth, delayed closure of anterior fontanelle (21m), prognathism, flat facies)	+(SH, PST, SFM, S5F, SPC)					
	P25	29m	F	moderate	2.18 (-1.6)	44.45	10 (-2.64)	82 (-2.09)	+(B, LAH, Microcephaly, SH)	+(L/FP-smooth, not long)	+(Sy, TE, LE, P, LDO, exotropia, astigmatism)	+(TUL, DCOM)	+(SH, PST)	+(SF)	+	c.2750A>G	missense	24
	P26	12y5m	M	moderate	2.778 (-1.7)	48 (-1.5)	20(6.9y) (-0.91)	110 (6.9y) (-2.05)	+(b, SH-thick)	+(DNB, AN, BNT)	+(AE, Sy, LE, P, HOF)	+(PHA, M/R, SN, Mild low-set and posteriorly rotated ears)	+(SH, PST, SFM, C5F, S5F)	+(SF, SOT-2-3)	+	c.3439C>G	missense	27
	P27	5m	F	severe	/	/	2.57 (-7.51)	48(-6.8)	+(B, LAH, microcephaly, Sh-thin)	+(DNB, L/FP, BNT)	+(AE,Sy, TE, LE)	+(TUL, DCOM, M/R, growly cry)	+(SH, SFM, S5F)	/	+	c.3644C>T	missense	29
The current case	P28	12y	M	mild	2.45	49	21	125.4	+(microcephaly, skull)	/	+(AE, LDO, bilatheral epicanthal foldings)	+(DA-Widely spaced teeth, uneven teeth),	+(C5F, S5F)	/	+	c.1942A>G	missense	18

**This case did not indicate the specific age at this time, only marked as 1st% in the report.*

B, brachycephaly; LAH, low anterior hairline; S, skull; Sh, scalp hair; AE, arched eyebrows; Sy, synnophrys; TE, thick eyebrows; LE, long eyelashes; P, ptosis; M, myopia; LDO, lacrimal duct obstruction; HOL, hooding of lids; DNB, depressed nasal bridge; AN, anteverted nostrils; L/FP, long/featureless philtrum; BNT, broad/bulbous nasal tip; TUL, thin upper lip; DCOM, downturned corners of mouth; PHA, palate high arch; PC, palate cleft; DA, dental anomalies (small/widely spaced); M/R, micrognathia/retrognathia; SN, short neck; SH, small hands; PST, proximally set thumbs; SFM, short first metacarpal; C5F, clinodactyly 5th finger; S5F, short 5th finger; SPC, Single Palmar crease; SF, small feet; SOT, syndactyly of toes.

There is a correlation between genotype and clinical phenotype to some extent in patients diagnosed with CdLS. As previously reported, *NIPBL* truncating, nonsense, splice site and frameshift pathogenic variants will produce more truncated and nonfunctional NIPBL proteins, and the NIPBL expression level is the lowest in patients with *NIPBL* variants compared with patients with *SMC3* variants, so the phenotype of patients carrying *NIPBL* variants will be more serious than those carrying *SMC3* variants. Using the severity of the cognitive developmental defects in patients as an example, patients with *NIPBL* variants are mostly moderate to profound and patients with *SMC3* variants are mostly mild to moderate. Similarly, patients with *NIPBL* variants have significantly more severe upper limb deformities than patients with *SMC3*. The former may have forearm loss, while brachydactyly and clinodactyly are more common in the latter. In terms of organ development, the incidence of cardiac, gastrointestinal, and urinary system defects in patients with *SMC3* variants is lower than that in patients with *NIPBL* variants. Interestingly, variants in *SMC3* were even found in some patients who were short and did not meet the diagnostic criteria for atypical CdLS, which includes intellectual and cognitive dysfunction (23).

In our study, only one of the 28 patients (P13) was found to be mosaic, but her phenotype can be classified as moderate according to the rating standard stated in 2007 (18). There was also a report analyzing the relationship between whether *NIPBL* mutant patients are mosaic and the severity of symptoms. The results showed that somatic mosaicism does not seem to be consistently connected with a milder phenotype. According to these reports, nearly 15 to 20% of patients with typical clinical characteristics of CdLS and *NIPBL* variants have the variants in other tissues and not in their lymphocytes (24, 25). Therefore, the international consensus statement suggests that clinicians should study patients' fibroblast cells, buccal cells, and bladder epithelial cells to confirm whether they are mosaic when variants of related genes cannot be detected in lymphocytes. Although patients with *SMC3* variants have relatively milder clinical symptoms than those with *NIPBL* variants, mosaicism should be taken into consideration in clinical settings.

This patient received rhGH treatment within a very short period and displayed a good effect with an estimated annual growth rate of 12 cm. However, they regrettably ceased the therapy for financial reasons. To date, on the basis of the literature we collected, only one report showed that rhGH had achieved good results in treating patients with short stature caused by CdLS (26). Although these two patients had a good response to rhGH, the number of cases was too small, and whether rhGH can be considered a commonly accepted treatment for patients with CdLS-induced short stature requires further clinical research.

The diagnosis and management of CdLS is challenging because of its multisystemic malformations. For patients with multiorgan involvement, facial dysmorphic features, growth retardation, cognitive disorder, and verbal and behavioral developmental defects, a suspicion of CdLS should be made. Molecular genetic testing assists in making a confirmative diagnosis of CdLS. Once the diagnosis is acquired, lifelong

medical care and multidisciplinary and social care are urgently needed to improve the patient's health and increase their quality of life (3, 27, 28). Interdisciplinary management integrates doctors from different disciplines to establish a treatment team, which enables patients with CdLS to be evaluated from different professional perspectives and it proposes syndrome-specific, individualized treatment plans. The team includes gastroenterologists for gastroesophageal reflux, cardiologists for congenital heart diseases, dentists for dysplasia of the teeth, psychotherapists for cognitive and behavioral defects, orthopedists for the correction of limb deformities, speech specialists for verbal defects, urologists for urinary system abnormalities, and geneticists who provide the necessary genetic counseling to the patients' parents (28). However, patients seldom have the chance to receive the therapies mentioned above. In the current case, our patient experienced delayed diagnosis and treatment, likely due to a lack of knowledge regarding CdLS by primary hospital caregivers, their geographic isolation and financial considerations. There is a long way to go in educating both caregivers and patients to achieve an early diagnosis, apply early interventions, diminish complications and improve the patients' quality of life.

CONCLUSION

SMC3 gene variants are a rare cause of CdLS. We reported a 11.7-year-old male carried a *de novo SMC3* variant, c.1942A>G (p.Met648Val), which was the first variant occurred in exon 18. Patients usually have mild to moderate typical clinical manifestations. Some facial features, such as arched eyebrows, long eyelashes and broad/bulbous nasal tips, as well as some intellectual developmental abnormalities and verbal development delay, are common clinical manifestations that require more attention in clinical settings. To our knowledge, the current case is the second case in which rhGH was used to improve the short stature of patients with CdLS. Although the results suggest that rhGH can be used as an effective treatment for the short stature caused by CdLS, more clinical evidence is necessary.

DATA AVAILABILITY STATEMENT

The data presented in the study are deposited in the SRA repository, accession number PRJNA751153.

ETHICS STATEMENT

Written informed consent was obtained from the patient's parents, for the publication of any potentially identifiable images or data included in this article.

AUTHOR CONTRIBUTIONS

All authors helped to perform the research. HZ conceived and designed the research. HZ, HP, LW and HY contributed to the project management. HL and MC helped to collect clinical samples. RL did molecular experiments. RL and BT took part in the statistical analysis. RL and BT wrote the manuscript. HY and LW took part in the revision of the manuscript. All authors contributed to the article and approved the submitted version.

FUNDING

This work was funded by the CAMS Innovation Fund for Medical Science (CAMS-2016-I2M-1-002, CAMS-2016-I2M-1-008) and the National Key Research and Development Program of China (No. 2016YFC0901501).

REFERENCES

1. Musio A. The Multiple Facets of the SMC1A Gene. *Gene* (2020) 743:144612. doi: 10.1016/j.gene.2020.144612
2. De Lange C. Sur Un Type Nouveau De Degenerescence (Typus Amsterlodamensis). *Arch Med Enfants* (1933) 36:713–9. (In French).
3. Kline AD, Moss JF, Selicorni A, Bisgaard AM, Deardorff MA, Gillett PM, et al. Diagnosis and Management of Cornelia De Lange Syndrome: First International Consensus Statement. *Nat Rev Genet* (2018) 19:649–66. doi: 10.1038/s41576-018-0031-0
4. Barisic I, Tokic V, Loane M, Bianchi F, Calzolari E, Garne E, et al. Descriptive Epidemiology of Cornelia De Lange Syndrome in Europe. *Am J Med Genet A* (2008) 146:51–9. doi: 10.1002/ajmg.a.32016
5. Kline AD, Grados M, Sponseller P, Levy HP, Blagowidow N, Schoedel C, et al. Natural History of Aging in Cornelia De Lange Syndrome. *Am J Med Genet C Semin Med Genet* (2007) 145:248–60. doi: 10.1002/ajmg.c.30137
6. Zhu Z, Wang X. Roles of Cohesin in Chromosome Architecture and Gene Expression. *Semin Cell Dev Biol* (2019) 90:187–93. doi: 10.1016/j.semcdb.2018.08.004
7. Watrin E, Kaiser FJ, Wendt KS. Gene Regulation and Chromatin Organization: Relevance of Cohesin Variants to Human Disease. *Curr Opin Genet Dev* (2016) 37:59–66. doi: 10.1016/j.gde.2015.12.004
8. Cochran L, Welham A, Oliver C, Arshad A, Moss JF. Age-Related Behavioural Change in Cornelia De Lange and Cri Du Chat Syndromes: A Seven Year Follow-Up Study. *J Autism Dev Disord* (2019) 49:2476–87. doi: 10.1007/s10803-019-03966-6
9. Deardorff MA, Kaur M, Yaeger D, Rampuria A, Korolev S, Pie J, et al. Variants in Cohesin Complex Members SMC3 and SMC1A Cause a Mild Variant of Cornelia De Lange Syndrome With Predominant Mental Retardation. *Am J Hum Genet* (2007) 80:485–94. doi: 10.1086/511888
10. Infante E, Alkorta-Aranburu G, El-Gharbawy A. Rare Form of Autosomal Dominant Familial Cornelia De Lange Syndrome Due to a Novel Duplication in SMC3. *Clin Case Rep* (2017) 5:1277–83. doi: 10.1002/ccr3.1010
11. Dowsett L, Porras AR, Kruszka P, Davis B, Hu T, Honey E, et al. Cornelia De Lange Syndrome in Diverse Populations. *Am J Med Genet A* (2019) 179:150–8. doi: 10.1002/ajmg.a.61033
12. Kaur M, Mehta D, Noon SE, Deardorff MA, Zhang Z, Krantz ID. NIPBL Expression Levels in CdLS Probands as a Predictor of Variant Type and Phenotypic Severity. *Am J Med Genet C Semin Med Genet* (2016) 172:163–70. doi: 10.1002/ajmg.c.31495
13. Gil-Rodriguez MC, Deardorff MA, Ansari M, Tan CA, Parenti I, Baquero-Montoya C, et al. De Novo Heterozygous Variants in SMC3 Cause a Range of Cornelia De Lange Syndrome-Overlapping Phenotypes. *Hum Mutat* (2015) 36:454–62. doi: 10.1002/humu.22761

14. Ansari M, Poke G, Ferry Q, Williamson K, Aldridge R, Meynert AM, et al. Genetic Heterogeneity in Cornelia De Lange Syndrome (CdLS) and CdLS-Like Phenotypes With Observed and Predicted Levels of Mosaicism. *J Med Genet* (2014) 51:659–68. doi: 10.1136/jmedgenet-2014-102573
15. Yuan B, Neira J, Pehlivan D, Santiago-Sim T, Song X, Rosenfeld J, et al. Clinical Exome Sequencing Reveals Locus Heterogeneity and Phenotypic Variability of Cohesinopathies. *Genet Med* (2019) 21:663–75. doi: 10.1038/s41436-018-0085-6
16. Yuan B, Pehlivan D, Karaca E, Patel N, Charng WL, Gambin T, et al. Global Transcriptional Disturbances Underlie Cornelia De Lange Syndrome and Related Phenotypes. *J Clin Invest* (2015) 125:636–51. doi: 10.1172/JCI77435
17. Dempsey MA, Johnson AEK, Swope BS, Moldenhauer JS, Sroka H, Chong K, et al. Molecular Confirmation of Nine Cases of Cornelia De Lange Syndrome Diagnosed Prenatally. *Prenat Diagn* (2014) 34:163–7. doi: 10.1002/pd.4279
18. Kline AD, Krantz ID, Sommer A, Kliewer M, Jackson LG, FitzPatrick DR, et al. Cornelia De Lange Syndrome: Clinical Review, Diagnostic and Scoring Systems, and Anticipatory Guidance. *Am J Med Genet A* (2007) 143:1287–96. doi: 10.1002/ajmg.a.31757
19. Clark DM, Sherer I, Deardorff MA, Byrne JLB, Loomes KM, Nowaczyk MJM, et al. Identification of a Prenatal Profile of Cornelia De Lange Syndrome (CdLS): A Review of 53 CdLS Pregnancies. *Am J Med Genet A* (2012) 158:1848–56. doi: 10.1002/ajmg.a.35410
20. Nizon M, Henry M, Michot C, Baumann C, Bazin A, Bessieres B, et al. A Series of 38 Novel Germline and Somatic Variants of NIPBL in Cornelia De Lange Syndrome. *Clin Genet* (2016) 89:584–9. doi: 10.1111/cge.12720
21. Nishiyama T. Cohesion and Cohesin-Dependent Chromatin Organization. *Curr Opin Cell Biol* (2019) 58:8–14. doi: 10.1016/j.ceb.2018.11.006
22. Shi Z, Gao H, Bai XC, Yu H. Cryo-EM Structure of the Human Cohesin-NIPBL-DNA Complex. *Science* (2020) 368(6498):1454–9. doi: 10.1126/science.abb0981
23. Boyle MI, Jespersgaard C, Brondum-Nielsen K, Bisgaard AM, Tumer Z. Cornelia De Lange Syndrome. *Clin Genet* (2015) 88:1–12. doi: 10.1111/cge.12499
24. Baquero-Montoya C, Gil-Rodriguez MC, Hernandez-Marcos M, Teresa-Rodrigo ME, Vicente-Gabas A, Bernal ML, et al. Severe Ipsilateral Musculoskeletal Involvement in a Cornelia De Lange Patient With a Novel NIPBL Variant. *Eur J Med Genet* (2014) 57:503–9. doi: 10.1016/j.ejmg.2014.05.006
25. Huisman SA, Redeker EJW, Maas SM, Mannens MM, Hennekam RCM. High Rate of Mosaicism in Individuals With Cornelia De Lange Syndrome. *J Med Genet* (2013) 50:339–44. doi: 10.1136/jmedgenet-2012-101477
26. de Graaf M, Kant SG, Wit JM, Redeker EJW, Santen GWE, Verkerk AJMH, et al. Successful Growth Hormone Therapy in Cornelia De Lange Syndrome. *J Clin Res Pediatr Endocrinol* (2017) 9:366–70. doi: 10.4274/jcrpe.4349
27. January K, Conway LJ, Deardorff M, Harrington A, Krantz ID, Loomes K, et al. Benefits and Limitations of a Multidisciplinary Approach to Individualized Management of Cornelia De Lange Syndrome and Related Diagnoses. *Am J Med Genet C Semin Med Genet* (2016) 172:237–45. doi: 10.1002/ajmg.c.31500
28. Mikolajewska E. Interdisciplinary Therapy in Cornelia De Lange Syndrome - Review of the Literature. *Adv Clin Exp Med* (2013) 22:571–7.

Conflict of Interest: The authors declare that the research was conducted in the absence of any commercial or financial relationships that could be construed as a potential conflict of interest.

Publisher's Note: All claims expressed in this article are solely those of the authors and do not necessarily represent those of their affiliated organizations, or those of the publisher, the editors and the reviewers. Any product that may be evaluated in this article, or claim that may be made by its manufacturer, is not guaranteed or endorsed by the publisher.

frontiers in Genetics

ORIGINAL RESEARCH
published: 22 December 2021
doi: 10.3389/fgene.2021.702540

Differential lncRNA/mRNA Expression Profiling and Functional Network Analyses in Bmp2 Deletion of Mouse Dental Papilla Cells

Feng Wang[1,2†], Ran Tao[1†], Li Zhao[1], Xin-Hui Hao[1], Yi Zou[3], Qing Lin[1], Meng Meng Liu[2], Graham Goldman[2], Daoshu Luo[1] and Shuo Chen[2]**

[1]Laboratory of Clinical Applied Anatomy, Department of Human Anatomy, School of Basic Medical Sciences, Fujian Medical University, Fuzhou, China, [2]Department of Developmental Dentistry, School of Dentistry, The University of Texas Health Science Center at San Antonio, San Antonio, TX, United States, [3]Greehey Children's Cancer Research Institute, The University of Texas Health Science Center at San Antonio, San Antonio, TX, United States

Bmp2 is essential for dentin development and formation. Bmp2 conditional knock-out (KO) mice display a similar tooth phenotype of dentinogenesis imperfecta (DGI). To elucidate a foundation for subsequent functional studies of cross talk between mRNAs and lncRNAs in Bmp2-mediated dentinogenesis, we investigated the profiling of lncRNAs and mRNAs using immortalized mouse dental Bmp2 flox/flox (iBmp2$^{fx/fx}$) and Bmp2 knock-out (iBmp2$^{ko/ko}$) papilla cells. RNA sequencing was implemented to study the expression of the lncRNAs and mRNAs. Quantitative real-time PCR (RT-qPCR) was used to validate expressions of lncRNAs and mRNAs. The Gene Ontology (GO) and Kyoto Encyclopedia of Genes and Genomes (KEGG) databases were used to predict functions of differentially expressed genes (DEGs). Protein–protein interaction (PPI) and lncRNA–mRNA co-expression network were analyzed by using bioinformatics methods. As a result, a total of 22 differentially expressed lncRNAs (16 downregulated vs 6 upregulated) and 227 differentially expressed mRNAs (133 downregulated vs. 94 upregulated) were identified in the iBmp2$^{ko/ko}$ cells compared with those of the iBmp2$^{fx/fx}$ cells. RT-qPCR results showed significantly differential expressions of several lncRNAs and mRNAs which were consistent with the RNA-seq data. GO and KEGG analyses showed differentially expressed genes were closely related to cell differentiation, transcriptional regulation, and developmentally relevant signaling pathways. Moreover, network-based bioinformatics analysis depicted the co-expression network between lncRNAs and mRNAs regulated by Bmp2 in mouse dental papilla cells and symmetrically analyzed the effect of Bmp2 during dentinogenesis via coding and non-coding RNA signaling.

Keywords: bone morphogenetic protein 2, dental mesenchymal papilla cells, coding and non-coding RNAs, bioinformatics, signal pathways

OPEN ACCESS

Edited by:
Liborio Stuppia, University of Studies G. d'Annunzio Chieti and Pescara, Italy

Reviewed by:
Paul Lasko, McGill University, Canada
Lu Zhang, Wuhan University, China

***Correspondence:**
Shuo Chen
chens0@uthscsa.edu
Daoshu Luo
luods2004@163.com

†These authors have contributed equally to this work and share first authorship

Specialty section:
This article was submitted to Genetics of Common and Rare Diseases, a section of the journal Frontiers in Genetics

Received: *29 April 2021*
Accepted: *29 November 2021*
Published: *22 December 2021*

Citation:
Wang F, Tao R, Zhao L, Hao X-H Zou Y, Lin Q, Liu MM, Goldman G, Luo D and Chen S (2021) Differential lncRNA/mRNA Expression Profiling and Functional Network Analyses in Bmp2 Deletion of Mouse Dental Papilla Cells. Front. Genet. 12:702540. doi: 10.3389/fgene.2021.702540

INTRODUCTION

Bone morphogenetic protein 2 (Bmp2) is a multiple-functional growth factor and is involved in many organ developments (Macias et al., 1997; Schlange et al., 2000; Ou et al., 2014). The bone morphogenetic proteins (BMPs) are structurally related to the transforming growth factor β (TGF-β) superfamily. The members of the BMP family play various biological functions during embryonic development (Hogan, 1996; Shi and Massagué, 2003; Wu et al., 2003; Chen et al., 2004; Miyazono et al., 2005), including a vital role in tooth development and formation (Meguro et al., 2019). Among the BMP family members, Bmp2 has been widely investigated for its diverse biological functions, particularly during dental cell differentiation (Casagrande et al., 2010; Wang et al., 2012; Yang et al., 2012; Guo et al., 2015; Yang et al., 2017; Malik et al., 2018). Bmp2 is expressed in mesenchymal cells and promotes mesenchymal progenitor/stem cell commitment to the odontoblast lineage by regulating a series of transcription factors and others (Yamashiro et al., 2003; Chen et al., 2005; Chen et al., 2008; Cho et al., 2010; Agas et al., 2013; Yang et al., 2017).

During tooth development, at the initiation stage (E10-12), the dental lamina is formed as an epithelial clustering, and the dental epithelium and mesenchyme are distinguished. The Bmp2 gene transcript is seen in those areas of the dental lamina where it started to form a bud (Aberg et al., 1997; Heikinheimo et al., 1998; Nadiri et al., 2004; Chen et al., 2008). At the bud stage (E12-13), Bmp2 expression is detectable in the dental epithelium and mesenchyme throughout the bud period. At the cap stage, Bmp2 expression is prominent at E14 and mainly localized at the epithelial enamel knot during the late cap stage, and Bmp2 expression expands to the neighboring inner dental epithelium where the secondary enamel knots will be formed and its signal is seen in dental mesenchyme. At the bell stage, Bmp2 expression is detected in the dental mesenchymal cells (Dong et al., 2014; Dong et al., 2016; Gao et al., 2018). Later, Bmp2 expression spreads to the dental papilla and is intense in the pre-odontoblasts. At the postnatal days (PN), Bmp2 is continually expressed in odontoblasts and ameloblasts and detected in the dental papilla as well as adjacent tissues including dental follicle, periodontal ligamental cells, cementoenamel junction, and Hertwig's epithelial root sheath (HERS) and osteoblasts in alveolar bones (Yamashiro et al., 2003; Kémoun et al., 2007).

The Bmp2 binds to two distinct types, type I serine/threonine kinase and type II receptors, which are necessary for signal transduction (Shi and Massagué, 2003; Chen et al., 2004; Miyazono et al., 2005). The Bmp signal regulates downstream gene expression through either the canonical Smad or non-canonical Smad pathway. Following heterodimerization, type I receptors are phosphorylated by type II receptors and subsequently activate the receptor-regulated R-Smad-1/-5/-8 through phosphorylation (Bhatt et al., 2013; Graf et al., 2016). The phosphorylated Smad-1/-5/-8 heterodimers form a complex with the common mediator Smad-4 (Co-Smad-4). Following nuclear translocation of the R-Smad-1/-5/-8/Co-Smad-4 complex, Bmp target gene expression is induced (Bhatt et al., 2013). On the other hand, Bmp2 also activates non-canonical Smad signaling pathways such as mitogen-activated protein kinases (MAPKs), c-Jun amino-terminal kinase (JNK), phosphoinositol-3 kinase (PI3K), Akt, and small GTPases (Derynck and Zhang, 2003). Thus, these canonical Smad pathways cooperate with non-canonical Smad pathways to regulate various cellular responses. Also, Bmp2 can crosstalk with other factors, such as Wnt, Fgf, and other factors, regulating cell proliferation, differentiation, and tissue development (Guo and Wang, 2009; O'Connell et al., 2012; Agas et al., 2013; Saito et al., 2016; Wu et al., 2016; Zhang et al., 2016; Chakka et al., 2020).

Global Bmp2 knockout (KO) mice are nonviable. Homozygous Bmp2 mutant embryos die at embryonic day 9.5 (E9.5) and exhibited defects in cardiac development, manifested by the abnormal development of the heart in the exocoelomic cavity (Zhang and Bradley, 1996). However, Bmp2 conditional KO mice were generated and viable. Teeth with Bmp2 cKO mice display the similar phenotype of dentin defects to that of dentinogenesis imperfecta (DGI) in humans and mice, the most common dentin genetic diseases, showing retardation of tooth growth, abnormal dentin structure with wide predentin, and thin dentin (Zhang et al., 2001; Lu et al., 2007; Lee et al., 2009). Accumulating evidence indicated that Bmp2 is capable of regulating a lot of bone/dentin-related gene expressions and transcriptional factors as well as dental cell proliferation and differentiation in tooth development (Chen et al., 2008; Cho et al., 2010; Oh et al., 2012; Yang et al., 2017). Additionally, cross talk has been described between Bmp signaling–associated mRNAs and non-coding RNAs during dental cell proliferation and differentiation (Wang F. et al., 2017; Wang J. et al., 2017; Liu et al., 2018; Liao et al., 2020; He et al., 2021).

High-throughput sequencing techniques have revolutionized our understanding of the human genome (Kapranov et al., 2007). The whole transcriptome study has demonstrated that although more than 90% of the genome can be transcribed into RNAs, only approximately 2% of the human genome contains protein-coding regions (Kapranov et al., 2007; Jalali et al., 2016). The remaining non-coding regions are transcribed into large amounts of non-coding RNAs (Jalali et al., 2016). lncRNAs are the largest class of non-coding RNAs composed of more than 200 nucleotides to over 100 kb in length, which lack protein-coding potential (Ponting et al., 2009). The lncRNAs comprise thousands of transcripts with distinct biogenesis, subcellular localization, and molecular functions (Chen, 2016). Studies have suggested that lncRNA genome complexity plays biological roles in regulating gene expression at transcriptional, post-transcriptional, and epigenetic levels in a lot of cellular and biological processes, such as signal transduction, cell proliferation, differentiation, and organ development (Batista and Chang, 2013; Fatica and Bozzoni, 2014; Quinn and Chang, 2016; Bunch, 2018; Statello et al., 2021). Therefore, alteration of lncRNA expression is related to numerous diseases (Fatica and Bozzoni, 2014; Wu and Du, 2017). lncRNAs can regulate the expression of growth factors, transcriptional and epigenetic factors, and vice versa (Yang et al., 2014). The pattern of cell- and tissue-specific lncRNA

expression provides new insights into tissue development, diagnosis, and treatment of several diseases (Chen et al., 2021). Up to date, over 100,000 lncRNAs have been identified in the human genome and new lncRNAs are being discovered and characterized rapidly (Zhao et al., 2021).

However, the interplay of Bmp2-mediated mRNAs and lncRNAs in the regulation of odontoblastic differentiation and function has not completely been understood. Previously, our group generated immortalized mouse dental Bmp2 flox/flox (iBmp2$^{fx/fx}$) and Bmp2 knock-out (iBmp2$^{ko/ko}$) papilla cells. In this study, we detected the differential lncRNA and mRNA expression profiles in these two types of dental papilla cell lines by RNA sequencing. A network-based bioinformatics analysis was performed to investigate the cross talk between lncRNAs and mRNAs via integrating lncRNA–mRNA interactions, gene co-expression, and protein–protein interactions. Our results demonstrated that the synergistic or competitive lncRNA–mRNA cross talk may play an important role in Bmp2-mediated odontoblastic differentiation.

MATERIALS AND METHODS

In Situ Alkaline Phosphatase Assay and Alizarin Red S Staining

Mouse dental iBmp2$^{fx/fx}$ and iBmp2$^{ko/ko}$ papilla cells were generated by our group as previously described (Wu et al., 2010; Wu et al., 2015). To induce cell differentiation, the cells were cultured in α-MEM supplemented with 10% fetal bovine serum (FBS), 1% antibiotics, 10 mM sodium β-glycerophosphate, 50 μg/ml ascorbic acid, and 100 nM dexamethasone for 7 and 10 days. Then, the cells were fixed and washed in PBS. *In situ* alkaline phosphatase (ALP) assay was carried out in accordance with the instructions. For cell mineralization assessment, the cells were fixed in 10% formalin as well as were treated with 1% Alizarin Red S dye (pH 4.2).

RNA-Seq and Gene Expression Analysis

The iBmp2$^{fx/fx}$ and iBmp2$^{ko/ko}$ cells were cultured in 100-mm^2 dishes to 80% confluence. The cells were harvested after 6, 48, or 72 h, and RNAs were extracted using TRIzol reagent (QIAGEN Inc.). The RNA quality was assessed using a bio-analyzer. The RNA-seq libraries were prepared from total RNAs in accordance with Illumina's RNA specimen preparation protocol (Illumina Inc. San Diego, CA, United States). Paired reads to the UCSC mm9 genome build were mapped by a TopHat2 aligner. To quantify gene expression, HTSeq was used to obtain raw read counts per gene and then converted to RPKM in accordance with the gene length and total mapped read count per sample. The DEGs were calculated, as gene expression levels were measured by Log_2-transformed RPKM ($|\log_2$ fold Change$|$ >1, p value <0.05). RNA-seq data were submitted and deposited to The Gene Expression Omnibus (GEO, http://www.ncbi.nlm.nih.gov/geo/). The GEO accession number is GSE174429.

Gene Ontology (GO) and Kyoto Encyclopedia of Genes and Genomes (KEGG) Analysis

GO analysis was used to investigate the roles of all differentially expressed mRNAs (https://david.ncifcrf.gov/). DAVID-based KEGG analysis was used to determine the significant pathways related to the differentially expressed mRNAs. Fisher's exact test and the x^2 test were used to select the significant GO categories and pathways. The threshold of significance was a p value < 0.05, and a false discovery rate (FDR) was calculated to correct the p value.

Generation of the Protein–Protein Interaction (PPI) Network

The differentially expressed genes (DEGs) were imported into a STRING database, and the species was limited to "Mus musculus" to obtain PPI information. The network relationships with high confidence (≥0.75) were screened and imported into Cytoscape 3.6.2 to draw a PPI network diagram. According to the calculation method of the MCC (maximum clique centrality) algorithm, the top 20 hub genes were screened by using the "cytoHubba" plug-in. Additionally, the interactive density region was extracted using the "MCODE" plug-in in Cytoscape.

Construction of the lncRNA–mRNA Co-Expression Network

The mRNA–lncRNA co-expression network, which was used to identify interactions between the differentially expressed lncRNAs and mRNAs, was constructed based on Pearson's correlation analysis. For each pair of genes, correlation coefficients of 0.95 or greater were selected to construct the network using the OmicStudio tools at https://www.omicstudio.cn/tool. In the network, each mRNA or lncRNA corresponds to a node, and the nodes are connected by edges.

Quantitative Reverse Transcription PCR (RT-qPCR)

Total RNA samples were isolated with TRIzol (Invitrogen, California, United States) and reverse transcribed into cDNA with the Prime Script RT reagent kit with gDNA Eraser (RR047A) following the manufacturers' guidelines (Takara, Japan). The RNA was reverse transcribed into cDNA at 37°C for 15 min, and the reaction was stopped at 85°C for 5 s. RT-qPCR was performed using the SYBR™ Select Master Mix (Applied Biosystems, California, United States) on a CFX96 system (Bio-Rad, California, United States). The relative gene expression was calculated with the $2^{-\Delta\Delta Ct}$ method using glyceraldehyde-3-phosphate dehydrogenase (GAPDH) as the reference housekeeping gene. The RT-qPCR primers are listed in **Table 1**.

TABLE1 | RT-qPCR primers.

Gene	Forward primer (5' --3')	Reverse primer (5'-- 3')
Fgf2	GCGACCCACACGTCAAACTA	TCCCTTGATAGACACAACTCCTC
Id2	ATGAAAGCCTTCAGTCCGGTG	AGCAGACTCATCGGGTCGT
Id3	CTGTCGGAACGTAGCCTGG	GTGGTTCATGTCGTCCAAGAG
Lhx1	CCAAGCGATCTGGTTCGCA	CCGGAGATAAACTAGGGTCACTG
Smad7	GACAGCTCAATTCGGACAACA	CAGTGTGGCGGACTTGATGA
Tcf7	ACAGTGCTCTAGGCTGTCC	CGACCTGAGAATGTTGGTGCT
Wnt1	TTCGGCAAGATCGTCAACCG	GCCAAAGAGGCGACCAAAATC
Wnt11	GCACTGAATCAGACGCAACAC	CGACAGGGCATACACGAAGG
Klf10	AGTGTCATCCGTCACACAGC	CACTGCAGCACAGGGTATGT
Lnc87211.1	GCCTCCCAGAGAAGTGTGAA	ATACACACTGCAGACAGCTACA
Lnc86888.1	GTGCGCATATCACAGTGTCG	AACAGGAAATCACTCGCCGT
Lnc87189.1	CTTGGTGTCCTTGGATGACCT	GCATAAGGAAAGAGAGCCACC
Gapdh	AGGTCGGTGTGAACGGATTTG	TGTAGACCATGTAGTTGAGGTCA

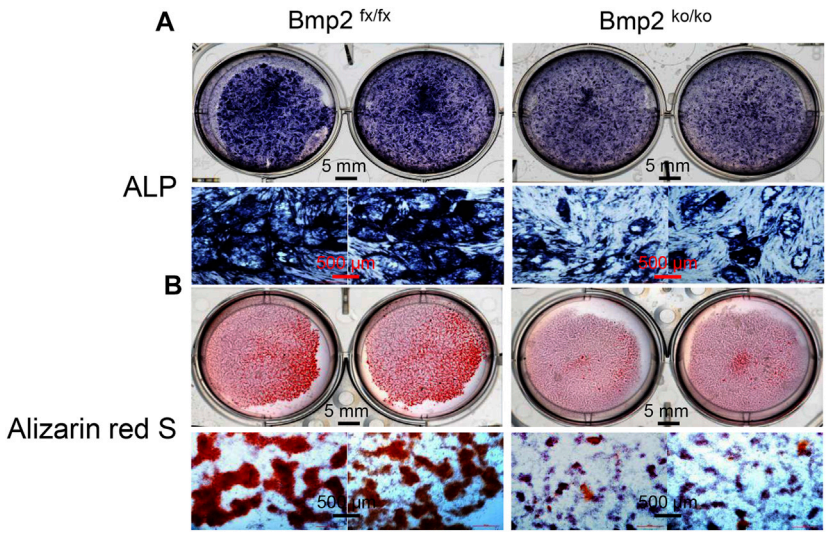

FIGURE 1 | Deletion of Bmp2 delays mouse dental papilla cell differentiation and mineralization. **(A)** iBmp2$^{fx/fx}$ and iBmp2$^{ko/ko}$ cells were cultured in the calcifying medium for 7 days. ALP activity was analyzed using *in situ* ALP staining. **(B)** For cell mineralization assay, both the iBmp2$^{fx/fx}$ and iBmp2$^{ko/ko}$ cells were treated with the calcifying medium for 10 days. Mineralized nodules were visualized with Alizarin Red S staining. fx, floxed; ko, knock-out.

Statistical Analysis

Data were presented as the mean ± SEM. RT-qPCR validation data presented were analyzed with Student's *t* test. $p < 0.05$ was considered statistically significant. Significant differences are noted by asterisks, with single asterisks representing $p < 0.05$, two asterisks representing $p < 0.01$, three asterisks representing $p < 0.001$, and four asterisks representing $p < 0.0001$.

RESULTS

Deletion of Bmp2 Causes Delay of Dental Papilla Mesenchymal Cell Differentiation and Mineralization

To determine the effect of Bmp2 on dental papilla cell differentiation and mineralization activities, we measured the alkaline phosphatase (ALP) activity by *in situ* ALP histochemistry since ALP is a marker of dental cell differentiation. Both cells were cultured in the calcifying medium in given time periods. This result showed delayed dental papilla cell differentiation in the iBmp2$^{ko/ko}$ cells compared to that in the Bmp2$^{fx/fx}$ cells. Additionally, deletion of the *Bmp2* gene led to low activity of the dental papilla cell mineralization as observed through Alizarin Red S staining (**Figure 1**).

Overview of Differential lncRNA/mRNA Expression Profiling

To identify DEGs between the iBmp2$^{fx/fx}$ and iBmp2$^{ko/ko}$ cells, we performed and analyzed the RNA-seq data by using the limma package. The cutoff criteria were as follows: |log fold change| (the absolute value of log2 in the fold change of gene expression) > 1 and p value <0.05. Our data demonstrated that 94 mRNAs were

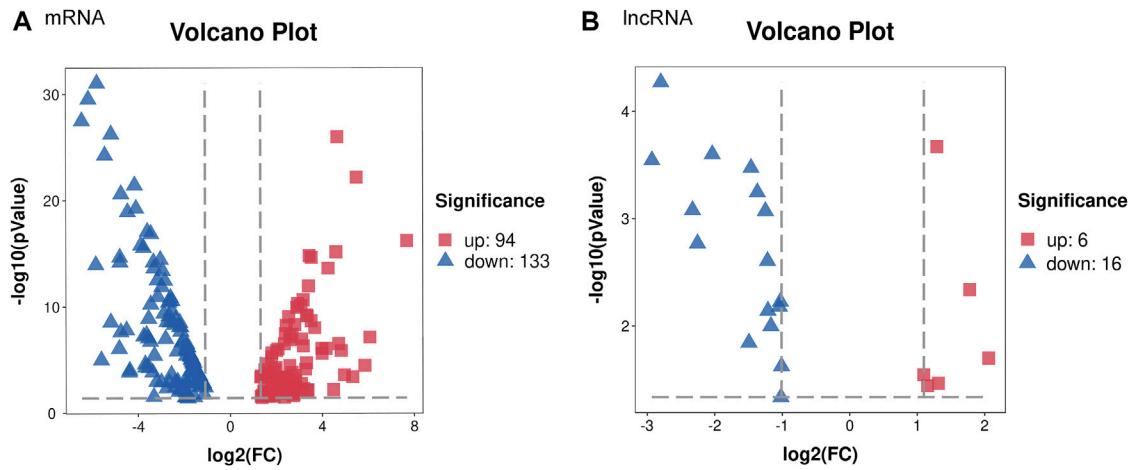

FIGURE 2 | Differentially expressed genes between the iBmp2$^{fx/fx}$ and iBmp2$^{ko/ko}$ groups. Our data showed that 94 mRNAs upregulated and 133 mRNAs downregulated in the iBmp2$^{ko/ko}$ cells compared to those in the iBmp2$^{fx/fx}$ cells **(A)**. Meanwhile, 6 lncRNAs upregulated and 16 lncRNAs downregulated (|log2FC| ≥1; Qvalue <=0.05) in the iBmp2$^{ko/ko}$ cells **(B)**. Red represents upregulated DEG, blue represents downregulated DEG.

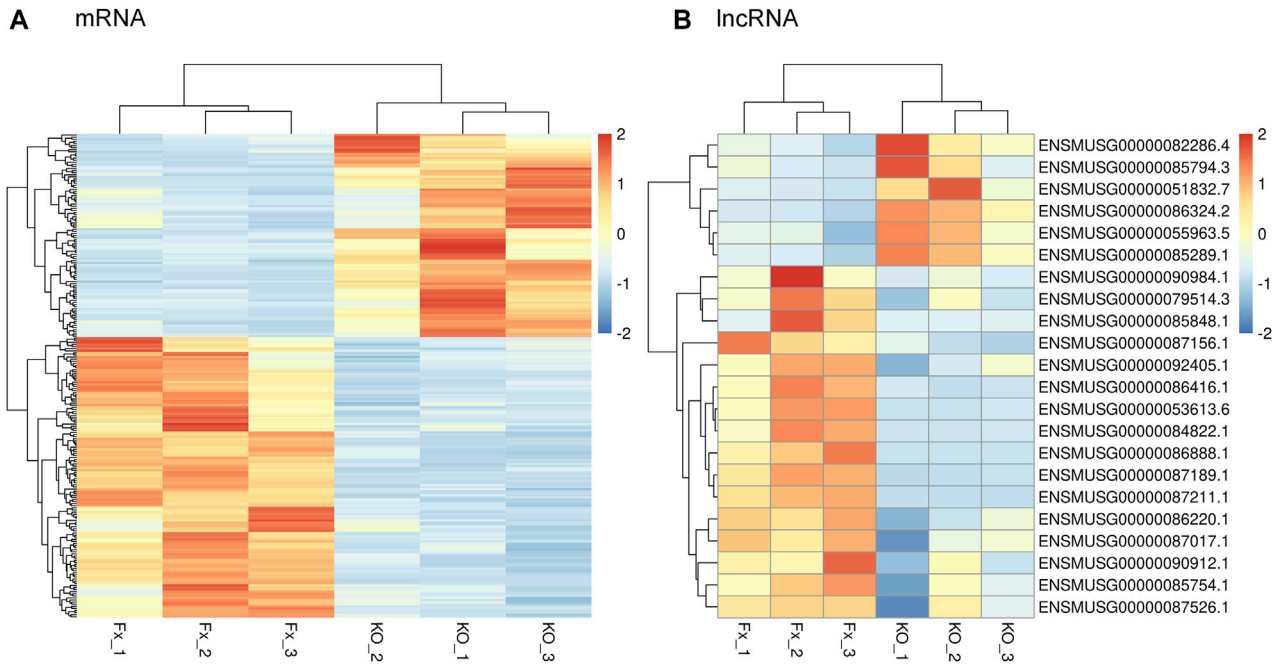

FIGURE 3 | Genetic clustering of differentially expression genes (|log2FC| ≥1; Q value <=0.001). **(A)** mRNAs; **(B)** and lncRNAs. The red color represents high fold-change, and the blue color represents low fold-change.

upregulated, while 133 mRNAs were downregulated in the iBmp2$^{ko/ko}$ cells compared with those in the iBmp2$^{fx/fx}$ cells (**Figure 2A**). Likewise, 6 lncRNAs were upregulated whereas 16 lncRNAs were downregulated in the iBmp2$^{ko/ko}$ cells compared to those in the iBmp2$^{fx/fx}$ cells (**Figure 2B**). The volcano maps of mRNA and lncRNA DEGs were drawn by the ggplot2 package. The heatmaps of mRNA and lncRNA DEGs were shown by the heatmap package (**Figure 3**).

Pathway and GO Analyses of Differentially Expressed mRNAs

The KEGG analysis showed that the DEGs were largely enriched in the TGF-β/BMP signaling pathway, Hippo signaling pathway, Wnt signaling pathway, and signaling pathways regulating pluripotency of stem cells (**Figure 4A**). These signal pathways are cross talks and are involved in dental and other cell proliferation and differentiation via regulating transcriptional

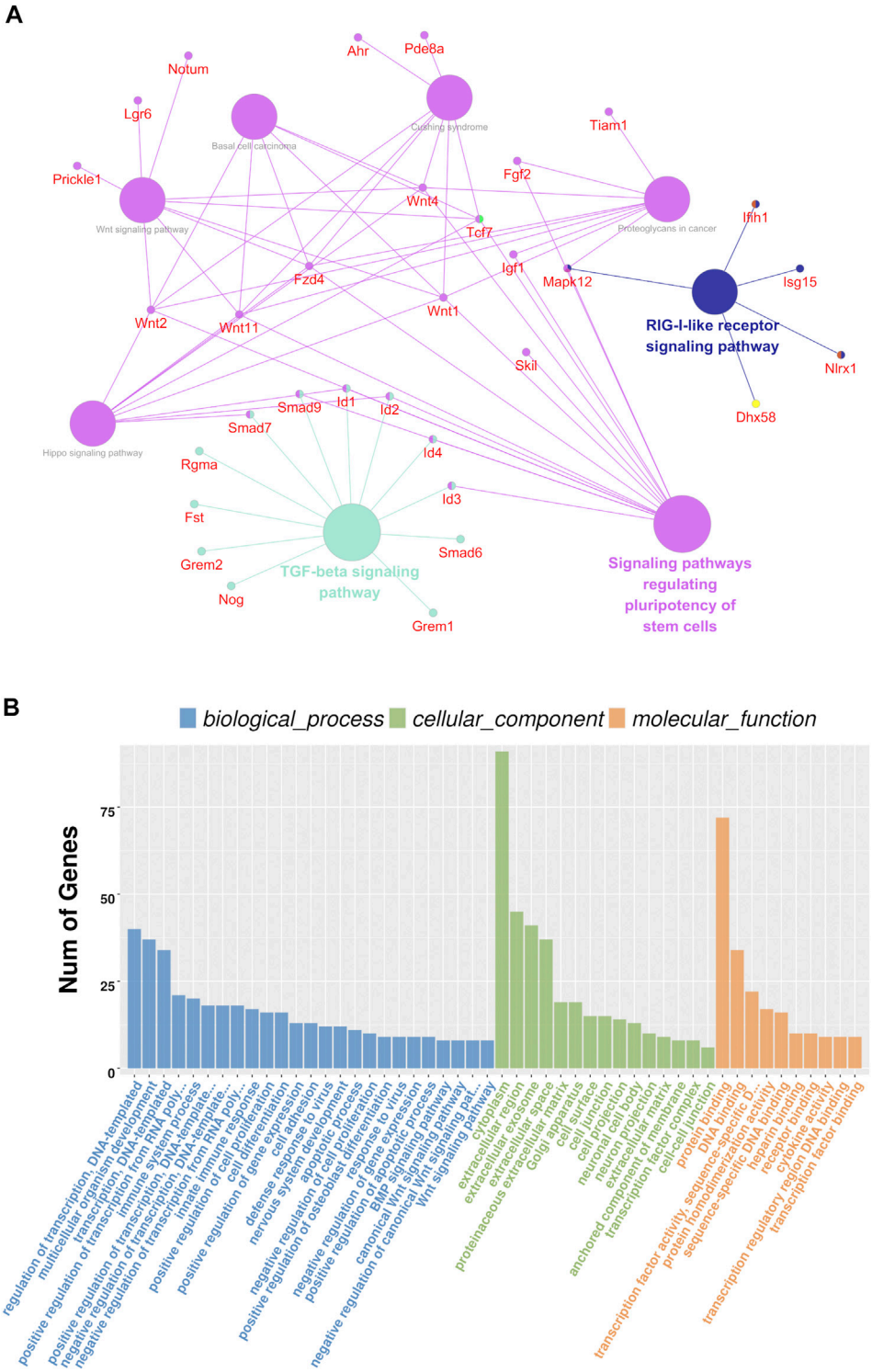

FIGURE 4 | Analysis results of KEGG and GO analyses. **(A)** Possible signaling pathways are represented by circles, and the involved genes are represented by red characters. The possible signaling pathways showed the larger diameters of the circle; the larger the diameters are the more significant the signal pathway is. **(B)** GO analysis in a cellular component, biological process, and molecular function.

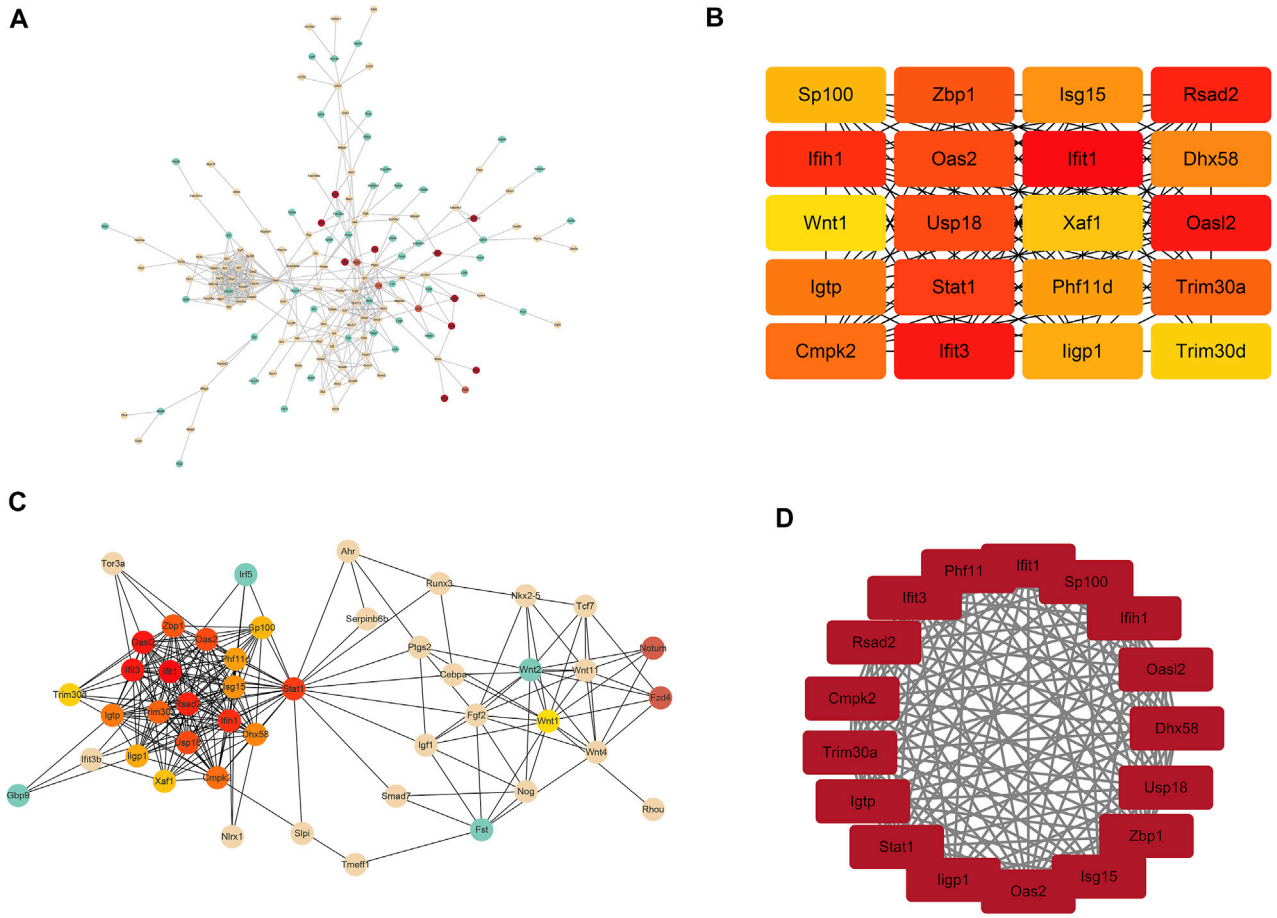

FIGURE 5 | Analysis results of PPI. **(A)** Total network interaction of all DEGs. The redder the color, the more important it is in the network relationship. **(B)** Top 20 hub genes in the interaction network. **(C)** Total network interaction of the top 20 hub genes and the differential genes that are directly related to them. **(D)** Top dense regions of the interactive density region in the PPI network.

and growth factors including *Id2*, *Id3*, *Fgf2*, *Klf10*, *Lhx1*, *Smad7*, *Tcf7*, *Wnt1*, and *Wnt11* (Ho et al., 2011; Koizumi et al., 2013; Sternberg et al., 2013; Bakopoulou et al., 2015; Chen et al., 2016; Zhang et al., 2016; Wang and Martin, 2017; Neves and Sharpe, 2018; Chen et al., 2019; Liu et al., 2019; Chakka et al., 2020; Niki et al., 2021).

The GO analysis showed that the following biological pathways (BPs) were notably enriched among the DEGs: regulation of gene transcription, regulation of transcription from RNA polymerase II promoter, multicellular organism development, positive regulation of cell proliferation, cell differentiation, Wnt signaling, and BMP signaling pathways, etc. (**Figure 4B**). Besides, the following cellular components (CCs) were found to be largely enriched in the extracellular exosome, proteinaceous extracellular matrix, anchored component of the membrane and transcription factor complex, cell–cell junction, and cell protection (**Figure 4B**). Additionally, the following molecular functions (MFs) were largely enriched in protein binding, transcription factor activity, sequence-specific DNA binding, receptor binding, and transcription regulatory region DNA binding (**Figure 4B**). This result suggests that Bmp2 and other signaling pathways regulate dental cell proliferation and cell differentiation as well as tissue development through those aforementioned pathways (Graf et al., 2016; Salazar et al., 2016; Wu et al., 2016; Migliorini et al., 2020).

Analysis Results of the Protein–Protein Interaction (PPI) Network

To gain more insights into the role of these 227 genes in the Bmp2 network and find the hub genes, which were significantly implicated in, a PPI network based on these 227 genes (94 upregulated genes and 133 downregulated genes) was established on the STRING database for functional association analysis, and the sequential visualization was performed on Cytoscape (**Figure 5A**). The plug-in "cytoHubba" determined the top 20 hub genes by MCC algorithm (**Figure 5B**) and related the differential genes according to the association grade difference between different genes (**Figure 5C**). The interactive density region in the PPI network by "MCODE" plug-in was also discovered. The figure below showed the top dense regions

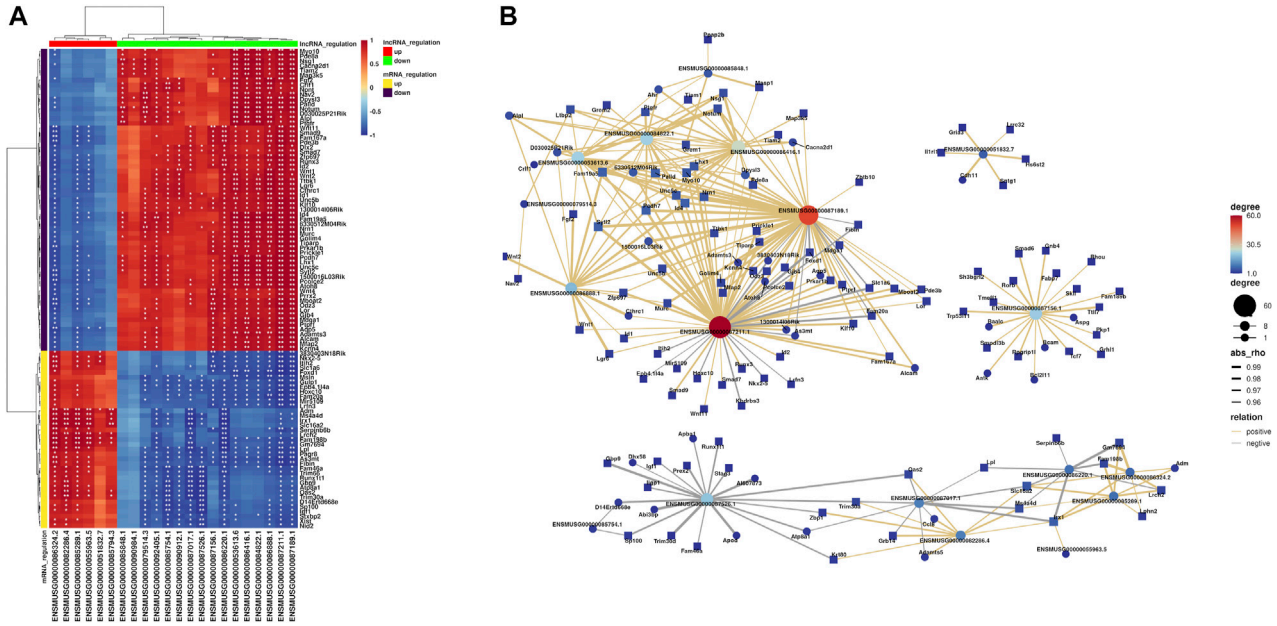

FIGURE 6 | Results of co-expression networks between mRNAs and lncRNAs. **(A)** Heatmaps are used to describe the relationship between lncRNAs and mRNAs (different colors of lncRNA or mRNA regulation). The differences that are statistically significant are denoted by asterisks, with single asterisks representing $p < 0.05$ and two asterisks representing $p < 0.01$. **(B)** Hub co-expression network between lncRNAs and mRNAs. The yellow line represents the positive regulation, the gray line represents the negative regulation, and the thickness of the line represents the relative strength. In addition, the size and color depth of the points represent the number of related genes.

(**Figure 5D**). The PPI analysis predicted that the 9 Bmp2-induced proteins tested can interact with each other. For instance, Fgf2 binds to Id3 and to Wnt11, Lhx1 to Wnt11, Smad7 to Klf10 and to Id2, Tcf7 to Wnt 1 and Id2, etc. On the other hand, one protein interacts with another *via* a third protein. For example, Id2 binds to Klf10 *via* Smad7; Lhx1 binds to Wnt1 *via* Wnt11 and Tcf7 *via* Wnt11; and Fgf2 binds to Id2 *via* Tcf7 and Lhx1 *via* Wnt11 as well as others. This study suggests that these proteins play synergistic roles in the regulation of dental cell proliferation and differentiation.

Analysis Results of Co-Expression Networks Between mRNAs and lncRNAs

Based on correlations between the differential expression levels of lncRNAs and mRNAs, a coding–noncoding gene co-expression network was established. We calculated the Pearson correlation coefficient (PCC) and used the R-value to calculate the correlation coefficient of the PCC between lncRNAs and mRNAs (lncRNA–mRNA PCC, not including lncRNA–lncRNA or mRNA–mRNA PCC). Those lncRNAs and mRNAs that had Pearson correlation coefficients (PCCs) ≥ 0.95 were selected to construct the co-expression network. The figure below showed the top 100 pairs of co-expression relationships (**Figure 6A**). Furthermore, visualization of the co-expression network between lncRNA and mRNAs was performed using the OmicStudio tools at https://www.omicstudio.cn/tool (**Figure 6B**). For instance, lncRNA ENSMUSG00000087211.1 (87,211.1) co-expressed with *Id2*, *Klf10*, *Smad7*, *Wnt1*, *Wnt11*, and *Lhx1*, while lncRNA ENSMUSG00000087189.1 (87,189.1) co-expressed with *Lhx1* and *Klf10*, lncRNA ENSMUSG00000086888.1 (86,888.1) co-expressed with *Fgf2* and *Wnt1*, and lncRNA ENSMUSG00000053613.6 (53,613.6) co-expressed with *Fgf2* and *Lhx1*. Although the co-expression of lncRNAs and mRNAs was identified in the dental papilla cells, the effect of cross talk between the mRNAs and lncRNA during dentinogenesis is required for further study.

Validation of Differentially Expressed lncRNAs and mRNAs

In order to verify the transcriptome sequencing results between the iBmp2$^{fx/fx}$ and iBmp2$^{ko/ko}$ cells and further analyze the possible signaling network mediated by Bmp2, the 9 representative mRNAs and 3 lncRNAs were selected for validation by using RT-qPCR since the 9 Bmp signal-associated mRNAs are involved in the dental cell proliferation, differentiation, and tooth development (Ho et al., 2011; Koizumi et al., 2013; Sternberg et al., 2013; Bakopoulou et al., 2015; Chen et al., 2016; Zhang et al., 2016; Chen et al., 2019; Liu et al., 2019; Chakka et al., 2020), and three novel lncRNAs (87,211.1, 87,189.1, and 86,888.1) co-expressed with these mRNAs (**Figure 6B**). The RT-qPCR results showed that the expression of lncRNA87211.1 and lncRNA87189.1 decreased in the iBmp2$^{ko/ko}$ cells, as same as the results of RNA-seq, but lncRNA86888.1 expression was increased in the iBmp2$^{ko/ko}$ cells which was opposite to the results of RNA-seq (**Figure 7A**). The mRNA expression of

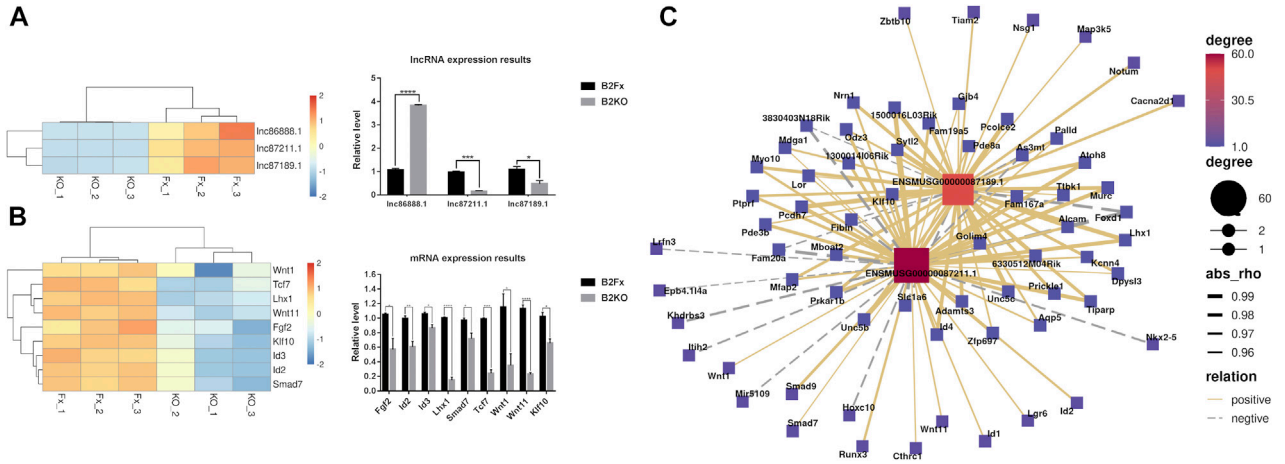

FIGURE 7 | RT-qPCR relative expression results. There are 9 mRNAs and 3 hub lncRNAs validated by RT-qPCR. **(A)** Results of the RNA-seq and RT-qPCR from the lncRNAs of lncRNA87211.1 (ENSMUSG00000087211.1), lncRNA87189.1 (ENSMUSG00000087189.1), and lncRNA86888.1 (ENSMUSG00000086888.1). **(B)** Results of the RNA-seq and RT-qPCR from 9 mRNAs including *Fgf2*, *Id2*, *Id3*, *Klf10*, *Lhx1*, *Smad7*, *Tcf7*, *Wnt1*, and *Wnt11*. The red color represents high fold-change, and the blue color represents low fold-change. The abscissa is the gene name, and the ordinate is the relative expression of the genes. **(C)** Hub co-expression network between two lncRNAs lncRNA87211.1 and lncRNA87189.1 and 6 mRNAs. The solid line shows positive regulation while the dashed line represents negative regulation.

Fgf2, *Id2*, *Id3*, *Lhx1*, *Smad7*, *Tcf7*, *Wnt1*, and *Wnt11* by RT-qPCR analysis was consistent with the result of the RNA-seq (**Figure 7B**). Furthermore, the 6 validated mRNAs (*Id2*, *Klf10*, *Lhx1*, *Smad7*, *Wnt1*, *and Wnt11*) were positively correlated with the expression of lncRNA 87211.1 and lncRNA 87189.1, which was in accordance with the predicted lncRNA–mRNA co-expression network (**Figure 7C**). Accordingly, the PCC can be used to predict the relation network between mRNAs and lncRNAs.

DISCUSSION

Bone morphogenetic proteins (BMPs), members of the TGF-β superfamily, are multiple regulators for organogenesis and homeostasis. Among them, Bmp2 has been proven to be able to induce osteogenesis or dentinogenesis, independently (Bais et al., 2009; Yang et al., 2012). Several canonical and non-canonical Bmp2 signaling pathways have been reported involved in odontogenesis (Cho et al., 2010; Qin et al., 2012a; Qin et al., 2012b; Washio et al., 2012; Qin et al., 2014). Recently accumulated evidence has demonstrated that lncRNAs play biological roles in dental cell proliferation, cell proliferation, and tooth development through the regulation of growth and transcriptional factors (Zheng and Jia, 2016; Liu et al., 2018; Gil and Ulitsky, 2020; Wang et al., 2020; Li et al., 2021; Mirzadeh Azad et al., 2021). The cross talk between the Bmp2 signaling pathway and lncRNAs in dental cell proliferation, cell differentiation, and odontogenesis remains largely unclear. In the present study, we, for the first time, sequenced transcriptome in the iBmp2$^{fx/fx}$ and iBmp2$^{ko/ko}$ cells and performed bioinformatics analysis to study Bmp2-mediated signaling pathways and downstream molecules as well as to predict the co-expression network between lncRNAs and mRNAs regulated by Bmp2 *in vitro*.

Our data indicated that 94 mRNAs were upregulated, and 133 mRNAs were downregulated. Moreover, 6 lncRNAs were upregulated and 16 lncRNAs were downregulated by RNA-seq from the iBmp2 $^{ko/ko}$ and iBmp2 $^{fx/fx}$ papilla cells. GO analysis indicated that the DEGs were closely related to cell proliferation, cell differentiation, transcriptional regulation, protein–protein interactions, BMP- and Wnt-signal pathways, and so forth. Through KEGG analysis, these DEGs were found to be largely enriched in developmentally signaling pathways including TGF-β/BMP signaling pathway, Hippo signaling pathway, Wnt signaling pathway, and signaling pathways regulating pluripotency of stem cells, suggesting that Bmp2 might mediate cross-talk between these signaling pathways and regulate dental papilla mesenchymal cell proliferation, differentiation, and dentinogenesis (Graf et al., 2016; Wu et al., 2016; Neves and Sharpe, 2018; da Silva Madaleno et al., 2020). YAP (Yes-associated protein) and transcriptional co-activator with PDZ-binding motif (TAZ) function as transcriptional cofactors of the Hippo pathway, which only indirectly bind to DNA and regulate target genes through interaction with other transcription factors such as Smads, Runx1/2, and their effectors of the transcriptional factor TEA domain (TEAD) family members (Piccolo et al., 2014). The cross talk between YAP/TAZ and BMP signaling has been documented. YAP was shown to support Smad1-dependent transcription and to be required for BMP-mediated suppression of neural differentiation in mouse embryonic stem cells, providing an example of long-term modulation of BMP signaling (Alarcón et al., 2009). Moreover, following stimulation with Bmp2, YAP modulated Smad1/5 phosphorylation and target gene expression in multiple cell types, while its early interaction

with nuclear Smad1/5/8 was documented to lead to a stabilization of Smad1/5/8 signaling in astrocytes (Huang et al., 2016). Likewise, YAP overexpression activated Smad-dependent BMP signaling and upregulated the mRNA and protein expression of several cementogenesis markers including ALP, Runx2, osteocalcin (Ocn), and dentin matrix acidic phosphoprotein 1 (Dmp1). Treatment with a specific BMP antagonist (LDN193189) prevented the upregulation of the mRNA levels of ALP, Runx2, Dmp1, and Ocn as well as the intensity of ALP-stained and mineralized nodules in cementoblasts (Yang et al., 2018). The PPI study predicted that Bmp-induced proteins related to tooth/bone development interact with each other, and one protein binds to another *via* a third protein (**Figure 5**). It suggests that these proteins synergically regulate tooth-related gene expression mediated by Bmp2 signaling. Furthermore, the lncRNA–mRNA co-expression network analysis revealed that lncRNAs87211.1, lnc87189.1, and lnc86888.1 co-expressed with *Id2*, *Klf10*, *Lhx1*, *Smad7*, *Wnt1*, and *Wnt11* (**Figure 6**).

Based on the results of the KEGG, the PPI, and lncRNA–mRNA co-expression, the 9 mRNAs (*Fgf2*, *Id2*, *Id3*, *Lhx1*, *Smad7*, *Tcf7*, *Wnt1*, *Wnt11*, and *Klf10*) and 3 lncRNAs (87,211.1, 87,189.1, and 86,888.1) were selected as representative genes for RT-qPCR validation as these genes are involved in the dental cell proliferation and differentiation as well as tooth development and formation induced by Bmp2 signaling (Tsuboi et al., 2003; Koizumi et al., 2013; Sternberg et al., 2013; Chen et al., 2016; Graf et al., 2016; Wu et al., 2016; Li et al., 2019; Liu et al., 2019; Qin et al., 2019; Nottmeier et al., 2021) and three novel lncRNAs co-expressed with those mRNAs in the dental papilla cells. Our study demonstrated that the validated 9 mRNAs and 2 lncRNAs by RT-qPCR were consistent with the results of the RNA-seq, and the PCC method can be used to predict co-expression networks between mRNAs and lncRNAs.

The selected 9 mRNAs are involved in the dental cell proliferation, differentiation, and homeostasis (Ho et al., 2011; Koizumi et al., 2013; Sternberg et al., 2013; Bakopoulou et al., 2015; Chen et al., 2016; Zhang et al., 2016; Wang and Martin, 2017; Neves and Sharpe, 2018; Chen et al., 2019; Liu et al., 2019; Chakka et al., 2020; Niki et al., 2021). The loss of Bmp2 resulted in a decrease of these gene expressions detected by RNA-seq and RT-qPCR (**Figures 2**, **7**). It suggested that Bmp2 regulates dental differentiation and dentinogenesis via these genes. It has been documented that the interplay of Bmp2 signal–associated mRNAs and lncRNAs regulates tooth development and formation (Liu et al., 2018; Zhong et al., 2020). This study showed that several novel lncRNAs such as lncRNA87211.1, lncRNA87189.1, and lncRNA86888.1 co-expressed with those mRNAs (**Figure 6**). However, whether the loss of Bmp2 downregulated expression of the selected 9 mRNAs through the lncRNA regulation needs to be further investigated although Liu's and Zhong's groups reported that lncRNAs inhibited microRNAs and indirectly upregulated Bmp2 gene expression, which enhanced the expression of Runx2, Dmp1, and Dspp genes as well as cell differentiation (Liu et al., 2018; Zhong et al., 2020).

Based on this study by the experimental and bioinformatics analyses, we suggest that Bmp2 signaling stimulates these mRNA expressions in the regulation of dental proliferation, differentiation, and homeostasis via direct or indirect lncRNA pathways. However, whether Bmp2 stimulates these 9 gene expressions *via* these lncRNAs during dentinogenesis needs to be further investigated.

Taken together, in the present study, we validated Bmp2 signal pathways and the possible signal molecules downstream of Bmp2 in the dental papilla cells using RNA-seq, RT-qPCR, and bioinformatics. Moreover, by performing bioinformatics analyses, we predicted several hub genes in the lncRNA–mRNA co-expression network regulated by Bmp2, which provides the direction and basis for further elucidating the regulation mechanism of Bmp2-mediated odontogenesis *via* the mRNA–lncRNA network.

DATA AVAILABILITY STATEMENT

The authors acknowledge that the data presented in this study must be deposited and made publicly available in an acceptable repository, prior to publication. Frontiers cannot accept a article that does not adhere to our open data policies.

ETHICS STATEMENT

Animal use was approved by the Institutional Animal Care and Use Committee (IACUC) of the University of Texas Health Science Center at San Antonio, Texas, United States.

AUTHOR CONTRIBUTIONS

FW and SC conceived and designed the experiments and revised the manuscript. FW and RT performed the experiments. YZ carried out RNA-seq. FW, ML, GG, RT, LZ, X-HH, QL, DL, and SC analyzed the data. FW and RT wrote the manuscript. All authors have read and approved the final manuscript.

FUNDING

This work was supported by the National Institutes of Health (NIH) grants, RO1DE019802, the Pilot Grant of School of Dentistry, UTHSCSA, the Natural Science Foundation of Fujian Province (No. 2021J01676), and the Joint Fund for Scientific and Technological Innovation of Fujian Province award (No. 2016Y9034).

ACKNOWLEDGMENTS

We thank Aries Okungbowa-Ikponmwosa and GG for editing the manuscript.

REFERENCES

Åberg, T., Wozney, J., and Thesleff, I. (1997). Expression Patterns of Bone Morphogenetic Proteins (Bmps) in the Developing Mouse Tooth Suggest Roles in Morphogenesis and Cell Differentiation. *Dev. Dyn.* 210, 383–396. doi:10.1002/(sici)1097-0177(199712)210:4<383:aid-aja3>3.0.co;2-c

Agas, D., Sabbieti, M. G., Marchetti, L., Xiao, L., and Hurley, M. M. (2013). FGF-2 Enhances Runx-2/Smads Nuclear Localization in BMP-2 Canonical Signaling in Osteoblasts. *J. Cel. Physiol.* 228, 2149–2158. doi:10.1002/jcp.24382

Alarcón, C., Zaromytidou, A.-I., Xi, Q., Gao, S., Yu, J., Fujisawa, S., et al. (2009). Nuclear CDKs Drive Smad Transcriptional Activation and Turnover in BMP and TGF-β Pathways. *Cell* 139, 757–769. doi:10.1016/j.cell.2009.09.035

Bais, M. V., Wigner, N., Young, M., Toholka, R., Graves, D. T., Morgan, E. F., et al. (2009). BMP2 Is Essential for post Natal Osteogenesis but Not for Recruitment of Osteogenic Stem Cells. *Bone* 45, 254–266. doi:10.1016/j.bone.2009.04.239

Bakopoulou, A., Leyhausen, G., Volk, J., Papachristou, E., Koidis, P., and Geurtsen, W. (2015). Wnt/β-catenin Signaling Regulates Dental Pulp Stem Cells' Responses to Pulp Injury by Resinous Monomers. *Dental Mater.* 31, 542–555. official publication of the Academy of Dental Materials. doi:10.1016/j.dental.2015.02.004

Batista, P. J., and Chang, H. Y. (2013). Long Noncoding RNAs: Cellular Address Codes in Development and Disease. *Cell* 152, 1298–1307. doi:10.1016/j.cell.2013.02.012

Bhatt, S., Diaz, R., and Trainor, P. A. (2013). Signals and Switches in Mammalian Neural Crest Cell Differentiation. *Cold Spring Harbor Perspect. Biol.* 5, a008326. doi:10.1101/cshperspect.a008326

Birjandi, A. A., Suzano, F. R., and Sharpe, P. T. (2020). Drug Repurposing in Dentistry: Towards Application of Small Molecules in Dentin Repair. *Ijms* 21, 6394. doi:10.3390/ijms21176394

Bunch, H. (2018). Gene Regulation of Mammalian Long Non-coding RNA. *Mol. Genet. Genomics* 293, 1–15. doi:10.1007/s00438-017-1370-9

Casagrande, L., Demarco, F. F., Zhang, Z., Araujo, F. B., Shi, S., and Nör, J. E. (2010). Dentin-derived BMP-2 and Odontoblast Differentiation. *J. Dent Res.* 89, 603–608. doi:10.1177/0022034510364487

Chakka, L. R. J., Vislisel, J., Vidal, C. d. M. P., Biz, M. T., Aliasger, K. S., and Salem, B. N. (2020). Application of BMP-2/FGF-2 Gene-Activated Scaffolds for Dental Pulp Capping. *Clin. Oral Invest.* 24, 4427–4437. doi:10.1007/s00784-020-03308-2

Chen, D., Zhao, M., and Mundy, G. R. (2004). Bone Morphogenetic Proteins. *Growth Factors* 22, 233–241. doi:10.1080/08977190412331279890

Chen, L.-L. (2016). Linking Long Noncoding RNA Localization and Function. *Trends Biochemical Sciences* 41, 761–772. doi:10.1016/j.tibs.2016.07.003

Chen, S., Gluhak-Heinrich, J., Martinez, M., Li, T., Wu, Y., Chuang, H.-H., et al. (2008). Bone Morphogenetic Protein 2 Mediates Dentin Sialophosphoprotein Expression and Odontoblast Differentiation via NF-Y Signaling. *J. Biol. Chem.* 283, 19359–19370. doi:10.1074/jbc.M709492200

Chen, S., Rani, S., Wu, Y., Unterbrink, A., Gu, T. T., Gluhak-Heinrich, J., et al. (2005). Differential Regulation of Dentin Sialophosphoprotein Expression by Runx2 during Odontoblast Cytodifferentiation. *J. Biol. Chem.* 280, 29717–29727. doi:10.1074/jbc.M502929200

Chen, X.-J., Shen, Y.-S., He, M.-C., Yang, F., Yang, P., Pang, F.-X., et al. (2019). Polydatin Promotes the Osteogenic Differentiation of Human Bone Mesenchymal Stem Cells by Activating the BMP2-Wnt/β-Catenin Signaling Pathway. *Biomed. Pharmacother.* 112, 108746. doi:10.1016/j.biopha.2019.108746

Chen, Y., Li, Z., Chen, X., and Zhang, S. (2021). Long Non-coding RNAs: From Disease Code to Drug Role. *Acta pharmaceutica Sinica B* 11, 340–354. doi:10.1016/j.apsb.2020.10.001

Chen, Z., Li, W., Wang, H., Wan, C., Luo, D., Deng, S., et al. (2016). Klf10 Regulates Odontoblast Differentiation and Mineralization via Promoting Expression of Dentin Matrix Protein 1 and Dentin Sialophosphoprotein Genes. *Cell Tissue Res* 363, 385–398. doi:10.1007/s00441-015-2260-2

Cho, Y.-D., Yoon, W.-J., Woo, K.-M., Baek, J.-H., Park, J.-C., and Ryoo, H.-M. (2010). The Canonical BMP Signaling Pathway Plays a Crucial Part in Stimulation of Dentin Sialophosphoprotein Expression by BMP-2. *J. Biol. Chem.* 285, 36369–36376. doi:10.1074/jbc.M110.103093

da Silva Madaleno, C., Jatzlau, J., and Knaus, P. (2020). BMP Signalling in a Mechanical Context - Implications for Bone Biology. *Bone* 137, 115416. doi:10.1016/j.bone.2020.115416

Derynck, R., and Zhang, Y. E. (2003). Smad-dependent and Smad-independent Pathways in TGF-β Family Signalling. *Nature* 425, 577–584. doi:10.1038/nature02006

Dinger, M. E., Pang, K. C., Mercer, T. R., and Mattick, J. S. (2008). Differentiating Protein-Coding and Noncoding RNA: Challenges and Ambiguities. *Plos Comput. Biol.* 4, e1000176. doi:10.1371/journal.pcbi.1000176

Dong, J., Lei, X., Wang, Y., Wang, Y., Song, H., Li, M., et al. (2016). Different Degrees of Iodine Deficiency Inhibit Differentiation of Cerebellar Granular Cells in Rat Offspring, via BMP-Smad1/5/8 Signaling. *Mol. Neurobiol.* 53, 4606–4617. doi:10.1007/s12035-015-9382-0

Dong, X., Shen, B., Ruan, N., Guan, Z., Zhang, Y., Chen, Y., et al. (2014). Expression Patterns of Genes Critical for BMP Signaling Pathway in Developing Human Primary Tooth Germs. *Histochem. Cel Biol* 142, 657–665. doi:10.1007/s00418-014-1241-y

Duan, J., Gherghe, C., Liu, D., Hamlett, E., Srikantha, L., Rodgers, L., et al. (2014). Wnt1/βcatenin Injury Response Activates the Epicardium and Cardiac Fibroblasts to Promote Cardiac Repair. *EMBO J.* 31, 429–442. doi:10.1038/emboj.2011.418

Fatica, A., and Bozzoni, I. (2014). Long Non-coding RNAs: New Players in Cell Differentiation and Development. *Nat. Rev. Genet.* 15, 7–21. doi:10.1038/nrg3606

Gao, Z., Wang, L., Wang, F., Zhang, C., Wang, J., He, J., et al. (2018). Expression of BMP2/4/7 during the Odontogenesis of Deciduous Molars in Miniature Pig Embryos. *J. Mol. Hist.* 49, 545–553. doi:10.1007/s10735-018-9792-1

Gil, N., and Ulitsky, I. (2020). Regulation of Gene Expression by Cis-Acting Long Non-coding RNAs. *Nat. Rev. Genet.* 21, 102–117. doi:10.1038/s41576-019-0184-5

Graf, D., Malik, Z., Hayano, S., and Mishina, Y. (2016). Common Mechanisms in Development and Disease: BMP Signaling in Craniofacial Development. *Cytokine Growth Factor. Rev.* 27, 129–139. doi:10.1016/j.cytogfr.2015.11.004

Guo, F., Feng, J., Wang, F., Li, W., Gao, Q., Chen, Z., et al. (2015). Bmp2 Deletion Causes an Amelogenesis Imperfecta Phenotype via Regulating Enamel Gene Expression. *J. Cel. Physiol.* 230, 1871–1882. doi:10.1002/jcp.24915

Guo, X., and Wang, X.-F. (2009). Signaling Cross-Talk between TGF-β/BMP and Other Pathways. *Cell Res* 19, 71–88. doi:10.1038/cr.2008.302

He, H., Yu, J., Liu, Y., Lu, S., Liu, H., Shi, J., et al. (2008). Effects of FGF2 and TGFβ1 on the Differentiation of Human Dental Pulp Stem Cells *In Vitro*. *Cel Biol. Int.* 32, 827–834. doi:10.1016/j.cellbi.2008.03.013

He, Q., Li, R., Hu, B., Li, X., Wu, Y., Sun, P., et al. (2021). Stromal Cell-derived Factor-1 Promotes Osteoblastic Differentiation of Human Bone Marrow Mesenchymal Stem Cells via the lncRNA-H19/miR-214-5p/BMP2 axis. *J. Gene Med.* 23, e3366. doi:10.1002/jgm.3366

Heikinheimo, K., Bègue-Kirn, C., Ritvos, O., Tuuri, T., and Ruch, J. V. (1998). Activin and Bone Morphogenetic Protein (BMP) Signalling during Tooth Development. *Eur. J. Oral Sci.* 106 (Suppl. 1), 167–173. doi:10.1111/j.1600-0722.1998.tb02171.x

Ho, C. C., and Bernard, D. J. (2010). Bone Morphogenetic Protein 2 Acts via Inhibitor of DNA Binding Proteins to Synergistically Regulate Follicle-Stimulating Hormone β Transcription with Activin A. *Endocrinology* 151, 3445–3453. doi:10.1210/en.2010-0071

Ho, C. C., Zhou, X., Mishina, Y., and Bernard, D. J. (2011). Mechanisms of Bone Morphogenetic Protein 2 (BMP2) Stimulated Inhibitor of DNA Binding 3 (Id3) Transcription. *Mol. Cell. Endocrinol.* 332, 242–252. doi:10.1016/j.mce.2010.10.019

Hogan, B. L. (1996). Bone Morphogenetic Proteins: Multifunctional Regulators of Vertebrate Development. *Genes Dev.* 10, 1580–1594. doi:10.1101/gad.10.13.1580

Huang, Z., Sun, D., Hu, J.-X., Tang, F.-L., Lee, D.-H., Wang, Y., et al. (2016). Neogenin Promotes BMP2 Activation of YAP and Smad1 and Enhances Astrocytic Differentiation in Developing Mouse Neocortex. *J. Neurosci.* 36, 5833–5849. doi:10.1523/jneurosci.4487-15.2016

Jalali, S., Gandhi, S., and Scaria, V. (2016). Navigating the Dynamic Landscape of Long Noncoding RNA and Protein-Coding Gene Annotations in GENCODE. *Hum. Genomics* 10, 35. doi:10.1186/s40246-016-0090-2

Kapranov, P., Cheng, J., Dike, S., Nix, D. A., Duttagupta, R., Willingham, A. T., et al. (2007). RNA Maps Reveal New RNA Classes and a Possible Function for Pervasive Transcription. *Science* 316, 1484–1488. doi:10.1126/science.1138341

Kémoun, P., Laurencin-Dalicieux, S., Rue, J., Vaysse, F., Roméas, A., Arzate, H., et al. (2007). Localization of STRO-1, BMP-2/-3/-7, BMP Receptors and Phosphorylated Smad-1 during the Formation of Mouse Periodontium. *Tissue and Cell* 39, 257–266. doi:10.1016/j.tice.2007.06.001

Koizumi, Y., Kawashima, N., Yamamoto, M., Takimoto, K., Zhou, M., Suzuki, N., et al. (2013). Wnt11 Expression in Rat Dental Pulp and Promotional Effects of Wnt Signaling on Odontoblast Differentiation. *Congenit. Anom.* 53, 101–108. doi:10.1111/cga.12011

Lee, S.-K., Lee, K.-E., Jeon, D., Lee, G., Lee, H., Shin, C.-U., et al. (2009). A Novel Mutation in the DSPP Gene Associated with Dentinogenesis Imperfecta Type II. *J. Dent Res.* 88, 51–55. doi:10.1177/0022034508328168

Li, J., Jin, F., Cai, M., Lin, T., Wang, X., and Sun, Y. (2021). LncRNA Nron Inhibits Bone Resorption in Periodontitis. *J. Dent Res.* 220345211019689, 002203452110196. doi:10.1177/00220345211019689

Li, J., Yang, Y., Fan, J., Xu, H., Fan, L., Li, H., et al. (2019). Long Noncoding RNA ANCR Inhibits the Differentiation of Mesenchymal Stem Cells toward Definitive Endoderm by Facilitating the Association of PTBP1 with ID2. *Cell Death Dis* 10, 492. doi:10.1038/s41419-019-1738-3

Li, Q., Hua, Y., Yang, Y., He, X., Zhu, W., Wang, J., et al. (2018). T Cell Factor 7 (TCF7)/TCF1 Feedback Controls Osteocalcin Signaling in Brown Adipocytes Independent of the Wnt/β-Catenin Pathway. *Mol. Cel Biol* 38. doi:10.1128/mcb.00562-17

Liang, Z., Hore, Z., Harley, P., Uchenna Stanley, F., Michrowska, A., Dahiya, M., et al. (2020). A Transcriptional Toolbox for Exploring Peripheral Neuroimmune Interactions. *Pain* 161, 2089–2106. doi:10.1097/j.pain.0000000000001914

Liao, C., Zhou, Y., Li, M., Xia, Y., and Peng, W. (2020). LINC00968 Promotes Osteogenic Differentiation *In Vitro* and Bone Formation *In Vivo* via Regulation of miR-3658/RUNX2. *Differentiation* 116, 1–8. doi:10.1016/j.diff.2020.09.005

Liu, J., Zhang, Z. Y., Yu, H., Yang, A. P., Hu, P. F., Liu, Z., et al. (2018). Long Noncoding RNA C21orf121/bone Morphogenetic Protein 2/microRNA-140-5p Gene Network Promotes Directed Differentiation of Stem Cells from Human Exfoliated Deciduous Teeth to Neuronal Cells. *J. Cel Biochem* 120, 1464–1476. doi:10.1002/jcb.27313

Liu, Z., Chen, T., Bai, D., Tian, W., and Chen, Y. (2019). Smad7 Regulates Dental Epithelial Proliferation during Tooth Development. *J. Dent Res.* 98, 1376–1385. doi:10.1177/0022034519872487

Lu, Y., Ye, L., Yu, S., Zhang, S., Xie, Y., Mckee, M. D., et al. (2007). Rescue of Odontogenesis in Dmp1-Deficient Mice by Targeted Re-expression of DMP1 Reveals Roles for DMP1 in Early Odontogenesis and Dentin Apposition *In Vivo*. *Dev. Biol.* 303, 191–201. doi:10.1016/j.ydbio.2006.11.001

Macias, D., Ganan, Y., Sampath, T. K., Piedra, M. E., Ros, M. A., and Hurle, J. M. (1997). Role of BMP-2 and OP-1 (BMP-7) in Programmed Cell Death and Skeletogenesis during Chick Limb Development. *Development* 124, 1109–1117. doi:10.1242/dev.124.6.1109

Malik, Z., Alexiou, M., Hallgrimsson, B., Economides, A. N., Luder, H. U., and Graf, D. (2018). Bone Morphogenetic Protein 2 Coordinates Early Tooth Mineralization. *J. Dent Res.* 97, 835–843. doi:10.1177/0022034518758044

Meguro, F., Porntaveetus, T., Kawasaki, M., Kawasaki, K., Yamada, A., Kakihara, Y., et al. (2019). Bmp Signaling in Molar Cusp Formation. *Gene Expr. Patterns* 32, 67–71. doi:10.1016/j.gep.2019.04.002

Migliorini, E., Guevara-Garcia, A., Albiges-Rizo, C., and Picart, C. (2020). Learning from BMPs and Their Biophysical Extracellular Matrix Microenvironment for Biomaterial Design. *Bone* 141, 115540. doi:10.1016/j.bone.2020.115540

Mirzadeh Azad, F., Polignano, I. L., Proserpio, V., and Oliviero, S. (2021). Long Noncoding RNAs in Human Stemness and Differentiation. *Trends Cell Biology* 31, 542–555. doi:10.1016/j.tcb.2021.02.002

Miyazono, K., Maeda, S., and Imamura, T. (2005). BMP Receptor Signaling: Transcriptional Targets, Regulation of Signals, and Signaling Cross-Talk. *Cytokine Growth Factor. Rev.* 16, 251–263. doi:10.1016/j.cytogfr.2005.01.009

Murayama, K., Kato-Murayama, M., Itoh, Y., Miyazono, K., Miyazawa, K., and Shirouzu, M. (2020). Structural Basis for Inhibitory Effects of Smad7 on TGF-β Family Signaling. *J. Struct. Biol.* 212, 107661. doi:10.1016/j.jsb.2020.107661

Nadiri, A., Kuchler-Bopp, S., Haikel, Y., and Lesot, H. (2004). Immunolocalization of BMP-2/-4, FGF-4, and WNT10b in the Developing Mouse First Lower Molar. *J. Histochem. Cytochem.* 52, 103–112. doi:10.1177/002215540405200110

Neves, V. C. M., and Sharpe, P. T. (2018). Regulation of Reactionary Dentine Formation. *J. Dent Res.* 97, 416–422. doi:10.1177/0022034517743431

Niki, Y., Kobayashi, Y., and Moriyama, K. (2021). Expression Pattern of Transcriptional Enhanced Associate Domain Family Member 1 (Tead1) in Developing Mouse Molar Tooth. *Gene Expr. Patterns* 40, 119182. doi:10.1016/j.gep.2021.119182

Nottmeier, C., Liao, N., Simon, A., Decker, M. G., Luther, J., Schweizer, M., et al. (2021). Wnt1 Promotes Cementum and Alveolar Bone Growth in a Time-dependent Manner. *J. Dent Res.* 100, 1501–1509. doi:10.1177/00220345211012386

O'Connell, D. J., Ho, J. W. K., Mammoto, T., Turbe-Doan, A., O'Connell, J. T., Haseley, P. S., et al. (2012). A Wnt-Bmp Feedback Circuit Controls Intertissue Signaling Dynamics in Tooth Organogenesis. *Sci. Signal.* 5, ra4. doi:10.1126/scisignal.2002414

Oh, S. H., Hwang, Y. C., Yang, H., Kang, J. H., Hur, S. W., Jung, N. R., et al. (2012). SHP Is Involved in BMP2-Induced Odontoblast Differentiation. *J. Dent Res.* 91, 1124–1129. doi:10.1177/0022034512461916

Ou, M., Zhao, Y., Zhang, F., and Huang, X. (2014). Bmp2 and Bmp4 Accelerate Alveolar Bone Development. *Connect. Tissue Res.* 56, 204–211. doi:10.3109/03008207.2014.996701

Pandur, P., Läsche, M., Eisenberg, L. M., and Kühl, M. (2002). Wnt-11 Activation of a Non-canonical Wnt Signalling Pathway Is Required for Cardiogenesis. *Nature* 418, 636–641. doi:10.1038/nature00921

Piccolo, S., Dupont, S., and Cordenonsi, M. (2014). The Biology of YAP/TAZ: Hippo Signaling and beyond. *Physiol. Rev.* 94, 1287–1312. doi:10.1152/physrev.00005.2014

Ponting, C. P., Oliver, P. L., and Reik, W. (2009). Evolution and Functions of Long Noncoding RNAs. *Cell* 136, 629–641. doi:10.1016/j.cell.2009.02.006

Qin, W., Lin, Z. M., Deng, R., Li, D. D., Song, Z., Tian, Y. G., et al. (2012a). p38a MAPK Is Involved in BMP-2-Induced Odontoblastic Differentiation of Human Dental Pulp Cells. *Int. Endod. J.* 45, 224–233. doi:10.1111/j.1365-2591.2011.01965.x

Qin, W., Liu, P., Zhang, R., Huang, S., Gao, X., Song, Z., et al. (2014). JNK MAPK Is Involved in BMP-2-Induced Odontoblastic Differentiation of Human Dental Pulp Cells. *Connect. Tissue Res.* 55, 217–224. doi:10.3109/03008207.2014.882331

Qin, W., Yang, F., Deng, R., Li, D., Song, Z., Tian, Y., et al. (2012b). Smad 1/5 Is Involved in Bone Morphogenetic Protein-2-Induced Odontoblastic Differentiation in Human Dental Pulp Cells. *J. endodontics* 38, 66–71. doi:10.1016/j.joen.2011.09.025

Qin, X., Jiang, Q., Miyazaki, T., and Komori, T. (2019). Runx2 Regulates Cranial Suture Closure by Inducing Hedgehog, Fgf, Wnt and Pthlh Signaling Pathway Gene Expressions in Suture Mesenchymal Cells. *Hum. Mol. Genet.* 28, 896–911. doi:10.1093/hmg/ddy386

Quinn, J. J., and Chang, H. Y. (2016). Unique Features of Long Non-coding RNA Biogenesis and Function. *Nat. Rev. Genet.* 17, 47–62. doi:10.1038/nrg.2015.10

Saito, E., Saito, A., Kato, H., Shibukawa, Y., Inoue, S., Yuge, F., et al. (2016). A Novel Regenerative Technique Combining Bone Morphogenetic Protein-2 with Fibroblast Growth Factor-2 for Circumferential Defects in Dog Incisors. *J. Periodontol.* 87, 1067–1074. doi:10.1902/jop.2016.150746

Salazar, V. S., Gamer, L. W., and Rosen, V. (2016). BMP Signalling in Skeletal Development, Disease and Repair. *Nat. Rev. Endocrinol.* 12, 203–221. doi:10.1038/nrendo.2016.12

Schlange, T., Andrée, B., Arnold, H.-H., and Brand, T. (2000). BMP2 Is Required for Early Heart Development during a Distinct Time Period. *Mech. Dev.* 91, 259–270. doi:10.1016/s0925-4773(99)00311-1

Sepponen, K., Lundin, K., Knuus, K., Väyrynen, P., Raivio, T., Tapanainen, J. S., et al. (2017). The Role of Sequential BMP Signaling in Directing Human Embryonic Stem Cells to Bipotential Gonadal Cells. *J. Clin. Endocrinol. Metab.* 102, 4303–4314. doi:10.1210/jc.2017-01469

Shi, Y., and Massagué, J. (2003). Mechanisms of TGF-β Signaling from Cell Membrane to the Nucleus. *Cell* 113, 685–700. doi:10.1016/s0092-8674(03)00432-x

Statello, L., Guo, C.-J., Chen, L.-L., and Huarte, M. (2021). Gene Regulation by Long Non-coding RNAs and its Biological Functions. *Nat. Rev. Mol. Cel Biol* 22, 96–118. doi:10.1038/s41580-020-00315-9

Sternberg, H., Kidd, J., Murai, J. T., Jiang, J., Rinon, A., Erickson, I. E., et al. (2013). Seven Diverse Human Embryonic Stem Cell-Derived Chondrogenic Clonal Embryonic Progenitor Cell Lines Display Site-specific Cell Fates. *Regenerative Med.* 8, 125–144. doi:10.2217/rme.12.117

Touat-Todeschini, L., Shichino, Y., Dangin, M., Thierry-Mieg, N., Gilquin, B., Hiriart, E., et al. (2017). Selective Termination of Lnc RNA Transcription Promotes Heterochromatin Silencing and Cell Differentiation. *Embo J.* 36, 2626–2641. doi:10.15252/embj.201796571

Tsuboi, T., Mizutani, S., Nakano, M., Hirukawa, K., and Togari, A. (2003). Fgf-2 Regulates Enamel and Dentine Formation in Mouse Tooth Germ. *Calcified Tissue Int.* 73, 496–501. doi:10.1007/s00223-002-4070-2

Vijaykumar, A., Root, S. H., and Mina, M. (2020). Wnt/β-Catenin Signaling Promotes the Formation of Preodontoblasts *In Vitro*. *J. Dent Res.* 100, 387–396. doi:10.1177/0022034520967353

Wang, F., Li, Y., Wu, X., Yang, M., Cong, W., Fan, Z., et al. (2017a). Transcriptome Analysis of Coding and Long Non-coding RNAs Highlights the Regulatory Network of cascade Initiation of Permanent Molars in Miniature Pigs. *BMC Genomics* 18, 148. doi:10.1186/s12864-017-3546-4

Wang, J., and Martin, J. F. (2017). Hippo Pathway: An Emerging Regulator of Craniofacial and Dental Development. *J. Dent Res.* 96, 1229–1237. doi:10.1177/0022034517719886

Wang, J., Samuels, D., Zhao, S., Xiang, Y., Zhao, Y.-Y., and Guo, Y. (2017b). Current Research on Non-coding Ribonucleic Acid (RNA). *Genes* 8, 366. doi:10.3390/genes8120366

Wang, Y., Li, L., Zheng, Y., Yuan, G., Yang, G., He, F., et al. (2012). BMP Activity Is Required for Tooth Development from the Lamina to Bud Stage. *J. Dent Res.* 91, 690–695. doi:10.1177/0022034512448660

Wang, Z., Huang, Y., and Tan, L. (2020). Downregulation of lncRNA DANCR Promotes Osteogenic Differentiation of Periodontal Ligament Stem Cells. *BMC Dev. Biol.* 20, 2. doi:10.1186/s12861-019-0206-8

Washio, A., Kitamura, C., Morotomi, T., Terashita, M., and Nishihara, T. (20122012). Possible Involvement of Smad Signaling Pathways in Induction of Odontoblastic Properties in KN-3 Cells by Bone Morphogenetic Protein-2: A Growth Factor to Induce Dentin Regeneration. *Int. J. dentistry* 2012, 1–6. doi:10.1155/2012/258469

Wu, L. A., Feng, J., Wang, L., Mu, Y.-d., Baker, A., Donly, K. J., et al. (2010). Immortalized Mouse Floxed Bmp2 Dental Papilla Mesenchymal Cell Lines Preserve Odontoblastic Phenotype and Respond to BMP2. *J. Cel. Physiol.* 225, 132–139. doi:10.1002/jcp.22204

Wu, L., Wang, F., Donly, K. J., Wan, C., Luo, D., Harris, S. E., et al. (2015). Establishment of Immortalized Mouse Bmp2 Knock-Out Dental Papilla Mesenchymal Cells Necessary for Study of Odontoblastic Differentiation and Odontogenesis. *J. Cel. Physiol.* 230, 2588–2595. doi:10.1002/jcp.25061

Wu, M., Chen, G., and Li, Y.-P. (2016). TGF-β and BMP Signaling in Osteoblast, Skeletal Development, and Bone Formation, Homeostasis and Disease. *Bone Res.* 4, 16009. doi:10.1038/boneres.2016.9

Wu, T., and Du, Y. (2017). LncRNAs: From Basic Research to Medical Application. *Int. J. Biol. Sci.* 13, 295–307. doi:10.7150/ijbs.16968

Wu, X.-B., Li, Y., Schneider, A., Yu, W., Rajendren, G., Iqbal, J., et al. (2003). Impaired Osteoblastic Differentiation, Reduced Bone Formation, and Severe Osteoporosis in Noggin-Overexpressing Mice. *J. Clin. Invest.* 112, 924–934. doi:10.1172/jci15543

Yamashiro, T., Tummers, M., and Thesleff, I. (2003). Expression of Bone Morphogenetic Proteins and Msx Genes during Root Formation. *J. Dent Res.* 82, 172–176. doi:10.1177/154405910308200305

Yang, B., Sun, H., Song, F., Wu, Y., and Wang, J. (2018). Yes-associated Protein 1 Promotes the Differentiation and Mineralization of Cementoblast. *J. Cel Physiol* 233, 2213–2224. doi:10.1002/jcp.26089

Yang, G., Yuan, G., MacDougall, M., Zhi, C., and Chen, S. (2017). BMP-2 Induced Dspp Transcription Is Mediated by Dlx3/Osx Signaling Pathway in Odontoblasts. *Sci. Rep.* 7, 10775. doi:10.1038/s41598-017-10908-8

Yang, G., Lu, X., and Yuan, L. (2014). LncRNA: a Link between RNA and Cancer. *Biochim. Biophys. Acta (Bba) - Gene Regul. Mech.* 1839, 1097–1109. doi:10.1016/j.bbagrm.2014.08.012

Yang, W., Harris, M. A., Cui, Y., Mishina, Y., Harris, S. E., and Gluhak-Heinrich, J. (2012). Bmp2 Is Required for Odontoblast Differentiation and Pulp Vasculogenesis. *J. Dent Res.* 91, 58–64. doi:10.1177/0022034511424409

Yin, Y., Yan, P., Lu, J., Song, G., Zhu, Y., Li, Z., et al. (2015). Opposing Roles for the lncRNA Haunt and its Genomic Locus in Regulating HOXA Gene Activation during Embryonic Stem Cell Differentiation. *Cell stem cell* 16, 504–516. doi:10.1016/j.stem.2015.03.007

Yuan, X., Liu, M., Cao, X., and Yang, S. (2019). Ciliary IFT80 Regulates Dental Pulp Stem Cells Differentiation by FGF/FGFR1 and Hh/BMP2 Signaling. *Int. J. Biol. Sci.* 15, 2087–2099. doi:10.7150/ijbs.27231

Zhang, F., Song, J., Zhang, H., Huang, E., Song, D., Tollemar, V., et al. (2016). Wnt and BMP Signaling Crosstalk in Regulating Dental Stem Cells: Implications in Dental Tissue Engineering. *Genes Dis.* 3, 263–276. doi:10.1016/j.gendis.2016.09.004

Zhang, H., and Bradley, A. (1996). Mice Deficient for BMP2 Are Nonviable and Have Defects in Amnion/chorion and Cardiac Development. *Development* 122, 2977–2986. doi:10.1242/dev.122.10.2977

Zhang, X., Zhao, J., Li, C., Gao, S., Qiu, C., Liu, P., et al. (2001). DSPP Mutation in Dentinogenesis Imperfecta Shields Type II. *Nat. Genet.* 27 (2), 151–152. doi:10.1038/84765

Zhao, L., Wang, J., Li, Y., Song, T., Wu, Y., Fang, S., et al. (2021). NONCODEV6: an Updated Database Dedicated to Long Non-coding RNA Annotation in Both Animals and Plants. *Nucleic Acids Res.* 49, D165–d171. doi:10.1093/nar/gkaa1046

Zheng, Y., and Jia, L. (2016). Long Noncoding RNAs Related to the Odontogenic Potential of Dental Mesenchymal Cells in Mice. *Arch. Oral Biol.* 67, 1–8. doi:10.1016/j.archoralbio.2016.03.001

Zhong, J., Tu, X., Kong, Y., Guo, L., Li, B., Zhong, W., et al. (2020). LncRNA H19 Promotes Odontoblastic Differentiation of Human Dental Pulp Stem Cells by Regulating miR-140-5p and BMP-2/FGF9. *Stem Cel Res Ther* 11, 202. doi:10.1186/s13287-020-01698-4

Conflict of Interest: The authors declare that the research was conducted in the absence of any commercial or financial relationships that could be construed as a potential conflict of interest.

Publisher's Note: All claims expressed in this article are solely those of the authors and do not necessarily represent those of their affiliated organizations, or those of the publisher, the editors, and the reviewers. Any product that may be evaluated in this article, or claim that may be made by its manufacturer, is not guaranteed or endorsed by the publisher.

Advantages of publishing in Frontiers

OPEN ACCESS
Articles are free to read for greatest visibility and readership

FAST PUBLICATION
Around 90 days from submission to decision

HIGH QUALITY PEER-REVIEW
Rigorous, collaborative, and constructive peer-review

TRANSPARENT PEER-REVIEW
Editors and reviewers acknowledged by name on published articles

Frontiers
Avenue du Tribunal-Fédéral 34
1005 Lausanne | Switzerland

Visit us: www.frontiersin.org
Contact us: frontiersin.org/about/contact

REPRODUCIBILITY OF RESEARCH
Support open data and methods to enhance research reproducibility

DIGITAL PUBLISHING
Articles designed for optimal readership across devices

FOLLOW US
@frontiersin

IMPACT METRICS
Advanced article metrics track visibility across digital media

EXTENSIVE PROMOTION
Marketing and promotion of impactful research

LOOP RESEARCH NETWORK
Our network increases your article's readership